Aldehyde functionalised poly(acryloyl hydrazide) polymers for modulating *E. coli* K-12 biofilm formation and subsequent biofilm functionality in the biocatalysis arena

by

Pavan Adoni

UNIVERSITY OF BIRMINGHAM

A thesis submitted to the University of Birmingham for the degree of

DOCTOR OF PHILOSOPHY

School of Chemical Engineering

College of Engineering and Physical Sciences

University of Birmingham

Abstract of Thesis

The use of bacterial biofilms in industry has emerged as an alternative to whole cell biotransformations, where they can use many of their resilient properties to overcome some of the environmental, physical and chemical stresses required for many industrial reactions, e.g. substrate/product or solvent toxicity. As such, a host of research can now be found to optimise biofilm mediated process by optimising biofilm properties, either through genetic regulation or through bacterial interaction with soft materials enabling a level control over biofilm structure. Recently, synthetic polymers have been used to interact and aggregate bacteria with interesting changes in phenotype, including the expression of biofilm factors. In this project, poly(acryloyl hydrazide) was used as the polymer scaffold onto which biologically relevant functional groups could be easily introduced post polymerisation, resulting in a library of functional poly(acryloyl hydrazide) polymers that could be used to aggregate bacteria to potentially induce and control biofilm levels. Firstly however, we describe the optimisation of poly(acryloyl hydrazide) synthesis via RAFT polymerisation, resulting in greater control over polymer chain lengths and dispersities. Then, the ability of aldehyde functionalised poly(acryloyl hydrazide) polymers to interact and aggregate the *E. coli* K-12 overproducing mutant PHL644 (which contains an *ompR234* mutation, leading to overexpression of the biofilm adhesin curli) and its parental MC4100 strain was investigated. In general, polymer induced cell aggregation and overall induced biofilm quantities were found to be directly modulated by polymer hydrophobicity, with the most hydrophobic polymers enabling MC4100 biofilm quantities (as measured by crystal violet) to exceed that of the overproducing PHL644. Importantly, the expression of curli within MC4100 polymer induced biofilms was influenced greatly by the addition of different polymers, with curli expression levels being highly linked to the physiochemical properties

of the aggregating polymer (hydrophobicity and heteroaromaticity) so much so that MC4100 curli expression levels were made to match and exceed that of the overproducing PHL644. The functionality of these polymer induced biofilms were then assessed in the biocatalytic arena, again with polymer induced biofilm properties being linked to the ability of the recombinant biofilms to convert 5-fluoroindole to 5-fluorotryptophan. We also harnessed the natural metabolic esterase generation of the polymer induced *E. coli* biofilms to catalyse the lipid ester 4-Nitrophenyl dodecanoate into 4-Nitrophenol in toxic reaction conditions.

Acknowledgements

I have learnt a great deal during this PhD; it has provided me with exciting challenges, and with a lot of hard work, a lot of fulfilment. I would thank my supervisors, I could not have asked for a better pairing and I am immensely grateful to all the hard work you have put in helping me along the way. Firstly to my primary supervisor Tim who has greatly helped me with the biological aspects of the project and for always having a positive outlook on my work. To my second supervisor Paco, you have helped immensely in guiding me through this project, your love of science and the generation of good data has always motivated me to go further. You're both great guys who I appreciate a lot. I would also like to thank my colleagues in both the schools of biochemical engineering and chemistry. From the Paco group; Oli Creese, Adam Kolodziej, Krystian Ubych, Manal Alanazi, Tom Leigh, Andrey Romanyuk, Sameh El Sayed, Charlotte Farrow, Carlos Guillen Posteguillo, Zelu Brioso Jimenez, Alex Antropenko, Nick Huniedi, Teyfick Selen, Amit Deb. And from the Overton group; Stacey Golub, Maria Charalambous, John Rolley, Wendy Allen, Dario Bazzoli, Ana de Magalhaes, Parissa Pordelkhaki, Nasim Mahmoodi, Hong Li, Ikhlaas Kasili. I have made some great friends and have had a lot of fun along the way. I would like to particularly thank Oli who showed me the ropes in polymer chemistry and for the nice work which resulted. I would like to also thank all the hark working and dedicated technicians that helped me along the way, from both schools with particular mention to; Allen Bowden (GPC), Cécile Le Duff (NMR), Elaine Mitchell and Ronnie Baglin (Biochemical engineering).

Last but not least, I would like to thank my family and friends; my mother Sharada and my brother Kishan, and to all my friends outside of academia for their continual support and encouragement.

List of Figures

Chapter 1

Chapter 2

Chapter 4

<u>Chapter 4 – Supplementary figures</u>

Chapter 5 (Written in the form of a publication)

Chapter 5 - Supplementary figures

Chapter 6

Table of Contents

Chapter 1 - Introduction

(i) A brief overview of bacterial biofilms

Bacteria have an incredible ability to adapt to their environment and this is why they have been able to colonise nearly everywhere on planet earth for billions of years. Evidence of this comes from early fossil records; putative biofilm microcolonies were identified within the 3.3-3.4 billion year old South African Kornberg formation[1] and filamentous biofilms were identified within 3.2 billion year old deep sea hydrothermal rocks in Australia[2]. The incredible prevalence of biofilms throughout the biosphere comes from the evolved ability of bacteria to sense and attach to nutrient rich surfaces[3,4] forming closely packed communities which are thought to have provided a localized homeostatic environment in the face of the adverse conditions of primitive earth (extremes in temperature, pH and exposure to UV light). From an evolutionary standpoint this facilitated the development of complex cell-cell interactions which lead to the development of advantageous/cooperative signalling pathways and chemotactic motility that biofilms have become known for[5] (and what differentiates cells in a biofilm from those in planktonic form) resulting in protection from predators and harsh environmental conditions through the division of labour, conservation of genotype[4] and the formation of a protective extracellular polymeric substance (EPS) 3D matrix which provides a physical and structural barrier against mechanical/chemical stresses[6].

Interestingly, the immediate appearance of biofilms growing in different environments are rather similar, suggesting that many of the convergent survival strategies adopted by biofilms may be in part due to structural specialisation[7] which in general results highly

heterogeneous matrix enclosed microcolonies with canal-like networks of water channels throughout the biofilm to allow for nutrient diffusion. It is thought that in general the EPS constitutes between 70-98% of the dry mass of a biofilm and that the vast majority of this is produced by the embedded bacteria that usually constitute only around 10% of dry cell mass[6,8]. Upon more detailed analysis of biofilm structure through the emergence of microscopy techniques such as scanning confocal laser microscopy (SCLM) subtle changes in the structure and morphology of biofilms can be seen for different biofilm growth conditions and strains of bacteria respectively. For example biofilms that grow in fast moving turbulent waters such as in streams or rivers are of a filamentous appearance and are known as 'streamers' which are attached to a surface by an upstream head connected to a downstream tail that oscillates due to the current[7,9]. In calmer/more still waters biofilms tend to be in the more widely studied mushroom like structures without any sort of patterning that would suggest a direction of flow[7] (see figure 1). Communities with access to higher levels of nutrients unsurprisingly tend to form thicker biofilms[9]. Additionally, as one would expect, there are subtle differences in biofilm structure between different strains of bacteria. *Pseudomonas aeruginosa* is widely seen as the model organism for the study of biofilms[10] mainly due to the fact that this species is highly associated with multidrug-resistant infections such as pneumonia, cystic fibrosis and other lung disorders with its pathogenicity being directly linked to its ability to colonise the host and form biofilms. Part of the reason for this multi-drug resistance is due to the fact that *P. aeruginosa* tend to produce very large amounts of protective EPS resulting in very thick, resistant biofilms[11,8,5]. *P. aeruginosa* biofilms tend to be very dense at the centre of colonies and become more sparsely populated toward the edges of the biofilm. For *Vibrio parahaemolyticus* biofilms the opposite arrangement is found, and both these species form biofilms that are

approximately twice as thick as *Pseudomonas fluorescens* biofilms when grow under the same conditions. Surprisingly despite the apparent thickness of *P. aeruginosa* biofilms, out of the three species, they contain the lowest ratio of bacterial dry cell mass to EPS dry mass[8]. The self-production of EPS by bacteria is unsurprisingly very influential on biofilm structure with different strains producing different amounts of EPS with differing components resulting in a vast array of biofilm morphologies ranging from smooth and flat looking biofilms to more rough or fluffy and porous ones[6]. For example, the production of alginate in *P. aeruginosa* is thought to be the reason for the thick, heterogenous biofilm appearance. Non-mucoid *P. aeruginosa* strains (that cannot make alginate) form more homogeneous looking flat biofilms[12]. In *Escherichia coli* K-12 biofilms, the polysaccharide EPS components poly-β-1,6-N-acetyl-D-glucosamine (PGA) and colanic acid are responsible for its 3D architecture, which is lost when the cells are not able to produce either component[13,14].

In general there are three main ways in which prokaryotic bacteria can become part of a structured biofilm; first is the redistribution of already attached cells (to a biofilm) to a different location by surface motility[15], the second is the division of biofilm associated cells whereby daughter cells grow outward and upward from the surface[16] and the third is the recruitment and attachment of prokaryotic cells from the bulk medium[17]. It is thought that the relative contributions of each of these mechanisms, the specific organisms involved and their adaptation to specific environmental cues via genetic regulation and/or selection which determine the overall structure of the biofilm[5].

In addition to all of this, biofilms are usually not limited to consist of only one species, in fact despite mono-species biofilms being the most widely studied, it is multi-species biofilms that predominate in nature[18] and again these communities have adapted to this over time. Interspecies interactions within a mixed species biofilms involve cell-cell communication and metabolic cooperation/competition. Due to the vast prevalence of these biofilms, it is clearly interspecies cooperation (not competition) within these biofilms that have prevailed in many cases[19]. A relevant example of interspecies cooperation is found in the biofilms that have invaded the lungs/oral cavities of cystic fibrosis (CF) patients, which mainly consist of *P. aeruginosa* and *Staphylococcus aureus* strains[20,18]. An exoproduct of *P. aeruginosa* enhances aminoglycoside resistance and other antibiotic resistance in *S. aureus* by triggering them to grow as small colony variants[21] with this at least in part contributing to the persistence of CF in humans.

(ii) Bacterial surface attachment and biofilm lifecycle

(a) Surface sensing

The process of bacteria sensing and attaching to a physical surface is one of the first stages of biofilm formation, where upon attachment bacteria transition from a motile planktonic state into a sessile, community oriented lifestyle through changes in genetic expression that mostly lead to the formation of biofilms. Due to the overwhelming diversity of bacteria and the almost infinite number of conditions that bacteria may find themselves in, all of which affect behaviour, it has been difficult to define a general bacterial mechanism for surface sensing. Still, this topic is of active interest and as such studies have been performed on certain model organisms. One of the first elucidations of a surface sensing mechanism was proposed in *V. parahaemolyticus* and was coined ‘flagella dynamometer’ whereby the

rotation of flagella (a filamentous protein structure that allows microorganisms to swim[22]) slows down upon surface contact or within viscous environments, thereby acting as a signal to the bacteria that it is on a surface[23,24]. In *E.coli*, upon contact with a surface, the periplasmic stress pathways Rcs and Cpx become activated, probably due to the disruptions caused in the cell wall/periplasmic space, again alerting the cell to its surface contact and causing sessile lifestyle genes to be expressed/upregulated[25]. The high local concentration of nutrients at surfaces also serves to trigger bacterial movement toward the chemical gradient (a process known as chemotaxis) and the transition from motile to sessile states[26]. In addition to this, the close proximity of bacteria to a surface causes local changes in pH and osmolarity which also plays its part in the transition[27]. Type IV pili (T4P) have also been shown to be involved with surface sensing. T4P are protein appendages attached to bacteria that have a wide array of functions including DNA uptake, microcolony formation and a specific surface associated type of movement known as 'twitching' whereby pili are elongated and retracted respectively to allow for crawling along a surface[28]. Recently T4P have been linked with surface sensing too with *Vibrio cholerae* using its flagellum and T4P to synergistically scan a surface mechanically before attaching to it[23,29].

(b) Surface attachment

After surface sensing, subsequent attachment immediately provides bacteria with many advantages; primarily organic material suspended within a bulk liquid tend to settle and become deposited on surfaces, thereby increasing local nutrient concentrations[30]. In addition it has been suggested that merely the process of surface attachment leads to increased resistance profiles. For example, low-biofilm forming bacteria that are attached to surfaces and that do not form a protective EPS matrix like a traditional biofilm exhibit similar

resistance profiles to cells in a biofilm. It was suggested that this was because surface attachment reduces the net negative charge on bacterial cells and in turn enhances the stability of its membrane. Upon surface detachment, the resistance was lost suggesting this type of resistance profile does not require changes in genotype[31].

The attachment of bacteria onto surfaces occurs in two phases, firstly cell attachment is reversible, occurs rapidly and involves non-specific interactions[27] which are gradually strengthened over time. Due to the non-specific nature of these primary surface interactions, it is not limited to living microbes; the absorption and desorption of both bacteria and polystyrene latex particles from a surface was shown to be very similarly mediated by van der Waals interactions and electrostatic repulsions[32], hence confirming that this initial reversible mode of attachment is due to mainly physiochemical rather than specific biological effects. After around 1-2 minutes, the gradually strengthening of interactions decrease the probability of desorption to a point where the attachment becomes effectively irreversible[33]. At this point, after overcoming any repulsive interactions, additional hydrophobic interactions between the cell wall/extracellular organelle moieties and surface hydrophobic groups further stabilises interfacial interactions[4].

This leads to the second irreversible mode of attachment which primarily involves biological effects; genes involving bacterial motility are downregulated and genes promoting a sessile lifestyle such as the production of EPS matrix components are upregulated[34]. Many of these processes are induced by the secretion of intracellular signalling molecules, the local concentrations of which are monitored by bacteria, effectively informing them of high local cell densities. This process, known as quorum sensing (QS) is one of the many ways that bacteria are able to communicate with each other, resulting in the transition to a sessile

lifestyle that allows for cell-cell cooperation within a biofilm community. Another particular signalling molecule that also induces many of these changes is the near ubiquitous secondary messenger cyclic di-GMP (c-di-GMP)[35]; high intracellular levels of this are recognised by bacteria which promote biofilm maturation both at the transcriptional and post translational levels[34] and it is usually at this point that cells will start to produce cell the EPS which not only provides protection, but further anchors the cell community to its surface[36]. As mentioned, the composition of the EPS matrix will differ among strains but in general it is thought that polysaccharides, proteins, lipids, eDNA, enzymes and ions form the main constituents[6,4,37]. The specific composition of EPS is species-specific[6].

(c) Biofilm maturation and cell detachment

After the initial attachment of bacteria and the expression of surface adhesins, there are two main characteristics of surface associated colonies; the ramping up of the production of EPS components, and resulting the development of colony/biofilm resistance[38]. At this stage, behaviour is vastly different to that of planktonic cells. The biofilm will start to look slimy, and the cells will usually begin to divide upward and outward into mushroom shaped microcolonies of multi-micron sized diameter (figure 1). Signalling molecules will be increasingly secreted, with the local concentration of these effectively allowing for high levels of cooperative cell-cell communication via quorum sensing (QS)[39] with this being one of the near ubiquitous pathways in which the cells of a biofilm and its EPS components will be modulated - dictating a variety of cellular functions; pathogenesis, nutrient acquisition, secondary metabolite production, conjugation and motility[40,4]. The length of time the biofilm will remain in this mature state will depend on various things, with the main limiting factor thought to be nutrient access[38]. When nutrients become depleted, cells at the outer

periphery of the matrix will begin to detach themselves and disperse into the bulk fluid, where some may then go on to attach to the surface at another location, starting off the cycle once again, hence this final step is vital for self-renewal of the microbial community[4]. However despite this, very little is actually known at this stage about the functions and regulatory pathways involved in cell detachment[38].

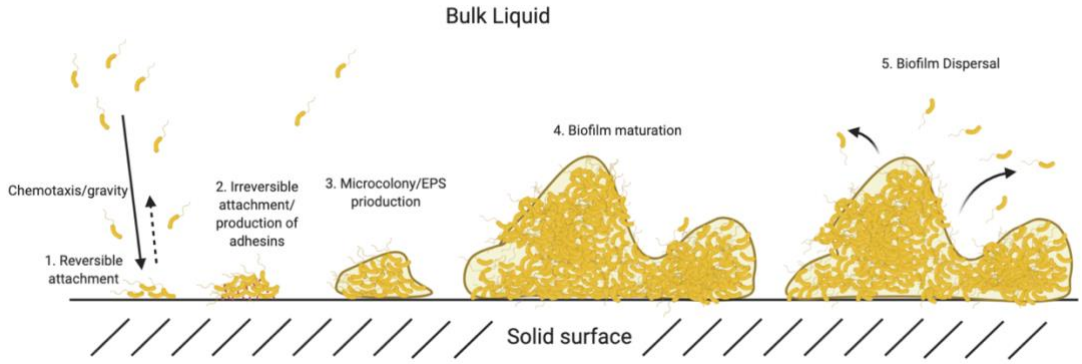

Figure 1: Five main stages of the biofilm lifecycle

(iii) *Escherichia coli* biofilms

E.coli is a Gram negative facultative anaerobe (can survive with or without oxygen) which has been widely used as a model organism in bioengineering and industrial microbiology[41]. Many strains of *E.coli* can be found within the intestinal tracts of warm blooded animals where they form biofilms and actually benefit the host by preventing the colonisation of other pathogenic strains[42]. There are however certain strains of *E.coli* that are pathogenic and may cause infection, with the preliminary stage being colonisation onto the infection site and biofilm formation which usually accompanies increased virulence and makes the infection harder to eradicate[43]. Unsurprisingly therefore, many studies have been conducted over the years to elucidate the mechanism of biofilm formation in *E.coli*[42,44,45]. The primary stage of *E.coli* biofilm formation is the initial adhesion of cells to a surface which initiates several signalling cascades resulting in the production of adhesins and other

exopolysaccharides that make up the EPS. The most widely studied adhesin in *E.coli* biofilms is known as curli, an amyloid fibre that projects from the cell surface and is known to bind to both biological and abiotic surfaces[46,47]. The expression of curli is mediated by two operons, *csgBA* and *csgDEFG*. The *csgBA* operon encodes the main structural subunit protein of curli, CsgA and the nucleator protein, CsgB. The *csgDEFG* operon encodes the proteins required for the assembly of CsgA into curli fibres with *csgD* acting as the master positive transcriptional regulator of the *csgBA* operon. Curli expression is maximal at temperatures of around 30 ^{o}C and in conditions of low osmolarity[48]. Other key adhesins include Antigen 43 (Ag 43) which plays a key role in adhesion to abiotic surfaces, and also mediates bacterial cohesion/autoaggregation[49,50]. Type 1 fimbriae or pili are filamentous protein appendages which can adhere in a specific manner to surfaces bearing mannose, hence type 1 pili promotes adhesion to eukaryotic mannose bearing host cells[45]. Type 4 pili (T4P) are additionally involved in surface twitching, allowing cells to move along a surface[51]. Later stages involve the production of exopolysaccharide EPS components. Poly-β-1,6-N-acetyl-D-glucosamine (PGA) is synthesised by the products of the *pgaABCD* operon and acts as an adhesin as well as maintaining biofilm structural stability[14] and it has been suggested that this is actually expressed almost immediately on surface contact[52]. Colanic acid (a branched polymer comprising fructose, galactose, glucuronic acid and glucose) production is controlled by the *wca* operon which encodes the enzymes necessary for colanic acid synthesis. In addition many *E. coli* strains produce cellulose as well, encoded by the *bcsQABZC* and *bcsEFG* operons. *E.coli* K-12 strains however do not produce cellulose due to absence of the *bcsQ* gene[53,54]. Overall, the matrix components heavily depend on the surrounding environment and as *E. coli* biofilms can be found in many different environments, it is clear that the regulation of EPS expression is tightly controlled and

extremely complex. Environmental stimuli is generally detected by two-component regulatory systems, whereby one gene (and its respective protein) is responsible for the detection of stimuli and the second is responsible for regulating the response. Generally in the context of biofilms many of these stimuli are detected during or after cell surface attachment and results in the activation of the sigma factor RpoS, which is a protein that regulates the expression of a group of genes involved in the regulation of stress response, normally resulting in the expression of protective biofilm factors. Several small messenger molecules such as cyclic-diguanylic acid (c-di-GMP) are also expressed and are essential for the transition of *E. coli* from planktonic to sessile state by taking part in the allosteric regulation of enzymes involved in biofilm formation. Quorum sensing also plays an extremely important role[44].

In *E. coli*, at least three two-component systems are involved in biofilm regulation and these are CpxA/CpxR, EnvZ/OmpR and the RcsC system. CpxA/CpxR is a stress response system that reacts towards cell envelope damage[55] on adhesion to a surface[45] with CpxA being the sensor and CpxR being the response regulator. Among the responses are modifications in cell-surface protein expression and repression of flagellar genes in order to prevent motility and chemotaxis resulting in optimal surface attachment. Conversely however, CpxA/R negatively regulates curli expression upon the overproduction of csgA[45,47]. In a similar way, the Rcs system also responds to envelope stress and also negatively regulates curli expression by repressing the expression of *csgD* and also represses expression of other adhesins such as Ag 43[56], however positively regulates the expression of colanic acid[57]. Both the CpxA/R and Rcs pathways serve to negatively regulate adhesins such as curli when overexpressed, suggesting that these adhesins are only really needed during the early stages of biofilm formation in *E.coli*[47]. The third system, EnvZ/OmpR responds to changes in

osmolarity; EnvZ being the sensor and OmpR regulating transcription of *ompF* and *ompC* porin encoding genes[45]. The system increases surface adhesion in response to moderate increases in osmolarity, which encourages bacteria to adhere to nutrient rich surfaces (where local osmolarity will be higher than in the bulk fluid)[58]. Additionally OmpR represses flagellar gene expression and positively regulates the expression of curli by activating the *csgD* promoter - the *csgD* gene is the curli master regulator. As mentioned, CpxR negatively regulates curli expression and it does this by binding to a region of the *csgD* gene hence preventing ompR from positively regulating it. Vidal et al, showed that an especially adherent *E. coli* K-12 mutant strain contained a point mutation in the *ompR* gene (*ompR234*) which was able to constitutively express curli potentially due to increased levels of OmpR234 binding and positive regulation with *csgD* when compared with the native OmpR protein. Hence these *ompR234* mutants are able to form more adherent, thicker biofilms[46]. Finally, quorum sensing is another very influential process in biofilm formation and is a cell density dependant chemical signalling system where individual bacteria secrete signal molecules known as autoinducers (AIs) which allows for cell-cell communication and coordination in high AI concentrations which serves to control many biofilm related genes and their expression. Gram negative bacteria produce two types of AIs; AI-1 which is an N-acyl-homoserine lactone (AHL) and AI-2, a furanosyl borate diester[42]. The AHL regulatory system consists of a *luxI* gene which encodes AHL synthase and *luxR* which acts as the response regulator. *E.coli* does not contain *luxI* or a similar homologue, but does have the *sdiA* gene which is a *luxR* homologue hence it is not able to synthesis AHLs (AI-1) but can detect them allowing for *E.coli* QS communication with other species. *sdiA* has also been shown to upregulate *uvrY* and *csrA* genes which enhance biofilm levels. AI-2 on the other hand is expressed by most bacterial species, including *E.coli*[44] via the *luxS* gene and is

responsible for both inter and intra species QS due to its universal nature. AI-2s have also been shown to increase biofilm formation through the MqsR system, which regulates flagellar motility and increases MotA and FliA expression which stimulates biofilm levels. In general it is thought that AI-2 concentrations are highest at the middle/end of the exponential phase and drop off during the stationary phase, suggesting QS is especially important during the initial stages of the biofilm lifecycle. Other QS systems may also be possible, for example an indole dependant QS system was reported in *E.coli*, which allowed for bacterial adaptation in response to starvation[59].

(iv) Influence of surface properties on bacterial attachment and subsequent phenotype

It is clear that biofilm formation is an extremely complex process which involves numerous overlapping metabolic pathways, which also differ vastly between strains. In general there are five stages of a biofilm and this lifecycle is briefly covered above and presented visually in figure 1. The stages are; irreversible followed by reversible attachment to a surface, formation of surface associated colonies, biofilm maturation and cell detachment. Clearly, each sequential stage will have a great influence on the proceeding step, and from this sense one may argue that the most influential stage of biofilm formation is the preliminary surface sensing and attachment process. Additionally due to the overwhelming complexity of genetic regulation upon surface attachment, it may be easier to control biofilm formation by controlling initial bacterial surface adherence (via non-specific interactions) rather than trying to genetically engineer an already complex system. As such, much research has been performed to find out how the physical properties of surfaces affect initial bacterial attachment and subsequent biofilm formaton[60,4,27]. Thermodynamics plays the central role in attachment to surfaces and as such, the current state of the art for studying bacterial

adhesion is based on theories of colloidal interactions, with the main one being known as the Derjaguin-Landau-Verwey-Overbeek (DLVO) theory which describes how bacterial adhesion to surfaces/particles are dictated by the interfacial free energies[32,61] of the system (including the bulk liquid). This theory however is not a perfect model for bacterial systems due to their living nature and the fact that bacteria, unlike colloids show structural and chemical heterogeneities[62]. To somewhat address this, the model was extended to what is now known as the extended DLVO theory (XDLVO)[61] which is now widely used in modelling bacterial-surface interactions. Still, one of its main drawbacks is due to limitations in the current methods required to obtain some of the variables used in its theoretical equations[32,63] and these will be discussed in the following sections.

As the basis of this project is to use synthetic polymers to interact and aggregate bacteria (to form biofilms), a brief summary of the physiochemical interactions that are included in the XDLVO theory is necessary to understand the basics of the thermodynamic processes that govern initial bacterial attachment to particles/surfaces, and so too which the formation of biofilms rely on. Due to the fact that biofilms are generally seen as problematic, much research has been performed on modifying surfaces to completely resist the initial thermodynamically driven bacterial attachment and therefore the subsequent formation of biofilms; this will be summarised too. Finally, more recent efforts to induce bacterial aggregation and alter phenotype via interaction with synthetic polymers will be discussed in detail.

(a) Influence of surface free energies in bacterial attachment

In general, the initial bacterial attachment to surfaces may be predicted by the XDLVO theory which considers interactions between particles in a bulk medium. In the case of bacteria-surface attachment, the medium will be aqueous and its surface energy will need to be taken into account along with those of the approaching particles. All materials possess surface energy; a particle in its bulk form will generally be stable with a balanced set of bonds/interactions. At its surface however the atoms will have an unbalanced set of bonds/interactions, and hence have the potential to form new interactions with another surface in close proximity[64]. This 'unrealised' energy is known as the materials' surface energy or interfacial free energy and is very important in dictating how a materials' surface will interact with another. For example, given there is a particle A in a liquid, the surface of that particle will form interactions with the liquids surface at the interface. If another particle B approaches, it may prefer to form surface interactions with particle B rather than the liquid. If the change in energy upon this is favourable (i.e. the particles form cooperative bonds that reduces the systems total energy), then the particles will form a surface with each other (i.e. positively interact). If the change in energy is not favourable (forms repulsive bonds with one another, or simply that the attraction between particle-liquid molecules is greater than that of particle-particle interaction), then the particle will stay interacting with the liquid surface and stay away from the other particle. In general therefore in the context of bacteria-surface/particle interactions, overall levels of adhesion/repulsion are governed by the balance of bacterial-solid, bacterial-liquid and solid-liquid interfacial Gibbs free energies[32].

Firstly, reversible interaction mechanisms are thought to initiate when cells approach a surface to within several hundred Angstroms – these are mainly Lifshitz-Van der Waals forces (LW) and electrostatic interactions (EL) and at this stage can be either attractive or repulsive. Normally, at large distances (over hundreds of Å) electrostatic interactions between the bacteria-surface tend to predominate, whilst at shorter ranges LW interactions become stronger[65]. Normally, these LW interactions are attractive while the EL interactions will depend on the surface charge. Most bacteria have a net negative charge as determined by zeta potential measurements[66,67] meaning they will preferentially bind to positively charged surfaces. In nature, most surfaces tend to have an overall slight negative charge meaning electrostatic repulsion with bacteria[68]. This repulsion however can be effectively screened by the presence of salts/ions in the liquid medium, and studies have shown increased initial bacterial attachment in high ionic strength liquids[69,70]. Therefore this attractive/reversible stage is represented by a secondary energy minimum on a Gibbs energy curve as shown in figure 2. Within seconds, these interactions are thought to strengthen and may overcome an energy barrier present at around 10 Å. At this point bacterial surface attachment becomes more irreversible in the primary interaction minimum due to additional short length acid-base interactions[32] that in general play the most important role in the initial physiochemical attachment of bacteria to surfaces[71]. After this, biological factors e.g. production of adhesive EPS take over and strengthen the surface interactions further[4].

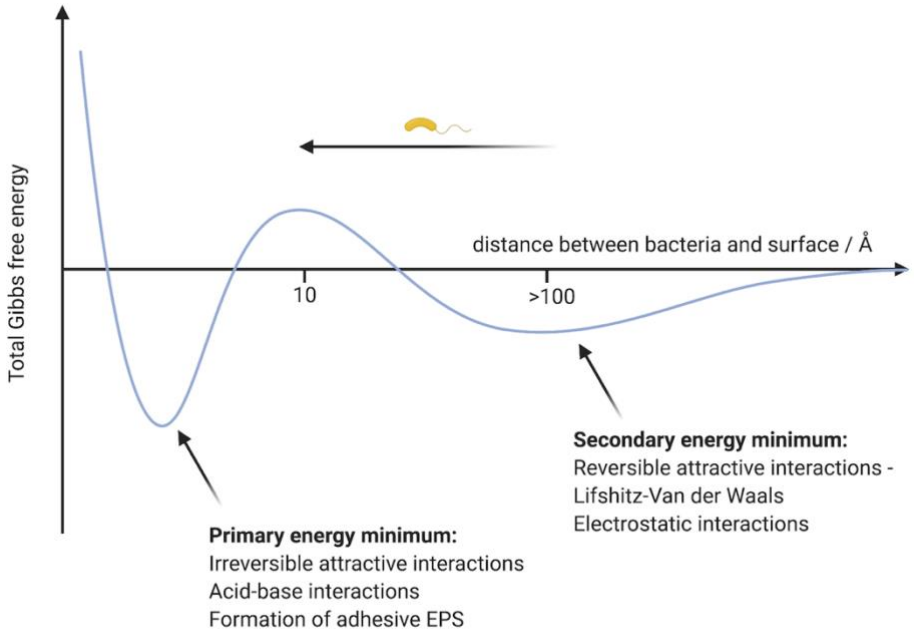

Figure 2: General schematic of distance dependant Gibbs free energy of interaction between bacteria and a surface, created using Biorender.com

Studies on bacterial-surface interactions can be modelled by theories of colloidal interactions, due to the fact that bacteria and colloids are of similar appearance and dimensions[72]. The original DLVO theory takes into account both Lifshitz-Van der Waals and electrostatic interactions which vary with colloidal separation[73], however this is only partly successful in describing interactions between biological entities[61] mainly because it does not take into account that bacterial surfaces are not chemically inert and will form hydrogen bonds/hydrophobic interactions whenever possible[62]. In order to take this into account, additional short range Lewis acid-base (AB) type interactions need to be considered in addition to LW and EL interactions. In general AB interactions are defined by electron donor/electron acceptor interactions between polar groups at the cell-surface interface in a liquid medium. These can either be attractive (representing adhesive hydrophobic interactions or hydrogen bonding) or repulsive (representing hydrophilic repulsion)

depending on the physiochemical properties of the bacteria/surface. The reason why attraction exists between hydrophobic substances is due to the hydrophobic effect which describes how water molecules surrounding a hydrophobic moiety form cohesive AB free energy reducing hydrogen bonds with each other, effectively forming water cages around the hydrophobic moieties which then bind together. Conversely, water molecules will form hydrogen bonds directly with hydrophilic substances if the AB free energy of cohesion between these is lower (i.e. thermodynamically favourable) than the AB free energy of cohesion between water molecules, therefore preventing interactions between hydrophilic moieties[74]. If the AB free energy of cohesion between hydrophilic cells and hydrophilic surfaces is lower (more favourable) than that of the cohesion between the water molecules and hydrophilic surface, hydrophilic attraction between cell and surface will predominate. In general therefore, total levels of adhesion/repulsion are governed by the balance of bacterial-solid (surface), bacterial-liquid (bulk liquid) and solid-liquid interfacial Gibbs free energies[32]. The combination of the three main physiochemical interactions; Lifshitz-Van der Waals forces, electrostatic interactions and the more recently investigated acid-base interactions determine the overall distance dependant Gibbs free energy of interaction, visualised in figure 2 for generic approaching particles/surface. This extended DLVO theory can be used to predict bacterial-surface adhesion or repulsion, and can be defined by equation 1.

$$\Delta G(y)^{Total} = \Delta G(y)^{LW} + \Delta G(y)^{EL} + \Delta G(y)^{AB} \quad \text{(Equation 1)}$$

Where y is the distance between bacteria and surface (or any two approaching particles), LW: Lifshitz-Van der Waals, EL: electrostatic, AB: Acid-base. A negative ΔG^{Total} value corresponds to a thermodynamically

favourable attractive interaction, a positive ΔG^{Total} corresponds to repulsion. The overall distance dependent $\Delta G(y)^{Total}$ can be visualised in figure 2.

An example where this theory was applied was in the investigation of reversible adhesion between three bacterial strains; *Staphylococcus epidermidis* HBH_2 169, *Acinetobacter calcoaceticus* RAG-1, *Streptococcus thermophilus* B and polystyrene particles, with three different solid surfaces; Glass, fluoroethyelenepropylene (FEP) and polymethylmethacrylate (PMMA) respectively under constant flow[32]. Water contact angles of each strain (and polystyrene) and surface were measured to determine hydrophobicity and were also used along with known surface free energies to predict distance dependant free energies of interaction (of each component given in equation 1) between the different strains/surfaces respectively. In most cases, when summing all the three individual contributions, a classical distance dependant Gibbs energy curve was obtained, much like as presented in figure 2. Alongside this, bacterial/particle deposition onto respective surfaces was measured experimentally and from this; initial deposition rates, initial desorption rates and final desorption rates were determined. As expected, initial desorption rates were much higher than final desorption rates indicating initial reversibility of adhesion followed by a presumed strengthening of interaction which lead to a stronger mode of attachment. Using the calculated distance dependant Gibbs energy curves (with the relative contributions of LW, EL and AB free energies of interaction), it was determined that final desorption rates of all strains (and particles) on glass and PMMA respectively, were directly related to the depth of secondary interaction minimum, hence bond strengthening in this case did not involve primary AB type interactions, but rather a strengthening of, or 'rolling down' the secondary interaction minimum (figure 2) involving EL and LW interactions. FEP however, which is

more hydrophobic than glass and PMMA, did not form adhesive LW or EL interactions and so the strong adhesion of the strains onto FEP could only be explained by the more irreversible primary AB type hydrophobic interactions.

As one would expect however there were indeed deviations from the XDLVO theory, for example no sensible primary interaction minimum was found using glass and PMMA surfaces - this may be understandable for the hydrophilic glass but PMMA is hydrophobic and would be expected to partake in primary AB interactions. In addition, the XDLVO theory does not take into account particle collisions during flow, meaning that larger adhering strains were more likely to be 'pulled off' a surface by a random collision with another flowing particle/strain. Furthermore XDLVO does not take into account the structural and chemical heterogeneity of cells which will also influence interactions, for example surface appendages may aid in initial adhesion. Given this, it can be said that the XDLVO theory still somewhat falls apart during this initial reversible bacterial adhesion process which in reality depends on additional biological factors other than surface free energies[32]. As mentioned before however, for most interactions with surfaces, AB type interactions are generally much larger and more influential on adhesion than LW and EL, hence a focus on this deeper primary irreversible interaction minimum could be said to be less prone to the drawbacks described above.

Another similar study by Ong et al. investigated these stronger primary AB hydrophobic interactions[75]. The surface adhesion of two isogenic *E.coli* K-12 strains; D21 and D21f2 (that varied in surface hydrophobicity, D21f2 > D21) onto four different surfaces of increasing hydrophobicity (mica > glass > polystyrene > Teflon) was investigated using AFM cantilevers coated with bacteria. When the bacteria/cantilever approaches a surface and interacts, it

becomes deflected. From this the force of interaction could be determined and indeed it was found that the bacterial-surface attraction increased with increasing surface hydrophobicities. Again, by measuring water contact angles and using known surface free energies, theoretical Gibbs curves of interaction were obtained for all cell-surface interactions, however this time adhesion was related to the primary interaction minimum which was always present at short ranges below around 10 Å[75].

(b) Influence of surface topography on bacterial surface attachment

Given that the vast majority of surfaces are not completely smooth, it is not surprising that many studies have been conducted to elucidate the effect of surface topography on bacterial attachment[68]. Despite this, and rather predictably due to the complexity and living nature of bacterial attachment, the mechanisms of topographical attachment still remain unclear. One of the main factors that define topography is surface roughness which describes the height variation on a surface. Because it can be calculated relatively easily, roughness is often used as the sole descriptor for surface topography, and this is especially the case in the field of biofouling[76]. In actuality, surface topography is effectively the configuration of a surface which is defined by vertical features (roughness), along with their spacial arrangement. In the literature there does not seem to be any type of conclusion for both surface roughness or topography on bacterial attachment[68]. A recent review by Cheng and Moraru, 2019 suggested that rather than looking directly at the effect of surface topography on bacterial attachment, investigating how surface topography influences bacterial-surface interactions by modulating interaction parameters such as physiochemical effects, chemical gradients, hydrodynamics and the conditioning of surfaces would provide a much better understanding of how surface topography influences attachment[68]. One such

study by Hoek and Agarwal focused on simulated colloid-surface interactions and it was found that the magnitude of repulsive interaction was lowered on a textured surface compared to a smooth one[77]. The overall interaction between colloid and surface was repulsive, however this repulsion was lowered when the surface contained nanoscale asperities separated by around 50 nm diameter troughs. It was deduced that these troughs often coincided with valleys where LW attractive interactions were present[77,78], furthermore it was suggested that these surface protrusions physically prevented the colloids from accessing the majority of the repulsive surface, hence reducing overall surface repulsion[78] (figure 3a, 3). Another more recent study by Feng et al. found that when a surface contained nanoscale asperities separated by only 15-25 nm, bacterial attachment was reduced compared to a smooth surface control. The reasoning was that when there are a large number of vertical asperities that are very tightly packed together, the surface area of contact with bacteria is greatly enhanced (and so too the repulsive interactions, figure 3a, 2). When the asperities were separated to around 50 nm (comparable to the previous computational study described), bacterial attachment similarly increased[79]. In general, it is thought that surfaces that contain vertical features that are between 20-150 nm in height and 20-200 nm separation, will increase LW interactions with particles/bacteria[80] .

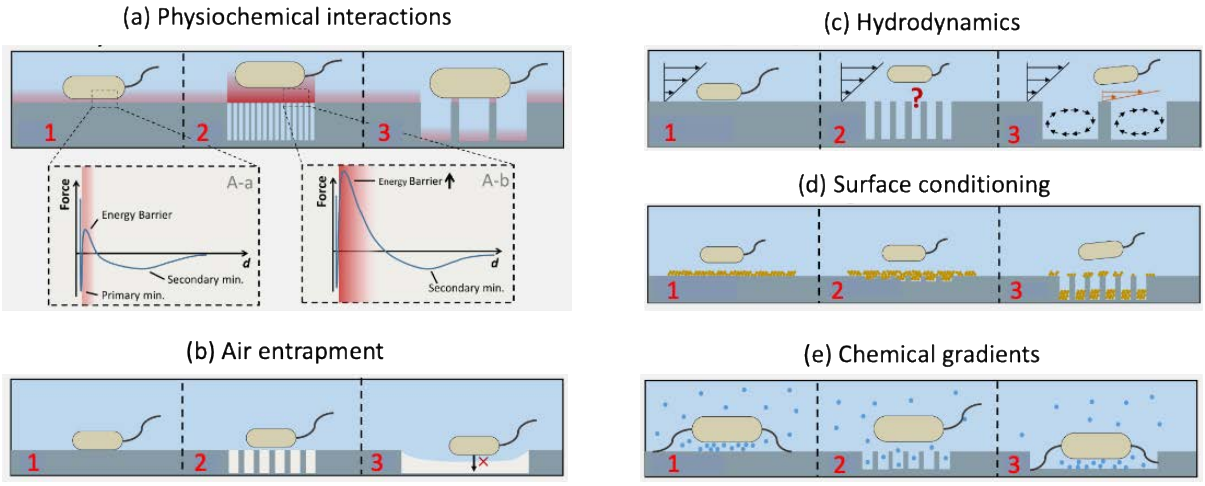

Figure 3: Scale-dependent effects of surface topography on various factors that influence initial bacterial attachment, e.g., surface topography may affect physiochemical interactions (a), local fluid mechanics at the interface (b and c), the depositioning of material onto the surface (d) and the resulting local chemical gradients all of which will influence bacterial attachment. Taken from Moraru et. al, ref 68

As previously mentioned, an important surface property that is very influential on bacterial attachment to a surface is its wettability (or hydrophobicity), which is expressed by the contact angle of a liquid on the surface. Contact angle measurements are usually taken on a macro scale and assume a completely smooth surface, when in reality the surface will rarely be smooth on the micro or nano scale[81]. Hence as contact angle measurements are normally used in XDVLO models, discrepancies may be present in the predictions of interactions between rougher/topologically more complex surfaces with bacteria. Surfaces that are rough are defined by vertical protrusions that are separated. The space between these protrusions may be filled with liquid or air depending on the surface topography[82] and hydrophobicity, which will then influence bacterial attachment (figure 3b). If the gaps are filled with air, then bacteria will usually not be able to access the solid surface by penetrating the liquid-air interface due to the high surface tension of water (figure 3b, 3). As such, surface topographies that are capable of stabilizing air-liquid interfaces between asperities may be useful antifouling surfaces[83].

Alongside influencing some of the physiochemical properties of surfaces on a nano/micro scale, topography may also influence bacterial attachment by altering the near surface microfluidic environment, which influences the hydrodynamic forces experienced by bacteria during surface attachment[84,85]. So far however, no study has been performed to elucidate the mechanisms of the effect of topography on local hydrodynamics, despite this being relevant to the formation of biofilms within high flow conditions. At present, it is thought that at the troughs between asperities provide a form of refuge for bacteria in flow conditions where it is thought that shear stress is especially high at the peaks of the asperities[85] (figure 3c, 3).

Another point to make is that bacterial cells may attach to surfaces that normally resist attachment due to the deposition of material onto them. Normally this deposition layer will contain small molecules, ions and proteins that are naturally found in the bulk liquid/media that settle onto the surface and alter its physiochemical properties. Additionally bacteria may secrete their own proteins to effectively condition the surface for bacterial attachment[27,4] and potentially leading to specific receptor based adhesion. Bakker et. al studied the effect of seawater conditioning on polyurethane surfaces and found that final water contact angles were similar for hydrophobic and hydrophilic polyurethanes surfaces after conditioning for 1h[86]. In addition to this, surface conditioning may alter the topological properties with Bakker et al. finding that the mean surface roughness of polyurethanes was increased by 4 nm after 1h exposure to the seawater and it is thought that this is due to protein aggregates in the conditioning layer. Usually the size of these aggregates is on the nanoscale meaning that surface topographies with originally nanoscale asperities may become smoother due to the aggregates filling themselves within the surface troughs/valleys[87] which may then reduce bacterial attachment in the absence of these

valleys where LW attractive interactions with bacteria is possible (figure 3d, 3). Surfaces with macroscale asperities may be less prone to this[68] (figure 3d, 2). Finally, surface topography may also alter chemical gradients at the liquid surface interface, which affects bacterial surface sensing and chemotaxis. As a result, chemical concentration dependant biofilm related signal transduction pathways may be altered resulting in differing levels of cell adhesion (figure 3e). For example, upon bacterial attachment to smooth surfaces, deposited chemicals may find themselves trapped between the solid surface and the bacterium, meaning a high local chemical concentration (figure 3e, 1 and 3). In the presence of closely packed asperities, the chemicals are able to escape from this due to pores between the bacteria and surface, meaning a low local concentration gradient (figure 3e, 2).

(c) Surface chemical modifications to modulate bacterial attachment

One of the main ways to modulate bacterial attachment to a surface is by controlling the surface chemistry as this will also change the physiochemical interactions upon bacterial approach which prove to be most important for initial bacterial attachment. Biofouling is a problem for a wide range of materials used in many different areas from the medical and food industries to textiles and water purification systems[60]. As such much research has been aimed at functionalising surfaces with chemical moieties that resist bacterial attachment. Figure 4 shows all the chemical structures of the anti-fouling surface coatings that will be discussed in this section. One very commonly used anti-fouling surface coating is poly(ethylene glycol) (PEG); one study described how hydrophilic PEG is able to resist the attachment of bacteria when PEG was grafted onto a hydrophobic substrate. As bacterial proteins approach the PEG chains, they compress leading to repulsive elastic forces. Additionally, as they approach the hydrated PEG layer, water molecules become displaced

which leads to a thermodynamically unfavourable osmotic penalty[88,60]. Despite the widespread use of PEG as protein resistant surfaces, their long term stability is questionable however as they are susceptible to oxidation damage[89]. This lead to the development of other protein resistant coatings, in the form of self-assembled monolayers (SAMs)[90] on surfaces. These SAMs usually consist of alkanethiols containing ethylene groups and present similar properties to PEG coatings[90,60]. In more recent years other types of SAMs such as those of hydrophilic peptides[91] and oxidatively stable dendritic polyglycerol[92] have also shown antifouling effects.

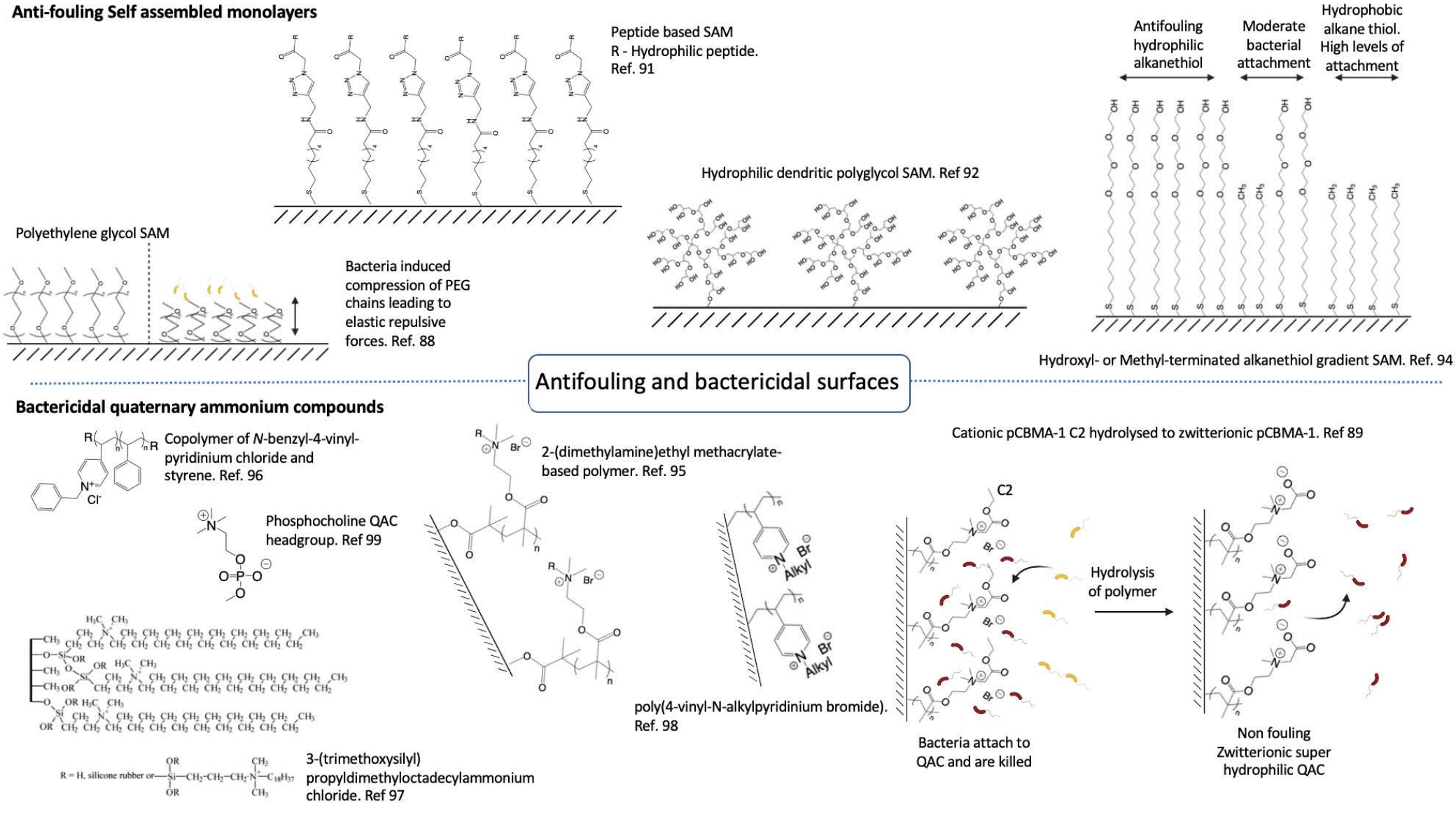

Figure 4: Chemical structures of antifouling and bactericidal polymer surface coatings

The real advantage of SAMs is that they have been widely studied, characterised in detail and can be prepared reproducibly[93], hence their coatings may allow for genuine control of surface energy/charge density and subsequent attachment and as such, SAMs have often been used a model system for studying bacterial attachment/biofilm formation on surfaces[4]. For example Burton et al. showed that SAMs consisting of a tri(ethylene glycol)-terminated alkanethiol were resistant to bacterial attachment (in a similar way to PEG), however upon introducing a more hydrophobic methyl-terminated alkanethiol to displace some of the original tri(ethylene glycol) terminated alkanethiol (forming a spacio-chemical gradient), bacterial attachment and subsequent biofilm formation was significantly increased in the region where the new hydrophobic alkanethiol SAMs were present[94].

As explained previously, electrostatic interactions between bacteria and surfaces are amongst the earliest and occur within seconds. Most bacteria have a net negative charge as determined by zeta potential measurements[66,67] meaning they will bind to positively charged surfaces. If a surface is highly positively charged, it may reduce bacterial viability through membrane disruption[95] and as such, much early research into the cell-surface adhesion and antimicrobial effect on bacteria involved the use of positively charged surface coatings; one such type are cationic quaternary ammonium compounds (QACs). For example, a cloth coated with a copolymer of *N*-benzyl-4-vinyl-pyridinium chloride and styrene (figure 4), and used as a filter for removing bacteria from water was shown to be 99.99% effective at filtering off a flow of *E.coli*[96]. Silicone rubber was covalently coupled to 3-(trimethoxysilyl) propyldimethyloctadecylammonium chloride, and this was shown to bind to and reduce the viability of gram-positive bacteria from 90% to 0% and the viability of gram negative bacteria from 90%-25%[97]. 2-(dimethylamine)ethyl methacrylate, which was

directly polymerised onto either filter paper or glass showed similar activity toward both *B.subtilis* and *E.coli*[95]. Tiller and Klibanov coated glass slides with poly(4-vinyl-N-alkylpyridinium bromide) which showed strong antifouling effects against gram positive *Staphylococcus aureus* and *Staphylococcus epidermidis* and gram negative *P.aeruginosa* and *E.coli*. Interestingly, the effectiveness of the QAC varied with alkyl chain length attached to the cationic quaternary nitrogen. If the chain length was too high, the chains would interact via hydrophobic interactions leading to physical screening of the positively charged nitrogen, and a reduction in antifouling[98].

One of the problems however with using QACs as antimicrobials is that once bacteria have adhered to the positively charged groups and been killed, they remain attached to the surface which eventually reduces its biocidal effect due to the relevant cationic groups being blocked off by dead cells[89]. Antiadhesive zwitterionic coatings are defined by the fact that they contain both cationic and anionic groups and one of the first classes were based on phosphorylcholine (PC)[99], designed due to its phospholipid-like structure which allowed for biocompatibility in the coatings of medical implants that need to be in the body for long periods[99]. One reason why it is thought that bacteria do not adhere to these zwitterionic PCs is due to their high polarity and consequent superhydrophilicity[100]. Usually bacteria are of low surface energy, and in aqueous solution will tend to bind to low energy surfaces too i.e. hydrophobic surfaces[27,101] hence the 'super' hydrophilicity of zwitterionic coatings make them useful antifouling materials. Studies have now combined the anti-microbial effects of positively charged adhesive coatings with the cell repelling zwitterionic coatings. One such study by Cheng et al. showed that poly(N,N-dimethyl-N-(ethoxycarbonylmethyl)-N-[2'-(methacryloyloxy)ethyl]ammonium bromide) (cationic pCBMA-1 C2) could be used as the initial cationic adhesive coating onto which bacteria bind to, and due to its highly positively

charged nature will kill 99.99%. Upon hydrolysis of the coating in situ, the pCBMA-1 C2 is converted to the anti-fouling zwitterionic pCBMA-1 which then releases up to 98% of the dead cells[89]. A similar study was also performed using a biocidal cationic morpholinone coating which could be hydrolysed to a cell releasing zwitterionic carboxy betaine[102]

(iv) Synthetic polymers for interacting and aggregating bacteria

So far, the discussion of bacterial-surface interactions has focused primarily on interactions with solid surfaces. Given that the most widely used theory in modelling bacterial-surface interactions (e.g. XDLVO) are based on approaching colloids, most of the information described in previous sections is applicable for bacteria interacting with polymeric substances in solution/suspension. As the main focus of this project is to use linear synthetic polymers to aggregate bacteria and stimulate/enhance biofilm formation, a discussion on the recent advances in suspended polymer-bacteria interactions is necessary.

In general, polymers can interact and aggregate particles/bacteria by three main mechanisms; bridging[103], charge neutralisation[104] and depletion aggregation[105] (figure 5). Bridging occurs when long multivalent polymers are able to simultaneously adsorb onto multiple particles, attaching them together. Charge neutralisation is one of the first stages in the flocculation/aggregation of particles by poly(electrolytes) and can be applied to bacteria-polymer suspensions too. When short chain cationic polymers are added to negatively charged bacteria, they adsorb onto the cell surface effectively screening the repulsive interactions between bacteria. This introduction of opposite charges allows for aggregates to form in the sub-micron range. When a longer polymer is added, larger aggregates may form from bridging of the smaller aggregates[104] (figure 5d).

Conversely, depletion aggregation occurs in environments where high concentrations of non-adsorbing polymers are present. In these conditions, when the polymers get too close to the particles/bacteria or become wedged in between particles/bacteria, their movement becomes constrained. As the number of polymeric chains is usually higher than that of the particles/bacteria, it is entropically favourable for the polymers to dissociate themselves from the particles. As the polymers move away, spontaneous motion will result in the particles/bacteria 'filling in the gap' and aligning themselves with one another (figure 5c). The more ordered and closely packed the particles become, the more the polymers are able to move out of the aggregates and into the bulk, increasing the entropy of the system. In addition to this, the resulting sharp gradient in polymer concentration between the aggregated particles and the bulk liquid establishes an unbalanced osmotic force that further hold the particle aggregates in place[105,106]. The following sections will discuss polymer bacteria interactions that result mainly from the bridging mechanism, however examples of charge neutralisation processes and depletion aggregation will be specifically mentioned too.

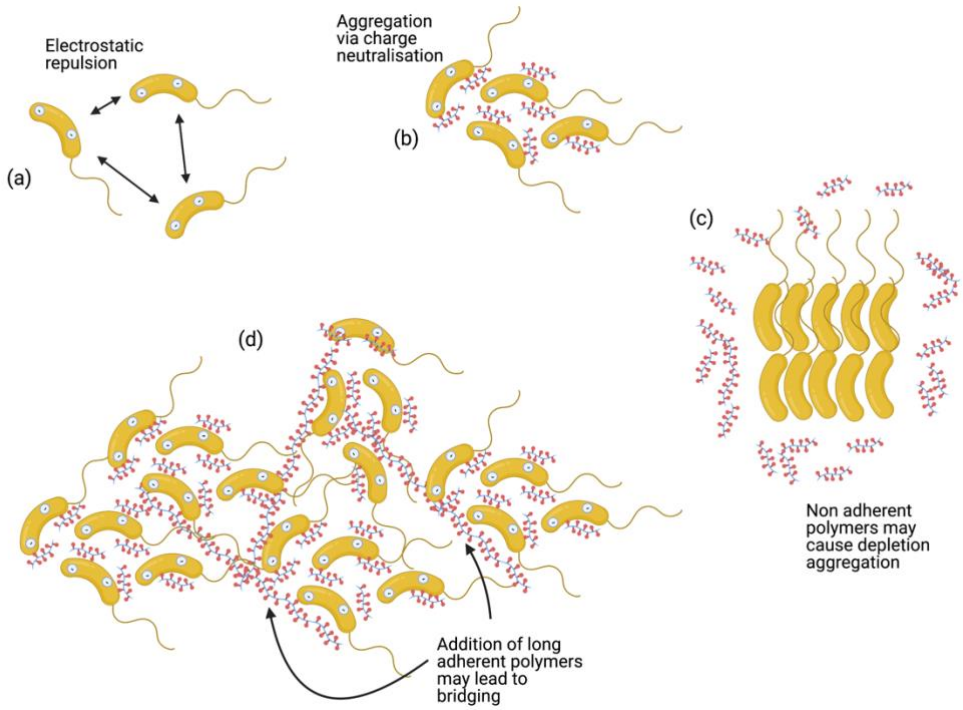

Figure 5: Mechanisms of polymer induced bacterial aggregation, created with BioRender.com. (a) electrostatic repulsion of negatively charged cells, (b) Charge neutralisation (with short polymers) can overcome electrostatic repulsion (c) interaction via depletion aggregation and (d) bridging interactions involving longer chain polymers

(a) Mechanisms of bacterial aggregation/flocculation with poly(electrolytes) – Chitosan

The adsorption of polyelectrolytes onto particles leading to their stabilisation (dispersion) or destabilisation (flocculation/aggregation) is essential in many industrial processes such as waste water treatment, paper making and food processing[103]. Usually these polyelectrolytes are positively charged in order to interact with negatively charged particles in suspension. For the case of weak polyelectrolytes (low charge density), their adsorption onto particles depends strongly on the ionic strength and pH of the bulk liquid. At low pHs with all charges present, polymer chains will electrostatically adsorb onto the particles forming a thin surrounding layer and effectively preventing further polyelectrolyte adsorption. As the polymers are of low charge density, increasing pH and/or increasing ionic strength may lead to more polymer adsorbing each particle (where electrostatic repulsion between polymer chains is effectively shielded by ions) leading to multiple layers. The polymers in the

outermost layers will tend to be weakly bound creating 'loops and tail' configurations, and if long enough, may allow for potential bridging with other flocs and consequent aggregation. For strong polyelectrolytes, a thin flat layer will adsorb onto the particles, however due to their large charge density may not completely surround each particle (due to polymer chain electrostatic repulsions) allowing for aggregation by charge neutralisation[103]. Most of this information has been gained from model dispersions using mineral particles and copolymers of acrylamide and cationic monomers[103]. Recently there is growing interest in using naturally occurring polymers for the stabilisation/flocculation of such particles, one such being chitosan. Chitosan refers to a family of linear polymers that are composed of two main monomers; 2-acetamido-2-deoxy- β-D-glucopyranose (GlcNAc) and 2-amino-2-deoxy-β -D-glucopyranose (GlcN) (for the chemical structure, please see figure 9 page 43). The composition is usually described by the molar fraction of acylated units (GlcNAc, denoted by F_A), which also adds a degree of hydrophobicity. However, in general it has been found that chitosans of higher charge density (lower F_A) induce more particle flocculation[107,108]. One of the first comprehensive studies on the flocculation/aggregation of bacteria (*E. coli*) by chitosans was performed by Strand et al. who showed that conversely, flocculation was actually increased with an increasing ratio of acylated units (and lower charge density), suggesting the presence of hydrophobic aggregating interactions. Surprisingly despite chitosan being a weak polyelectrolyte, it was found that pH had little effect on overall bacterial flocculation[108] between pH 4-6.8 despite the prevalence of protonatable groups in chitosan. Under basic conditions however where cationic charges may be removed, lower levels of flocculation were observed. Investigation of the effect of ionic strength on flocculation pointed towards a bridging mechanism. Chitosans of low F_A (high charge density) induced small amounts of clustering via charge neutralisation, however upon the

increasing levels of ionic strength more aggregation was observed, presumably due to a thicker polymer coating leading to bridging between flocs. Lower charge density chitosans (high F_A) on the other hand showed greater levels of flocculation even with very low amounts of chitosan suggesting that these chitosans were bound weakly in a 'loop and tail' configurations allowing for bridging and consequent aggregation at lower chitosan concentrations. Increasing ionic strength again increased the level of flocculation, but this time only to a certain point after which the bacteria become stabilised (dispersed). A reason for this may be that upon adsorption of more chitosan in high ionic strength media, the layer around each bacteria becomes larger and larger, reducing the likelihood of bridging between cells. The molecular weight of chitosans also had an effect with larger chitosans inducing larger amounts of flocculation, again pointing toward a bridging flocculation mechanism. Furthermore, by measuring zeta potentials of cells after the addition of increasing levels of chitosan, bridging was confirmed as aggregation always occurred at polymer concentrations that preceded the charge neutralisation point[103].

(b) Non-toxic pathogen sequestering polymers

The following sections will discuss some of the recent advances in polymer induced bacterial aggregation, with a focus on how aggregation affects bacterial phenotype, with many involving changes in biofilm expression.

One of the most important classes of antimicrobials are synthetic cationic polymers and in general they are designed with two main components in mind; cationic groups designed to electrostatically bind with the negatively charged bacterial cell wall, and hydrophobic groups which are thought to insert into and disrupt the membrane leading to cell death[109,110]. One of the disadvantages of solid surfaces modified with antimicrobials/antifouling moieties is that they become susceptible to the natural deposition of material (e.g. proteins) onto the surface in physiological conditions which effectively masks the anti-adhesive/antimicrobial layer[27]. Additionally as bacteria are being killed, it may lead to antimicrobial resistance. As with all antimicrobials, the minimum inhibitory concentration (MIC) is key, and interestingly it has been observed that cationic polymers added to bacterial suspensions at sub-inhibitory concentrations actually induce rapid aggregation of bacteria without necessarily having a toxic effect. As such this alternative method was identified as a possible route to anti-adhesion therapy, whereby rather than binding with and infecting a known surface, the bacteria will aggregate around the polymer. Additionally the lack of polymer toxicity minimises evolutionary pressure and as such the chances of antimicrobial resistance[111]. One such example of anti-adhesive polymers was demonstrated by Perez-Soto et. al. (figure 6) where they showed that two separate primary and tertiary displaying cationic methacrylamide polymers were able to

competitively bind to *V. cholerae* and reduce its adhesion with Caco-2 cell lines (*V. cholerae:* an infectious agent that causes the cholera disease by binding to gut epithelia, forming biofilms and releasing toxins). Overall, the tertiary amine bearing polymer showed greater activity, likely due to its higher level of hydrophobicity. Both polymers showed little disruption to the Caco-2 cells at the low concentrations required for bacterial sequestration, lowered *V. cholerae* virulence and interestingly increased biofilm expression levels. *In vivo* studies were also performed and showed that these polymer reduced the accumulation of GFP expressing *V.cholerae* in the intestinal tract of zebrafish[112].

A similar study was conducted by Foster et. al where they showed that the high biofilm forming *Pseudomonas aeruginosa* could be aggregated by a cationic quaternary amine bearing polymer, reducing initial bacterial attachment to a surface[113].

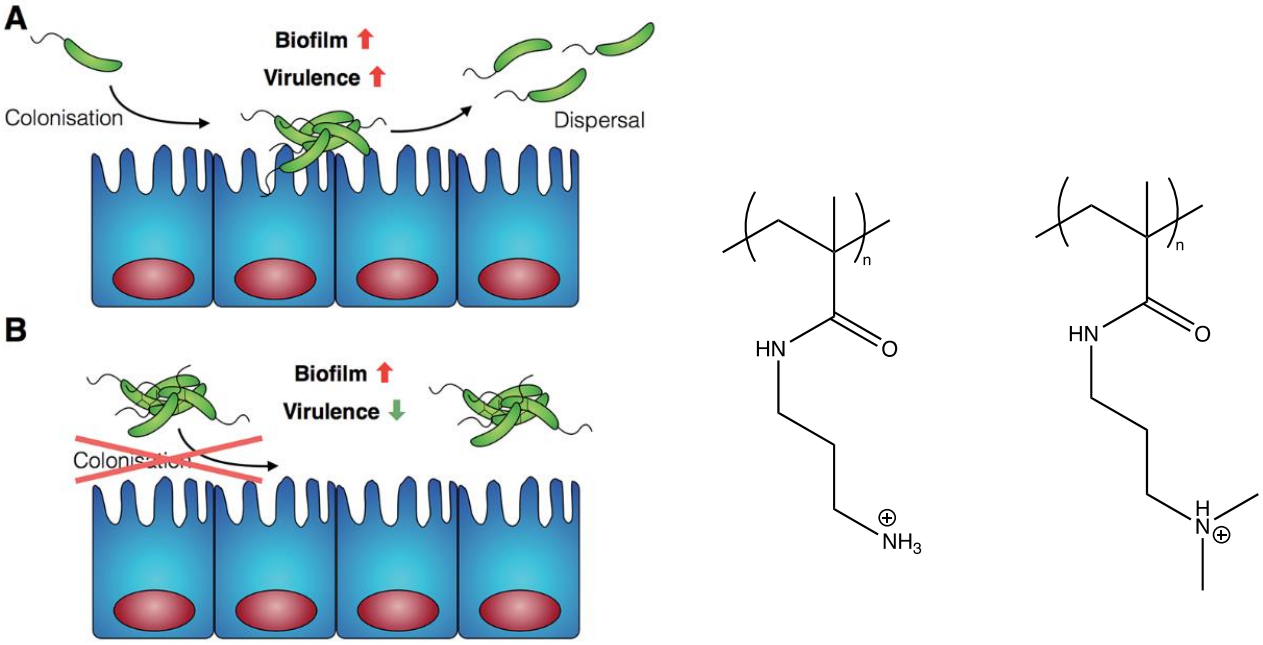

Figure 6: Anti-adhesive, sequestering effect of cationic methacrylamide polymers on V. cholerae, taken from Perez-Soto et. al, ref 112. (A) showing the general mechanism by which V. cholerae infects the gut epithelia. (B) Schematic of the anti-adhesive effect of the aggregating primary (left) and tertiary (right) cationic methyl methacrylamide polymers. Bacteria is sequestered around the polymers rather that adhering to and colonising the gut.

(c) Polymers for the aggregation and detection of bacteria

Synthetic polymers – Non-specific interactions

As mentioned, one of the ways to prevent bacteria attaching to a solid surface is to add an adhesive polymer which sequesters the bacteria, preventing surface fouling/biofilm formation. However, preventing surface adhesion/biofilm is only one of the many potential applications of this technique; polymer mediated aggregation of bacteria could be useful in bioremediation, downstream processing and could also be incorporated into cleaning materials used in clinical, industrial or even domestic settings[114,103]. Another very interesting application could be in the rapid isolation and selective detection of pathogens, and unsurprisingly much research has been performed in this area. Pernagallo et. al used a polymer microarray assay to identify materials which could selectively bind to and aggregate the foodborne pathogen *Salmonella enterica* serovar *Typhimurium* (*S. typhimurium*), and *E. coli*. Two polymer classes were used in the study; 22 poly(acrylates) PAs, and 14 poly(urethanes) PUs. Each of the polymers were of slightly different composition, for example the PAs contained varying amounts of acrylate and imidazolium groups and the PUs varied with diol composition. Bacterial binding to polymers was detected by GFP expression, and it was revealed that bacterial binding onto polymers was highly dependent on polymer composition. PAs would bind strongly to both strains given a sufficient ratio of hydrophobic imidazolium in the polymer. PUs in general stimulated strong binding in both strains however a few selected PAs showed selective binding toward the pathogenic *S. typhimurium* over *E. coli*[114]. A study by Yuan et. al showed that a single quaternary ammonium cationic polymer could selectively bind to either fungi (*C. albicans*), Gram positive (*B. subtilis*) or Gram negative bacteria (*E. coli*) respectively by simply varying the ionic strength of the culture. To explain this, isothermal titration microcalorimetry (ITC)

was employed to investigate the thermodynamic changes of the bacterial system upon addition of the polymer to cultures of different ionic strengths. The enthalpies of polymer interaction changed significantly with ionic strength for *C. albicans* and *E. coli* demonstrating that electrostatics dominated this interaction (an increase in ionic strength will reduce electrostatic interaction as the ions in solution screen the polymer charge), while for *B. subtilis*, hydrophobic interactions dominated. By combining the distribution coefficients, K of the different interactions and performing confocal microscopy to visualise the polymer induced aggregates it was found that at low ionic strength (5 mM), strong and selective electrostatic interactions between the polymer and *C. albicans* dominated. At higher ionic strengths (around 20 mM), interactions between polymer and *E. coli* dominated whist at very high ionic strengths (less electrostatics between polymer and cells) the polymer selectively bound *B. subtilis* via hydrophobic interactions. In addition to this, the detection of cells in a mixed culture was also realised. Each species binds to the polymer with a given distribution coefficient. On binding, the polymer is able to fluoresce with an intensity which is directly linked to the strength of the polymer bacteria interaction, hence the fluorescent intensities (normalised for cell culture density) of differently mixed cultures also will vary and can be compared to a standard graph of all polymer induced fluorescent intensities of known mixed species[115]. One of the more recent dynamic approaches to bacterial detection involves the direct polymerisation of monomers on the surface of bacteria, leading to the production of 'templated' polymers with high affinity to the specific bacterial species that 'instructed' their synthesis on its surface. In other words the polymers produced are self-selective binding agents for the 'instructing' cell types. Work by Magennis et. al showed how this was possible by harnessing the reducing properties of bacteria to convert Co(II) into Co(I), thereby providing an reducing environment for the atom transfer radical

polymerisation (ATRP catalysed by Co(I)) of two separate monomers directly onto the cell surface. The two monomers consisted of a cationic quaternary amine and a sulfobetaine acrylate; the cation to increase binding onto the negatively charged cell wall and a hydrophilic acrylate to increase solubility. *E. coli* and *P. aeruginosa* were chosen as the instructing bacteria and monomers were added respectively to both strains with ATRP polymerisation occurring within 5 minutes. The authors noted that monomers that were bound at the surface of the bacteria would polymerise first to generate templated polymers with high affinity for that particular bacterial strain. Additionally due to the highly reductive environment, polymerisation would also occur away from the bacteria – these polymers however would not be templated by the bacteria and so would have low affinity for it. Both types of polymer were isolated and purified and it was found that upon its addition to a culture, polymer induced clustering would only occur in samples where the correct templated polymer was added to its instructing bacteria. Untemplated polymers and polymers made in the absence of bacteria showed little or no aggregating capabilities. This technique therefore defines a new platform for making novel polymeric materials for detection that can be adapted for a range of cell types[116].

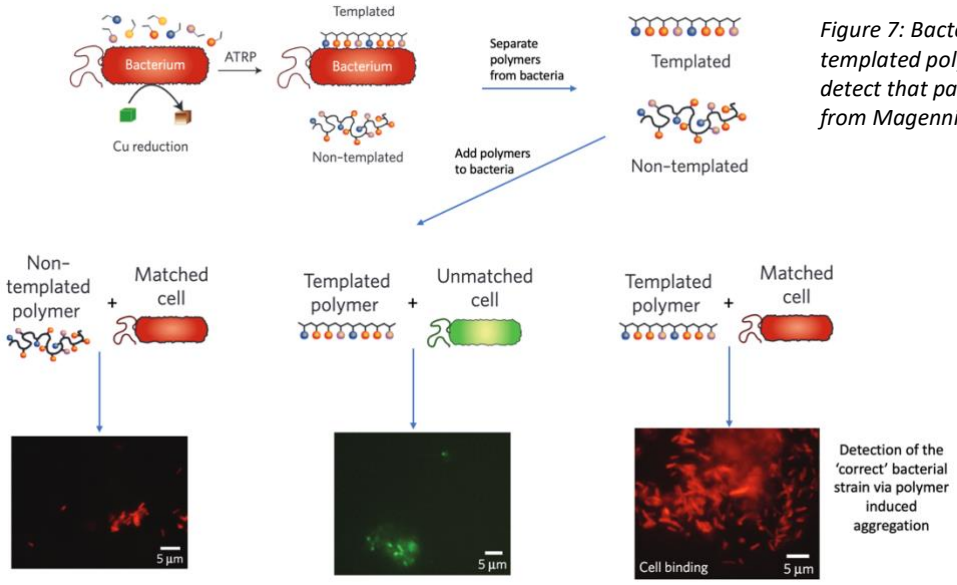

Figure 7: Bacteria instructed synthesis of templated polymer, which can then be used to detect that particular strain of bacteria, taken from Magennis et. al, ref 116

Carbohydrate functionalised polymers – Specific receptor based interactions

Another type of polymer that has been used to selectively bind to and/or detect bacteria are polymers that have carbohydrate functional groups. In many cases bacteria bind to carbohydrates on the surface they infect, these receptor-specific type of interactions usually occur in the irreversible stage of surface attachment and as such, examples of designing carbohydrate bearing polymers to bind to and detect bacteria can be found throughout the literature. One of the first examples was shown by Disney et. al who demonstrated that *E. coli* bearing the mannose specific receptor FimH was able to bind to a carbohydrate functionalised fluorescent polymer leading to aggregates of high fluorescence. When the same experiment was performed on a mutant FimH strain, no aggregation or fluorescence could be observed[117]. A very similar study was also performed by Xue et. al, this time with a very soluble, hydrophilic poly(ethylene glycol) polymer bearing mannose groups where again polymer induced aggregation was found for *E.coli* bearing FimH but not for the mutant FimH strain[118]. This study goes to show how polymers that usually repel bacteria when coated onto solid surfaces (e.g. PEG) can have a completely different effect when added to a suspension of bacteria in non-lethal doses. Phillips et. al described how this detection method could be optimised by increasing polymer sensitivity toward the sugar binding domains of bacteria. Interestingly they showed that placing the repeating carbohydrate substituents (mannose in this case) further away from the backbone (by increasing the size of the polymer linker group) lead to increased binding and aggregation of *E. coli*. Making the carbohydrate substituents more complex (i.e. having three bearing mannose groups instead of one) also had a greater aggregating effect[119].

Another interesting, different type of study by Wang et. al showed how fluorescent, mannose bearing oligomers that are attached to a graphene oxide (GO) surface could be used to detect FimH bearing *E. coli*. GO is able to quench fluorescence very efficiently via fluorescence resonance energy transfer (FRET) and so there will be little fluorescence given off by the oligomers when bound to GO. Upon the binding of bacteria to the oligomers, the contact of the graphene and oligomers becomes effectively shielded preventing the FRET. Therefore the oligomers will be able to fluoresce without GO quenching in the presence of mannose binding *E. coli*[120] (figure 8).

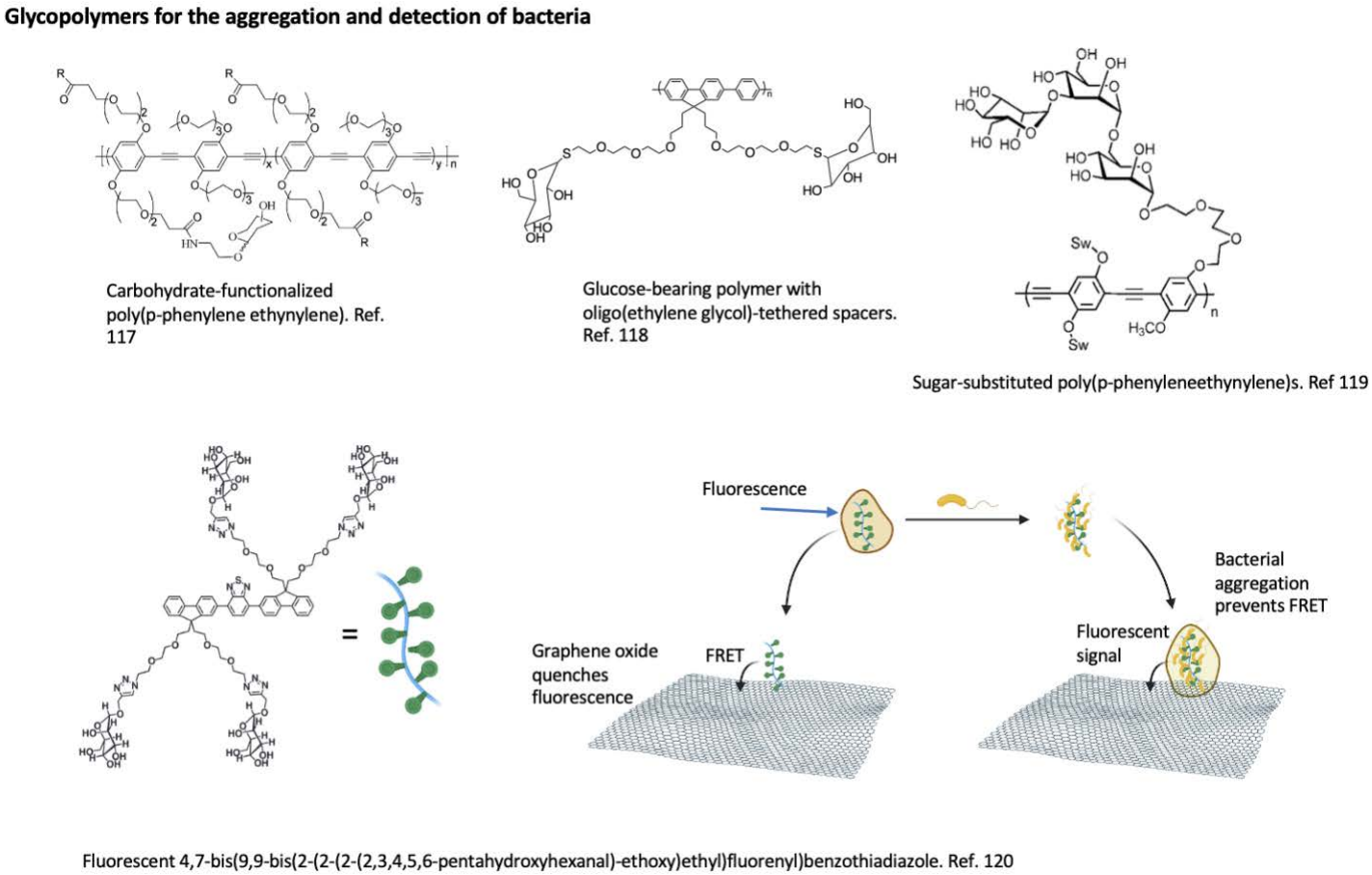

Figure 8: Chemical structures of bacteria aggregating glycopolymers for the detection of bacteria as described in the text. Glycopolymers show ability to bind to mannose specific FimH bacterial envelope receptors and hence can aggregate FimH expressing species .

(d) Polymers for the modulation of quorum sensing

The first stage of the biofilm lifecycle is the attachment of bacteria to a surface, whether that may be to a solid surface or to polymers added to a culture. This brings bacteria together in a high cell density aggregated form, leading to high local concentrations of excreted signalling molecules known as autoinducers (AIs), effectively informing the bacteria to transition to a sessile/cooperative biofilm lifestyle and may also directly impact on other behaviours such as virulence and antibiotic resistance. This type of cell-cell communication known as quorum sensing (QS) can be defined as is the regulation of gene expression in response to fluctuations in cell-population density[121]. As such many studies on the impact of polymer mediated bacterial aggregation on QS and resulting cell behaviour (transition to biofilm mode) can be found. The polymer structures described in this section can be found in figure 9. A study by Xue et. al took advantage of this link between cell aggregation and QS to produce polymers that would be able to simultaneously aggregate *V. harveyi* (hence providing an anti-adhesive sequestering effect) and reduce quorum sensing through hijacking the AI-2 QS network. A key compounds in the AI-2 mediated QS pathway is 4,5-dihydroxy-2,3-pentanedione (DPD) which only becomes activated upon reaction with boric acid to give the active furanosyl borate ester. Therefore a polymer was designed to simultaneously aggregate bacteria and sequester borate to prevent activation of DPD leading to the hijacking of the AI-2 QS network. Dopamine has known affinity for borate and as such an *N*-dopamine meth-acrylamide monomer was copolymerised with a water soluble, bacteria binding cationic methacrylamide. Indeed the dual activity of the polymer was confirmed with it both aggregating *V. harveyi* and reducing its QS signal as measured by *V. harveyi* QS modulated luminescence[122]. Similarly, Piletska et. al computationally designed a set of polymers targeted to reduce *V. fischeri* QS, this time without necessarily interacting

with the cells. The QS signal molecule N-(β-ketocaproyl)-L-homoserine lactone (3-oxo-C6-AHL) was targeted by the set of polymers which resulted in its sequestration when mixed with a *V. fischeri* culture, leading to a reduction in QS as given again by QS modulated *V. fischeri* luminescence[123]. Conversely, another study by Zhang et al. showed how *E. coli* aggregated by a polymer bearing dendronized cationic amine groups was able to produce the autoinducer AI-2 for longer periods than that without the addition of polymer. The authors also showed how this leads directly to an increase in overall biofilm production and a decreased susceptibility to antibiotics (ampicillin)[124], a trait often shown by infectious biofilms.

Unlike most strains of bacteria where an increase in quorum sensing leads to an upregulation of biofilm gene expression, the production of autoinducers actually represses biofilm genes in *V. cholerae* leading to dissipation of bacteria back to the environment. Previous work by Perez et al. (described above, section b) showed how cationic methacrylamide polymers were able to aggregate *V. cholerae* and actually increase biofilm levels contrary to how one would expect given the assumed high concentration of autoinducers within *V. cholerae* aggregates[112]. The group therefore decided to investigate the mechanistic basis of this behaviour and indeed found that quorum sensing was significantly increased within polymer induced *V. cholera* clusters due to rapid secretion and high local concentration of autoinducers, mainly CAI-1. However, it was found that the polymers also increased the expression of the biofilm regulator VpsR and the biofilm structural protein RbmA, bypassing the usual suppression of biofilm levels in the presence of high concentrations of autoinducers[125]. Normally, *V. cholerae* in biofilm form are highly virulent, however as previously found virulence decreased for these polymer induced aggregates/biofilms[112]. This is an excellent example of how polymers may be used to

mediate biofilm formation whilst providing interesting and unexpected behavioural changes.

So far all the studies outlined above describe how the local concentration of QS autoinducer molecules increase sharply within the confines of aggregated bacteria, more specifically polymer induced bacterial aggregates. A study by Qin et al. however describes how quorum sensing is actually reduced within non-toxic cationic chitosan induced *E. coli* aggregates. Firstly, *E. coli* was transformed with a GFP reporter plasmid which could act as a biosensor for the detection of a quorum sensing homoserine lactone autoinducer, 3OC6HSL. The strain could not however produce its own autoinducer, hence 3OC6HSL was added directly to the chitosan/*E.coli* mixture. The effect of the added chitosan on the bacteria interacting with the autoinducer and expressing GFP was then measured. Firstly however, bacteria aggregation was highly dependent on chitosan concentration with too low (<4 ug/ml) or too high (>12 ug/ml) concentrations not inducing any aggregates for *E. coli* at OD 0.7. The authors reasoned that the addition of too much chitosan would lead to excess amounts being adsorbed onto the bacterial surface leading to an excess of positive charge, thereby preventing aggregation via electrostatics. Between these concentrations however, bacterial aggregates were formed and at these concentrations quorum sensing was surprisingly severely reduced as determined by GFP expression. The authors reasoned that these chitosan induced aggregates actually shielded the entrapped bacteria from the external added autoinducer[126]. This study highlights how quorum sensing can be reduced with aggregating bacteria that do not make their own autoinducers whilst on the contrary, for bacteria that do secrete their own autoinducers, local concentrations of these within aggregates can be very high.

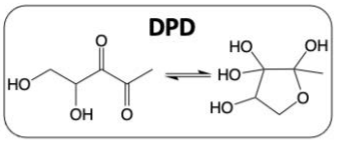

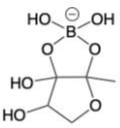

Activated DPD (component in AI-2 pathway)

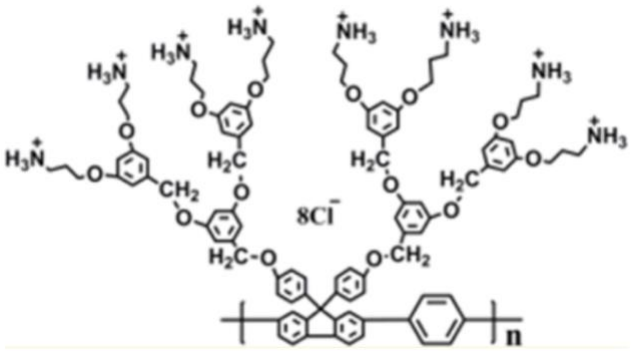

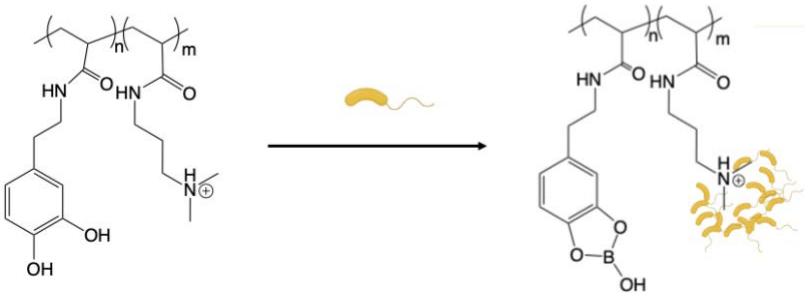

- Dendronized polymer (PFP-G2) bearing cationic amine groups
  - Polymer induces *E. coli* aggregation
- Resulting in prolonged generation of AI-2 and higher biofilm levels
  - Ref 124

- Copolymer with N-dopamine methacrylamide and N-[3-(dimethylamino)propyl]methacrylamide units.
  - Polymer induces *E. coli* aggregation
    - Reduces quorum sensing
- Excellent properties for anti-adhesive bacterial sequestering polymers
  - Ref 122

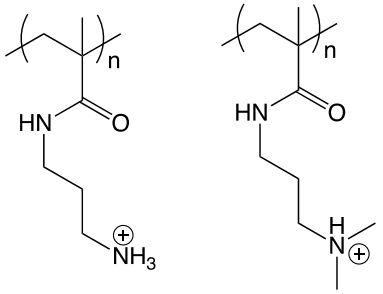

- Cationic methacrylamide polymers
- Polymers stimulate *V. cholerae* aggregation
  - Resulting in increased QS
- Causes induction of biofilm specific regulator VspR and the biofilm structural protein RbmA
  - Ref 125

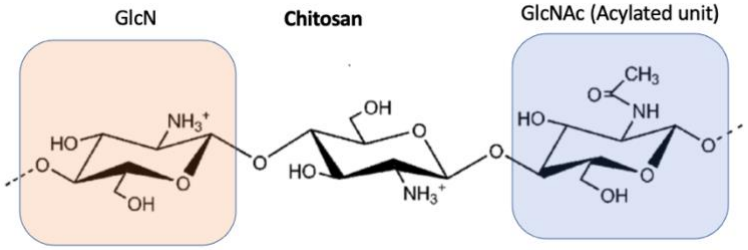

- Chitosan aggregates *E. coli* but shields away externally added autoinducers
  - Reduces QS
  - Ref 126

Figure 9: Polymers described in this section that are able to modulate QS through polymer mediated bacterial aggregation

(v) Applications of functional bacterial biofilms in the biotechnology industry

Bacteria within biofilms are known for their resistant characteristics toward environmental and chemical stresses. Biofilms may possess resilience to toxic molecules (such as antibiotics), organic solvents, and changes in conditions such as pH, temperature, salt concentration and water content, all of which are normally known be detrimental to the metabolic state of planktonic bacteria[127,7]. As such the formation of biofilms has been seen as a constant source of detrimental and persistent contamination onto surfaces, leading to surface biofouling and/or persistent infections upon invasion of a host organism. These same resilient properties of biofilms can however be exploited in the field of biotechnology where the metabolic activity of biofilms is exploited for industrial purposes in conditions that are normally detrimental to planktonic cells. As such biofilms have been used in a wide range of industrial processes including environmental remediation (e.g. wastewater treatment, air filters and soil remediation), biocatalysis and have recently also found applications in microbial fuel cells[128,129]. This section will therefore describe some of the recent advances in these 'functional biofilms' whilst also describing some of the techniques used in optimising biofilm performance either through genetic control of biofilm formation or through the design of templated surfaces which act to modulate the spatial distribution of cells within the engineered biofilm.

(a) Biofilms for bioremediation processes

Some bacterial communities are able to metabolize organic pollutants and oxidise heavy metal contaminants in their natural state in the environment, however their low abundance in these conditions, along with lack of nutrients to allow for sufficient metabolic activity, prevent these naturally occurring processes from removing enough toxins from the environment at a sufficient rate[130]. Bacteria cultured specifically for the remediation of toxic materials are also are less likely to survive in these conditions due lack of protection in the planktonic state. In addition to their low activity, there is also the low bioavailability of pollutants which tend not to be in the aqueous phase and these factors therefore lead to insignificant remediation levels by planktonic bacteria[130,131]. By contrast bacteria within biofilms grow within a protective matrix which provides structural integrity and physical protection from toxic compounds. Biofilms are also genetically diverse and can often be composed of multiple species of aerobic and anaerobic bacteria that may possess different useful metabolic bioremediating pathways that complement each other and allow for survival in a range of different conditions and for the removal of multiple types of pollutants its environment[131].

Bioremediation of persistent organic pollutants (POPs)

Organic compounds represent some of the most widespread environmental pollutants found in air, water and sediments produced as by-products of industrial processes[132]. These include polycyclic aromatic hydrocarbons (PAHs), polychlorinated ethenes (PCEs), polychlorinated dibenzo-*p*-dioxins and difurans (PCDD/Fs) and polychlorinated byphenyls (PCBs), xenobiotic compounds such as pharmaceutical and personal care products (PPCPs)

as well as other organic pollutants such as fertilizers, pesticides and herbicides found in wastewater[130,133].

Polycyclic hydrocarbons (PAHs)

PAHs are consumed by organisms found in wastewater and can make their way up the food chain with potential carcinogenic effects. *Sphingomonas* (a type of gram negative, aerobic bacteria) and mycobacteria are known to degrade PAHs[134] however one of the main limitations is their limited bioavailability due to the fact PAHs are solubilised the form of crystals in the non-aqueous phase[135,136]. To mitigate this, bacteria may produce biosurfactants to increase PAH water solubility[137] however this is still in dispute[138]. Johnsen et. al found that solubilisation of PAHs was primarily driven by the formation of *Sphingomonas* biofilms. They isolated three separate polysaccharides excreted by *Sphingomonas* biofilms and found that these EPS components dramatically increased the solubilisation of PAHs. Conversely, planktonic cells did not increase solubility, confirming that the solubilisation of PAHs through did not occur through the bacterial excretion of surfactants in this strain. *Sphingomonas* biofilm formation was therefore responsible for the increased solubility and mass transfer of PAHs into bacteria for biotransformation.

Polychlorinated ethenes (PCEs)

Chlorinated ethenes are a predominant source of contamination in drinking water. So far, only one known group of bacteria known as *Dehalococcoides* are able to degrade chlorinated ethenes via reductive chlorination[139]. Work by Chung et. al showed that biofilms formed by *Dehalococcoides* inside a denitrifying membrane biofilm reactor could reductively

dechlorinate trichloroethenes, and that the biofilm was actually enriched by this normally toxic source of food[140].

Polychlorinated biphenyls (PCBs) and dioxins

Despite the fact that PCBs and dioxins were banned over thirty years ago, they can still be found as pollutants in soil, sediment and even in the air[132]. A group of anaerobic microorganisms known as dechlorinating *Chloroflexi* are known to reductively dechlorinate highly chlorinated PCB congeners into less chlorinated structures that can then be degraded by other anaerobic bacteria[141]. Macedo et al. formed biofilms that originated from bacteria found in soil contaminated with polychlorinated biphenyls. The biofilms were grown onto a substrate containing PCB oil, and the mature biofilm was shown to invade the oil droplets resulting in PCB degradation. The dominant strains of bacteria within the biofilm were *Herbaspirillum* and *Bradyrhizobium*[142].

Pharmaceutical and personal care products (PPCPs)

Xenobiotic chemicals such as PPCPs can also be found also be found as pollutants in water streams. One particular compound of concern is triclosan, an antibacterial and antifungal agent which is photo-transformed into dioxins. Therefore due to the antibacterial nature of triclosan, dioxin degrading bacteria are killed leading to the additional replenishment of dioxin in wastewater. Hence biofilms, which are less susceptible to antibiotics need to be used for the remediation of triclosan. A study by Bower et al. described how mixed species biofilms (initially inoculated from wastewater sludge containing triclosan's) grown onto sand columns were able to degrade 10 out of 14 PPCPs tested; these included biphenylol, *p*-chloro-*m*-cresol, chlorophene, 5-fluorouracil, gemfibrozil, ibuprofen,

ketoprofen, naproxen, triclosan, and valproic acid[143].

Bioremediation of heavy metal pollutants

Heavy metals have been a source of pollution ever since the onset of the industrial revolution. The main form of metal remediation involves dredging up contaminated sediments and debris followed by expensive ex-situ treatment to remove contaminants[144]. These processes are not only very expensive, but also cause the wholesale disruption of the immediate environment and its ecosystem[145]. Remediation by biological systems therefore provide a cheaper, more environmentally friendly method of removing metal pollutants. In the natural environment, metals are usually found in their mineral form so it is assumed that bacteria can interact with them and use them as metabolites. A study by Costley et al. described how biofilms were able to remove metals from water containing cadmium, copper and zinc. Mixed species bacteria were inoculated from activated sludge found in sewage water and grown as a biofilm on a rotating biological contactor (RBC). The RBC was submerged into the metal contaminated water for a period of 24h (one absorption cycle) after which the biofilm was treated with an acid wash to remove the absorbed metals. The washed biofilm was then placed back into the contaminated water and the cycle was repeated. Interestingly, the absorption efficiency of the biofilms did not deteriorate as shown by the equally high levels of biofilm mediated metal removal even after three acid wash cycles. Hence this process is only possible in biofilms which are highly resistant to changes in external conditions. Furthermore, the use of mixed species biofilms may be more beneficial in biofilm remediation, due to interspecies co-operation allowing for a wider network of metabolic pathways that may further enhance resilience and ability to survive in adverse environments. For example von Canstein et al. showed how mixed species biofilms

within a packed bed reactor were able to remove more mercury from mercury contaminated water when compared with a monospecies biofilm[131]. Diels et al. showed how mixed species biofilms composed of the metal absorbing bacterial strains *Pseudomonas mendocina* AS302 and *Arthrobacter* sp. BP7/26 along with a heavy metal resistant and bioprecipitating *Ralstonia eutropha* CH34 strain, were able to remove the heavy metals found in metal-bearing wastewater (Cd, Zn, Cu, Pb, Hg, Ni and Co) through biosorption onto the biofilm structure which could then be washed away[146]. Another study by Jong et al. showed how biofilms formed from sulphate reducing bacteria (SRB) found in water samples from a wetland filter, were able to remove metals and sulphates from contaminated water. Sulphate reduction occurred after the initial lag phase of the biofilm which led to an increase in pH of the wastewater resulting in the precipitation of metals which were then able to bind to the biofilm and consequently removed from the wastewater. This treatment resulted in removal of 98 % of Zn, Cu, Ni, and 82% and 78 % of Fe and As[146].

(b) Optimising biofilm bioremediation through control over biofilm formation

As explained, biofilm formation is an extremely complex process that is controlled by a vast number of regulatory networks, which continue to be investigated for their effect on biofilm formation. Quorum sensing is a near ubiquitous and important regulatory system employed by bacteria to modulate the formation of biofilms. In most strains, an initial increase in quorum sensing results in an increase in biofilm development, whilst disrupting QS signalling may result in the attenuation of biofilm formation[121]. Furthermore QS signalling may be responsible for the self-regulation of the biofilm lifecycle; when QS signalling molecules reach a certain threshold, biofilm formation is slowed down and may lead to the dispersal of

the biofilm[147,148]. Membrane systems are commonly used in wastewater treatment and may involve the formation of bioremediating biofilms onto the inner section of the membrane. The biofilms are then able to purify water as it flows along the membrane. A major problem however is the 'overgrowing' of the biofilm which results in blockages within the membrane, reducing remediation efficiency. To mitigate this Wood et al. constructed a QS-based gene circuit to engineer an *E.coli* biofilm forming strain[147] to control its biofilm thickness. The gene circuit contained the LasI/LasR QS module of *P. aeruginosa* which is one of the best characterised QS systems and plays a key role in the regulation of *P. aeruginosa* biofilms[148]. On the expression of the LasI protein, it synthesises the QS signal molecule N-(3-oxo-dodecanoyl)-L-homoserine lactone (3oC12HSL) which is released by the cells which then transition to a sessile biofilm lifestyle when local concentrations are high. However, when the concentration of 3oC12HSL reaches a certain upper limit threshold, the QS signals bind to LasR which results in the production of the biofilm dispersal protein BdcA E50Q, hence the LasI/LasR system regulates the *P. aeruginosa* biofilm thickness through regulation of the QS modulated biofilm lifecycle. As such The LasI/LasR gene circuit was transformed into an *E. coli* strain additionally engineered to produce an epoxide hydrolase that is able to remove the environmental pollutant epichlorohydrin from water. The resulting engineered strain was able to produce membrane bound biofilms with self-regulated thickness, and was shown to efficiently remove epichlorohydrin from water. Additionally, the strain was also engineered to produced nitric acid which prevented colonisation of the biofilm by other species, hence preventing the build-up of biofilm of other species on the membrane which could lead to its blockage[147].

In addition to QS systems, the near ubiquitous messenger molecule cyclic di-GMP (c-di-GMP) is also part of the regulatory systems involving biofilm formation. Usually when c-di-GMP is expressed in high levels, it leads to the formation of biofilms. Conversely at low concentrations biofilm formation is supressed[149]. As such several studies have attempted to engineer biofilm formation through modulation of c-di-GMP resulting in enhancement of biofilm mediated processes[150]. Wu et al. constructed a plasmid containing the c-di-GMP synthase gene YedQ taken from a *Comamonas testosteroni* biofilm forming strain. The YedQ plasmid was transformed into an *E.coli* strain, which resulted in the formation of higher levels of biofilm which consequently lead to improved levels of degradation of an organic soil pollutant, 3-chloroaniline in a biofilm bioreactor[151]. Mukherjee et. al engineered an *E.coli* strain by introducing a c-di-GMP based genetic circuit to reduce biofouling and biofilm overgrowth on the membranes of water purification columns, similarly to Wood et al who conversely used a QS-based gene circuit to control biofouling[147]. The levels of c-di-GMP are regulated by two groups of enzymes; diguanylate cyclases (DCGs) which catalyse the synthesis of c-di-GMP and phosphodiesterases (PDEs) which catalyses the hydrolysis of c-di-GMP. As such a genetic circuit was constructed consisting of a near infrared (NIR) light regulated DCE gene which expresses the DCE, BphS. The circuit also consisted of a blue light activated PDE gene which expresses the PDE, EB1. Hence through modulation of light, c-di-GMP levels could be controlled to prevent biofilm overgrowth, which could lead to excessive membrane fouling. Additionally, the circuit was also made to consist of a *O. anthropi* based quorum quenching gene, aiiO which when expressed degrades N-Acyl Homoserine Lactones (AHLs) resulting in the hijacking of the AHL based quorum sensing system. As a result, the engineered *E.coli* strain formed biofilms of light responsive thickness and biovolume onto a water purification membrane, and also inhibited biofouling of the

membrane by other bacteria such as *P. stewartia* (a strain widely involved in biofouling) through *E.coli* mediated quorum quenching[152,150]. Note *E. coli* does not produce AHL signalling molecules but rather uses other QS pathways (e.g. involving AI-2), hence quorum sensing in the engineered *E.coli* strain was unaffected.

(c) Biofilm based microbial fuel cells

Microbial fuel cells (MFCs) are a promising new technique in biotechnology due to the fact that bacteria are able to convert chemical energy into electricity. The concept of MFCs is based on the capacity of bacteria to perform or participate in extracellular electron transfer (EET) toward reducing an anode[153]. Direct EET is when electrons are naturally pumped out of the cell through outer membrane proteins[154] or through bacterial appendages[155]. These electrons are then directed towards the anode which gets reduced (i.e. builds up negative charge). Indirect EET involves the use of small molecules (mediators/redox shuttles) which act to shuttle the electrons from the bacteria to the anode[156]. In addition, bacteria may soak up electrons from a mediator that is easily oxidised and transfer them to the anode either directly or through other electron shuttling mediators. In this sense therefore, bacteria may be able to remove organic pollutants from a solution (which get oxidised by the bacteria), while simultaneously generating electricity[157]. In general, the bacteria that are responsible for current generation are grown directly onto the anode in the form of a biofilm[157] (figure 10).

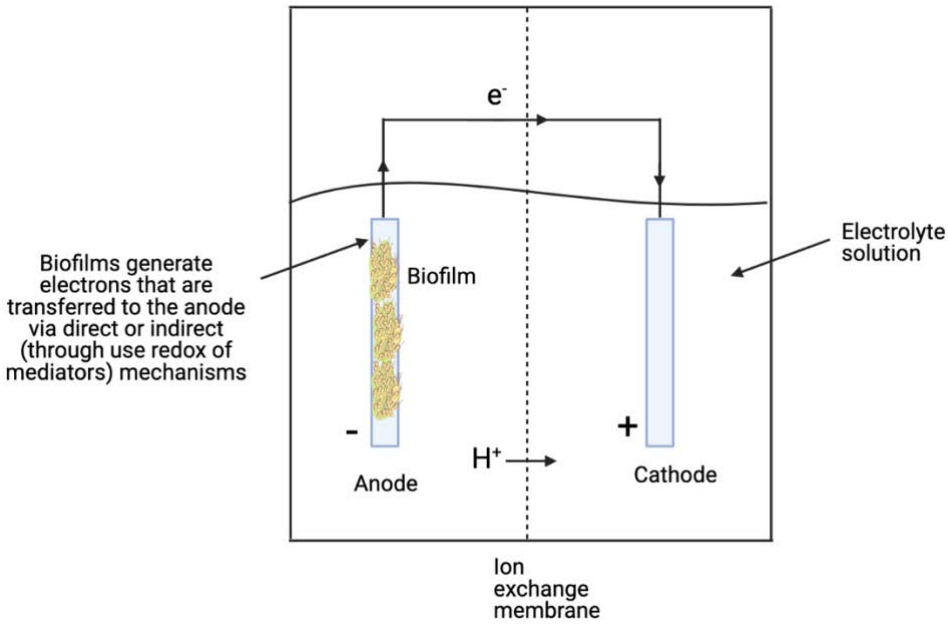

Figure 10: Schematic of a generic anode biofilm-based microbial fuel cell

Initially, the cells of the biofilm are able to pump out electrons which are transferred to the anode. This then sets up a difference in electrical potential between the anode and the cathode and subsequently, electrons begin to flow towards the cathode generating a current. A comprehensive study performed by Rabaey et al. investigated the link between biofilm structure and composition on subsequent current generation[153]. Intriguingly, they found that cell of biofilms grown onto the anode in a closed system (figure 10) were more viable closer to the electrode where EET is more likely to take place. In an open system, no current could be generated and the anode cannot accept electrons. In this case, oxidising agents (formate and nitrate) were added to the electrolyte solution so as to accept electrons generated by the biofilm (figure 11).

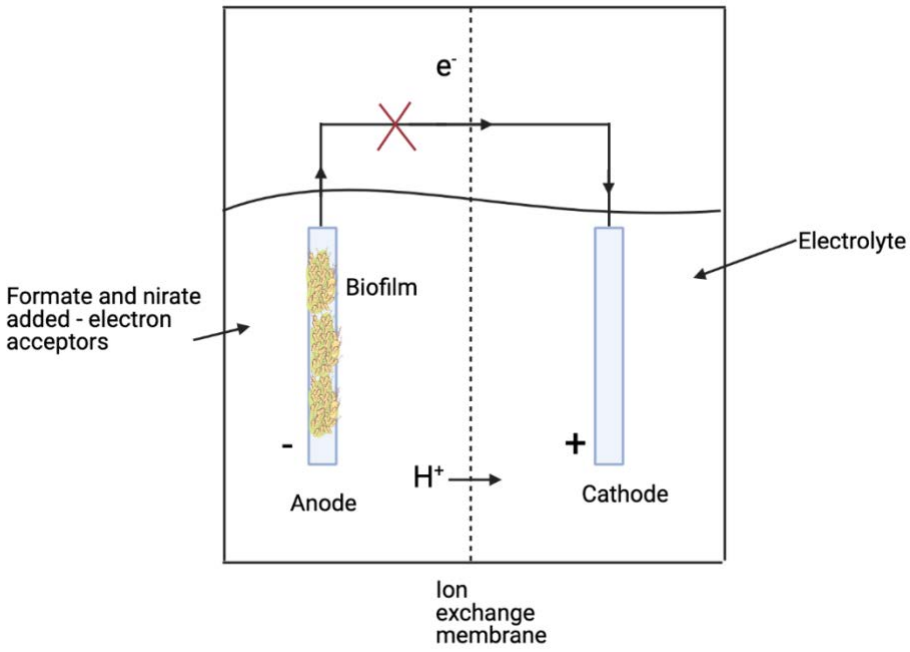

Figure 11: Schematic of an open biofilm-based microbial fuel cell – no current generation

In this open system it was conversely found that the cells in the biofilm were more viable away from the electrode at the top of the biofilm where cells have ready access to the soluble electron acceptors. Therefore from this it can be said that the cells of a biofilm used

in a microbial fuel cell are more active and viable at sites where EET can occur rapidly, with another study suggesting this leads to increased bacterial growth rates[158]. Additionally, biofilms grown in an open circuit were generally thicker than those grown in a closed circuit. This is because the reduction potential of the solutes (formate and nitrate) in an open circuit is greater that the reduction potential of the anode. Hence it is thermodynamically more favourable to reduce the solutes than to reduce the anode, leading to increased growth rates in an open circuit biofilm. The authors also notes differences in the biofilms of Gram negative and Gram positive bacteria, with Gram negative bacteria forming thicker biofilms. The suggested reason for this was that Gram positive bacteria have less potential to pump out their own electrons and that ideally, Gram positive bacteria need the presence of redox mediators to take part in EET. Unsurprisingly therefore, gram positive bacteria formed thinner biofilms than their Gram negative counterparts which readily take part in EET and generate more current. Finally, the authors investigated biofilm formation and subsequent current production in mixed culture biofilms composed of gram positive and Gram negative bacteria. In general, they found that the Gram positive bacteria would coat the electrode, whilst the gram negative bacteria grew on top of the biofilm, forming tower-like projections on the biofilm periphery. Current generation in mixed species biofilms was significantly higher than that of the respective monoculture species and was thought this was related to interspecies co-operation in EET. For example, gram negative bacteria readily secrete redox mediators, which can then be used by the Gram positive bacteria for EET. Hence it is likely that a mixed culture biofilm uses both direct and indirect methods of EET to boost current production with respect to either monospecies biofilm. In addition, the more complex topography of mixed species biofilms (i.e. the presence of projecting towers) may also increase the bioavailability of nutrients whilst maintaining contact with the anode[153].

(d) Biofilms as robust biocatalysts

Biocatalysts such as bacteria and the enzymes they produce have been used in many industrial applications due to their effectiveness and their environmentally friendly nature. Another advantage of biocatalysis is the high level of stereoselectivity of products when compared with chemically catalysed reactions, as enzymes are normally expressed in one particular orientation leading to stereospecific enzyme catalysis of substrates. Using whole cells or purified enzymes in these bioprocesses however have certain limitations due to their vulnerability toward potentially adverse reaction conditions which may limit the effectiveness of the biocatalytic process. Biofilms therefore have emerged as a new generation of biocatalysts, in the which bio-catalysing cells are protected within the EPS of the biofilm. Also, biofilms are very cell dense structures, therefore allowing for higher productivities in relation to the high local concentrations of biomass. Additionally, as described previously for bioremediating biofilms, biocatalytic biofilms can also be recycled and used multiple times which could save costs and time[159]. Some of the drawbacks of biofilm mediated processes however include limitations in mass transfer throughout the biofilm structure, the usually long periods of time required for the initial immobilisation process (i.e. biofilm formation) and system blockages due to biofilm overgrowth[160]. Hence much work has to be performed in optimising specific biofilm mediated process before efficient use on industrial scale, this includes selecting the correct bacterial strains for specific biocatalytic reactions and control over subsequent biofilm formation to form optimal biofilm structures for the particular bioprocess in question. For example most biocatalytic biofilms that can be found in the literature are heterogenous in structure and topography rather than flat homogeneous biofilms which in general are metabolically less active. The reason for this is due to the fact that heterogeneous biofilms contain many

different sub-communities separated by voids and channels which can increase the mass transfer of nutrients and oxygen throughout the biofilm, leading to increased cell growth and metaboilism[161,162]. As such, heterogeneous biofilms have been shown as effective biocatalysts for the production of chemicals used in the bioenergy industry (e.g. alcohols and biohydrogen), enzymes, amino acids, antibiotics, exopolysaccharides and surfactants amongst others from cheap, readily available substrates many of which are already environmental pollutants. Hence biocatalytic biofilms may be used to simultaneously remove pollutants whilst producing new and useful products[159].

Biocatalytic biofilms for the production of alcohols and hydrogen gas (bioenergy)

Mohan et. al showed how a mixed consortium of bacteria obtained from wastewater were able to form biofilms which could then use industrial wastewater as a carbon source for the metabolic biocatalytic reactions required for the bio-generation of H_2 gas[163], which is known to be the most promising and green alternative to fossil fuels for energy generation[164]. Single species biofilms have been used widely for the production of alcohols such as ethanol and butanol, from sugar based substrates. For example *Zymomonas mobilis* biofilms have been widely used to produce ethanol from sources such as starch[165], glucose[166] and more recently rice bran hydrolysate[167]. Napoli et al. showed how *Clostridium acetobutylicum* biofilms were able to produce butanol from water containing cheese whey, an abundant lactose based pollutant in wastewater.

Biofilms for the production of fine chemicals

Fine chemicals are pure chemical compounds that are produced in small amounts by industrial processes. These chemicals are then used for the synthesis of products such as pharmaceuticals, fragrances, food additives, biocides and other specialty chemicals used as starting materials in various industrial processes[168]. Unlike bulk chemicals which are produced in large scale, fine chemical synthesis is very expensive and energy intensive. Therefore biofilm mediated biocatalysis of cheap starting materials to yield valuable fine chemicals has attracted much attention, with many reports of biofilm mediated fine chemical synthesis. For example, Li et al. showed that *Zymomonas mobilis* biofilms were able continuously catalyse benzaldehyde into the fine chemical benzyl alcohol despite benzaldehyde normally being extremely toxic to planktonic cultures. Additionally biofilm biocatalytic efficiency did not reduce over the 45h continuous process, despite the continual addition of benzaldehyde to the biofilm[169]. Gross et al. used a biofilm forming *Pseudomonas sp.* Strain to catalyse styrene into an enantiomerically pure (S)-styrene oxide. *Pseudomonas sp.* strain VLB12 is known for its ability to mineralise and uptake styrene via (S)-styrene oxide using its enzyme styrene monooxygenase, StyAB. Hence *Pseudomonas sp*. strain VLB120ΔC with a knock-out mutation in the gene coding for the isomerase enzyme responsible for the uptake of (S)-styrene oxide was used, such that (S)-styrene oxide remained in the reaction and could be isolated. The biofilm was found to be biocatalytically active for a period of at least 55 days in a continual process[170].

Recombinant biofilms for biocatalysis

A relatively new field in biofilm mediated biocatalysis of chemicals involves the use of recombinant genes to allow the bacteria within the biofilm to express specific enzymes for use in specific biocatalysis reactions. Despite the widespread use of recombinant planktonic cultures in biocatalysis, there are only a few literature examples which describe the use of recombinant biofilms. The first study by Zhou et al. described biofilm mediated biocatalysis of ethanol from lignocellulosic biomass[171] using a recombinant *E.coli* strain. According to Zaldevar et. al, the production of ethanol from renewable lignocellulosic biomass (i.e. from waste crops) has the potential to significantly contribute to global fuel requirements while minimising the release of greenhouse gasses[172]. Therefore an *E.coli* KO11 strain was developed by Ingram et al[173] such that it contained chromosomally integrated genes from *Zymomonas mobilis* that coded for pyruvate decarboxylase, *pdc* and alcohol dehydrogenase II, *adhB* which when expressed at high levels is able to divert pyruvate metabolism from acid production (lactic acid) to ethanol (pyruvate is an intermediate product in the degradation of cellulosic sugars)[173,171]. As such, Zhou et al. used this recombinant strain to produce biofilms which were shown to be more resilient to ethanol production than planktonic cultures, leading to a higher and more stable ethanol yield for up to 40 days of continuous ethanol production from the biocatalysis of xylose (a hemicellulose)[171].

Another study by Lee et al. used a recombinant *Acetobacter xylinum* strain transformed with D-amino acid oxidase (DAAO) activity which when expressed can catalyse D-amino acids to its corresponding α-ketoacid, ammonia and hydrogen peroxide[174]. The DAAO gene was taken from *Rhodosporidium toruloides*. α-ketoacids are valuable chemicals that can be subsequently used in feeds, food additives, pharmaceuticals and chemical synthesis

processes[175]. The authors showed that the recombinant *Acetobacter xylinum* was able to form cellulose based biofilms at the air/liquid interface – commonly known as floating biofilms or pellicles. Although the biofilm associated cells only showed around 10% of the DAAO activity of whole cell planktonic cultures, it provided benefits which included increased thermal and operational stability, and easy retrieval of biofilm cells for re-use[174]. Another study, which was performed in our labs at Birmingham used recombinant *E. coli* K-12 biofilms for the conversion of haloindoles into halotryptophans which are an important class of pharmaceutical intermediates. The biofilm forming *E. coli* K-12 strain PHL644 was transformed with a plasmid (pSTB7) which contained the tryptophan synthase gene, *trpBA* taken from *Salmonella enterica* serovar Typhimurium TB1533, which when expressed catalyses the conversion of haloindoles to halotryptophans. Biofilms of recombinant PHL644 were prepared by spin coating the strain onto glass slides (by centrifugation) and growing the biofilm for 7 days. The spin coated biofilms matured faster and were more heterogeneous than the naturally formed biofilms (i.e. without spin coating). Furthermore, the spin coated recombinant biofilms were able to convert higher amounts of haloindole into halotryptophan than the corresponding naturally formed recombinant biofilm, recombinant planktonic bacteria and the purified immobilised tryptophan synthase[127]. Additionally the engineered PHL644 biofilms could be recycled, with no loss of activity even after 3 sequential cycles of the conversion of 5-chloroindole[176]. Given this promising data, a further study was performed to optimise the biocatalytic reaction. This time, four separate *E. coli* K-12 strains were spin coated onto glass slides and matured for 7 days, these strains were; the parental K-12 strains MC4100 and MG1655 and their respective isogenic mutant strains PHL644 and PHL628. Both mutant strains PHL644 and PHL628 contained a point mutation in the *ompR* gene (*ompR234*), which allowed for the overproduction of curli

resulting in thicker biofilms (see section iii) than their parental strains. In general for the biotransformation of 5-chloroindole and 5-fluoroindole (to their respective halotryptophans), the overproducing recombinant biofilms performed better with the reactions initially proceeding faster and generating more halotryptophan for longer periods than the parental recombinant biofilms. The planktonic recombinant cells were able to initially induce high rates of haloindole depletion and halotryptophan generation, however in general after 10h the rate of conversion dropped to zero whilst recombinant biofilms were able to stay biocatalytically active for over 20h. Initially, it was thought that the catalytic longevity of recombinant biofilms is due to the increased protection of cells provided by the EPS, however a further study by Tong et al. showed that the catalytic longevity was at least in part due to the ability of cells within a biofilm to constantly and completely regenerate the recombinant tryptophan synthase enzyme[177]. This was found through SILAC (stable isotopic labelled amino acids in cell cultures) analysis in which pulses of differently labelled isotopic acids are administered to the culture over a period of time, after which the protein of interest is extracted to find the amount of incorporated isotope labelled amino acid in the protein. Two amino acids; lysine and phenylalanine are abundant in tryptophan synthase hence these two amino acids were labelled with a stable isotope. The respective unlabelled amino acids (phenylalanine and lysine) and labelled amino acids ([2,6-$^{2}H_2$]-L-phenylalanine and [4,4,5,5-$^{2}H_4$]-L-lysine) can be differentiated through mass spectrometry and as such any protein that is able to incorporate these labelled amino acids will be also be of altered and known final mass corresponding to the number of incorporated labelled amino acids with respect to the native protein.

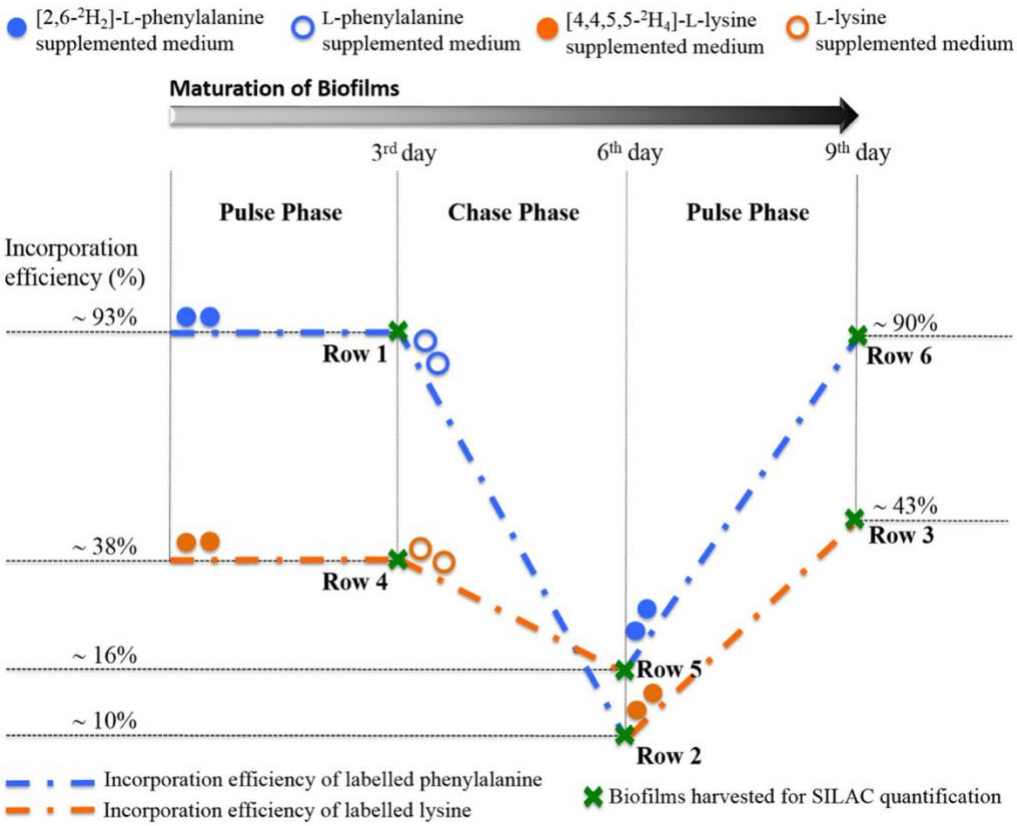

Figure 12: Workflow showing changes in the incorporation of SILAC amino acids into tryptophan synthase, taken from Tong et al. Ref 177. Biofilms were grown for three days (pulse phase) in the presence of either [2,6-2H2]-L-phenylalanine (solid double blue dots) or [4,4,5,5-2H$_4$]-L-lysine (solid double orange dots), resulting in the incorporation of the respective labelled amino acid within recombinant tryptophan synthase produced from the respective biofilm. The chase phase (days 3-6) involved further growing biofilms in the same unlabelled media (empty dots) as in the pulse phase. The second pulse phase involves growth of the biofilm in the original labelled media, showing its constant incorporation within biofilm produced tryptophan synthase

Initially, PHL644 was grown in the presence of either labelled phenylalanine or labelled lysine. After the cultures had grown in the presence of either label, the cells were spin coated respectively onto glass slides that were then placed into deep wells with fresh media containing the same isotope labelled amino acid. The two separate biofilms were then grown for 3 days (pulse phase, figure 12), after which an aliquot of each was taken for protein analysis. The culture that grew in the presence of [2,6-$^2H_2$]-L-phenylalanine was shown produce tryptophan synthase in which 93% of phenylalanine was in labelled form. The culture that was grown in [4,4,5,5-$^2H_4$]-L-lysine produced enzyme in which 38% of the lysine residues were labelled. After this, the media of each biofilm sample was removed and re-supplemented with media that contained the same unlabelled amino acid. This was then

matured for another 3 days (chase phase), after which an aliquot was again taken from each sample for protein analysis. The amount of incorporated labelled amino acid in both samples dropped dramatically to 10% labelled phenylalanine and 16% labelled lysine. Finally, the media of the now 6 day old biofilm samples was removed again and supplemented with the other labelled amino acid. The biofilm was further matured for another 3 days (2nd pulse phase) after which protein analysis was again performed. The resulting tryptophan synthase was found to now contained a similar portion of the other labelled amino acid. This data therefore demonstrates the constant and complete regeneration of tryptophan synthase within PHL644 biofilms, even after 9 days of maturation which is thought to contribute to its striking biocatalytic longevity[177].

Optimising biofilm meditated biocatalysis through genetic control over biofilm formation

As described earlier, biofilm mediated process can be optimised through control over biofilm formation[150]. Previous studies have shown how biofilm thickness can be modulated by control over c-di-GMP expression which leads to improved levels of bioremediation of pollutants and control over excessive biofouling[151,152]. Therefore following from this, Cao et al. introduced a near infrared light (NIR) responsive genetic circuit to modulate cellular levels of c-di-GMP to control biofilm formation in *E.coli* BL21. In addition, the cells were also transformed with the pSTB7 plasmid, allowing the cells to express tryptophan synthase for the biocatalysis of indole into tryptophan. Upon the exposure of NIR light, almost twice the amount of biofilm was induced when compared to natural biofilm formation in the dark, due to increased levels of NIR dependant c-di-GMP expression, which consequently lead to a 30% increase in *E.coli* BL21 biofilm mediated tryptophan yield[178]. A second study

performed by Lorenzo et al. again introduced a genetic circuit to modulate c-di-GMP expression, this time into *Pseudomonas putida* KT244. The genetic circuit was composed of a *YedQ* gene (coding for c-di-GMP synthase) that could be expressed in the presence of a chemical inducer (cyclohexanone). The resulting biofilm was significantly more abundant than without the presence of cyclohexanone, and showed greater biocatalytic activity toward degrading the common industrial pollutant 1-chlorobutane[179].

(vi) New approaches toward designing spatially defined functional biofilms

Up till this point, all the studies that have been described have all made the use of functional biofilms that have been immobilised onto a solid surface. Furthermore, the functionality of these biofilms have been manipulated and optimised through genetic control over biofilm expression factors that may have great influence over subsequent biofilm functionality. Most of these studies have involved the use of genetic circuits to modulate specific biofilm related genes to increase or reduce biofilm thickness, and to modulate its composition. A more recent approach involves the embedding of bacteria into spatially controlled hydrogels allowing for the creation of 'living materials' with controlled three dimensional (3D) shape, microstructure and resulting dynamic metabolic response. In contrast to immobilising bacteria onto solid surfaces, enclosing bacteria into a spatially defined hydrogel provides an ideal living environment that contains lots of water to allow for the flow of nutrients and waste products into and out of the living material. Once the bacteria have been entrapped within the hydrogel, biofilm factors begin to be expressed resulting in the formation of EPS substances. For example *Acetobacter xylinum* are able to secrete their own nanocellulose hydrogels which have great mechanical strength. As such

biofilm produced cellulose has widely been used in the medical industry in tissue engineering due to its biocompatibility. So far however, bacterial cellulose has been mainly produced in biofilms deposited onto solid surfaces. However immobilising the bacteria into a spatially defined viscoelastic matrix would allow for the production of cellulose of defined macrostructure and chemical composition which could be vital depending on the application e.g. production of skin grafts of defined shapes. Moreover overcoming geometrical constraints and the lack of spatial control of current solid surface associated biofilm growth could lead to new and novel designs for biofilms to be used in microbial fuel cells, bioremediation, biocatalysis. Additionally, spacial control over bacterial distribution could be a used as a model for studying biofilm dynamics and metabolic processes[180,181,182].

(a) 3D printing of bacteria into functional biofilms

The most recent development into controlling biofilm architecture involves the use of a 3D printing platform which allows for the digital fabrication of cell dense hydrogels, with full control over the spacial distribution of cells within a self-supporting 3D printed hydrogel[180]. This is possible by initially loading the desired strain of bacteria into a 'hydrogel ink' which can then be loaded into a 3D printing machine, and printed (extrusion) into desired shapes and morphologies whilst providing a rich environment in which bacteria can survive and go on to express biofilm EPS (figure 13). Usually the 'ink' that the bacteria are initially embedded within is composed of biocompatible and viscoelastic hydrogels such as hyaluronic acid (HA), k-carrageenan (k-CA), fumed silica (FS)[180], gelatine, agarose[181] or a mixture of these.

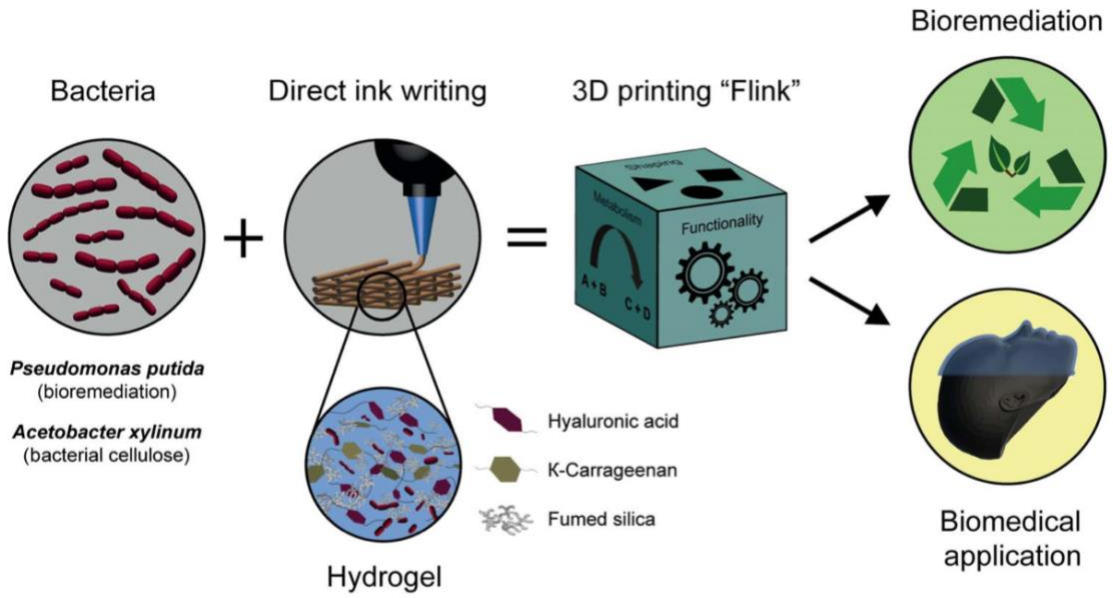

Figure 13: Schematic of the 3D bacteria-printing platform for the creation of functional living materials which can be used in various industries, taken from Schaffner et al ref 180

A landmark study by Schaffner et al. presented two examples of 3D printed living materials with defined geometry and architecture (figure 14 a-d), and with functionality in terms of bioremediation and cellulose production. Firstly the authors designed a hydrogel with appropriate rheological properties to allow for the deposition of distortion free and precise 3D hydrogel architectures. The hydrogel was composed of glycidyl methacrylate hyaluronic acid (GMHA) and fumed silica (FS) which are both viscous, combined with k-carrageenan (k-CA) to induce elasticity. After printing, the hydrogel can be re-enforced by exposure to UV light which results in the cross linking of GMHA to yield mechanically stable hydrogels which mimic the natural physiological conditions that bacteria thrive in. To produce a functional living material, the bacterial strain *Pseudomonas putida* was incorporated into the hydrogel ink, with this strain being capable of phenol degradation. As such the bacterial ink was printed into a grid-like architecture (figure 14b) which would provide a high surface area for the biotransformation of phenol. Following this the 'living grid' was re-enforced by UV light and placed into a solution containing phenol. This first incubation lead to a complete

removal of phenol within 140h, after which the grid was rinsed and reused which lead to increased phenol degradation kinetics, with complete removal at around the 20h mark, comparable with the degradation kinetics of planktonic *Pseudomonas putida.* A second 3D printed living material was also prepared, this time a hydrogel ink with *Acetobacter xylinum*. This strain is capable of producing cellulose as its EPS component when oxygen is present. As such *Acetobacter xylinum* was embedded into the same hydrogel composed of HA, k-CA and FS, followed by incubation of the printed structure for 4-7 days to allow for biofilm proliferation and cellulose production. In this case, to promote biofilm growth (and consequent swelling of the hydrogel), no cross linker was used. After the incubation period, the bacteria within the hydrogel were washed out using water/ethanol mixtures, thereby leaving only the structurally defined cellulose network produce by the embedded bacteria (figure 14e, g). Bacterial cellulose formation depends on oxygen availability and the viscosity of the hydrogel ink. This was investigated by producing circular prints of living material containing 3, 4.5 and 6 wt % hydrogel components and covering them with glass slides so as to only allow oxygen through to the sides of the living material (figure 14f). In general, cellulose was only produced on the edges of the material (as confirmed by using a cellulose specific fluorescent dye) where oxygen was available, however the amount produced was inversely proportional to the ink viscosity, due to the high level of immobilisation of bacteria within viscous structures which reduce cellulose expression. This technique could therefore be used in the preparation of films and coatings where the thickness of the coating is to be modulated (figure 14f)[180].

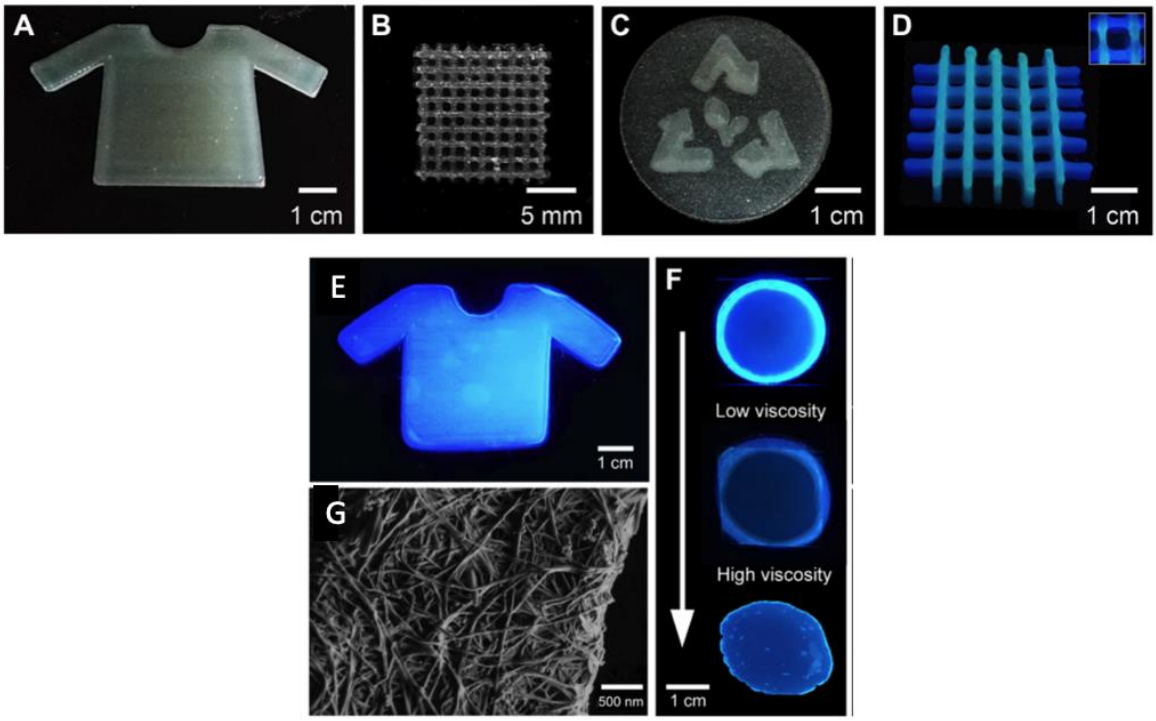

Figure 14: (a-c) Examples of 3D living hydrogel architectures (d) Multimeric 3D printing with spacial segregation of bacterial strains: Pseudomonas putida labelled with DAPI stain (blue) is located in the horizontal lines whilst Bacillus subtilis labelled with Nile red (green fluorescence) is found on the vertical lines. (e) formation of bacterial cellulose by 3D printed Acetobacter xylinum in the shape of a T-shirt, cellulose is visualised through the use of a cellulose specific fluorescent stain. (g) Bacterial cellulose nanofibril network visualised by scanning electron microscopy (f) Bacterial cellulose production is dependent on oxygen availability – the printed living circular structures were covered with glass slides to only allow oxygen transfer through the sides of the printed biofilm, hence cellulose (stained with a cellulose specific fluorescent marker) was only found coating the outer layer of the circular structures. Increasing viscosity of the ink leads to lower cellulose production due to the entrapment of bacterial cells within a viscous ink. Figure taken from Schaffner et al. Ref 180.

Few other examples of printable living materials can be found in the literature, as this technique is still in its infancy. Lehner et al. printed a living system platform with *E.coli* as the living part, and alginate as the printable ink[182]. Zhong et al. printed a highly flexible and tuneable living functional materials platform based on the TasA amyloid machinery of the bacterium *Bacillus subtilis*. TasA is an amyloid protein that is produced by *Bacillus subtilis*, and as such the authors developed genetically programmable TasA fusion proteins with defined functionality for a range of applications, including fluorescence detection, conjugation chemistry, bioremediation and defined nanoparticle templating onto the TasA fusion proteins. As such, biofilms of *Bacillus subtilis* and their extracellular TasA-fusion

proteins were printed into defined structures with high functionality and defined viscoelastic properties for the specific application of use[183] (figure 15).

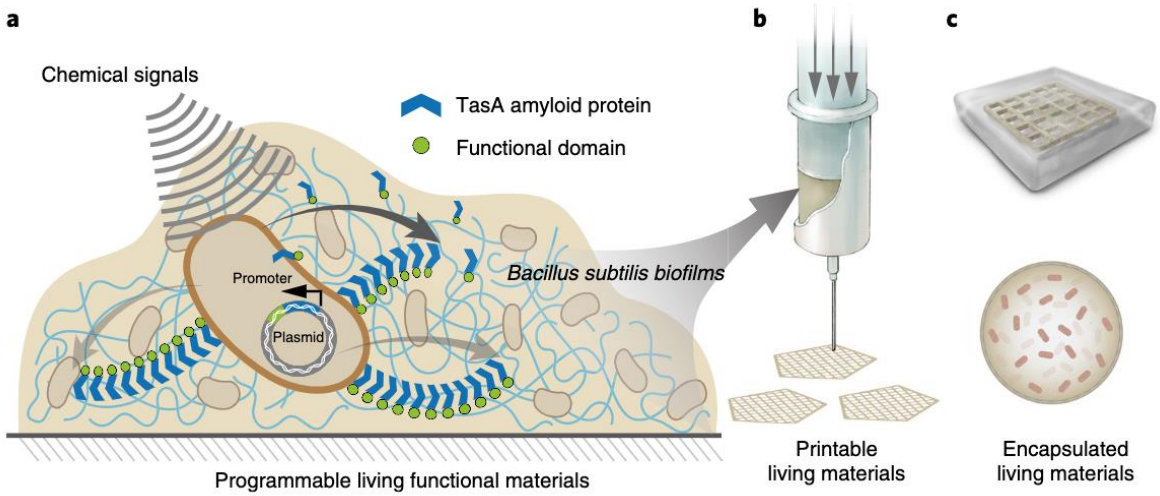

Figure 15: Schematic of 3D printed Bacillus based living materials with programmable amyloid functionality. TasA amyloid proteins produced by Bacillus subtillis can be functionalised with specific moieties for a plethora of potential uses. Taken from Zhong et al. ref 183

(b) A simple and cheaper method of controlling biofilm morphology and functionality through the use of synthetic polymers

In the following chapters, we show that synthetic hydrophobic polymers based on a poly(acryloyl hydrazide) scaffold are able to interact and aggregate biofilm forming *E.coli* K-12 strains in a predictable manner that is dependent on polymer hydrophobicity. Upon addition of our hydrophobic polymers into the aqueous culture, the polymers immediately precipitate into insoluble aggregates of defined size onto which the bacteria adhere in a predictable manner and proceed to form biofilms of defined aggregate size. For example we show that the most hydrophobic polymers induce rapid cell aggregation which leads to the production of large polymer-induced aggregates with high biofilm content after incubation. Therefore, rather than using expensive printing methods to form functional biofilms, the addition of polymers of defined physiochemical properties to induce cell aggregation provides enough stimulation to form size defined bacterial aggregates/functional biofilms.

Biocatalytic functionality was introduced to the cells by transforming the pSTB7 plasmid containing the tryptophan synthase gene which allows for polymer-induced biofilm mediated biocatalysis of haloindole to halotryptophans. The kinetics of the reaction was found to be highly dependent on the specific polymer used to aggregate the bacteria into defined sizes via hydrophobic interactions. To our knowledge, there is only one previous study involving the aggregation of microbes onto synthetic polymer gels in solution resulting in the generation of protected functional living materials. Pines and Freeman showed how a polyacrylamide scaffold partially functionalised with acyl hydrazide groups (rather similar to polyacryloyl hydrazide) was able to immobilise the yeast *Saccharomyces cerevisiae* within its hydrogel which was formed via crosslinking using glyoxal. The ability of the resulting immobilised yeast biofilms to convert glucose to ethanol was monitored with the immobilised system showing significantly greater resistance toward the continuous production of ethanol than free yeast[184].

(vii) Concluding Statements

Bacterial biofilms are surface associated bacterial colonies that differ vastly in their behaviour to planktonic cells through complex genetic regulation networks that vary between different strains of bacteria and under different environmental conditions. Cells within a biofilm live in a sessile state and are able to survive through intercellular cooperation resulting in protection from predators and harsh environmental conditions through the division of labour, conservation of genotype, and the formation of a protective extracellular polymeric substance (EPS) matrix which provides a physical and structural barrier against mechanical, physical and chemical stresses such as the addition of

antibiotics. Due to their persistent characteristics, biofilms have been historically seen as problematic; their robust structure makes them difficult to remove from surfaces that they may contaminate and they are commonly associated with wide range of bacterial infections. Due to the overwhelmingly complex genetic modulation of biofilm formation, strategies to eradicate biofilms from surfaces commonly involve the design of antifouling surfaces. The first stage of biofilm formation involves the initial attachment of bacteria onto a surface which is initially modulated by non-specific physiochemical interactions between the bacteria and surface, and can be somewhat modelled by theories of colloidal interactions involving electrostatic, van der Waals and acid-base type interactions (e.g. hydrophobic or hydrophilic interactions, and hydrogen bonding). From this surfaces have been deliberately designed to modulate and reduce physiochemical interactions with bacteria, through the design of antifouling surfaces. A relatively new method of preventing bacterial adhesion to surfaces involve the use of anti-adhesive bacterial sequestering polymers which are designed to interact and aggregate bacteria away from the potential site of infection through physiochemical interactions. Studies into the effect of these aggregating polymers on bacteria have shown that polymers are able to modulate bacterial phenotype, including biofilm expression factors. Hence polymers themselves may be used to aggregate bacteria and stimulate biofilm formation. The persistent and resistant characteristics of biofilms, though normally seen as problematic may be utilised in the field of biotechnology where metabolising cells are protected from harsh reactor conditions that would not usually be suitable for planktonic bacteria. As such functional biofilms have found their way into processes such as bioremediation, biocatalysis and microbial fuel cells where the metabolic activity of biofilms can be used in harsh environmental conditions. A such, a relatively new field has opened up which is concerned with modulating and optimising functional biofilm

formation and performance through the use of characterizable materials of defined structure resulting in the spacial control of functional cells within a biofilm. This usually involves the printing of bacteria-laden hydrogels into defined shapes termed functional living materials. A more simple method of controlling functional biofilm formation involves the use of polymers designed to aggregate bacteria into defined sizes which then go on to form biofilms, the characteristics of which may directly be related to the physicochemical properties of the aggregating polymer. This concept forms the bulk of this project.

(viii) Project Objectives

This project is centred around the use of functional polymers to interact and aggregate the *E. coli* K-12 strains MC4100 and its isogenic mutant PHL644, to modulate biofilm expression and resulting biofilm biocatalytic performance in the biotransformation of 5-fluoroindole to 5-fluorotryptophan. A recently developed poly(acryloyl hydrazide) scaffold was used to provide a platform for easy post-polymerisation functionalisation, allowing for the production of a library of functional poly(acryloyl hydrazide) polymers to test with bacteria. Before this however, a collaborative study was conducted in our labs to optimise the RAFT polymerisation of boc-poly(acryloyl hydrazide) through modulation of polymerisation temperature – this work is presented in the form of a published journal paper in chapter 3. Following this, a library of functional polymers based on the now optimised poly(acryloyl hydrazide) scaffold was synthesised and tested with *E.coli* K-12 to induce cell aggregation, the first stage in the biofilm lifecycle, in the hope of modulating biofilm expression factors and boosting biofilm levels. Finally, the functionality of the polymer-induced aggregates/biofilms was tested in the biocatalytic arena. This body of work is presented in

chapters 4 and 5 of this thesis. Before this however, and due to the highly interdisciplinary nature of this project - spanning the fields of polymer chemistry, microbiology and biochemical engineering, the next chapter (chapter 2) will go through and describe background theory related to the experiments conducted in this project in a way that is representative of the workflow of the overall project. Chapter 2 also contains the materials and methods section.

(ix) References

1. Westall F, De Wit MJ, Dann J, Van der Gaast S, De Ronde CEJ, Gerneke D. Early archean fossil bacteria and biofilms in hydrothermally-influenced sediments from the Barberton greenstone belt, South Africa. *Precambrian Res*. 2001. doi:10.1016/S0301-9268(00)00127-3
2. Rasmusssn B. Filamentous microfossils in a 3,235-million-year-old volcanogenic massive sulphide deposit. *Nature*. 2000. doi:10.1038/35015063
3. Baty AM, Eastburn CC, Techkarnjanaruk S, Goodman AE, Geesey GG. Spatial and temporal variations in chitinolytic gene expression and bacterial biomass production during chitin degradation. *Appl Environ Microbiol*. 2000. doi:10.1128/AEM.66.8.3574-3585.2000
4. Renner LD, Weibel DB. Physicochemical regulation of biofilm formation. *MRS Bull*. 2011. doi:10.1557/mrs.2011.65
5. Stoodley P, Sauer K, Davies DG, Costerton JW. Biofilms as complex differentiated communities. *Annu Rev Microbiol*. 2002. doi:10.1146/annurev.micro.56.012302.160705
6. Flemming HC, Wingender J. The biofilm matrix. *Nat Rev Microbiol*. 2010. doi:10.1038/nrmicro2415
7. Hall-Stoodley L, Costerton JW, Stoodley P. Bacterial biofilms: From the natural environment to infectious diseases. *Nat Rev Microbiol*. 2004. doi:10.1038/nrmicro821
8. Lawrence JR, Korber DR, Hoyle BD, Costerton JW, Caldwell DE. Optical sectioning of microbial biofilms. *J Bacteriol*. 1991. doi:10.1128/jb.173.20.6558-6567.1991
9. Stoodley P, Dodds I, Boyle JD, Lappin-Scott HM. Influence of hydrodynamics and nutrients on biofilm structure. In: *Journal of Applied Microbiology Symposium*

Supplement. ; 1999. doi:10.1111/j.1365-2672.1998.tb05279.x

10. Mann EE, Wozniak DJ. Pseudomonas biofilm matrix composition and niche biology. *FEMS Microbiol Rev*. 2012. doi:10.1111/j.1574-6976.2011.00322.x

11. Maurice NM, Bedi B, Sadikot RT. Pseudomonas aeruginosa biofilms: Host response and clinical implications in lung infections. *Am J Respir Cell Mol Biol*. 2018. doi:10.1165/rcmb.2017-0321TR

12. Tielen P, Strathmann M, Jaeger KE, Flemming HC, Wingender J. Alginate acetylation influences initial surface colonization by mucoid Pseudomonas aeruginosa. *Microbiol Res*. 2005. doi:10.1016/j.micres.2004.11.003

13. Danese PN, Pratt LA, Kolter R. Exopolysaccharide production is required for development of Escherichia coli K-12 biofilm architecture. *J Bacteriol*. 2000. doi:10.1128/JB.182.12.3593-3596.2000

14. Itoh Y, Rice JD, Goller C, et al. Roles of pgaABCD genes in synthesis, modification, and export of the Escherichia coli biofilm adhesin poly-β-1,6-N-acetyl-D-glucosamine. *J Bacteriol*. 2008. doi:10.1128/JB.01920-07

15. Dalton HM, Goodman AE, Marshall KC. Diversity in surface colonization behavior in marine bacteria. *J Ind Microbiol Biotechnol*. 1996. doi:10.1007/bf01574697

16. Heydorn A, Nielsen AT, Hentzer M, et al. Quantification of biofilm structures by the novel computer program COMSTAT. *Microbiology*. 2000. doi:10.1099/00221287-146-10-2395

17. Suh SJ, Silo-Suh L, Woods DE, Hassett DJ, West SEH, Ohman DE. Effect of rpoS mutation on the stress response and expression of virulence factors in Pseudomonas aeruginosa. *J Bacteriol*. 1999;181(13):3890-3897. doi:10.1128/jb.181.13.3890-3897.1999

18. Elias S, Banin E. Multi-species biofilms: Living with friendly neighbors. *FEMS Microbiol Rev*. 2012. doi:10.1111/j.1574-6976.2012.00325.x

19. Periasamy S, Kolenbrander PE. Aggregatibacter actinomycetemcomitans builds mutualistic biofilm communities with Fusobacterium nucleatum and Veillonella species in saliva. *Infect Immun*. 2009. doi:10.1128/IAI.00345-09

20. Bittar F, Richet H, Dubus JC, et al. Molecular detection of multiple emerging pathogens in sputa from cystic fibrosis patients. *PLoS One*. 2008. doi:10.1371/journal.pone.0002908

21. Hoffman LR, Déziel E, D'Argenio DA, et al. Selection for Staphylococcus aureus small-colony variants due to growth in the presence of Pseudomonas aeruginosa. *Proc Natl Acad Sci U S A*. 2006. doi:10.1073/pnas.0606756104

22. Haiko J, Westerlund-Wikström B. The role of the bacterial flagellum in adhesion and virulence. *Biology (Basel)*. 2013. doi:10.3390/biology2041242

23. O'Toole GA, Wong GCL. Sensational biofilms: Surface sensing in bacteria. *Curr Opin Microbiol*. 2016. doi:10.1016/j.mib.2016.02.004

24. McCarter L, Hilmen M, Silverman M. Flagellar dynamometer controls swarmer cell differentiation of V. parahaemolyticus. *Cell*. 1988. doi:10.1016/0092-8674(88)90197-3

25. Otto K, Silhavy TJ. Surface sensing and adhesion of Escherichia coli controlled by the Cpx-signaling pathway. *Proc Natl Acad Sci U S A*. 2002. doi:10.1073/pnas.042521699

26. Monds RD, Newell PD, Gross RH, O'Toole GA. Phosphate-dependent modulation of c-di-GMP levels regulates Pseudomonas fluorescens Pf0-1 biofilm formation by controlling secretion of the adhesin LapA. *Mol Microbiol*. 2007. doi:10.1111/j.1365-2958.2006.05539.x

27. Tuson HH, Weibel DB. Bacteria-surface interactions. *Soft Matter*. 2013. doi:10.1039/c3sm27705d

28. Craig L, Forest KT, Maier B. Type IV pili: dynamics, biophysics and functional consequences. *Nat Rev Microbiol*. 2019. doi:10.1038/s41579-019-0195-4

29. Utada AS, Bennett RR, Fong JCN, et al. Vibrio cholerae use pili and flagella synergistically to effect motility switching and conditional surface attachment. *Nat Commun*. 2014. doi:10.1038/ncomms5913

30. Zobell CE. The Effect of Solid Surfaces upon Bacterial Activity1. *J Bacteriol*. 1943. doi:10.1128/jb.46.1.39-56.1943

31. John AK, Schmaler M, Khanna N, Landmann R. Reversible daptomycin tolerance of adherent staphylococci in an implant infection model. *Antimicrob Agents Chemother*. 2011. doi:10.1128/AAC.00172-11

32. Meinders JM, van der Mei HC, Busscher HJ. Deposition Efficiency and Reversibility of Bacterial Adhesion under Flow. *J Colloid Interface Sci*. 1995. doi:10.1006/jcis.1995.9960

33. Boks NP, Kaper HJ, Norde W, Busscher HJ, van der Mei HC. Residence time dependent desorption of Staphylococcus epidermidis from hydrophobic and hydrophilic substrata. *Colloids Surfaces B Biointerfaces*. 2008. doi:10.1016/j.colsurfb.2008.08.021

34. Berne C, Ellison CK, Ducret A, Brun Y V. Bacterial adhesion at the single-cell level. *Nat Rev Microbiol*. 2018. doi:10.1038/s41579-018-0057-5

35. Jenal U, Reinders A, Lori C. Cyclic di-GMP: Second messenger extraordinaire. *Nat Rev Microbiol*. 2017. doi:10.1038/nrmicro.2016.190

36. MARSHALL KC, STOUT R, MITCHELL R. Mechanism of the Initial Events in the Sorption of Marine Bacteria to Surfaces. *J Gen Microbiol*. 1971. doi:10.1099/00221287-68-3-

337

37. Vasudevan R. Biofilms: Microbial Cities of Scientific Significance. *J Microbiol Exp*. 2014. doi:10.15406/jmen.2014.01.00014

38. O'Toole G, Kaplan HB, Kolter R. Biofilm formation as microbial development. *Annu Rev Microbiol*. 2000. doi:10.1146/annurev.micro.54.1.49

39. Borlee BR, Goldman AD, Murakami K, Samudrala R, Wozniak DJ, Parsek MR. Pseudomonas aeruginosa uses a cyclic-di-GMP-regulated adhesin to reinforce the biofilm extracellular matrix. *Mol Microbiol*. 2010. doi:10.1111/j.1365-2958.2009.06991.x

40. Harmsen M, Yang L, Pamp SJ, Tolker-Nielsen T. An update on Pseudomonas aeruginosa biofilm formation, tolerance, and dispersal. *FEMS Immunol Med Microbiol*. 2010. doi:10.1111/j.1574-695X.2010.00690.x

41. Lee SY. High cell-density culture of Escherichia coli. *Trends Biotechnol*. 1996. doi:10.1016/0167-7799(96)80930-9

42. Sharma G, Sharma S, Sharma P, et al. Escherichia coli biofilm: development and therapeutic strategies. *J Appl Microbiol*. 2016. doi:10.1111/jam.13078

43. Reisner A, Maierl M, Jörger M, et al. Type 1 fimbriae contribute to catheter-associated urinary tract infections caused by Escherichia coli. *J Bacteriol*. 2014. doi:10.1128/JB.00985-13

44. Markova JA, Anganova E V., Turskaya AL, Bybin VA, Savilov ED. Regulation of Escherichia coli Biofilm Formation (Review). *Appl Biochem Microbiol*. 2018. doi:10.1134/S0003683818010040

45. Beloin C, Roux A, Ghigo JM. Escherichia coli biofilms. *Curr Top Microbiol Immunol*. 2008. doi:10.1007/978-3-540-75418-3_12

46. Vidal O, Longin R, Prigent-Combaret C, Dorel C, Hooreman M, Lejeune P. Isolation of an Escherichia coli K-12 mutant strain able to form biofilms on inert surfaces: Involvement of a new ompR allele that increases curli expression. *J Bacteriol*. 1998.

47. Barnhart MM, Chapman MR. Curli Biogenesis and Function. *Annu Rev Microbiol*. 2006. doi:10.1146/annurev.micro.60.080805.142106

48. Römling U, Sierralta WD, Eriksson K, Normark S. Multicellular and aggregative behaviour of Salmonella typhimurium strains is controlled by mutations in the agfD promoter. *Mol Microbiol*. 1998. doi:10.1046/j.1365-2958.1998.00791.x

49. Danese PN, Pratt LA, Dove SL, Kolter R. The outer membrane protein, Antigen 43, mediates cell-to-cell interactions within Escherichia coli biofilms. *Mol Microbiol*. 2000. doi:10.1046/j.1365-2958.2000.02008.x

50. Hufnagel DA, Depas WH, Chapman MR. The Biology of the Escherichia coli Extracellular Matrix. *Microbiol Spectr*. 2015. doi:10.1128/microbiolspec.mb-0014-2014

51. Shi W, Sun H. Type IV pilus-dependent motility and its possible role in bacterial pathogenesis. *Infect Immun*. 2002. doi:10.1128/IAI.70.1.1-4.2002

52. Wang X, Preston JF, Romeo T. The pgaABCD Locus of Escherichia coli Promotes the Synthesis of a Polysaccharide Adhesin Required for Biofilm Formation. *J Bacteriol*. 2004. doi:10.1128/JB.186.9.2724-2734.2004

53. Leech J, Golub S, Allan W, Simmons MJH, Overton TW. Non-pathogenic Escherichia coli biofilms: effects of growth conditions and surface properties on structure and curli gene expression. *Arch Microbiol*. 2020. doi:10.1007/s00203-020-01864-5

54. Serra DO, Richter AM, Hengge R. Cellulose as an architectural element in spatially structured escherichia coli biofilms. *J Bacteriol*. 2013. doi:10.1128/JB.00946-13

55. Hung DL, Raivio TL, Jones CH, Silhavy TJ, Hultgren SJ. Cpx signaling pathway monitors biogenesis and affects assembly and expression of P pili. *EMBO J*. 2001. doi:10.1093/emboj/20.7.1508

56. Ferrières L, Clarke DJ. The RcsC sensor kinase is required for normal biofilm formation in Escherichia coli K-12 and controls the expression of a regulon in response to growth on a solid surface. *Mol Microbiol*. 2003. doi:10.1046/j.1365-2958.2003.03815.x

57. Laverty G, Gorman SP, Gilmore BF. Biomolecular mechanisms of Pseudomonas aeruginosa and Escherichia coli biofilm formation. *Pathogens*. 2014. doi:10.3390/pathogens3030596

58. Prigent-Combaret C, Brombacher E, Vidal O, et al. Complex regulatory network controls initial adhesion and biofilm formation in Escherichia coli via regulation of the csgD gene. *J Bacteriol*. 2001. doi:10.1128/JB.183.24.7213-7223.2001

59. Kim J, Park W. Indole: a signaling molecule or a mere metabolic byproduct that alters bacterial physiology at a high concentration? *J Microbiol*. 2015. doi:10.1007/s12275-015-5273-3

60. Banerjee I, Pangule RC, Kane RS. Antifouling coatings: Recent developments in the design of surfaces that prevent fouling by proteins, bacteria, and marine organisms. *Adv Mater*. 2011. doi:10.1002/adma.201001215

61. van Oss CJ. Acid-base interfacial interactions in aqueous media. *Colloids Surfaces A Physicochem Eng Asp*. 1993. doi:10.1016/0927-7757(93)80308-2

62. Hermansson M. The DLVO theory in microbial adhesion. *Colloids Surfaces B Biointerfaces*. 1999. doi:10.1016/S0927-7765(99)00029-6

63. Bellon-Fontaine MN, Mozes N, van der Mei HC, et al. A comparison of

thermodynamic approaches to predict the adhesion of dairy microorganisms to solid substrata. *Cell Biophys*. 1990. doi:10.1007/BF02989805

64. What is Surface Energy? Calculation Models and More Explained | Ossila. https://www.ossila.com/pages/a-guide-to-surface-energy. Accessed January 6, 2021.

65. Hori K, Matsumoto S. Bacterial adhesion: From mechanism to control. *Biochem Eng J*. 2010. doi:10.1016/j.bej.2009.11.014

66. Soni KA, Balasubramanian AK, Beskok A, Pillai SD. Zeta potential of selected bacteria in drinking water when dead, starved, or exposed to minimal and rich culture media. *Curr Microbiol*. 2008. doi:10.1007/s00284-007-9046-z

67. Katsikogianni MG, Missirlis YF. Interactions of bacteria with specific biomaterial surface chemistries under flow conditions. *Acta Biomater*. 2010. doi:10.1016/j.actbio.2009.08.006

68. Cheng Y, Feng G, Moraru CI. Micro-and nanotopography sensitive bacterial attachment mechanisms: A review. *Front Microbiol*. 2019. doi:10.3389/fmicb.2019.00191

69. Bunt CR, Jones DS, Tucker IG. The effects of pH, ionic strength and polyvalent ions on the cell surface hydrophobicity of Escherichia coli evaluated by the BATH and HIC methods. *Int J Pharm*. 1995. doi:10.1016/0378-5173(94)00205-J

70. Vigeant MAS, Ford RM. Interactions between motile Escherichia coli and glass in media with various ionic strengths, as observed with a three-dimensional-tracking microscope. *Appl Environ Microbiol*. 1997. doi:10.1128/aem.63.9.3474-3479.1997

71. Nguyen VT, Chia TWR, Turner MS, Fegan N, Dykes GA. Quantification of acid-base interactions based on contact angle measurement allows XDLVO predictions to attachment of Campylobacter jejuni but not Salmonella. *J Microbiol Methods*. 2011.

doi:10.1016/j.mimet.2011.04.005

72. Missirlis YF, Katsikogianni M. Theoretical and experimental approaches of bacteria-biomaterial interactions. *Materwiss Werksttech*. 2007. doi:10.1002/mawe.200700240

73. Bos R. Physico-chemistry of initial microbial adhesive interactions – its mechanisms and methods for study. *FEMS Microbiol Rev*. 1999;23(2):179-229. doi:10.1016/S0168-6445(99)00004-2

74. Van Oss CJ. Long-range and short-range mechanisms of hydrophobic attraction and hydrophilic repulsion in specific and aspecific interactions. *J Mol Recognit*. 2003. doi:10.1002/jmr.618

75. Ong YL, Razatos A, Georgiou G, Sharma MM. Adhesion forces between E. coli bacteria and biomaterial surfaces. *Langmuir*. 1999. doi:10.1021/la981104e

76. Bollen CM, Lambrechts P, Quirynen M. Comparison of surface roughness of oral hard materials to the threshold surface roughness for bacterial plaque retention: a review of the literature. *Dent Mater*. 1997. doi:10.1016/s0109-5641(97)80038-3

77. Hoek EMV, Agarwal GK. Extended DLVO interactions between spherical particles and rough surfaces. *J Colloid Interface Sci*. 2006. doi:10.1016/j.jcis.2005.12.031

78. Hoek EMV, Bhattacharjee S, Elimelech M. Effect of membrane surface roughness on colloid-membrane DLVO interactions. *Langmuir*. 2003. doi:10.1021/la027083c

79. Feng G, Cheng Y, Wang SY, et al. Alumina surfaces with nanoscale topography reduce attachment and biofilm formation by Escherichia coli and Listeria spp. *Biofouling*. 2014. doi:10.1080/08927014.2014.976561

80. Martines E, Csaderova L, Morgan H, Curtis ASG, Riehle MO. DLVO interaction energy between a sphere and a nano-patterned plate. *Colloids Surfaces A Physicochem Eng Asp*. 2008. doi:10.1016/j.colsurfa.2007.11.035

81. Wenzel RN. Resistance of solid surfaces to wetting by water. *Ind Eng Chem*. 1936. doi:10.1021/ie50320a024

82. Chunbo R, Guqiao D, Weichang L, Yan D, Wentao H. Wetting on nanoporous alumina surface: Transition between Wenzel and Cassie states controlled by surface structure. *Langmuir*. 2008. doi:10.1021/la801461j

83. Nguyen DHK, Pham VTH, Truong VK, et al. Role of topological scale in the differential fouling of: Pseudomonas aeruginosa and Staphylococcus aureus bacterial cells on wrinkled gold-coated polystyrene surfaces. *Nanoscale*. 2018. doi:10.1039/c7nr08178b

84. Halder P, Nasabi M, Lopez FJT, et al. A novel approach to determine the efficacy of patterned surfaces for biofouling control in relation to its microfluidic environment. *Biofouling*. 2013. doi:10.1080/08927014.2013.800192

85. Lee YK, Won YJ, Yoo JH, Ahn KH, Lee CH. Flow analysis and fouling on the patterned membrane surface. *J Memb Sci*. 2013. doi:10.1016/j.memsci.2012.10.010

86. Bakker DP, Busscher HJ, van Zanten J, de Vries J, Klijnstra JW, van der Mei HC. Multiple linear regression analysis of bacterial deposition to polyurethane coatings after conditioning film formation in the marine environment. *Microbiology*. 2004. doi:10.1099/mic.0.26983-0

87. Anselme K, Davidson P, Popa AM, Giazzon M, Liley M, Ploux L. The interaction of cells and bacteria with surfaces structured at the nanometre scale. *Acta Biomater*. 2010. doi:10.1016/j.actbio.2010.04.001

88. Jeon SI, Lee JH, Andrade JD, De Gennes PG. Protein-surface interactions in the presence of polyethylene oxide. I. Simplified theory. *J Colloid Interface Sci*. 1991. doi:10.1016/0021-9797(91)90043-8

89. Cheng G, Xue H, Zhang Z, Chen S, Jiang S. A switchable biocompatible polymer surface with self-sterilizing and nonfouling capabilities. *Angew Chemie - Int Ed*. 2008. doi:10.1002/anie.200803570

90. Prime KL, Whitesides GM. Self-assembled organic monolayers: Model systems for studying adsorption of proteins at surfaces. *Science (80-)*. 1991. doi:10.1126/science.252.5009.1164

91. Chelmowski R, Köster SD, Kerstan A, et al. Peptide-based SAMs that resist the adsorption of proteins. *J Am Chem Soc*. 2008. doi:10.1021/ja8065754

92. Siegers C, Biesalski M, Haag R. Self-assembled monolayers of dendritic polyglycerol derivatives on gold that resist the adsorption of proteins. *Chem - A Eur J*. 2004. doi:10.1002/chem.200306073

93. Ulman A. Formation and structure of self-assembled monolayers. *Chem Rev*. 1996. doi:10.1021/cr9502357

94. Burton EA, Simon KA, Hou S, Ren D, Luk YY. Molecular gradients of bioinertness reveal a mechanistic difference between mammalian cell adhesion and bacterial biofilm formation. *Langmuir*. 2009. doi:10.1021/la803261b

95. Lee SB, Koepsel RR, Morley SW, Matyjaszewski K, Sun Y, Russell AJ. Permanent, nonleaching antibacterial surfaces, 1. Synthesis by atom transfer radical polymerization. *Biomacromolecules*. 2004. doi:10.1021/bm034352k

96. Kawabata N, Inoue T, Tomita H. Removal of micro-organisms by filtration through unwoven cloth coated with a pyridinium-type polymer. *Epidemiol Infect*. 1992. doi:10.1017/S0950268800049578

97. Gottenbos B, Van Der Mei HC, Klatter F, Nieuwenhuis P, Busscher HJ. In vitro and in vivo antimicrobial activity of covalently coupled quaternary ammonium silane

coatings on silicone rubber. *Biomaterials*. 2002. doi:10.1016/S0142-9612(01)00263-0

98. Tiller JC, Liao CJ, Lewis K, Klibanov AM. Designing surfaces that kill bacteria on contact. *Proc Natl Acad Sci U S A*. 2001. doi:10.1073/pnas.111143098

99. Lewis AL. Phosphorylcholine-based polymers and their use in the prevention of biofouling. *Colloids Surfaces B Biointerfaces*. 2000. doi:10.1016/S0927-7765(99)00152-6

100. Hirota K, Murakami K, Nemoto K, Miyake Y. Coating of a surface with 2-methacryloyloxyethyl phosphorylcholine (MPC) co-polymer significantly reduces retention of human pathogenic microorganisms. *FEMS Microbiol Lett*. 2005. doi:10.1016/j.femsle.2005.05.019

101. Absolom DR, Lamberti F V., Policova Z, Zingg W, van Oss CJ, Neumann AW. Surface thermodynamics of bacterial adhesion. *Appl Environ Microbiol*. 1983. doi:10.1128/aem.46.1.90-97.1983

102. Cao Z, Mi L, Mendiola J, et al. Reversibly switching the function of a surface between attacking and defending against bacteria. *Angew Chemie - Int Ed*. 2012. doi:10.1002/anie.201106466

103. Strand SP, Vårum KM, Østgaard K. Interactions between chitosans and bacterial suspensions: Adsorption and flocculation. *Colloids Surfaces B Biointerfaces*. 2003. doi:10.1016/S0927-7765(02)00043-7

104. Flocculation | Theory and Background. https://www.mt.com/gb/en/home/applications/L1_AutoChem_Applications/L2_ParticleProcessing/Formulation_Flocculation.html. Accessed January 19, 2021.

105. Schwarz-Linek J, Dorken G, Winkler A, et al. Polymer-induced phase separation in suspensions of bacteria. *EPL*. 2010. doi:10.1209/0295-5075/89/68003

106. Secor PR, Michaels LA, Ratjen A, Jennings LK, Singh PK. Entropically driven aggregation of bacteria by host polymers promotes antibiotic tolerance in Pseudomonas aeruginosa. *Proc Natl Acad Sci U S A*. 2018. doi:10.1073/pnas.1806005115

107. Ashmore M, Hearn J. Flocculation of model latex particles by chitosans of varying degrees of acetylation. *Langmuir*. 2000. doi:10.1021/la991648w

108. Strand SP, Vandvik MS, Vårum KM, Østgaard K. Screening of chitosans and conditions for bacterial flocculation. *Biomacromolecules*. 2001. doi:10.1021/bm005601x

109. Yang Y, Cai Z, Huang Z, Tang X, Zhang X. Antimicrobial cationic polymers: From structural design to functional control. *Polym J*. 2018. doi:10.1038/pj.2017.72

110. Ganewatta MS, Tang C. Controlling macromolecular structures towards effective antimicrobial polymers. *Polymer (Guildf)*. 2015. doi:10.1016/j.polymer.2015.03.007

111. Krachler AM, Orth K. Targeting the bacteria-host interface strategies in anti-adhesion therapy. *Virulence*. 2013. doi:10.4161/viru.24606

112. Perez-Soto N, Moule L, Crisan DN, et al. Engineering microbial physiology with synthetic polymers: Cationic polymers induce biofilm formation in: Vibrio cholerae and downregulate the expression of virulence genes. *Chem Sci*. 2017. doi:10.1039/c7sc00615b

113. Foster LL, Yusa SI, Kuroda K. Solution-mediated modulation of pseudomonas aeruginosa biofilm formation by a cationic synthetic polymer. *Antibiotics*. 2019. doi:10.3390/antibiotics8020061

114. Pernagallo S, Wu M, Gallagher MP, Bradley M. Colonising new frontiers - Microarrays reveal biofilm modulating polymers. *J Mater Chem*. 2011. doi:10.1039/c0jm01987a

115. Yuan H, Liu Z, Liu L, Lv F, Wang Y, Wang S. Cationic conjugated polymers for

discrimination of microbial pathogens. *Adv Mater*. 2014. doi:10.1002/adma.201400636

116. Magennis EP, Fernandez-Trillo F, Sui C, et al. Bacteria-instructed synthesis of polymers for self-selective microbial binding and labelling. *Nat Mater*. 2014. doi:10.1038/nmat3949

117. Disney MD, Zheng J, Swager TM, Seeberger PH. Detection of bacteria with carbohydrate-functionalized fluorescent polymers. *J Am Chem Soc*. 2004. doi:10.1021/ja047936i

118. Xue C, Velayudham S, Johnson S, et al. Highly water-soluble, fluorescent, conjugated fluorene-based glycopolymers with poly(ethylene glycol)-tethered spacers for sensitive detection of escherichia coli. *Chem - A Eur J*. 2009. doi:10.1002/chem.200801875

119. Phillips RL, Kim IB, Carson BE, et al. Sugar-substituted poly(p-phenyleneethynylene)s: Sensitivity enhancement toward lectins and bacteria. *Macromolecules*. 2008. doi:10.1021/ma8016025

120. Wang L, Pu KY, Li J, et al. A graphene-conjugated oligomer hybrid probe for light-up sensing of lectin and Escherichia coli. *Adv Mater*. 2011. doi:10.1002/adma.201102227

121. Miller MB, Bassler BL. Quorum sensing in bacteria. *Annu Rev Microbiol*. 2001. doi:10.1146/annurev.micro.55.1.165

122. Xue X, Pasparakis G, Halliday N, et al. Synthetic polymers for simultaneous bacterial sequestration and quorum sense interference. *Angew Chemie - Int Ed*. 2011. doi:10.1002/anie.201103130

123. Piletska E V., Stavroulakis G, Karim K, et al. Attenuation of vibrio fischeri quorum sensing using rationally designed polymers. *Biomacromolecules*. 2010.

doi:10.1021/bm901451j

124. Zhang P, Lu H, Chen H, et al. Cationic Conjugated Polymers-Induced Quorum Sensing of Bacteria Cells. *Anal Chem*. 2016. doi:10.1021/acs.analchem.5b03920

125. Perez-Soto N, Creese O, Fernandez-Trillo F, Krachler AM. Aggregation of Vibrio cholerae by Cationic Polymers Enhances Quorum Sensing but Overrides Biofilm Dissipation in Response to Autoinduction. *ACS Chem Biol*. 2018. doi:10.1021/acschembio.8b00815

126. Qin X, Emich J, Goycoolea FM. Assessment of the quorum sensing inhibition activity of a non-toxic chitosan in an N-Acyl homoserine lactone (AHL)-based Escherichia coli biosensor. *Biomolecules*. 2018. doi:10.3390/biom8030087

127. Tsoligkas AN, Winn M, Bowen J, Overton TW, Simmons MJH, Goss RJM. Engineering Biofilms for Biocatalysis. *ChemBioChem*. 2011. doi:10.1002/cbic.201100200

128. Qureshi N, Annous BA, Ezeji TC, Karcher P, Maddox IS. Biofilm reactors for industrial bioconversion process: Employing potential of enhanced reaction rates. *Microb Cell Fact*. 2005. doi:10.1186/1475-2859-4-24

129. Angelaalincy MJ, Navanietha Krishnaraj R, Shakambari G, Ashokkumar B, Kathiresan S, Varalakshmi P. Biofilm Engineering Approaches for Improving the Performance of Microbial Fuel Cells and Bioelectrochemical Systems. *Front Energy Res*. 2018. doi:10.3389/fenrg.2018.00063

130. Edwards SJ, Kjellerup B V. Applications of biofilms in bioremediation and biotransformation of persistent organic pollutants, pharmaceuticals/personal care products, and heavy metals. *Appl Microbiol Biotechnol*. 2013. doi:10.1007/s00253-013-5216-z

131. Von Canstein H, Kelly S, Li Y, Wagner-Döbler I. Species diversity improves the

efficiency of mercury-reducing biofilms under changing environmental conditions. *Appl Environ Microbiol*. 2002. doi:10.1128/AEM.68.6.2829-2837.2002

132. Roots O, Roose A, Kull A, Holoubek I, Cupr P, Klanova J. Distribution pattern of PCBs, HCB and PeCB using passive air and soil sampling in Estonia. *Environ Sci Pollut Res*. 2010. doi:10.1007/s11356-009-0147-z

133. Lammel G, Lohmann R. Identifying the research needs in the global assessment of toxic compounds 10 years after the signature of the Stockholm Convention. *Environ Sci Pollut Res*. 2012. doi:10.1007/s11356-012-0967-0

134. Johnsen AR, Karlson U. Evaluation of bacterial strategies to promote the bioavailability of polycyclic aromatic hydrocarbons. *Appl Microbiol Biotechnol*. 2004. doi:10.1007/s00253-003-1265-z

135. Volkering F, Breure AM, Sterkenburg A, van Andel JG. Microbial degradation of polycyclic aromatic hydrocarbons: effect of substrate availability on bacterial growth kinetics. *Appl Microbiol Biotechnol*. 1992. doi:10.1007/BF00170201

136. Harms H, Bosma TNP. Mass transfer limitation of microbial growth and pollutant degradation. *J Ind Microbiol Biotechnol*. 1997. doi:10.1038/sj.jim.2900259

137. Déziel É, Paquette G, Villemur R, Lépine F, Bisaillon JG. Biosurfactant production by a soil Pseudomonas strain growing on polycyclic aromatic hydrocarbons. *Appl Environ Microbiol*. 1996. doi:10.1128/aem.62.6.1908-1912.1996

138. Willumsen PA, Karlson U. Screening of bacteria, isolated from PAH-contaminated soils, for production of biosurfactants and bioemulsifiers. *Biodegradation*. 1996. doi:10.1007/bf00056425

139. Löffler FE, Ritalahti KM, Zinder SH. Dehalococcoides and Reductive Dechlorination of Chlorinated Solvents. In: *Bioaugmentation for Groundwater Remediation*. ; 2013.

doi:10.1007/978-1-4614-4115-1_2

140. Chung J, Krajmalnik-Brown R, Rittmann BE. Bioreduction of trichloroethene using a hydrogen-based membrane biofilm reactor. *Environ Sci Technol*. 2008. doi:10.1021/es702422d

141. Fagervold SK, Watts JEM, May HD, Sowers KR. Sequential reductive dechlorination of meta-chlorinated polychlorinated biphenyl congeners in sediment microcosms by two different Chloroflexi phylotypes. *Appl Environ Microbiol*. 2005. doi:10.1128/AEM.71.12.8085-8090.2005

142. Macedo AJ, Kuhlicke U, Neu TR, Timmis KN, Abraham WR. Three stages of a biofilm community developing at the liquid-liquid interface between polychlorinated biphenyls and water. *Appl Environ Microbiol*. 2005. doi:10.1128/AEM.71.11.7301-7309.2005

143. Onesios KM, Bouwer EJ. Biological removal of pharmaceuticals and personal care products during laboratory soil aquifer treatment simulation with different primary substrate concentrations. *Water Res*. 2012. doi:10.1016/j.watres.2012.02.001

144. Mulligan CN, Yong RN, Gibbs BF. An evaluation of technologies for the heavy metal remediation of dredged sediments. *J Hazard Mater*. 2001. doi:10.1016/S0304-3894(01)00226-6

145. Kwon YT, Lee CW. Application of multiple ecological risk indices for the evaluation of heavy metal contamination in a coastal dredging area. *Sci Total Environ*. 1998. doi:10.1016/S0048-9697(98)00069-2

146. Diels L, Spaans PH, Van Roy S, et al. Heavy metals removal by sand filters inoculated with metal sorbing and precipitating bacteria. In: *Hydrometallurgy*. ; 2003. doi:10.1016/S0304-386X(03)00161-0

147. Wood TL, Guha R, Tang L, Geitner M, Kumar M, Wood TK. Living biofouling-resistant membranes as a model for the beneficial use of engineered biofilms. *Proc Natl Acad Sci U S A*. 2016. doi:10.1073/pnas.1521731113

148. Williams P, Cámara M. Quorum sensing and environmental adaptation in Pseudomonas aeruginosa: a tale of regulatory networks and multifunctional signal molecules. *Curr Opin Microbiol*. 2009. doi:10.1016/j.mib.2009.01.005

149. Hengge R. Principles of c-di-GMP signalling in bacteria. *Nat Rev Microbiol*. 2009. doi:10.1038/nrmicro2109

150. Mukherjee M, Cao B. Engineering controllable biofilms for biotechnological applications. *Microb Biotechnol*. 2020. doi:10.1111/1751-7915.13715

151. Wu Y, Ding Y, Cohen Y, Cao B. Elevated level of the second messenger c-di-GMP in Comamonas testosteroni enhances biofilm formation and biofilm-based biodegradation of 3-chloroaniline. *Appl Microbiol Biotechnol*. 2015. doi:10.1007/s00253-014-6107-7

152. Mukherjee M, Hu Y, Tan CH, Rice SA, Cao B. Engineering a light-responsive, quorum quenching biofilm to mitigate biofouling on water purification membranes. *Sci Adv*. 2018. doi:10.1126/sciadv.aau1459

153. Read ST, Dutta P, Bond PL, Keller J, Rabaey K. Initial development and structure of biofilms on microbial fuel cell anodes. *BMC Microbiol*. 2010. doi:10.1186/1471-2180-10-98

154. Holmes DE, Bond DR, Lovley DR. Electron Transfer by Desulfobulbus propionicus to Fe(III) and Graphite Electrodes. *Appl Environ Microbiol*. 2004. doi:10.1128/AEM.70.2.1234-1237.2004

155. Gorby YA, Yanina S, McLean JS, et al. Electrically conductive bacterial nanowires

produced by Shewanella oneidensis strain MR-1 and other microorganisms. *Proc Natl Acad Sci U S A*. 2006. doi:10.1073/pnas.0604517103

156. Rabaey K, Boon N, Höfte M, Verstraete W. Microbial phenazine production enhances electron transfer in biofuel cells. *Environ Sci Technol*. 2005. doi:10.1021/es048563o

157. Gatti MN, Milocco RH. A biofilm model of microbial fuel cells for engineering applications. *Int J Energy Environ Eng*. 2017. doi:10.1007/s40095-017-0249-1

158. Heijnen JJ, Kleerebezem R. Bioenergetics of microbial growth. *Encycl Ind Biotechnol Bioprocess, Biosep Cell Technol*. 1999.

159. Todhanakasem T. Developing microbial biofilm as a robust biocatalyst and its challenges. *Biocatal Biotransformation*. 2017. doi:10.1080/10242422.2017.1295230

160. Cheng KC, Demirci A, Catchmark JM. Advances in biofilm reactors for production of value-added products. *Appl Microbiol Biotechnol*. 2010. doi:10.1007/s00253-010-2622-3

161. Costerton JW. Overview of microbial biofilms. *J Ind Microbiol*. 1995. doi:10.1007/BF01569816

162. de Beer D, Stoodley P, Roe F, Lewandowski Z. Effects of biofilm structures on oxygen distribution and mass transport. *Biotechnol Bioeng*. 1994. doi:10.1002/bit.260431118

163. Mohan SV, Mohanakrishna G, Veer Raghavulu S, Sarma PN. Enhancing biohydrogen production from chemical wastewater treatment in anaerobic sequencing batch biofilm reactor (AnSBBR) by bioaugmenting with selectively enriched kanamycin resistant anaerobic mixed consortia. *Int J Hydrogen Energy*. 2007. doi:10.1016/j.ijhydene.2007.04.043

164. Mu Y, Wang G, Yu HQ. Kinetic modeling of batch hydrogen production process by mixed anaerobic cultures. *Bioresour Technol*. 2006.

doi:10.1016/j.biortech.2005.05.014

165. Weuster-Botz D, Aivasidis A, Wandrey C. Continuous ethanol production by Zymomonas mobilis in a fluidized bed reactor. Part II: Process development for the fermentation of hydrolysed B-starch without sterilization. *Appl Microbiol Biotechnol*. 1993. doi:10.1007/BF00164450

166. Reddy Kunduru M, Pometto AL. Continuous ethanol production by Zymomonas mobilis and Saccharomyces cerevisiae in biofilm reactors. *J Ind Microbiol*. 1996. doi:10.1007/BF01570029

167. Todhanakasem T, Narkmit T, Areerat K, Thanonkeo P. Fermentation of rice bran hydrolysate to ethanol using Zymomonas mobilis biofilm immobilization on DEAE-cellulose. *Electron J Biotechnol*. 2015. doi:10.1016/j.ejbt.2015.03.007

168. Panizza M. Fine chemical industry, pulp and paper industry, petrochemical industry and pharmaceutical industry. In: *Electrochemical Water and Wastewater Treatment*. ; 2018. doi:10.1016/B978-0-12-813160-2.00013-4

169. Li XZ, Webb JS, Kjelleberg S, Rosche B. Enhanced benzaldehyde tolerance in Zymomonas mobilis biofilms and the potential of biofilm applications in fine-chemical production. *Appl Environ Microbiol*. 2006. doi:10.1128/AEM.72.2.1639-1644.2006

170. Gross R, Hauer B, Otto K, Schmid A. Microbial biofilms: New catalysts for maximizing productivity of long-term biotransformations. *Biotechnol Bioeng*. 2007. doi:10.1002/bit.21547

171. Zhou B, Martin GJO, Pamment NB. Increased phenotypic stability and ethanol tolerance of recombinant Escherichia coli K011 when immobilized in continuous fluidized bed culture. *Biotechnol Bioeng*. 2008. doi:10.1002/bit.21800

172. Zaldivar J, Nielsen J, Olsson L. Fuel ethanol production from lignocellulose: A

challenge for metabolic engineering and process integration. *Appl Microbiol Biotechnol*. 2001. doi:10.1007/s002530100624

173. Ohta K, Beall DS, Mejia JP, Shanmugam KT, Ingram LO. Genetic improvement of Escherichia coli for ethanol production: Chromosomal integration of Zymomonas mobilis genes encoding pyruvate decarboxylase and alcohol dehydrogenase II. *Appl Environ Microbiol*. 1991. doi:10.1128/aem.57.4.893-900.1991

174. Setyawati MI, Chien LJ, Lee CK. Self-immobilized recombinant Acetobacter xylinum for biotransformation. *Biochem Eng J*. 2009. doi:10.1016/j.bej.2008.09.002

175. Song Y, Li J, Shin H dong, Liu L, Du G, Chen J. Biotechnological production of alpha-keto acids: Current status and perspectives. *Bioresour Technol*. 2016. doi:10.1016/j.biortech.2016.08.015

176. Winn M, Foulkes JM, Perni S, Simmons MJH, Overton TW, Goss RJM. Biofilms and their engineered counterparts: A new generation of immobilised biocatalysts. *Catal Sci Technol*. 2012. doi:10.1039/c2cy20085f

177. Tong X, Barberi TT, Botting CH, et al. Rapid enzyme regeneration results in the striking catalytic longevity of an engineered, single species, biocatalytic biofilm. *Microb Cell Fact*. 2016. doi:10.1186/s12934-016-0579-3

178. Hu Y, Liu X, Ren ATM, Gu JD, Cao B. Optogenetic Modulation of a Catalytic Biofilm for the Biotransformation of Indole into Tryptophan. *ChemSusChem*. 2019. doi:10.1002/cssc.201902413

179. Benedetti I, de Lorenzo V, Nikel PI. Genetic programming of catalytic Pseudomonas putida biofilms for boosting biodegradation of haloalkanes. *Metab Eng*. 2016. doi:10.1016/j.ymben.2015.11.004

180. Schaffner M, Rühs PA, Coulter F, Kilcher S, Studart AR. 3D printing of bacteria into

functional complex materials. *Sci Adv*. 2017. doi:10.1126/sciadv.aao6804

181. Balasubramanian S, Aubin-Tam ME, Meyer AS. 3D Printing for the Fabrication of Biofilm-Based Functional Living Materials. *ACS Synth Biol*. 2019. doi:10.1021/acssynbio.9b00192

182. Lehner BAE, Schmieden DT, Meyer AS. A Straightforward Approach for 3D Bacterial Printing. *ACS Synth Biol*. 2017. doi:10.1021/acssynbio.6b00395

183. Huang J, Liu S, Zhang C, et al. Programmable and printable Bacillus subtilis biofilms as engineered living materials. *Nat Chem Biol*. 2019. doi:10.1038/s41589-018-0169-2

184. Pines G, Freeman A. Immobilization and characterization of Saccharomyces cerevisiae in crosslinked, prepolymerized polyacrylamide-hydrazide. *Eur J Appl Microbiol Biotechnol*. 1982. doi:10.1007/BF00500730

Chapter 2 - Experimental procedures and background theory

Introduction

This project can be split into two main sections; RAFT mediated polymerisation of poly(acryloyl hydrazide) and its optimisation (chapter 3), and the use of functional poly(acryloyl hydrazide) polymers to induce functional biofilm formation in *E. coli* (Chapters 4 and 5). Hence the experimental techniques used in the project span the fields of polymer chemistry, microbiology and bioengineering. Due to the interdisciplinary nature of this project, it was decided to include this extended chapter primarily for the benefit of the reader which goes through and describes background theory related to the wide ranging techniques used, in an order that is reflective of the workflow of the project.

(a) Optimisation of boc-poly(acryloyl hydrazide) synthesis

The first part of the project involved the polymerisation synthesis and optimisation of the polymer scaffold to be used to interact with *E. coli*. A recently developed poly(acryloyl hydrazide) scaffold (pAH) was chosen due to its relatively easy synthesis and its ability for simple post polymerisation functionalisation with a wide range of biologically relevant aldehyde molecules, yielding a library of functional polymers that can be screened for biological applications in a high throughput manner e.g. with bacteria (figure 1)[1].

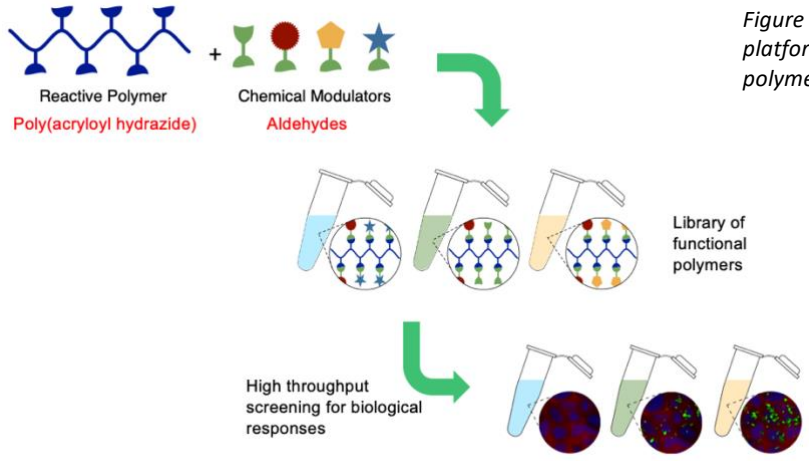

Figure 1: Poly(acryloyl hydrazide) provides a platform for the screening of functional polymers for biological applications

The polymer is synthesised via a mechanism known as reversible addition fragmentation polymerisation (RAFT), a technique which allows for the synthesis of polymers with defined molecular weight and low molar mass dispersity[2]. However upon the synthesis of high molecular weight poly(acryloyl hydrazide) polymers (≥ DP50), the level of control over the polymerisation is somewhat lost, possibly as a result of temperature dependant degradation of the RAFT agent through intramolecular nucleophilic attack from the growing polymer chains[3]. As such, the first experimental chapter of this thesis; Chapter 3 (which is presented in the form of a journal paper) describes the optimisation of poly(acryloyl hydrazide) RAFT polymerisation via the modulation of reaction temperature. Before this however and for the purposes of aiding the reader, this chapter will describe background theory relating to RAFT polymerisation, post-polymerisation functionalisation, and the subsequent polymer characterisation techniques that are based on nuclear magnetic resonance spectroscopy (NMR) and gel permeation chromatography (GPC). The overall reaction scheme toward the synthesis of functional poly(acryloyl hydrazide) polymers is shown in figure 2.

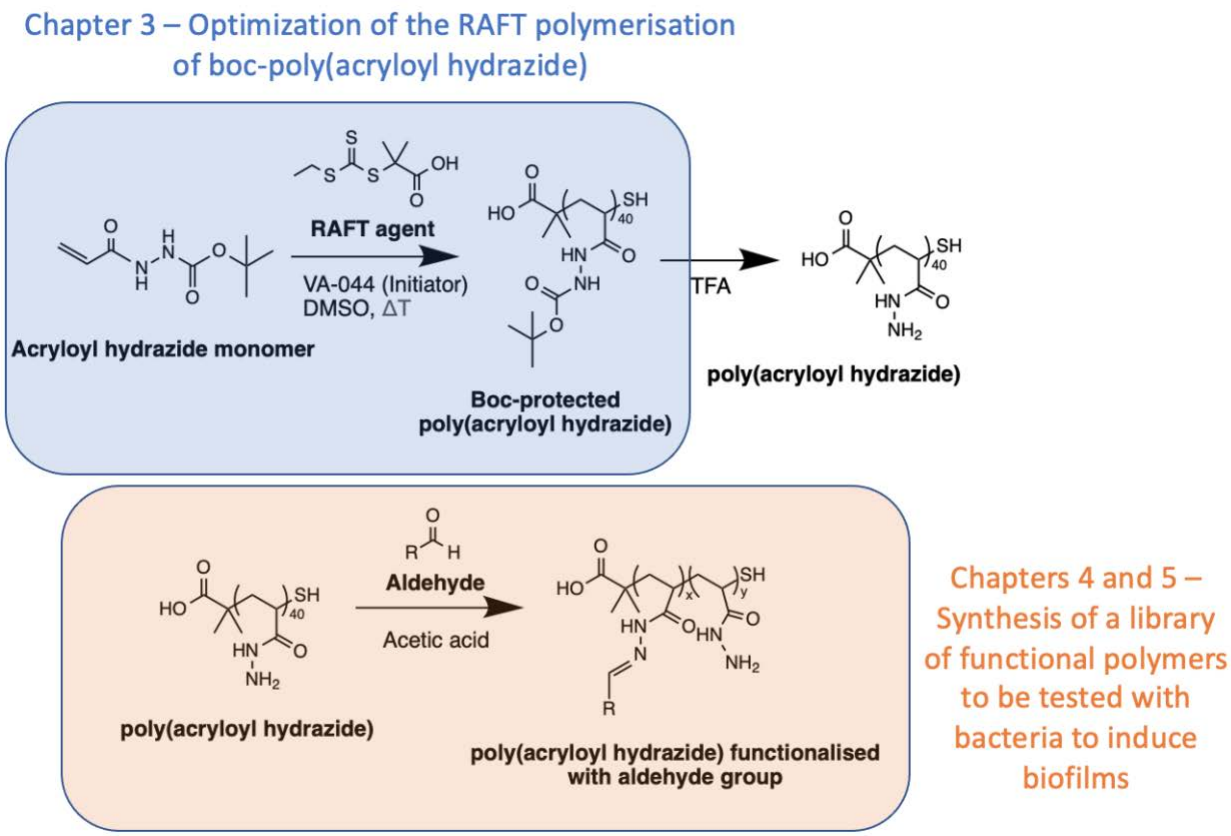

Figure 2: (a) Polymerisation of an acryloyl hydrazide monomer to yield a boc-poly(acryloyl hydrazide) which is then deprotected with TFA to yield poly(acryloyl hydrazide). (b) Post polymerisation functionalisation of poly(acryloyl hydrazide) to yield aldehyde functionalised polymers

(b) Use of functional poly(acryloyl) hydrazide polymers for modulating bacterial aggregation and subsequent biofilm formation

The second part of this project involved using the functional poly(acryloyl hydrazide) polymers to induce bacterial aggregation via non-specific physiochemical interactions, in the hope of subsequent polymer induced biofilm stimulation after incubation with minimal media. These polymer-induced aggregates/biofilms were then analysed using various biological techniques as shown in figure 3. This material will be covered in chapters 4 and 5 and the materials and methods section for this is presented in this chapter.

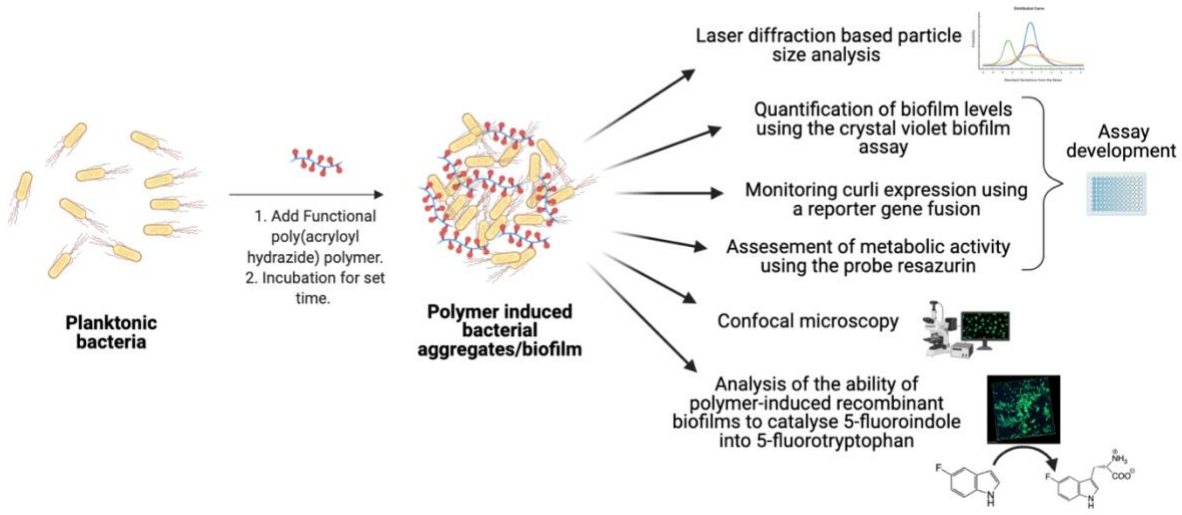

Figure 3: Chapters 4 and 5 involve the stimulation of polymer-induced biofilms using functional poly(acryloyl hydrazide) polymers. The subsequent biofilms are then analysed for biofilm expression and biofilm functionality using various techniques

(i) Background theory related to polymer synthesis and characterisation techniques

(a) Basic theory of RAFT polymerisation

The first stage of this project involved the optimisation of the synthesis of boc-poly(acryloyl hydrazide) (boc-pAH), using temperature control. Boc-pAH is synthesised relatively easily from a boc-protected acryloyl hydrazide monomer using reversible addition-fragmentation chain transfer (RAFT) polymerisation (figure 1). RAFT polymerisation is a type of reversible deactivation radical polymerisation (RDRP), also known as living or controlled radical polymerisation[2]. Polymerisation occurs through radical propagation whilst being controlled by reversible deactivation processes. Since its first reporting in by Moad, Rizzaro and Thang (1998)[4], RAFT has become a popular and versatile method in the controlled polymerisation of monomers yielding polymers of predictable molecular weight, low molar mass dispersities and high end group fidelity allowing for further controlled polymer chain growth if nessasary[2].

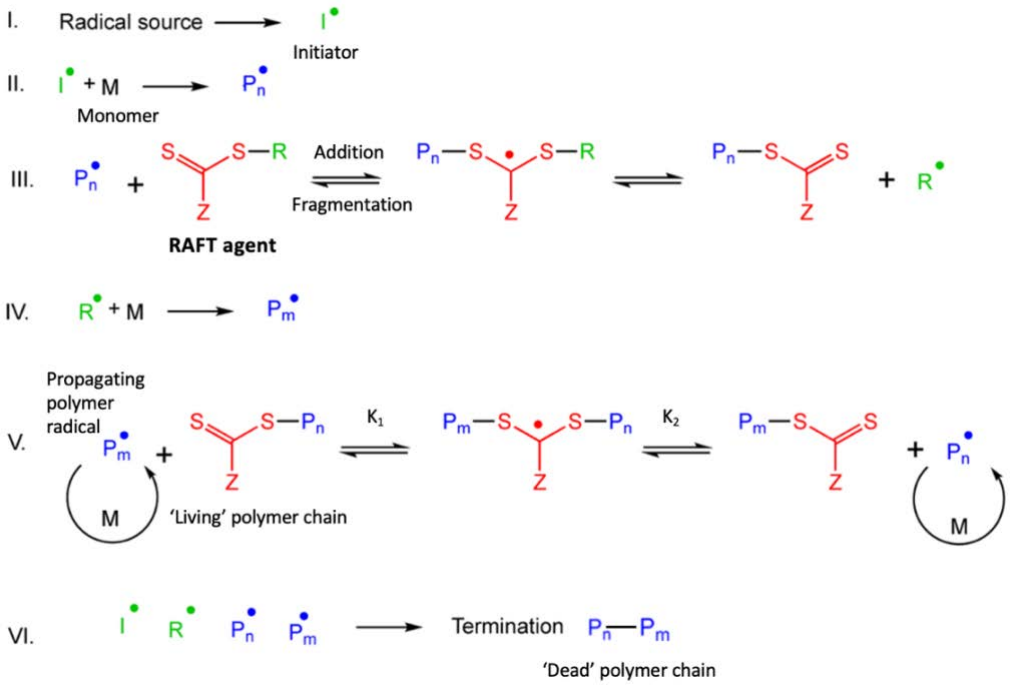

Figure 4: Mechanism of RAFT polymerisation, taken from Perrier (2017). Ref 2

The mechanism of the RAFT process is illustrated in figure 4 and consists of three main starting materials; an initiator (I), a monomer (M) and a RAFT agent as shown in figure 4. The RAFT agent takes the form Z−(C=S)-S−R, where the Z and R groups are tailored depending on the type of monomer to be used. The mechanism is as follows; firstly the initiator is activated by a specific source (e.g. heat, application of light etc) and splits into the active radicals (step 1, figure 4). The initiator radical $I^{\bullet}$ then reacts with the monomer, M to form the start of the propagating radical chain, $P_n^{\bullet}$ (step 2). The $P_n^{\bullet}$ radical then reacts with the RAFT agent which sets up the first addition-fragmentation equilibrium (step 3). Fragmentation of the RAFT agent leads to the production of another type of initiator radical, $R^{\bullet}$ which is then free to react with another monomer molecule forming the second propagating radical chain, $P_m^{\bullet}$ (step 4). This leads to the formation of the main addition-fragmentation equilibrium between the two propagating radical species, $Pn^{\bullet}$ and $Pm^{\bullet}$ (step 5). The rate of propagation (i.e. $P_n^{\bullet}$ or $P_m^{\bullet}$ + M of step 5) must be significantly slower than the rate of addition/fragmentation such that on average, less than one monomer is added to $P_n^{\bullet}$ or $P_m^{\bullet}$ during one addition fragmentation cycle. This allows for the controlled propagation of $P_n^{\bullet}$ and $P_m^{\bullet}$ meaning they will be of the same degree of polymerisation at any one time during the reaction, leading to final polymers of low molecular weight dispersities. The final step is the bimolecular termination process where $P_n^{\bullet}$ and $P_m^{\bullet}$ (ideally both the same size) attach to form the final polymer (step 6). The rate of termination should be significantly lower than the rate of propagation to prevent early termination of propagating radicals ($P_n^{\bullet}$ and $P_m^{\bullet}$) which leads to the formation of smaller final polymers, and an increase in polymer dispersity. In addition the amount of RAFT agent should be significantly higher than that of the initiator. If initiator concentrations are too high, then the concentration of propagating radicals also becomes very high leading to increasing early termination events.

Due to the highly controlled nature of RAFT polymerisation, it is possible to target polymers of a certain chain length by varying the molar ratio of monomer to RAFT agent. Suppose the initial molar ratio of monomer to RAFT agent is 50:1, it means that on average given that propagation goes to completion, the final $P_m^{\bullet}$ and $P_n^{\bullet}$ will be of chain length 25 per molecule of RAFT agent. Hence on bimolecular termination, the final polymer will be of chain length 50. Therefore the molar ratio of monomer to RAFT agent theoretically determines the targeted polymer chain length given that the polymerisation remains 'living' throughout – that is that the main addition-fragmentation stage 5 allows for the continual and controlled chain extension of the propagating chains via attachment to the RAFT agent, up until all the monomer molecules have ran out. Degradation of the RAFT agent mid reaction will lead to loss of the 'livingness' of the polymerisation and leads to the loss of control over chain length (leading to shorter polymers), resulting in the overall formation of polymers with high dispersities[2]. Degradation of the living RAFT agent has been reported in the polymerisation of acrylamides such as that of the boc-protected acryloyl hydrazide monomer used in the polymerisation of boc-poly(acryloyl hydrazide)[5]. Previous work on the synthesis of boc-poly(acryloyl hydrazide) polymers of different chain lengths showed that the polymerisation reaction did not go to completion and it was suspected that this was because of mid-reaction RAFT agent degradation[1]. The paper presented in chapter 3 describes the efforts towards minimising RAFT degradation during the polymerisation of boc-poly(acryloyl hydrazide), leading to an improved control over the polymerisation[3].

(b) Basic theory of Proton Nuclear Magnetic Resonance spectroscopy [6,7,8]

The primary characterisation technique used for the intermediates and the final polymers made in this project was proton nuclear magnetic resonance (^{1}H-NMR). ^{1}H-NMR works by measuring the magnetic properties of each hydrogen atom (or proton) within a molecule. Subatomic particles (protons, neutrons and to a lesser extent electrons) can be imagined as spinning on their axis, which causes them to act like a magnet, with their own magnetic field. When these subatomic particles are brought together into an atom, the relative spinning (and direction) of all the subatomic particles within the nucleus of the atom are summed. When an atom contains an even number of total protons and neutrons, the individual spins within the atom nucleus will all cancel each other out, such that the nucleus of the atom will not possess its own overall spin/magnetic field. In some cases however, when an atom contains an uneven number of protons and neutrons, the spins do not cancel and as such the nucleus of the atom will possess its own overall spin/magnetic field (e.g. in the case of ^{1}H and ^{13}C). When an additional external magnetic field is applied to a spinning ^{1}H nucleus (which possesses its own magnetic field) the energy level of the nucleus get split such that a proportion of nuclei will be aligned with the magnetic field (and of low energy) and a proportion that may absorb the correct and exact amount of energy required to jump to the higher energy level with spin aligned against the external magnetic field (figure 5).

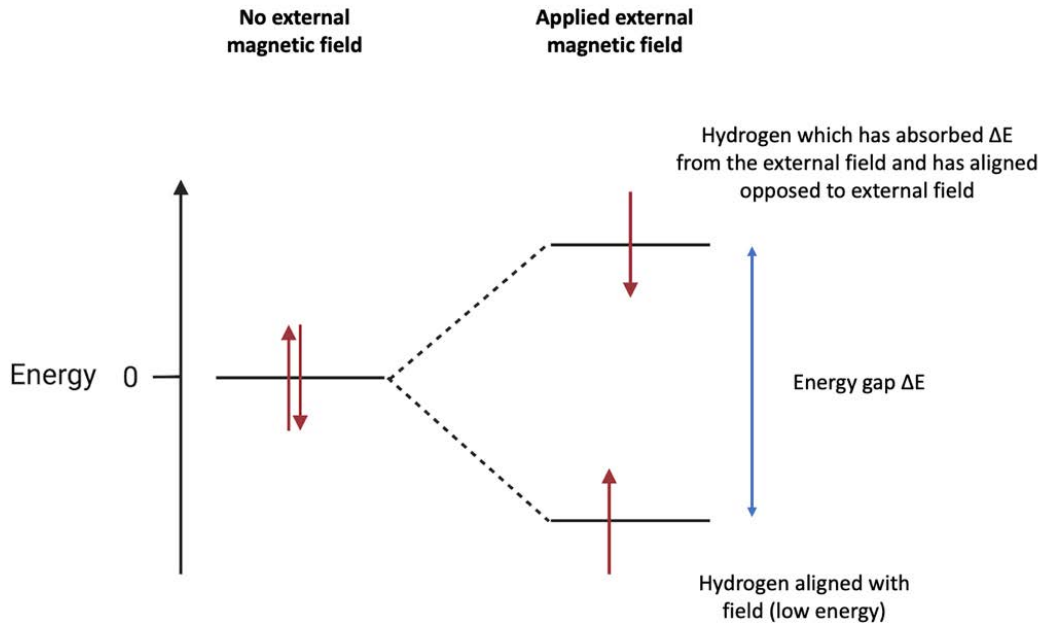

Figure 5: Energy levels for a hydrogen nucleus with and without an external magnetic field

It is important to note that hydrogen nuclei (protons) which are aligned to the field and of lower energy will only make the transition to the higher energy level if they absorb the exact amount of energy required to make this transition i.e. ΔE on figure 5, and these are usually similar energies to that of radio waves. It is possible to detect this interaction between the correct energy radio waves and the proton as it flips and moves against the external field (known as the resonance condition), and this is represented as a peak on an ^{1}H-NMR trace. So far, all this information corresponds to an isolated hydrogen but in reality, hydrogens within a molecule will be surrounded by electrons which actually serve to reduce the effect of an external magnetic field on the nucleus (known as a shield effect). Hence a hydrogen with a high density of electrons surrounding it will require a larger external magnetic field to make the jump to the higher energy level. In general, protons/hydrogens within a molecule will each be in slightly differing environments which depend on the slightly differing electron densities surrounding each proton. These differences mean that the resonance conditions of each proton/hydrogen will be slightly different, leading to separate peaks

corresponding to each hydrogen on a ^{1}H-NMR trace. For example, take two hydrogens bonded to different atoms, X and Y:

The positioning of the electrons within the bond will depend on the electronegativities of X and Y respectively. All atoms possess electronegativity, which is a measure of the tendency of an atom to attract electrons within a chemical bond. If Y is an electronegative atom, then the electrons within the Y-H bond will be closer in proximity to Y meaning that this hydrogen nucleus will feel an external magnetic field more so that the hydrogen bonded to X which is surrounded by a high density of electrons which reduce (or shield) the effect of the external magnetic field. Therefore the resonance energy required for X-H will be higher than that required for Y-H, and this is inversely reflected in a parameter called the chemical shift recorded in parts per million (ppm).

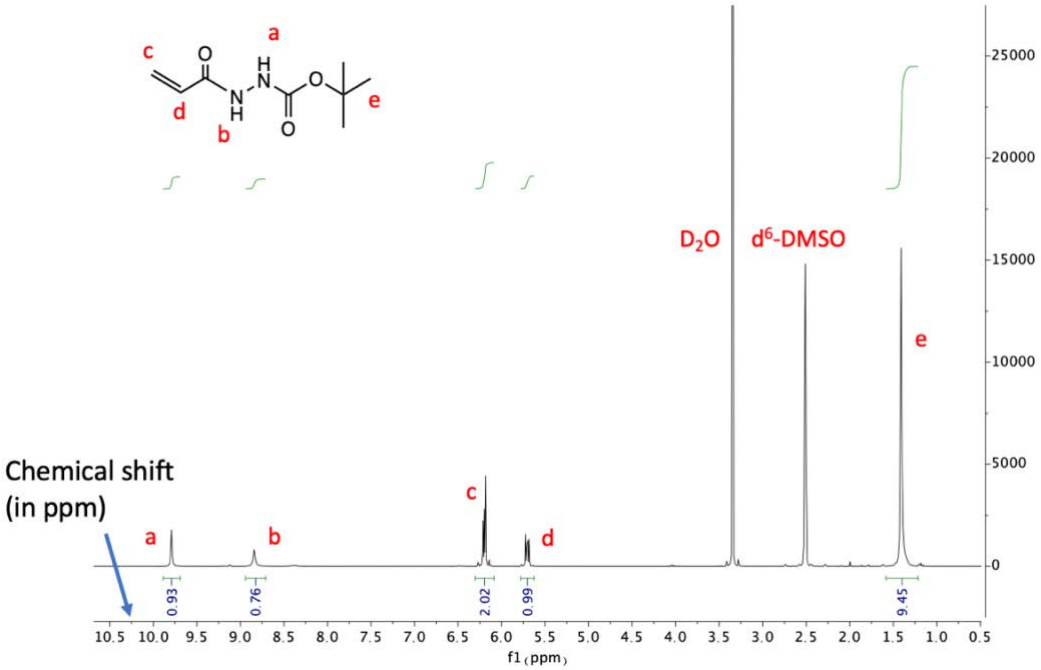

Figure 6: Example ^{1}H-NMR of tert-butyl 2-acryloylhydrazinecarboxylate, referred to as boc protected acryloyl hydrazide

An example of a ^{1}H-NMR spectrum of boc protected acryloyl hydrazide is shown in figure 6. In this case there are five different hydrogen environments, with each environment labelled on the chemical structure. The least electronegative atom in the molecule is carbon, hence any hydrogen atom attached to a carbon will be somewhat shielded from the applied external magnetic field by electrons within the C-H bond. Therefore a high amount of energy is required for C-H hydrogens to jump energy levels and this is reflected in low chemical shift values, the lowest being for the 9 hydrogens of the boc group e, at 1.41 ppm (figure 6). Two C-H peaks can also be found between 5.5 and 6.5 ppm and these correspond to the vinyl hydrogens, c and d which are slightly deshielded by the high electron density of the double bond (electrons tend to be pulled toward regions of high electron density), hence the slightly higher chemical shifts. Conversely, the most electronegative atom is nitrogen which will attract electrons away from the attached hydrogens, effectively deshielding them. Hence these hydrogens will now feel a higher effect of the external magnetic field meaning less resonance energy is required for N-H hydrogens to jump energy levels, reflected in the highest chemical shifts b and a at 8.84 and 9.79 ppm respectively. Furthermore, the area under each peak corresponds directly to the number of hydrogen nuclei within that particular environment. Peaks can be integrated using NMR software such as MNova and can be found at the bottom of the NMR trace of figure 6 for boc protected acryloyl hydrazide, with all integrals reasonably matching the number of hydrogen atoms in each environment. Finally, each peak also gives information about the number of hydrogens attached to the adjacent (next door) carbon atom, depending on the way that the peak is spilt. The source of peak splitting is down to a phenomenon known as spin-spin coupling which describes the magnetic interactions between neighbouring, non-equivalent hydrogens with the hydrogen environment in question. The n+1 rule is used to interpret

peak splitting, where n is the number of hydrogen atoms directly adjacent (i.e. attached to the carbon atom next door) to the hydrogen/s in question - n+1 is the number of times that peak is spilt.

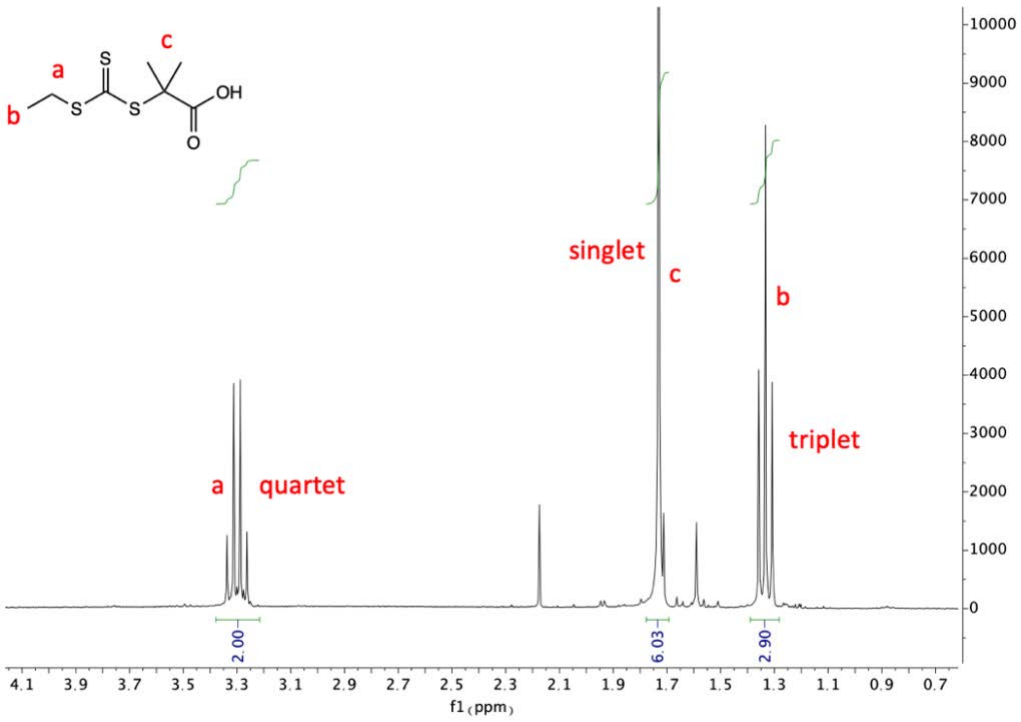

Figure 7: ^{1}H-NMR of 2-((Ethylthio)carbonothioyl)thio-2-methylpropanoic acid (RAFT agent), zoomed in to view peak splitting

Figure 7 shows a ^{1}H-NMR of the RAFT agent used in the polymerisation of acryloyl hydrazide, which clearly shows the peak splitting phenomenon. The hydrogens in the least electronegative environment (and therefore the least deshielded) are those attached to carbon b which represent three hydrogen atoms (1.3 ppm). Next to b, there is a carbon atom (a) that is attached to two further hydrogens, hence peak b will be split 2+1 times giving a triplet peak b. The six hydrogens attached to the two identical methyl groups, c are also in a shielded environment (they are attached to carbons), however there are no hydrogen atoms attached next door to carbon environment c, hence the splitting will be 0+1

giving a singlet at 1.7 ppm. The hydrogens that find themselves in the most electronegative environment are those attached to carbon a, as this is directly next to the most electronegative sulphur atom. Furthermore carbon a is directly next to carbon b which has three hydrogens. Hence carbon a will be split 3+1 times, giving a quartet which is the most deshielded at 3.3 ppm.

(c) ^{1}H-NMR for the characterisation of polymers

Polymers are defined by fact that they contain multiple monomer repeating units. In the case of boc-protected pAH, the monomer unit is the boc-protected acryloyl hydrazide. When in solution, the polymer will end up folding into its lowest energy configuration meaning that each repeating monomer unit within the polymer will find itself in a slightly different environment (depending on the polymer orientation). This results in the broadening of any peak representing the monomer unit within the polymer.

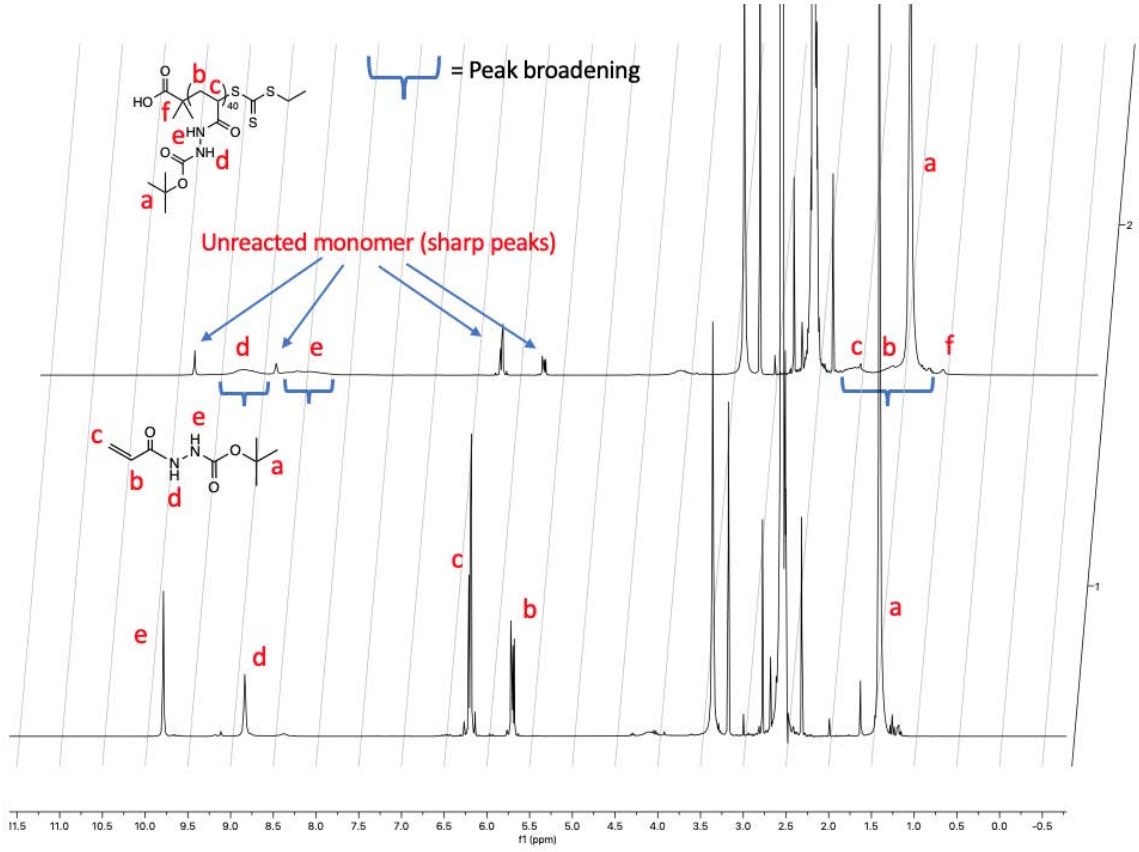

Figure 8: ^{1}H-NMR (top) of crude Boc-protected poly(acryloyl hydrazide) and (bottom) aliquot of boc-acryloyl hydrazide starting material before polymerisation.

Figure 8 shows a ^{1}H-NMR trace of the monomer (bottom) and the resulting crude polymer (top). Unsurprisingly, both ^{1}H-NMRs are very similar as they are made from the same molecule (i.e. boc protected acryloyl hydrazide). The main difference is that the polymer ^{1}H-NMR shows peak broadening for any hydrogen atom that originated from the monomer

unit, representing many identical repeating units at ever so slightly differing chemical shifts within the polymer. Hence the sharp N-H (peaks d and e) and boc peak (peak a) of boc acryloyl hydrazide broaden after polymerisation (figure 8). The only real change in environments between the monomer and polymer can be found at the reactive part of the monomer, where the vinyl region (5.3-6.2 ppm) is converted into the broad C-C backbone saturated chain (peaks b and c, figure 8 top). As the final polymer product is crude (not purified), we are still able to see a small amount of the monomer in the product as represented by the left over vinyl peaks (figure 8, top). This allows us to calculate exactly how much of the monomer has become part of the polymer by simply monitoring the reduction of the initial monomer vinyl integral.

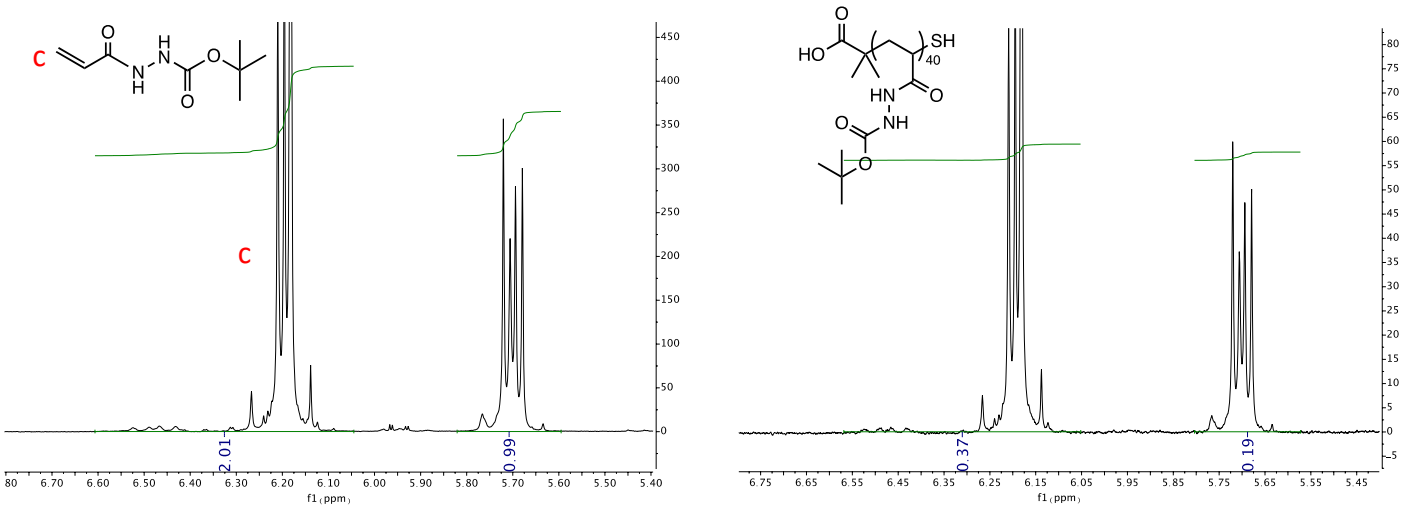

Figure 9: ^{1}H-NMR (right) of crude Boc-protected poly(acryloyl hydrazide) and (left) aliquot of boc-acryloyl hydrazide starting material, zoomed in to the vinyl regions

By looking at the vinyl integrals (figure 9), it can be deduced that in this case around 81.5% of the vinyl peak c disappears during the polymerisation (integral of peak c drops from 2.01 to 0.37), hence 81.5% of the starting monomer becomes part of the polymer. One of the real advantages of RAFT polymerisation is the high level of control over the polymerisation, resulting in predictable polymer chain lengths and low dispersities. One can control the

polymer chain length (degree of polymerisation, DP) by mixing the monomer and RAFT agent at defined ratios. For example if 50 moles of monomer are added to 10 moles of RAFT agent, the final polymer chain will theoretically contain 50/10 = 5 chain units (DP) if the reaction goes to completion i.e. all the monomer gets used up. For the synthesis of boc-poly(acryloyl hydrazide) the [monomer] : [RAFT] agent molar ratio upon mixing was 100:2 targeting a chain length of 50. We know that the reaction has not gone to completion as only 81.5% of the monomer become incorporated into polymer, hence we can deduce that our final polymer will have a chain length of 50 x 0.815= 40.75 or around DP 40. This is only possible due to the controlled nature of RAFT polymerisation whereby all chains grow at very similar rates, confirmed by the narrow size distribution of the polymer via size exclusion chromatography (figure 13).

Upon the synthesis of boc-poly(acryloyl hydrazide), it is purified by dialysis against water and then boc deprotected using trifluoroacetic acid (TFA). The final pAH is then further purified by dialysis to remove any excess TFA to afford a white fluffy powder (figure 10 bottom).

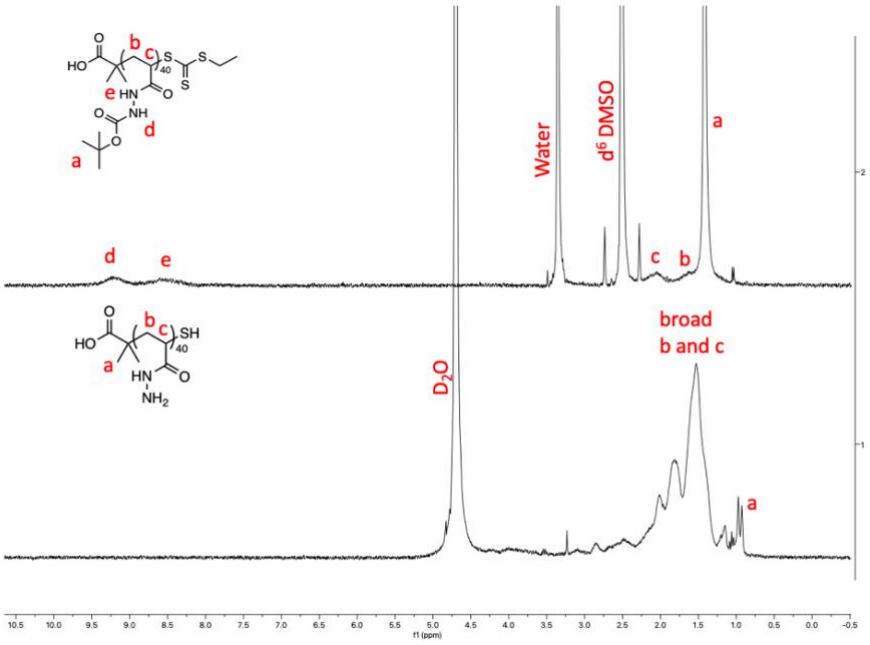

Figure 10: (top) ^{1}H-NMR of purified boc-pAH, (bottom) ^{1}H-NMR of pAH

Finally, pAH is now ready to be post-polymerisation functionalised with a range of aldehydes by reacting molar equivalents of aldehyde and polymer hydrazide.

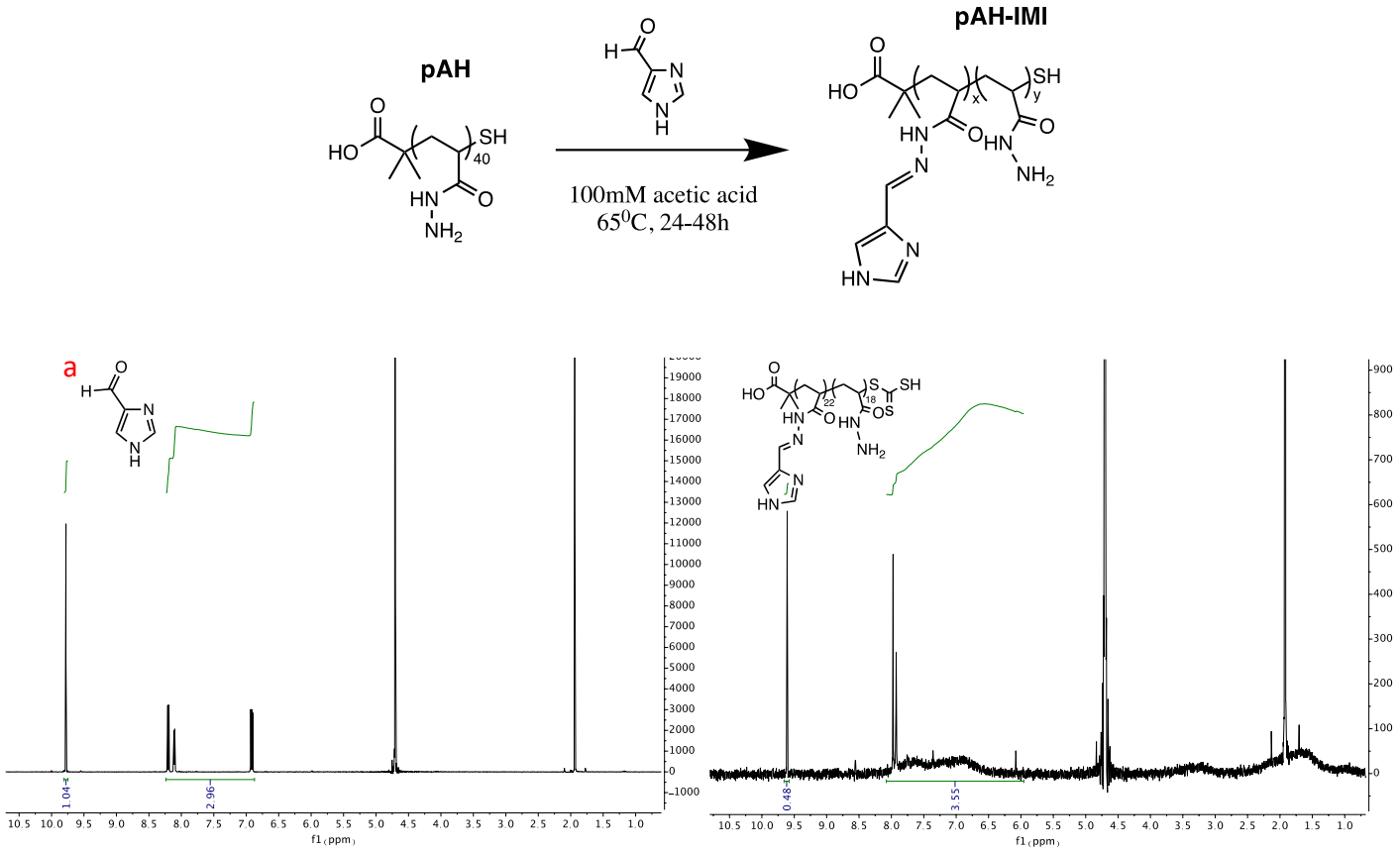

Figure 11: (top) Reaction scheme for post polymerisation functionalisation with Imidazole-4-carboxaldehyde. (bottom left) ^{1}H-NMR of Imidazole-4-carboxaldehyde (bottom right) ^{1}H-NMR of pAH functionalised with Imidazole-4-carboxaldehyde (pAH-IMI)

Note we do not add molar equivalents of aldehyde and pAH, but rather aldehyde and hydrazides. To find the number of moles of hydrazides for a given amount of pAH, the mass of pAH needs to be taken and converted into moles using the molecular weight of the hydrazide segment of the polymer (86 g/mol) and not the molecular weight of pAH. Once the moles of hydrazide has been obtained, an equimolar amount of aldehyde is to be added and left to incubate for 24h-48h at 60^{o}C in either 95% d^6-DMSO/5% 100 mM acetic acid (v/v) or 100mM acetic acid reaction solvent as the reaction is acid catalysed. Imidazole-4-carboxaldehyde is water soluble (upon addition of heat) hence the above reaction is

performed in 100 mM acetic acid. This is also the case for the functionalisation of pAH with 2-Amino 3-formylpyridine. The more hydrophobic aldehydes that were used in this project are not water soluble hence are coupled onto pAH in 95% d^6-DMSO/5% 100 mM acetic acid (v/v). Due to the fact the aldehyde and hydrazide are being added in an equimolar amount, the amount of aldehyde incorporated into the polymer can be calculated from the decrease of the free aldehyde peak integral as it is converted into a hydrazone. In the case of pAH-IMI functionalisation, the Imidazole-4-carboxaldehe aldehyde peak a (figure 11, bottom left) decreases from 1.04 to 0.48 (figure 11, bottom right), a decrease of 54% as it reacts with the pAH hydrazide groups. Therefore the final pAH-IMI contains 54% of the imidazole moiety (i.e. 54% of the hydrazide groups of pAH have become functionalised). All ^{1}H-NMRs of each pAH coupling reaction performed during this project can be found in the supplementary figures of chapter 6

(d) Characterisation of polymers by gel permeation chromatography (GPC)

Gel permeation chromatography is a type of size exclusion chromatography (SEC) which is used commonly in the characterisation of polymers. GPC separates molecules of differing sizes by filtration through a gel (stationary phase). The gel is made up of spherical beads containing small pores which trap smaller molecules. Upon addition of a sample into the gel, smaller molecules become temporarily trapped inside of the pores while bigger molecules may be too big to fit inside them, hence bigger molecules continue their journey down through the column gel and are eluted much faster than the smaller molecules which require more time to escape from the pores. Consequently, molecules (or polymers) are

separated based on their sizes, with molecules of large molecular weight eluting faster than those of lower molecular weights (figure 12).

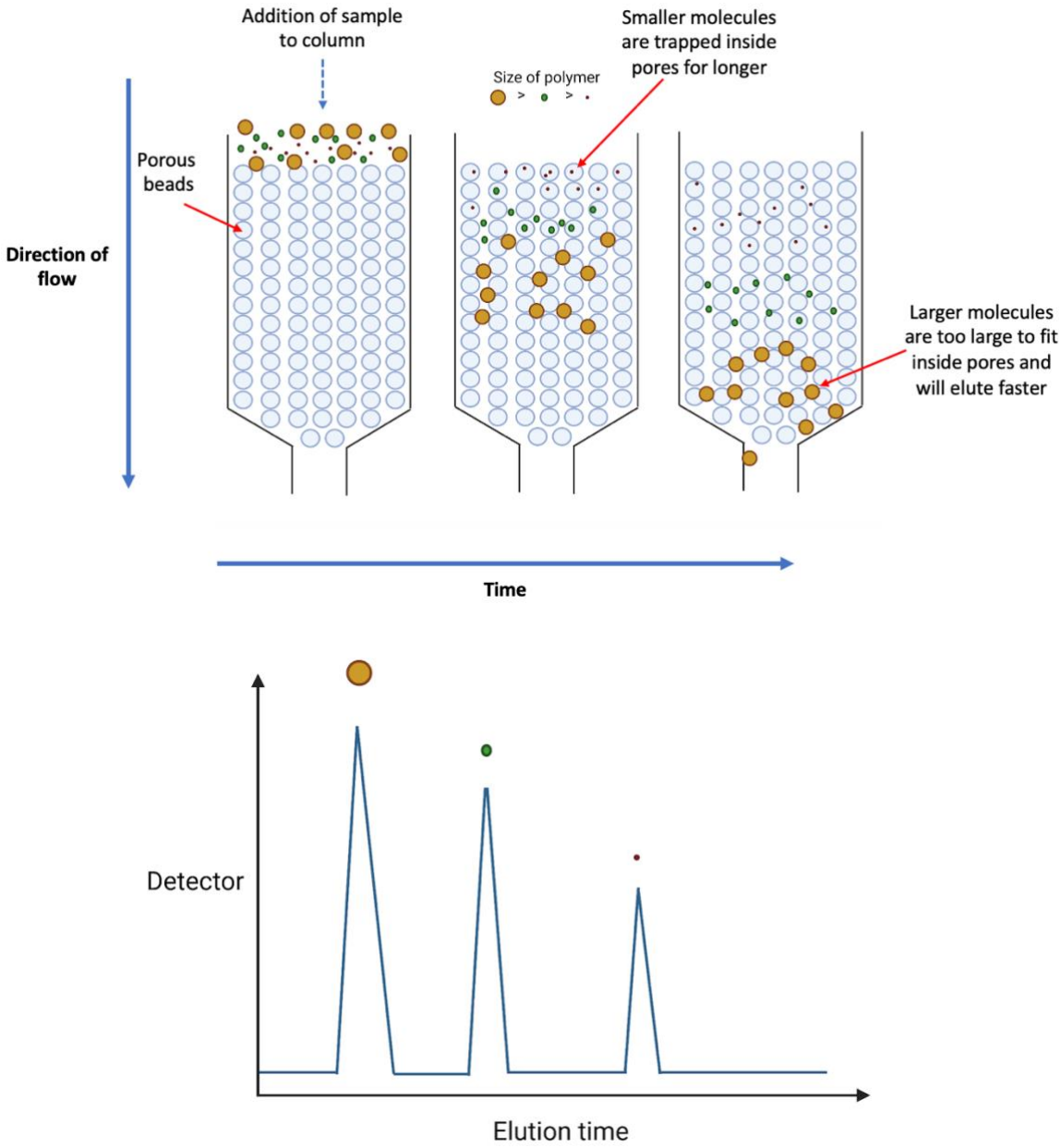

Figure 12: (top) Schematic representation of the separation of molecules based on their size (moleculaer weight) within a size exclusion column. (bottom) Schematic of a typical chromatogram with each peak corresponding to one type of molecule or polymer, seperated by size.

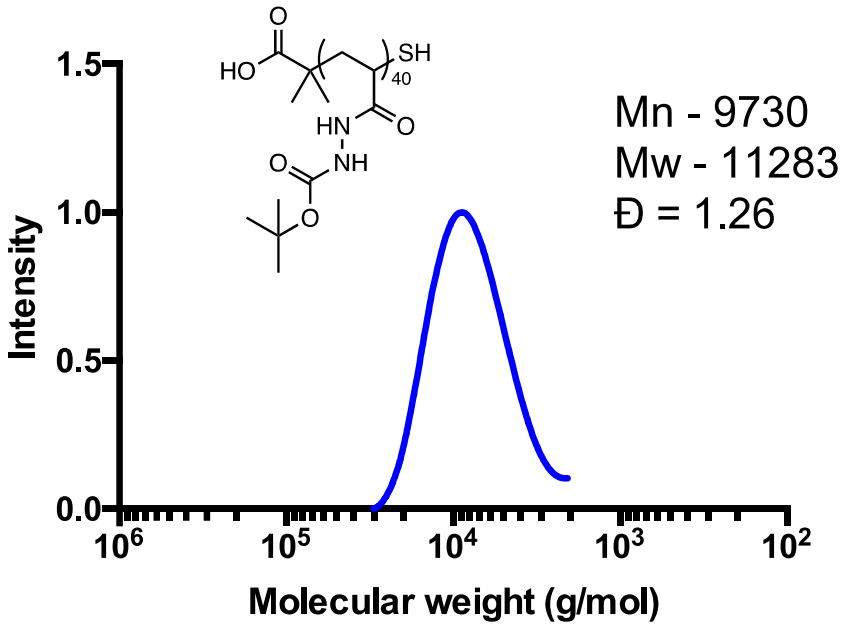

Figure 13: GPC trace of pAH (DP 40) with a narrow dispersity of 1.26

A detector, placed downstream to the column will detect eluting polymers by order of size. Usually for GPC, the detector will be a differential refractometer which will detect the difference in refractive index when the sample is eluted (compared with the RI of the eluting solvent). Commonly UV detectors are also used which detect UV absorption by the eluting sample. The resulting elution time chromatogram of a sample (figure 12, bottom) is then transformed into a molecular weight chromatogram by comparing and normalising with elution time chromatograms of known molecular weight polymer standards (e.g. PMMA, PEO or PEG standards). Once a molecular weight distribution of the sample is obtained, the dispersities (Đ) of each peak (that is the molecular weight distribution) can be obtained from the raw data. A perfectly controlled polymerisation will result in polymers of identical size corresponding to a dispersity of 1. This however very rarely happens and in reality, controlled polymerisations such as RAFT should result in polymers with dispersities between 1 and 1.4. Above this, it can be said that the polymerisation is not controlled (i.e.,

polymer chains do not grow at the same rate, resulting in final polymers of vastly differing sizes).

(e) Determining hydrophobicity of functional polymers[9]

The term lipophilicity refers to the ability of a molecule to be dissolved in lipids, fats, oils and other non-polar solvents rather than water. Hydrophobicity is the physical property of a molecule that is repelled by water molecules. Usually, the terms lipophilicity and hydrophobicity are used interchangeably due to the fact that most hydrophobic molecules are lipophilic. The most commonly used measure of lipophilicity is the term LogP which is defined as the partition coefficient of a molecule between the aqueous and lipophilic phase, normally this is water and octanol. As such, the experimental method for determining LogP involves dissolving the molecule of interest into a volume of water and octanol. The two phases are immiscible, hence once the molecule is added shaking is required. After addition and shaking, the two phases separate from each other and the relative concentrations of the molecule in each solvent can be determined. The equation below is then used to determine LogP:

$$LogP_{oct/water} = \log\left(\frac{[solute]_{oct}}{[solute]_{water}}\right)$$

This is however a rather time consuming and tedious method, hence there are now a number of software tools that calculate predicted clogP values. The software usually works by using a large data set of known LogP values for a range of chemical groups, the contributions of which are summed for a particular molecule giving an overall calculated LogP value (clogP). The term LogP however, does not take into account groups within a

molecule that may be ionised at different pHs. The distribution constant LogD is therefore used when a molecule contains groups that may be charged at certain pHs. Therefore LogD is measured in a similar way to LogP, but instead of using water, the aqueous phase is adjusted to a defined pH. Hence LogD is pH dependant.

$$LogD_{oct/water} = \log\left(\frac{[solute]_{octanol}}{[solute]_{ionised\ water} + [solute]_{neutral\ water}}\right)$$

Again, there is software available that calculate the clogD of a molecule based on its constituents, however this time clogD is pH dependant. We therefore decided to employ clogD values of the functional polymers at pH 7, due to the fact that that polymers were added to bacterial suspensions at pH 7. cLogD values of each functional polymer were calculated from MarvinSketch by drawing out the full polymer and using the partition plugin.

(f) Determining functional polymer pKa values[10]

The Brønsted-Lowry theory states that an acid is a chemical that is able to donate a proton (H^+) into the solution that it is dissolved in, whilst a base is a chemical that is able to accept a proton from the solution. The concept of proton exchange is variable between different chemicals; different chemicals that are acidic may be able to donate protons to a varying extent, and the same is with different bases. A strong acid is defined by the fact that when it is added into solution, a vast majority of the acid molecules will donate protons to the solution, whilst a weak acid may only partially donate protons. A strong base is one that is

able to effectively accept protons into each base molecule, whilst a weak base will only be partially protonated in solution when added.

The kinetics for proton exchange for acids/bases can be treated like any other equilibrium reaction. For example, an acid will set up the following equilibrium when dissolved in solution:

$$HA \leftrightharpoons H^+ + A^-$$

Where HA is the acid of concern, which is able to dissociate into the conjugate acid (A^-) and a proton (H^+). The equilibrium constant for this dissociation is given by the equation below:

$$K_a = \frac{[H^+][A^-]}{[HA]}$$

A strong acid will dissociate in a way that gives a high concentration of $[H^+]$ and $[A^-]$ (that is, it donates a large amount of H^+) whilst a weak acid will dissociate into low concentrations of $[H^+]$ and $[A^-]$ with respect to [HA]. Therefore, acids can be defined as strong or weak based on their equilibrium constant of dissociation, K_a. By definition, the overall pH of a solution containing HA can therefore be obtained by measuring the final concentration of the conjugate acid (A^-) to obtain the concentration of $[H^+]$ ions in solution (as $[H^+] = [A^-]$). From this the pH of the solution containing HA is given by:

$$pH = -\log_{10}([H^+])$$

So far, we have discussed the addition of an acid or base to a neutral solution, i.e., pH 7. Clearly the value of K_a will depend on the pH of the solution, if the pH is below 7 (i.e. acidic),

then one would expect the dissociation constant of an acid to be lower than what it would be if added to a neutral solution. The same can be said for the addition of base into an already basic solution. Another term, the pKa of a compound defines the pH at which the exactly half of the acid molecules will dissociate. For example, say an acidic compound HA has a defined pKa of 3; at pH 3 exactly half of the [HA] will dissociate into $[H^+]$ and $[A^-]$ respectively. Below pH 3, the HA will not dissociate as much and above pH 3 over half the HA will dissociate. Hence the relative acidity of a molecule depends on the pH of the solution it has been dissolved in. The pKa of a molecule however is a set value and is used to define the relative acidity of a molecule – its equation is given below:

$$pK_a = -\log\left(\frac{[H^+][A^-]}{[HA]}\right)$$

The relative charge of a compound (that is [A-]/[HA]) at a given pH can be calculated by rearranging the above equation:

$$\frac{[A^-]}{[HA]} = 10^{(pH-pKa)}$$

Of all the functional pAH that have been made in this project, only the unfunctionalised pAH, pAH-2AFP and pAH-IMI contain protonatable functional groups. The relative charges of these polymers at pH 2.8 (i.e., the pH of 100mM acetic acid that they are synthesised in) and pH 7 (the pH of the bacterial suspensions that the polymers are to be added to) were determined by drawing out the full polymers onto MarvinSketch, and using the protonation plugin to determine the pKa's of each functional moiety attached to each polymer. The pKa values of functional groups within the same polymer will vary slightly due to the fact that

each repeating functional group will be in a slightly different environment, depending on the orientation of the dissolved polymer. From this, the average pKa of the functional groups of the polymer can be determined and are used to estimate the relative charge of each polymer at pH 2.8 and 7.

(ii) Materials and Methods

(a) Chemical Synthesis and Characterisation

Nuclear Magnetic Resonance (NMR) spectra were recorded on either a Bruker Avance III 300 MHz or a Bruker Avance III 400 MHz spectrometer. Chemical shifts are reported in ppm (units) referenced to the following solvent signals: dimethylsulfoxide (DMSO)-d^6 H 2.50 and D_2O H 4.79. Ultraviolet/visible (UV-vis) measurements were performed using a Cary 50 spectrophotometer. Fluorescence measurements/assays were performed using a CLARIOstar PLUS plate reader. Purification of polymers was performed by dialysis in deionised water at room temperature for a minimum of 48 hours using a Spectra/Por 6 1000 Molecular weight cut-off (MWCO) 38 mm width membrane. Azobis[2-(2-imidazolin-2-yl)propane] dihydrochloride (VA-044) was purchased from Fluorochem and used without further purification. All aldehydes were purchased from either Sigma-Aldrich®, Fisher Scientific®, VWR® or Acros®, and used without further purification. All solvents were Reagent grade or above, purchased from Sigma-Aldrich®, Fisher Scientific® or VWR®, and used without further purification.

*(i) tert-Butyl-2-acryloylhydrazine-1-carboxylate (**Boc-protected acryloyl hydrazide**)*

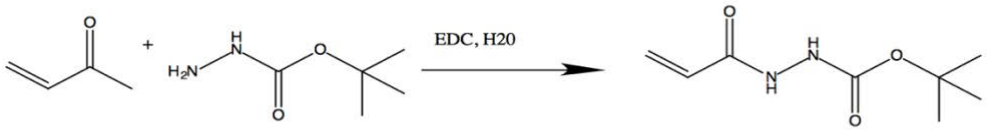

Acrylic acid (7.9 ml, 110 mmol) and tert-butyl carbazate (12 g yield, 90.8 mmol) were dissolved in a H2O : THF mixture (2:1, 360 ml) at room temperature. N-(3-Dimethylaminopropyl)-N'-ethylcarbodiimide hydrochloride (24.6 g, 128 mmol) was added in portions to the solution over 15 minutes and left stirring for 3 h. The solution was extracted with ethyl acetate (EtOAc) (3 × 60 ml) and the organic layer was washed with H2O (50 ml) and brine (2 × 50 ml). The organic phase was dried with Na_2SO_4 and the solvent was removed under reduced pressure to afford the crude product as a white solid. The crude product was purified by recrystallization from EtOAc (70 °C to r.t.) to afford a white crystalline powder (4.37 g, 26 %). ^{1}H NMR (300 MHz, DMSO-d^6) δ (ppm) 9.79 (s, 1H), 8.84 (s, 1H), 6.17-6.22 (m, 2H), 5.67-5.74 (m, 1H), 1.41 (s, 9H).

*(ii) 2-((Ethylthio)carbonothioyl)thio-2-methylpropanoic acid (**RAFT agent**)*

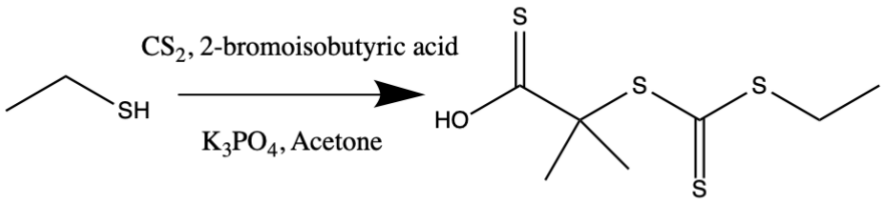

As followed from the literature[11], ethane thiol (3.6 ml, 47.64 mmol) was added to a suspension of tripotassium phosphate (15.4 g, 71.46 mmol) in acetone (150 mL) and stirred for 10 min. Carbon disulfide (7.2 ml, 119.10 mmol) and 2-bromoisobutyric acid (7.3 g, 42.88

mmol) was then added and the mixture left stirring overnight. The solution was concentrated by purging with argon and filtered. The cream coloured solid residue was dissolved in 1 M HCl (150 mL) and extracted with DCM (3 x 100 mL). The organic layer was collected and washed further with 0.1M HCl (2 x 100 mL), water (2 x 100 mL) and brine (2 x 100 mL) and dried with anhydrous Na_2SO_4. The solution was concentrated under reduced pressure to afford an orange oil. The crude product was purified by recrystallisation from hexane (55 °C to 0 °C followed by overnight cooling in freezer) to afford a bright yellow powder (3.9 g, 40 %). ^{1}H NMR (300 MHz, DMSO-d^6) δ (ppm) 12.59-13.22 (br, 1H, COO*H*), 3.30 (q, 2H, SC*H*$_2$CH$_3$), 1.62 (s, 6H, ((C*H*$_3$)$_2$), 1.25 (t, 3H, C*H*$_3$).

*(iii) Poly(tert-butyl-2-acryloylhydrazine-1-carboxylate) (**boc-pAH**)*

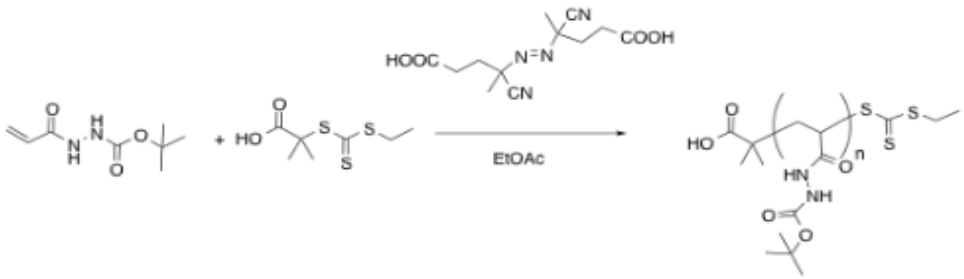

2,2'-azobis[2-(2-imidazolin-2-yl) propane]dihydrochloride (VA-044, Fluorchem) (23.4 mg, 0.072 mmol), 2-ethylthiocarbonothioylthio-2-methylpropanoic-acid (CTA) (80.5 mg, 0.36 mmol) and N'-(tert-butoxycarbonyl)acryloyl hydrazide (3.33 g, 17.9 mmol) were dissolved in DMSO (20.0 mL) and a 100 µL sample was taken at this stage to calculate monomer conversion into polymer. The molar ratios given were used to target a DP 50 polymer. The solution vessel was sealed with a septum, securely fastened with electrical tape to maintain the seal, and degassed by bubbling with argon for 25 minutes. The suspension was then left

to react for 30 mins at 60 °C with stirring. The reaction was stopped by exposing to air after which another 100 µL sample was taken to calculate monomer conversion (80 %). The polymer solution was then purified by dialysis against deionised water for approximately 1 week, with several changes of water. A solid off-white powder was obtained (2.3 g, 68 %) after removing the water by lyophilisation and drying in a vacuum desiccator. ^{1}H NMR (300 MHz, DMSO-d^{6}) δ (ppm) 8.85-9.53 (br, 1H, N*H*), 8.10-8.87 (br, 1H, N*H*), 1.90-2.23 (br, 1H, CH_2CH), 1.64 (br, 11H, 9H in $C(CH_3)_3$, 2H in $CHCH_2$), 1.02 (m, 6H, $(C(CH_3)_2$). Conversion 80% to give a DP 40 polymer. Gel Permeation Chromatography (GPC) was performed with a Shimadzu Prominence LC-20A fitted with a Thermo Fisher Refractomax 521 Detector and a SPD20A UV-vis Detector. Boc-pAH was analysed using 0.05 M LiBr in dimethylformamide (DMF) at 60 °C as the eluent and a flow rate of 1 mL min^{-1} . The instrument was fitted with a Polymer Labs PolarGel guard column (50 × 7.5 mm, 5 µm) followed by two PLGel PL1110–6540 columns (300 × 7.5 mm, 5 µm). Molecular weights were calculated based on a standard calibration method using polymethylmethacrylate.

*(iv) Poly(acryloyl hydrazide) (**pAH**)*

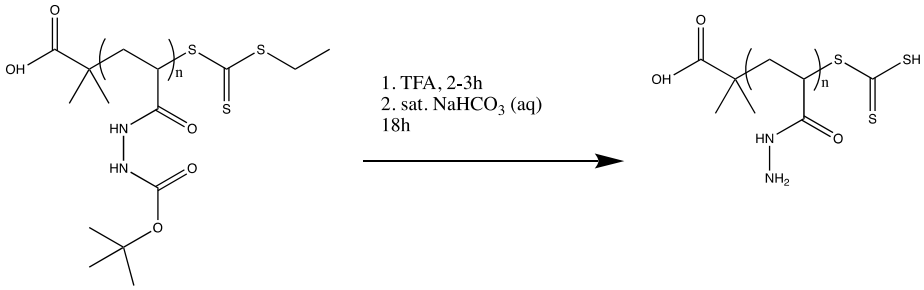

Trifluoroacetic acid (TFA) (10 mL) was added dropwise to poly(tert-butyl-2-acryloylhydrazine-1-carboxylate) (400 mg, 0.053 mmol) and the yellow solution was stirred at r.t. overnight. Excess of TFA was removed by blowing a steady stream of Argon and the resulting oil was diluted in water (10 mL). The Polymer·TFA salt formed was neutralised by

adding $NaHCO_3$ until the solution was pH neutral. The crude polymer was purified by dialysis against water for approximately 1 week, with several changes of water. The water was removed by lyophilisation and the polymer dried in a vacuum desiccator to give a fluffy white powder (81.3 mg, 43 %). ^{1}H NMR (300 MHz, D_2O) δ (ppm) 1.27-2.30 (br, 3H), 0.97 (s, 3H), 0.92 (s, 3H). Gel Permeation Chromatography (GPC) was performed with a Shimadzu Prominence LC-20A fitted with a Thermo Fisher Refractomax 521 Detector and a SPD20A UV-vis Detector. Poly(acryloyl hydrazide) (**pAH**) was analysed using Dulbecco's Phosphate Buffered Saline (0.0095 M PO_4) without Ca and Mg as the eluent and a flow rate of 1 mL min−1 . The instrument was fitted with an Agilent PL aquagel-OH column (300 × 7.5 mm, 8 mm) and run at 35 °C. Molecular weights were calculated based on a standard calibration method using poly(ethylene oxide).

(v) poly(tert-butyl-2-acryloylhydrazine-1- carboxylate) N-(2-aminoethyl) propionamide (Boc-pAH-NH_2)

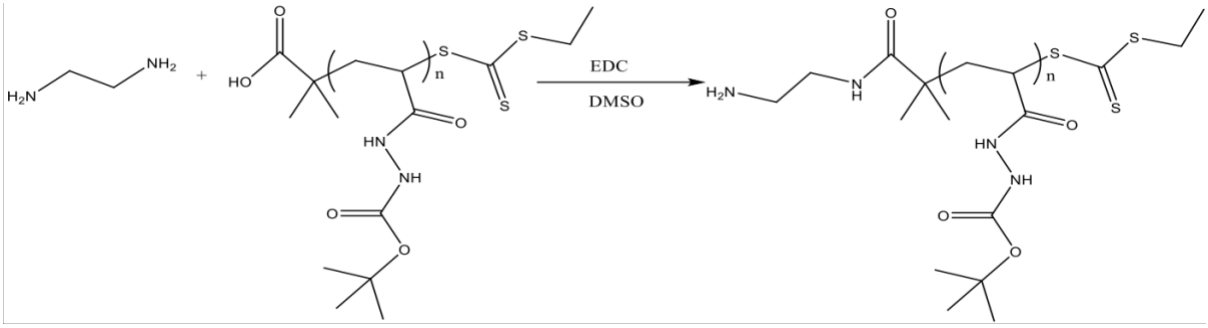

Boc-pAH (2 g, 0.29 mmol), and ethylene diamine (10 ml, 150 mmol) were dissolved in DMSO (20 ml). EDC (9 g, 47 mmol) was added in portions over 15 minutes and the mixture stirred at r.t for 3 hours. The resulting mixture was purified by dialysis against deionised water and lyophilized to a white powder (1.31 g, 65 %). ^{1}H NMR (300 MHz, DMSO-d^6) δ (ppm) 8.88-

9.58 (br, 1H, N*H*), 7.57-8.87 (br, 1H, N*H*), 3.17 (br, 4H, NCH_2CH_2N), 2.04 (br, 1H, C*H*CH_2), 1.64 (br, 11H, 9H in $C(CH_3)_3$, 2H in CHCH_2), 0.98 (br, 6H, $(C(CH_3)_2)$.

*(vi) MCCA-poly(tert-butyl-2-acryloylhydrazine-1- carboxylate) N-(2-aminoethyl) propionamide (**Boc-pAH-NH$_2$-MCCA**)*

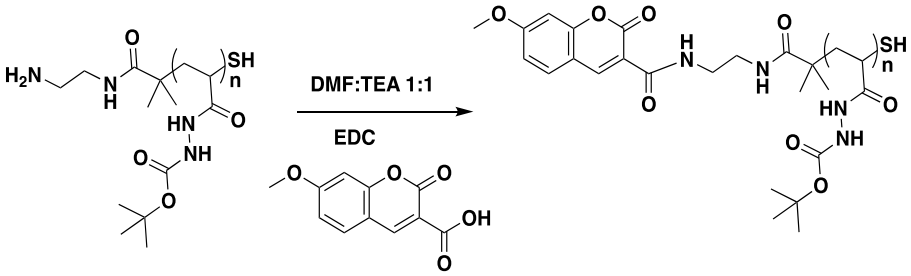

Working in the dark, boc-pAH-NH_2 (245 mg, 0.032 mmol), 7-methoxycoumarin-3- carboxylic acid (30 mg, 0.14 mmol) and EDC (30 mg, 0.16 mmol) was dissolved in DMF/triethylamine (24.2 mL 1:1, v/v). In an ice bath and with stirring, DMAP (3 mg, 0.025 mmol) was added and the resulting mixture was left to react overnight. The crude mixture was purified by dialysis against deionised water (5 L) and lyophilised to yield a light off white solid (168 mg, 67 %). ^{1}H NMR (300 MHz, DMSO-d^6) δ (ppm) 8.88-9.79 (br, 1H, N*H*), 7.49-8.87 (br, 1H, N*H*), 2.05 (br, 1H, C*H*CH_2), 1.63 (br, 11H, 9H in $C(CH_3)_3$, 2H in CHCH_2), 1.02 (m, 6H, $(C(CH_3)_2)$.

*(vii) MCCA-poly(acryloyl hydrazide) N-(2- aminoethyl) propionamide (**pAH-NH$_2$-MCCA**)*

Trifluoroacetic acid (TFA) (2 mL) was added dropwise to Boc-pAH-NH_2-MCCA (80 mg) and stirred at r.t. overnight. Excess of TFA was removed by blowing a steady stream of Argon and the resulting oil was diluted in water (2 mL). The Polymer·TFA salt formed was neutralised by adding $NaHCO_3$ until the solution was pH neutral. The crude polymer was purified by dialysis against water for approximately 1 week, with several changes of water. The water was removed by lyophilisation and the polymer dried in a vacuum desiccator to

give a fluffy off white powder. ^{1}H NMR (300 MHz, D_2O) δ (ppm) 1.26-2.31 (br, 3H, C*H*C*H*$_2$), 0.9-1.25 (m, 6H, (C(CH_3)$_2$).

(viii) Poly(acryloyl hydrazide) - aldehyde coupling reactions

Note: Aldehydes were mixed with pAH such that a 1:1 ratio of aldehyde : hydrazide groups was formed (not a 1:1 ratio of pAH:aldehyde). Typically this involved incubating pAH (8.01mg, 0.093 mmol hydrazides for a DP 40 polymer) with a molar equivalent of the required aldehyde to give a 125mM solution in 95% DMSO-d^6/5% 100mM acetic acid for all aldehyde couplings except 2-Amino 3-formylpyridine and Imidazole-4-carboxaldehyde which were reacted in 100mM acetic acid. The mixture was incubated and stirred at 60 ^{o}C for 24-48h to give the functional polymer which was then characterised by ^{1}H-NMR and GPC and used without further purification.

(ix) Determination of polymer partition coefficients at pH 7 (cLogD)

Full polymer structures were drawn out on MarvinSketch, and cLogD determined using the partition plugin.

(x) Determination of polymer pKa

Full polymer structures were drawn out, and an estimation of overall polymer pKa was made using the pKa plugin on MarvinSketch.

(b) Bacterial protocols

(i) Bacterial Strains and plasmids

Two *Escherichia coli* K-12 strains MC4100: *araD139* Δ*(argF-lac)U169 rpsL150 relA1 flbB5301 deoC1 ptsF25 rbsR* and PHL644: MC4100 *malA-kan ompR234* (Vidal et al. 1998[12]) were used in this study. Reporter plasmid pJLC-T comprises the *E. coli* MC4100 *csgD-csgB* intergenic region upstream of the gene encoding eGFP with a C-terminal AANDEN-YALVA tag which reduces GFP half-life to around 60 min[13] cloned into the *Eco*RI-*Hin*dIII sites of pPROBE'-TT upstream of the *gfp* gene[14]. pPROBE'-TT encodes tetracycline resistance and has a pBBR1 origin of replication. pSTB7, a pBR322-based plasmid containing the *Salmonella enterica* serovar Typhimurium TB1533 *trpBA* genes and encoding ampicillin resistance (Kawasaki et al., 1987), was purchased from the American Type Culture Collection (ATCC 37845). *E.coli* strains were transformed with plasmids using the heat shock method.

(ii) Media and preparation of polymer-cell suspensions

E.coli was grown on Luria-Bertani-agar plates (10 g/L tryptone, 5 g/L yeast extract, 10 g/L NaCl, 15 g/L bacteriological agar) (Sigma, UK). Cultures were prepared by selecting a single colony from the plate of the required strain and grown overnight in 10 ml Luria-Bertani (LB) broth (5 g/L tryptone, 2.5 g/L yeast extract, 5 g/L NaCl (Sigma, UK). For experiments involving monitoring the expression of curli using the reporter plasmid pJLC-T, growth media was supplemented with 10 µg/ml tetracycline. For experiments involving biotransformations using the plasmid pSTB7, growth media was supplemented with 100 µg/ml ampicillin.

For the protocols used in chapter 5:

Cells were re-inoculated to 1% in LB in the morning and grown for 3h until an OD of 0.2 was reached Cells were then centrifuged down (10 mins, 3900 rpm) and washed twice with water (2 x 10 ml). The pellet was resuspended in 0.1 M KH_2PO_4/K_2HPO_4 pH 7 so that an OD of 0.2 was reached. The respective polymers were then added to the culture at 0.1 mg/ml, and then the culture supplemented with an equal volume of standard M63 minimal media (100 mM KH_2PO_4, 15 mM$(NH_4)_2SO_4$, 1 mM $MgSO_4$, 1.8 µM $FeSO_4$, 10 mM glucose, 0.5% thiamine, 40 µg/ml L-cysteine adjusted to pH 7 using KOH pellets). Hence final polymer concentration was 0.05 mg/ml in 1:1 (v/v) 0.1 M KH_2PO_4/K_2HPO_4 and 1X M63. The total volume used varied between experiments and details of this can be found in the relevant sections below. This was then incubated at 30 ^oC, 150 rpm for the required amount of time, after which analysis would be performed.

For protocols used in chapter 4:

Cells from an overnight inoculum were directly washed twice with water (2 x 10 ml) and resuspended in 0.1 M KH_2PO_4/K_2HPO_4 pH 7 so that an OD of 1 was reached. The culture was split into 1 ml aliquots in plastic cuvettes and the respective polymers were added at a concentration of 0.5 mg/ml and incubated at 30^oC with shaking at 150 rpm for the required amount of time, after which analysis could be performed (see details below).

In most experiments performed, an identical control experiment was also performed whereby the respective aldehyde (rather than the polymer-aldehyde conjugate) was added to the cells at the same concentration. Polymer control experiments were also performed without the presence of bacteria.

(iii) Spectrophotometric monitoring of polymer mediated cell aggregation

MC4100 was grown overnight in 10 ml LB. The morning after, the cells were centrifuged down and washed twice with water (2 x 10 ml). The pellet was resuspended in 0.1 M KH_2PO_4/K_2HPO_4 so as an OD of 1 was reached. The culture was split into 1 ml aliquots in plastic cuvettes. Polymers were then added respectively to a final concentration of 0.5 mg/ml and OD_{600} was measured immediately, then every 30 minutes for 4h and finally once at 24h whilst incubating at 30 ^oC, 150 rpm between measurements. An identical experiment was performed using the respective aldehydes (0.05 mg/ml) rather than adding polymer so as to serve as a control. Further control experiments without bacteria were also performed, whereby the respective polymers were added to 0.1 M KH_2PO_4/K_2HPO_4 to a final concentration of 0.5 mg/ml and OD measured in the same way.

(iv) Biofilm quantification using crystal violet

Polymer-cell suspensions were prepared as detailed to a final total volume of 1 ml in 15 ml falcon tubes and incubated at 30 ^oC, 150 rpm for 24 and 48h respectively. After incubation, the polymer-cell clusters (sedimented at the bottom of the falcon tube) were washed with water by taking out 900 µl of the suspension and gently adding back 900 µl of water. This was repeated again with extra care so as to not disrupt the sedimented clusters. Using a table lamp to enhance visualisation is recommended. After the second wash, 900 µl of supernatant was removed and 1ml of a 1% crystal violet solution in water was added. A pipette tip was used to gently mix the crystal violet into the polymer-cells sediment and this was left at r.t. for 1h. Gently the stained suspension was washed three times with water by taking out 800 µl of solution and adding back 800 µl of water, again ensuring not to disrupt

the sediment. 20 minutes were left between washes so as to reduce sediment disruption. After the final addition of water, the suspension was centrifuged down (30s, 3900 rpm) and the supernatant removed. The pellet was then resuspended in 2ml of 33% acetic acid and further diluted by adding 3 ml water and the absorbance (550 nm) of the solutions then measured. Aldehyde controls were performed in the exact same way, as too the polymer controls without the presence of bacteria to ensure the crystal violet was simply not just staining the added polymer.

(v) Polymer-cell aggregate size analysis

Polymer-cell suspensions were prepared as detailed to a final total volume of 2 ml in 15 ml falcon tubes and incubated at 30 ^{o}C, 150 rpm for 48h respectively. Polymer-cell cluster sizes were analysed using a Malvern Mastersizer 2000. Plastic pipettes were used to carefully transfer the whole 2ml suspensions respectively into the mastersizer dispersion chamber filled with 100 ml water mixing at 500 rpm, the obscuration was set to 1% and the cluster sizes were measured whilst mixing. To determine the maximum peak sizes, particle size distributions were deconvoluted using the peakfit.m command (http://terpconnect.umd.edu/~toh/spectrum/InteractivePeakFitter.htm#command) and the relative proportion of cells in clusters bigger than 10 µm was analysed on MATLAB R2016a.

(vi) Monitoring curli expression

Both strains used in this experiments had been transformed with pJLC-T. Polymer-cell suspensions were prepared as described in an f-bottom clear 96 well plate to a final volume of 300 µl. The plate was put into a microplate reader where it was incubated at 30 ^{o}C with

shaking at 100 rpm in orbital mode. During this time, fluorescence emission at 510 nm was measured every hour for 48h (excitation 488 nm). The total amount of curli expressed after 48h was determined by calculation of the area under the graph over 48h using Prism.

(vii) 5-Fluoroindole biotransformations

Both strains (PHL644 and MC4100) used in this experiment were transformed with pSTB7 using the heat shock method. Polymer-cell suspensions were prepared as detailed to a final volume of 1 ml in eppendorf tubes and incubated at 30 ^{o}C, 150 rpm for 24 and 48h respectively. After this, the polymer-cell/naturally formed sediment was washed once by gently removing as much supernatant as possible (and measuring OD_{600}) without disrupting the sediment and adding back an equal volume of water. The supernatant was removed again and 1 ml of reaction buffer (0.1 M KH_2PO_4, 7 mM serine, 0.1 mM pyridoxal-5'-phosphate, 1 mM 5-fluoroindole adjusted to pH 7 with KOH and supplemented with 5% (v/v) DMSO) was added. The samples were placed back into an incubator at 30 ^{o}C, 150 rpm for 24h after which the biotransformation was stopped by centrifugation (16000 g, 10 minutes). The sample supernatants (1 ml) were then filtered through a 0.45 µm PTFE filter and analysed by HPLC.

The relative concentrations of 5-fluoroindole and 5-fluorotryptopan were measured using HPLC by monitoring the decrease in sample peak integral corresponding to 5-fluoroindole from a 1 mM 5-fluoroindole control sample, and the relative increase in sample peak integral corresponding to 5-fluorotryptophan by comparing with the peak integral corresponding to 1 mM 5-fluoroindole (theoretical maximum yield from 1 mM

5-fluroindlole). Samples were analysed using a Shimadzu HPLC with a C-18 column resolved with methanol versus water at 0.7 ml/min. A UV detector was used for the analysis. Both solvents were acidified using 0.1% formic acid and run using the gradient shown in figure SI33 of chapter 5.

(viii) 4-Nitrophenyldodecanoate biotransformations

Polymer-cell suspensions were prepared as detailed to a final volume of 15 ml in eppendorf tubes and incubated at 30 ^{o}C, 150 rpm for 24h respectively. After this, the polymer-cell/naturally formed sediment was washed once by gently removing as much supernatant as possible (and measuring OD_{600}) without disrupting the sediment and adding back an equal volume of water. The supernatant was removed again and 15 ml of a ethanol/water mixture (33% v/v) containing 0.08 mM of 4-Nitrophenyldodecanoate was added, and the reaction mixture incubated at 30 ^{o}C, 150 rpm for 240h. The reaction was monitored by recording the absorbance of the solution at 410 nm, at set timepoints throughout the reaction. In an experiment involving 'unchallenged conditions', the same protocols were performed, except this time the reaction solution was made of 10% ethanol in water with 0.008 mM 4-Nitrophenyldodecanoate.

(ix) Confocal Microscopy

Strains used for microscopy were transformed with pJLC-T and the aggregating polymer used was the blue fluorescent MCCA-pAH-2AFP. Polymer – bacterial suspensions were prepared as described previously to a total volume of 20 ul in 8 well slides (u-Slide, 8 well, Ibidi) and incubated at 30^{o}C with 150 rpm shaking for 24h. Slides were imaged using a Nikon

A1R inverted confocal microscope. Image acquisition and analysis was carried out using ImageJ.

(iii) References

1. Crisan DN, Creese O, Ball R, et al. Poly(acryloyl hydrazide), a versatile scaffold for the preparation of functional polymers: Synthesis and post-polymerisation modification. *Polym Chem*. 2017. doi:10.1039/c7py00535k
2. Perrier S. 50th Anniversary Perspective: RAFT Polymerization - A User Guide. *Macromolecules*. 2017. doi:10.1021/acs.macromol.7b00767
3. Creese O, Adoni P, Su G, Romanyuk A, Fernandez-Trillo P. Poly(Boc-acryloyl hydrazide): the importance of temperature and RAFT agent degradation on its preparation. *Polym Chem*. 2019;10(41):5645-5651. doi:10.1039/C9PY01222B
4. Matyjaszewski K, Janzen E, He YZ, et al. Living Free-Radical Polymerization by Reversible Addition - Fragmentation Chain Transfer : The RAFT Process. *Macromolecules*. 1998.
5. Abel BA, McCormick CL. Mechanistic Insights into Temperature-Dependent Trithiocarbonate Chain-End Degradation during the RAFT Polymerization of N-Arylmethacrylamides. *Macromolecules*. 2016. doi:10.1021/acs.macromol.5b02463
6. high resolution nuclear magnetic resonance (nmr) spectra. https://www.chemguide.co.uk/analysis/nmr/highres.html#top. Accessed February 25, 2021.
7. NMR Spectroscopy - Theory. https://teaching.shu.ac.uk/hwb/chemistry/tutorials/molspec/nmr1.htm. Accessed

February 25, 2021.

8. 13.6: Spin-Spin Splitting in ^{1}H NMR Spectra - Chemistry LibreTexts. https://chem.libretexts.org/Bookshelves/Organic_Chemistry/Map%3A_Organic_Chemistry_(McMurry)/13%3A_Structure_Determination_-_Nuclear_Magnetic_Resonance_Spectroscopy/13.06%3A_Spin-Spin_Splitting_in_H_NMR__Spectra. Accessed February 25, 2021.
9. LogD | Cambridge MedChem Consulting. https://www.cambridgemedchemconsulting.com/resources/physiochem/logD.html. Accessed March 15, 2021.
10. pH, pKa, pI and protein charge. https://www.petercollingridge.co.uk/tutorials/bioinformatics/ph-pKa-pi-and-protein-charge/. Accessed March 22, 2021.
11. Skey J, O'Reilly RK. Facile one pot synthesis of a range of reversible addition-fragmentation chain transfer (RAFT) agents. *Chem Commun*. 2008. doi:10.1039/b804260h
12. Vidal O, Longin R, Prigent-Combaret C, Dorel C, Hooreman M, Lejeune P. Isolation of an Escherichia coli K-12 mutant strain able to form biofilms on inert surfaces: Involvement of a new ompR allele that increases curli expression. *J Bacteriol*. 1998.
13. Andersen JB, Sternberg C, Poulsen LK, Bjørn SP, Givskov M, Molin S. New unstable variants of green fluorescent protein for studies of transient gene expression in bacteria. *Appl Environ Microbiol*. 1998. doi:10.1128/aem.64.6.2240-2246.1998
14. Miller WG, Leveau JHJ, Lindow SE. Improved gfp and inaZ broad-host-range promoter-probe vectors. *Mol Plant-Microbe Interact*. 2000.

doi:10.1094/MPMI.2000.13.11.1243

Chapter 3 – Poly(boc-acryloyl hydrazide): the importance of temperature and RAFT agent degradation on its preparation (*Publication*)

O. Creese, P. Adoni, G. Su, A. Romanyuk, P. Fernandez-Trillo, *Polym. Chem.* 2019, **124**, 14922-7

Declaration

All experiments were designed by O. Creese and P. Fernandez Trillo unless stated. All data was independently analysed by O. Creese, P. Adoni, P. Fernandez-Trillo and A. Romanyuk. All polymerisations reported in the paper were characterised by GPC to obtain M_n, M_w, Đ and all conversion calculations were obtained using NMR. All polymerisations and characterisation was performed by O. Creese unless stated as below. O. Creese and P. Fernandez-Trillo wrote the manuscript. Baseline correction of GPC traces was performed by A. Romanyuk.

Experimental contributions to the chapter:

P. Adoni carried out synthesis and characterisation steps towards the synthesis of small molecule analogue of a DP= 1 of N'-(tert-butoxycarbonyl)acryloyl hydrazide, (data presented in Scheme S1, Figure S3, Figure S5), chain extension of "living" and "dead" poly(boc-acryloyl hydrazide), (data presented in figure S6, S7 and S8), and polymerisation kinetics for conditions: DP150 100^{o}C, DP50 80^{o}C and DP100 65^{o}C.

A. Romanyuk (University of Birmingham) carried out baseline correction of GPC data prior to final analysis and publication.

G. Su carried out monomer synthesis of N'-(tert- butoxycarbonyl)acryloyl hydrazide (**1**), and performed some of the initial kinetic experiments.

All co-authors contributed actively to discussions during the work and were involved with the proof reading of the final manuscript.

Poly(Boc-acryloyl hydrazide): the importance of temperature and RAFT agent degradation on its preparation

Oliver Creese, Pavan Adoni, Guanlong Su, Andrey Romanyuk and Paco Fernandez-Trillo, ,

Polym. Chem. 2019, **124**, 14922-7

Abstract

Poly(acryloyl hydrazide) is a versatile polymer scaffold readily functionalised through post-polymerisation modification with aldehydes to yield polymers for biological applications. However, its polymerisation is affected by nucleophilic degradation of the RAFT agent that leads to early termination, an issue often overlooked in the polymerisation of primary acrylamides. Here we report the effect of temperature on the RAFT polymerisation of N'-(tert-butoxycarbonyl)acryloyl hydrazide (1) and demonstrate that by carefully selecting this polymerisation temperature, a balance between rate of polymerisation and rate of degradation of the RAFT agent can be achieved. This way greater control over the polymerisation process is achieved, allowing the synthesis of Boc-protected poly(acryloyl hydrazide) with higher degrees of polymerisation (DP) than those obtained previously, while still maintaining low dispersities ($Đ_M$).

Introduction

Synthetic polymers are increasingly becoming an attractive means of interfacing biological systems via multivalent binding, displaying activities orders of magnitude higher than those of their monovalent components.[1–5] Thus, polymers are now widely researched for biomedical applications including as antimicrobials,[6,7] as drug and gene delivery vehicles,[2,8]

as biological sensors,[9,10] or as "smart" biomaterials with antifouling properties.[11] Highly functional polymers developed for specific applications generally involve the use of functional monomers which either already possess the final desired functionality, or have the capability of undergoing post-polymerisation modification to introduce the desired functionality. This latter approach can greatly broaden the scope of chemical functionalities used. Post-polymerisation modification has normally relied on click chemistries,[12] and has now been greatly expanded through the use of oxime[13] and hydrazone chemistry,[14,15] reductive amination,[16] and epoxide ring opening.[17] A common limitation when developing synthetic polymers for biomedical applications is the need to screen large libraries of compounds which is costly and time consuming. In this regard, poly(acryloyl hydrazide) has been recently reported as a versatile platform for the synthesis and screening of polymers for biomedical applications.[14,18–20] Functional polymers are obtained by simple incubation of poly(acryloyl hydrazide) with functional aldehydes, both under aqueous or organic conditions,[14] and this polymer has now been applied to the development of glycan arrays,[18] pH sensitive drug-delivery,[21] and nucleic acid delivery.[20,22,23] In our laboratories poly(acryloyl hydrazide) was prepared from Boc-protected precursor Boc-Px (Scheme 1) following deprotection with TFA.[14] Reversible addition–fragmentation chain-transfer (RAFT) polymerisation of N'-(tert-butoxycarbonyl) acryloyl hydrazide (1) resulted in a small library of polymers. However, control over the polymerisation was lost with increasing conversion and degree of polymerisation, possibly as a result of degradation of the RAFT agent through intramolecular nucleophilic attack. This degradation has been reported in the RAFT polymerisation of other acrylamide derivatives,[24,25] including closely related methacryloyl hydrazide,[26] with better control reported when the polymerisation is carried out at low temperatures.[25,27] This side-reaction is often overlooked in the polymerisation of primary

and secondary acryl- and methacrylamides, and makes synthesising highly functional polymers from this type of monomers inherently challenging.[28] The need for greater control over these materials is more significant when looking to understand better the nature of the structure–activity relationship throughout post-polymerisation modification and biological screening. Here, we report the effect of temperature and the decomposition rate of the initiator on the polymerisation of N'-(tertbutoxycarbonyl)acryloyl hydrazide (1), as a route to optimise the preparation of poly(acryloyl hydrazide). Polymerisations were carried out using 2,2'-azobis[2-(2-imidazolin-2-yl) propane]dihydrochloride (VA-044) as a low temperature initiator, so that the rate of generation of radicals could be readily modified as a function of temperature. Our results suggest that while increasing the temperature increases the polymerisation rate, it also speeds up RAFT degradation and thus, loss of control. Conditions have been identified for which the polymerisation "outperforms" this side reaction and polymers with good control over molecular mass and dispersities ($Đ_M$) can be obtained. More importantly, these conditions allowed us to prepare Boc-Px with higher degrees of polymerisation and lower $Đ_M$, not accessible with our previous conditions.[14] This improved control over the polymerisation of Boc-protected poly(acryloyl hydrazide) will be of value when DP and $Đ_M$ may underpin future applications.

Experimental section

Materials

2-((Ethylthio)carbonothioyl)thio-2-methylpropanoic acid (CTA) [29] and N'-(tert-butoxycarbonyl)acryloyl hydrazide (1) [14,20] were synthesised according to protocols described in the literature. 2,2'-Azobis[2-(2-imidazolin-2-yl)propane] dihydrochloride (VA-

044) was purchased from Fluorochem and used without further purification. All other chemicals were purchased from Sigma-Aldrich®, Fisher Scientific®, VWR® or Acros®, and used without further purification. All solvents were Reagent grade or above, purchased from Sigma-Aldrich®, Fisher Scientific® or VWR®, and used without further purification. Polymethylmethacrylate standards were purchased from Agilent®.

Characterisation

Nuclear Magnetic Resonance (NMR) spectra were recorded on either a Bruker Avance III 300 MHz or a Bruker Avance III 400 MHz spectrometer. Chemical shifts are reported in ppm (units) referenced to the following solvent signals: dimethylsulfoxide (DMSO)-d6 H 2.50. Gel Permeation Chromatography (GPC) was performed with a Shimadzu Prominence LC-20A fitted with a Thermo Fisher Refractomax 521 Detector and a SPD20A UV-vis Detector. Poly(N'-(tert-butoxycarbonyl)acryloyl hydrazide) (Boc-Px) was analysed using 0.05 M LiBr in dimethylformamide (DMF) at 60 °C as the eluent, and a flow rate of 1 mL min−1 . The instrument was fitted with a Polymer Labs PolarGel guard column (50 × 7.5 mm, 5 µm) followed by two PLGel PL1110-6540 columns (300 × 7.5 mm, 5 µm). Molecular masses were calculated based on a standard calibration method using polymethylmethacrylate standards.

RAFT polymerisation of N'-(tert-butoxycarbonyl)acryloyl hydrazide (1)

In a typical kinetic experiment 2,2'-azobis[2-(2-imidazolin-2-yl) propane]dihydrochloride (VA-044) (11.7 mg, 0.036 mmol), 2-ethylthiocarbonothioylthio-2-methylpropanoic-acid (CTA) (40.3 mg, 0.18 mmol) and N'-(tert-butoxycarbonyl)acryloyl hydrazide (1) (1.666 g, 8.950 mmol) were dissolved in DMSO (10.0 mL) and a 100 µL sample was taken at this stage

to calculate conversion (ρ). The solution vessel was sealed with a septum, securely fastened with electrical tape to maintain the seal, and degassed by bubbling with argon for 25 minutes. Using a cannula, 1 mL of the solution was transferred to sealed glass vials containing stirrer bars, each degassed for 5 minutes. Vials were then left to react at a pre-set temperature (30–150 °C) for the required amount of time. The reaction was stopped by allowing the tube to cool using a water bath and exposing it to air. 100 µL aliquots of each timepoint were taken at this stage to calculate conversion (ρ) and for GPC analysis. NMR and GPC analysis of each timepoint was carried out from the crude mixture. The natural logarithm of the inverse of the fractional concentration of monomer – ln(M0/Mt) – was plotted against time, and the data fitted using GraphPad Prism version 6.0 for Mac Os X, GraphPad Software, La Jolla California USA, http://www.graphpad.com. The in-built segmental line regression was used to fit the data to two intersecting lines. This model was used to identify when a change in the polymerisation kinetics was observed (t_{dead}).

Results and discussion

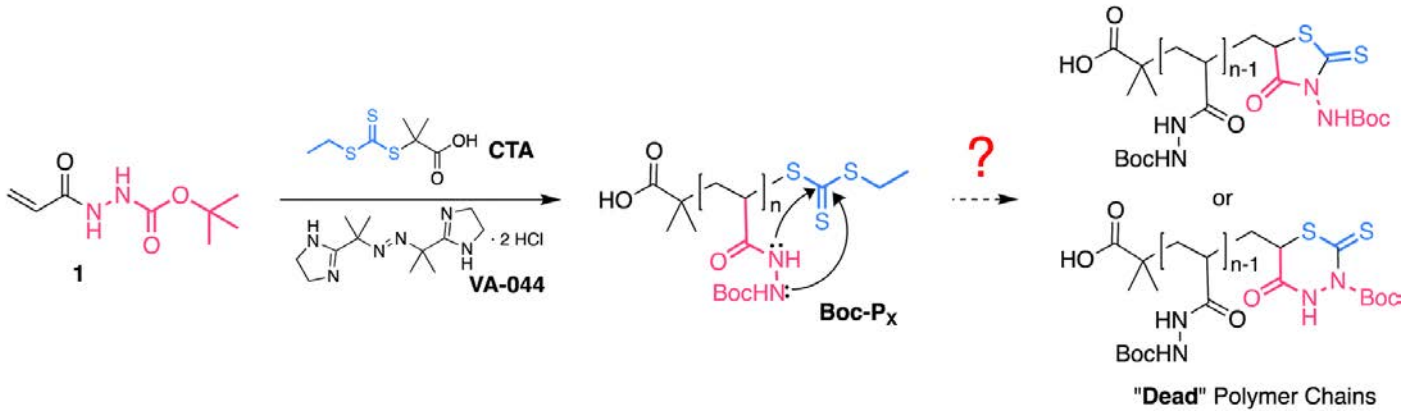

Scheme 1: RAFT polymerisation of N'-(tert-butoxycarbonyl)acryloyl hydrazide (1) and potential degradation by-products.

As reported, our initial efforts to optimise the polymerisation of Boc-protected acryloyl hydrazide **1** focused on reducing the temperature of the polymerisation.[14] RAFT polymerisation of acrylamides and methacrylamides often suffers from cleavage of the RAFT agent through intramolecular addition–elimination of the weakly nucleophilic amides to the trithiocarbonate group (Scheme 1).[25] Under our previously reported conditions for the polymerisation of **1**, a change in the rate of polymerisation was observed with increasing conversion (Fig. S1A†) which we associated with this degradation of the terminal trithiocarbonate in the growing chain. It has been proposed that reducing the polymerisation temperature would significantly reduce the rate of this side reaction.[25] Thus, optimisation of the polymerisation was at that time carried out under the same conditions but using initiators with different 10 hours half-life decomposition temperatures (t_{10}) (Fig. S1†). This way, the rate of formation of radicals was kept as similar as possible for all polymerisations while reducing the temperatures to 50 °C (V-65) or 44 °C (VA-044). Despite the use of lower temperatures, in all cases, a change in the kinetics of the polymerisation was observed, although this change was not as obvious for the polymerisations performed at 44 °C (Fig. S1A,† right). To identify when this change in rate of polymerisation was occurring, the natural logarithm of the inverse of the fractional concentration of monomer – $\ln(M_0/M_t)$ – was plotted against time, and the data fitted to a segmental line regression. This function fits the data to two different lines, before and after a breakpoint. In our case, we termed the breakpoint t_{dead} because we think that after this point, side reactions have a predominant effect on the kinetics of the polymerisation resulting in an increasing number of dead polymer chains. This change in kinetics was reflected on the relatively high dispersity in molecular mass ($Đ_M$ = 1.38–1.95) obtained for the polymers prepared under

these conditions.[14] Overall, no clear benefit from reducing the temperature was observed, with a t_{dead} of approximately 4 and 4.5 hours for polymerisations at 50 °C and 70 °C respectively. Interestingly, t_{dead} for the polymerisation performed at 44 °C was observed at approximately 2.5 h, which would suggest degradation was occurring faster at this temperature. This was not expected and may suggest that other mechanisms beyond the simple degradation of the RAFT agent may be at play. For instance, polymerisation decay can also be caused by diminishing initiator efficiency at high monomer conversions, which has been observed for some azo-initiators.[30,31] However, this factor normally becomes significant at much higher conversions than the ones we reported. Attempts to perform the polymerisation at an even lower temperature (30 °C) using VA-044 as the source of radicals resulted in a very long induction period followed by a short period of linear increase of the fractional concentration of monomer until a change in kinetics was again evident (Fig. S2†). The maximum conversion in this case was 50% – ln (M_0/M_t) = 0.83, worse than that observed for the polymerisations performed at higher temperatures. In order to determine if degradation of the RAFT agent was indeed possible at low temperatures, we attempted to synthesise a small molecule analogue which mimicked an n = 1 polymer (Scheme S1†). To this end, 2-bromopropionic acid (2) was reacted with tert-butyl carbazate, and the resulting bromine derivative **3** reacted under standard conditions for the formation of the RAFT agent. ^{1}H NMR analysis of this reaction revealed a very complex mixture, where only traces of something that could resemble trithiocarbonate 4 could be identified (Fig. S4†). This observation was in line with our previous results, and suggested that hydrazide containing trithiocarbonates such as **4** were very amenable to intramolecular nucleophilic attack. Attempts to isolate this trithiocarbonate **4** were unsuccessful, with the main isolated product of this reaction being tentatively assigned to a mixture of the 5- and 6-membered

rings in a 6 : 4 ratio (Fig. S5†). Seeing how lowering the temperature had no beneficial effect on the kinetics of the polymerisation of **1**, and a change in kinetics was still observed, we decided to explore the use of "Ultra-Fast" polymerisation conditions in an attempt to outrun the side reaction.[32–34] Our hypothesis was that by using a low temperature initiator such as VA-044 at a significantly higher temperature (e.g. 100 °C) than the reported t_{10} (44 °C), an increase in the concentration of radicals in solution would be achieved. This way, the concentration of propagating radicals would be higher with a greater number of chains growing at the same time, resulting in the synthesis of polymers with better control over the molecular mass and $Đ_M$. This methodology is particularly suitable for fast-propagating monomers such as acrylamides, and since the rate of polymerisation is directly proportional to the concentration of these propagating radicals (and the monomer concentration, Rp = kp[M][P•]), we postulated that running the polymerisation under these conditions could outperform the side reaction observed under standard RAFT polymerisation conditions. In a first attempt, the polymerisation conditions previously reported by us for the polymerisation of **1** (Fig. S1†) [14] were modified so that the initiator used was VA-044 and the polymerisation temperature was 100 °C. A shorter polymer was targeted this time and, as expected, the polymerisation was very fast, reaching up to 70% conversion in less than five minutes (Fig. 1A, CTA : VA-044 5:1 ●).

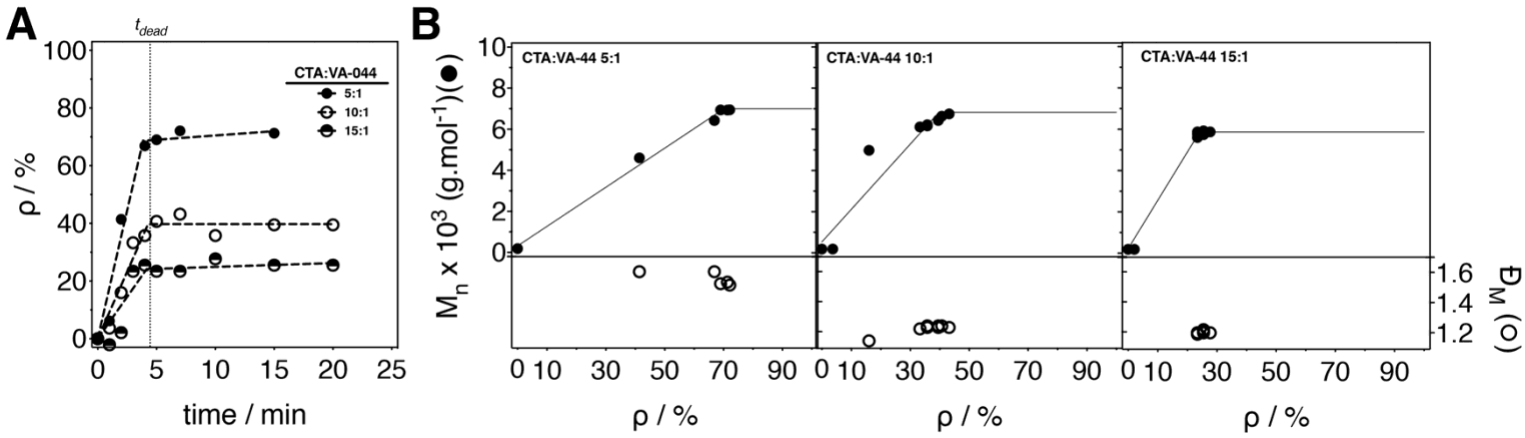

Fig. 1 (A) Plot of conversion (ρ) vs. time and (B) measured number average molecular mass (Mn) vs. conversion (●) and dispersity in molecular mass ($Đ_M$) vs. conversion (○), for polymerisations of N'-(tert-butoxycarbonyl)acryloyl hydrazide (1) performed with different CTA : VA-044 ratios. Conditions: [M] = 0.9 M, [M]/[CTA] = 50/1. Mn and $Đ_M$ calculated by GPC using 0.05 M LiBr in dimethylformamide (DMF) at 60 °C.

The change in reaction rate could not be suppressed and was again evident, with a t_{dead} of approximately 4.5 min. Before t_{dead}, the polymerisation retained the features of a controlled polymerisation, with the molecular mass of the polymer directly proportional to the conversion and, comparable dispersities (Fig. 1B, left) to those observed with our previous conditions.[14] These results were promising and we therefore explored decreasing the concentration of initiator in our polymerisations, in an attempt to suppress termination, increase the number of chains growing from the RAFT agent and thus optimising the dispersities. However, while dispersities were decreased, reducing the concentration of initiator in these polymerisations resulted in slower reactions, with no effect observed in t_{dead} (Fig. 1A). As a result, the maximum conversion obtained when the CTA : VA-044 ratio was increased to 10 : 1 or 15 : 1 (40% and 24% conversion respectively) was lower than in the previous case (70%). We decided next to run the polymerisations at 150 °C, in an attempt to further increase the concentration of radicals during early stages of

polymerisation, and thus the rate of propagation. However, these conditions not only resulted in lower conversions (Fig. S9†) but a colour change of the reaction mixture from yellow to dark brown, suggesting that thermal decomposition of the trithiocarbonate group was ocurring.[35] Thermal decomposition of the RAFT agent was confirmed via ^{1}H NMR where signals consistent with the β-elimination of the trithiocarbonate could be observed (Fig. S10†).[35,36]

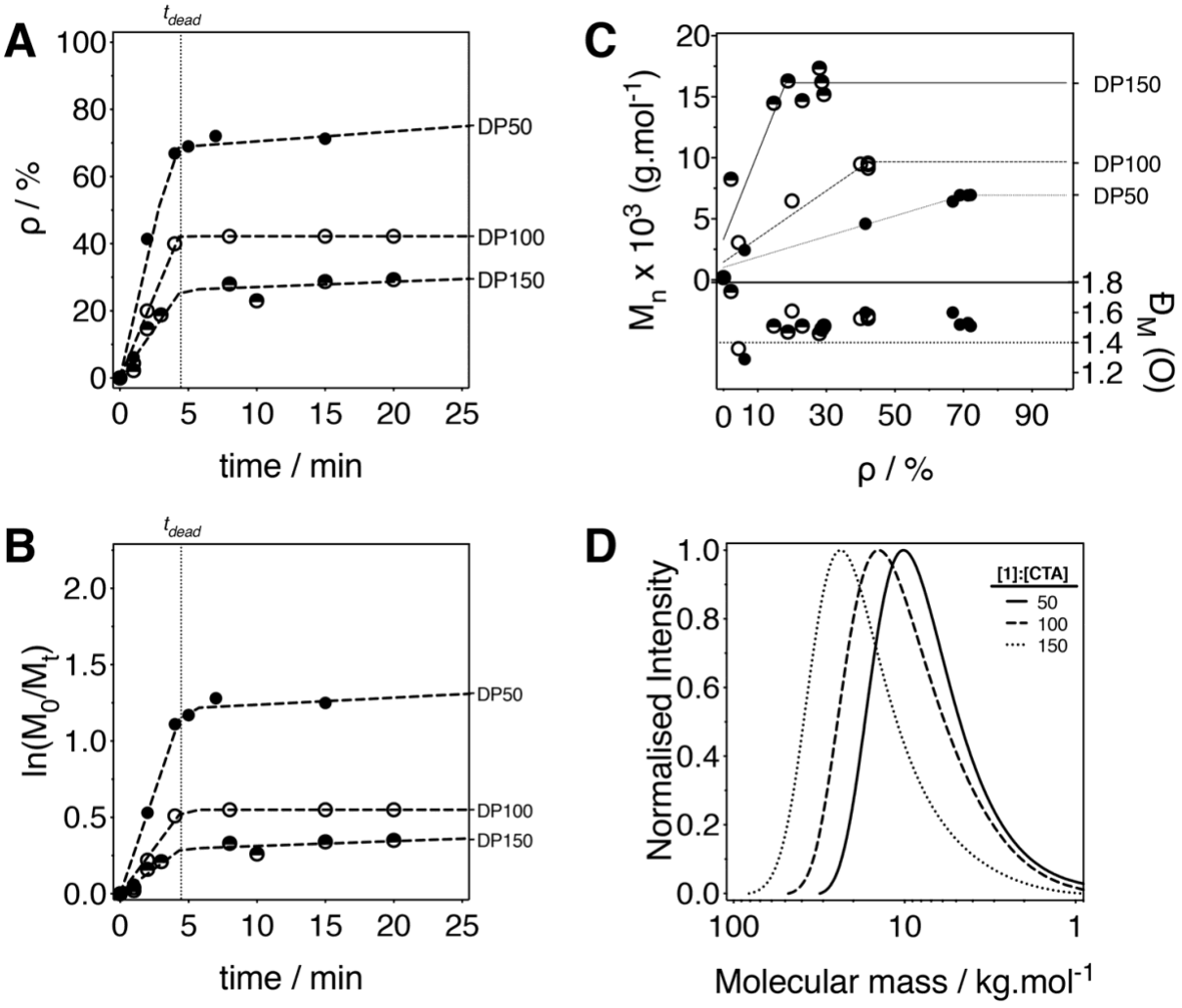

Fig. 2 (A) Plot of conversion (ρ) vs. time, (B) fractional concentration of monomer ln(M_0/M_t) vs. time, and (C) measured number average molecular mass (Mn) vs. conversion (ρ) (top) and dispersity in molecular mass ($Đ_M$) vs. conversion (ρ) (bottom), for polymerisations of N'-(tert-butoxycarbonyl) acryloyl hydrazide (1) performed at 100 °C with different 1 : CTA ratios. (D) GPC chromatograms of the resulting polymers at the highest conversion obtained. Conditions: [M] = 0.9 M, [CTA]/[VA-044] = 5/1. Mn and $Đ_M$ calculated by GPC using 0.05 M LiBr in dimethylformamide (DMF) at 60 °C.

Having identified conditions to run the polymerisation of **1** at 100 °C, which resulted in similar conversions and dispersities to those previously reported, we decided to explore the use of these conditions to prepare polymers of higher DP (Fig. 2), which were harder to control using our previously reported method.[14] Three different DPs were targeted (i.e. [1]/[CTA] = 50, 100 and 150), by maintaining the concentration of **1** and reducing the amount of RAFT agent and initiator used. As expected, this resulted in slower polymerisations, while t_{dead} still remained at around 4.5 min (Fig. 2A). As a consequence, polymerisations targeting 100 and 150 monomer units only reached low conversions (~40% and 30% respectively). In any case, control over the molecular mass of the polymer was still observed during the first stages of the polymerisation, with the average molecular mass (Mn) increasing linearly with time until the change in polymerisation rate was evident (t_{dead}) (Fig. 2B). A clear shift towards lower retention time was observed in the gel permeation chromatograms when higher DPs were targeted, suggesting that, at least during the initial phase of the reaction, the polymerisation was maintaining features of a controlled radical polymerisation. $Đ_M$ remained similar across the three targeted molecular masses which demonstrates an improvement compared to our previous conditions where $Đ_M$ increased with increasing targeted DP. At this point, our results suggested that a compromise could be obtained between increasing the rate of propagation by increasing the polymerisation temperature, and delaying t_{dead} by reducing the polymerisation temperature.

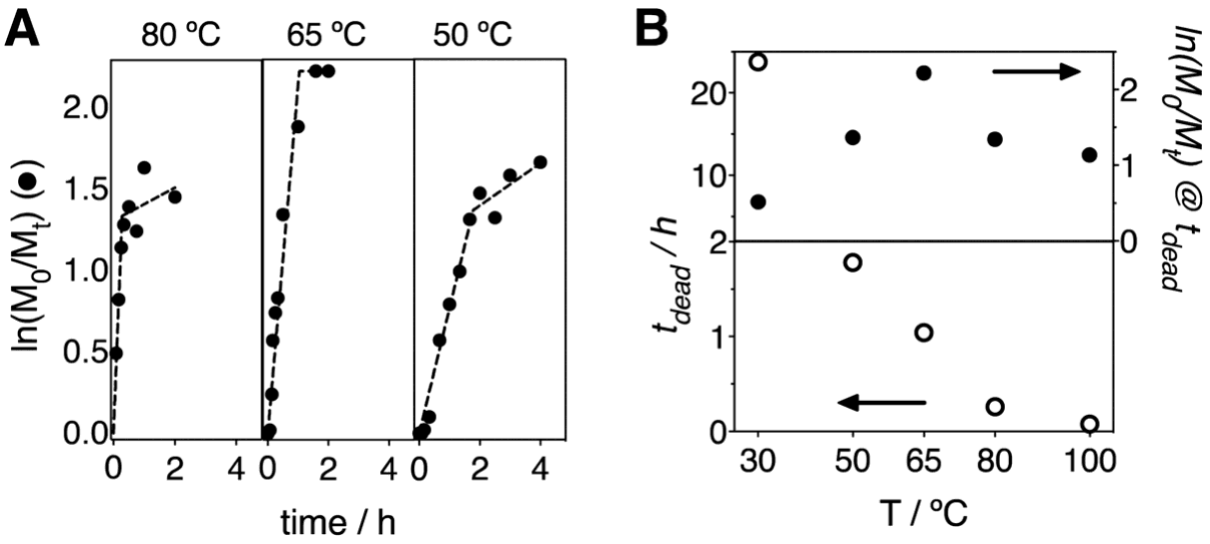

Fig. 3 (A) Plot of fractional concentration of monomer ln(M0/Mt) vs. time for polymerisations of N'-(tert-butoxycarbonyl)acryloyl hydrazide (1) performed at different temperatures. (B) Effect of temperature on the time at which deviation from linearity for the plot of ln[M]0/[M]t vs. time is observed (tdead) (○), and the fractional concentration of monomer ln(M0/Mt) at this point (●). Conditions: [M] = 0.9 M, [M]/[CTA]/[VA-044] = 50/1/0.2.

Therefore, we investigated polymerisations at intermediate temperatures (Fig. 3). While a change in polymerisation rate was still evident for the new temperatures investigated, higher conversions could be achieved for the polymerisation performed at 65 °C (90%) while the next highest conversions at 80 °C and 50 °C were 77% and 80% respectively (Fig. 3B, ●). Temperature had a significant effect on the time at which a change in polymerisation rate was evident (t_{dead}), with this inflection point happening sooner as the temperature was increased (Fig. 3B, ○). With encouraging results from the polymerisations at 65 °C, we set out to probe the "livingness" of the polymer before and after t_{dead} and thus whether t_{dead} was due to degradation of the RAFT agent. To this end, we isolated and purified two polymerisations of **1**, one that had been stopped at intermediate conversions (ρ = 47%, t = 30 min), before t_{dead} (Fig. S6A†) and one that was stopped at maximum conversion (ρ = 85%, t = 120 min), after t_{dead} (Fig. S6B†). As expected, Boc-Px isolated before t_{dead} was able to undergo complete chain extension with further addition of **1** and initiator (Fig. S6A†), thus

demonstrating that at intermediate conversions the RAFT agent was still present in significant amounts. GPC analysis of Boc-Px isolated after t_{dead} indicated that no chain extension had occurred, instead showing a bimodal distribution of molecular mass and high dispersities (Fig. S6B†) demonstrating that after t_{dead} the RAFT group had been degraded. To probe if the RAFT agent degradation was temperature driven, we isolated and purified a second "living" Boc-Px at intermediate conversions (ρ = 52% t = 30 min) (Fig. S7†). This polymer was then heated for 90 minutes under standard polymerisation conditions, but this time without addition of **1** and initiator. We anticipated that heating the polymer this way should result in degradation of the RAFT agent, a hypothesis that was confirmed upon attempting to chain extend this terminated Boc-Px. In this case, high dispersities, together with a shoulder at high molecular mass, were observed, indicating that the Boc-Px which had been subjected to further heating was "dead" (Fig. S7†). Additional evidence of the RAFT agent degradation was obtained from NMR spectroscopy, where the protons associated with both the R and Z end group of the polymer chain could be observed for the "living" Boc-Px whereas "dead" Boc-Px showed a loss of the Z group (Fig. S8†). Seeing how running the polymerisations at 65 °C gave the highest conversions (90%) at t_{dead} of all the conditions evaluated, we decided to target different degrees of polymerisation using these conditions (Fig. 4). As before, targeting higher DPs resulted in slower rates of polymerisation, in particular for DP200 and DP300. While slower rates had a significant effect on the maximum conversion achieved (approx. 90%, 89%, 68% and 55% for DP 50, 100, 200 and 300 respectively), little effect was observed on the t_{dead}, with most polymerisations "stopping" after 1 h (Fig. 4A).

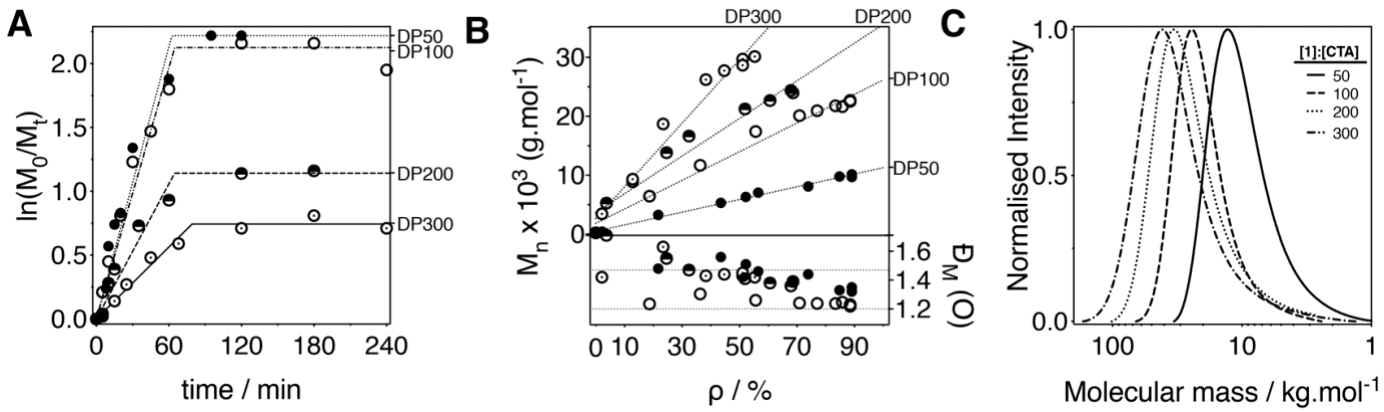

Fig. 4 (A) Plot of fractional concentration of monomer ln(M0/Mt) vs. time. (B) Measured number average molecular mass (Mn) vs. conversion (ρ) (top) and dispersity in molecular mass (ĐM) vs. conversion (ρ) (bottom), for polymerisations of N'-(tert-butoxycarbonyl)acryloyl hydrazide (1) performed at 65 °C with different 1 : CTA ratios. (C) GPC chromatograms of the resulting polymers at the highest ρ obtained. Conditions: [M] = 0.9 M, [CTA]/[VA-044] = 5/1. Mn and ĐM calculated by GPC using 0.05 M LiBr in dimethylformamide (DMF) at 60 °C.

Under these optimised conditions, the polymerisations retained features of a controlled polymerisation, with the molecular mass of the polymers increasing linearly with conversion, narrow dispersities in molar mass (Fig. 4C) and good end group fidelity if isolated before t_{dead}. In all cases, the dispersities obtained were similar or lower to those reported previously.[14] This improvement was particularly the case when targeting DPs of 100 and 200 with dispersities of <1.4 being observed at maximum conversion

Conclusion

Here we have demonstrated the role of temperature and RAFT agent degradation in the polymerisation of N'-(tert-butoxycarbonyl)acryloyl hydrazide (1). Our results highlight that the polymerisation of this hydrazide monomer **1** via RAFT can be severely hampered by the degradation of the chain transfer agent and that, under some circumstances, this degradation cannot be eliminated but rather outperformed if the rate of polymerisation is tuned. We demonstrate that by using a low temperature initiator such as VA-044, optimal

polymerisation conditions can be achieved at 65 °C. This way, poly(N'-(tertbutoxycarbonyl)acryloyl hydrazide)s with high degrees of polymerisation could be obtained while still maintaining low dispersities. We believe that further improvement of the polymerisation could be achieved through the choice of RAFT agents such as pyrazole or quaternised pyridinium dithiocarbamates,[37,38] the use of photopolymerisation,[39] or the use of alternative controlled polymerisation techniques. Our efforts in these directions will be reported in due course.

References

1. Gestwicki JE, Cairo CW, Strong LE, Oetjen KA, Kiessling LL. Influencing receptor-ligand binding mechanisms with multivalent ligand architecture. J Am Chem Soc. 2002. doi:10.1021/ja027184x
2. Duncan R. The dawning era of polymer therapeutics. Nat Rev Drug Discov. 2003. doi:10.1038/nrd1088
3. Zhu C, Liu L, Yang Q, Lv F, Wang S. Water-soluble conjugated polymers for imaging, diagnosis, and therapy. Chem Rev. 2012. doi:10.1021/cr200263w
4. Li J, Yu F, Chen Y, Oupický D. Polymeric drugs: Advances in the development of pharmacologically active polymers. J Control Release. 2015. doi:10.1016/j.jconrel.2015.09.043
5. Green JJ, Elisseeff JH. Mimicking biological functionality with polymers for biomedical applications. Nature. 2016. doi:10.1038/nature21005
6. Muñoz-Bonilla A, Fernández-García M. Polymeric materials with antimicrobial activity. Prog Polym Sci. 2012. doi:10.1016/j.progpolymsci.2011.08.005

7. Kenawy ER, Worley SD, Broughton R. The chemistry and applications of antimicrobial polymers: A state-of-the-art review. Biomacromolecules. 2007. doi:10.1021/bm061150q

8. Pack DW, Hoffman AS, Pun S, Stayton PS. Design and development of polymers for gene delivery. Nat Rev Drug Discov. 2005. doi:10.1038/nrd1775

9. Kim HN, Guo Z, Zhu W, Yoon J, Tian H. Recent progress on polymer-based fluorescent and colorimetric chemosensors. Chem Soc Rev. 2011. doi:10.1039/c0cs00058b

10. Richards SJ, Jones MW, Hunaban M, Haddleton DM, Gibson MI. Probing bacterial-toxin inhibition with synthetic glycopolymers prepared by tandem post-polymerization modification: Role of linker length and carbohydrate density. Angew Chemie - Int Ed. 2012. doi:10.1002/anie.201202945

11. Cao Z, Mi L, Mendiola J, et al. Reversibly switching the function of a surface between attacking and defending against bacteria. Angew Chemie - Int Ed. 2012. doi:10.1002/anie.201106466

12. Theato P, Klok HA. Functional Polymers by Post-Polymerization Modification: Concepts, Guidelines, and Applications.; 2013. doi:10.1002/9783527655427

13. Collins J, Xiao Z, Müllner M, Connal LA. The emergence of oxime click chemistry and its utility in polymer science. Polym Chem. 2016. doi:10.1039/c6py00635c

14. Crisan DN, Creese O, Ball R, et al. Poly(acryloyl hydrazide), a versatile scaffold for the preparation of functional polymers: Synthesis and post-polymerisation modification. Polym Chem. 2017. doi:10.1039/c7py00535k

15. Kölmel DK, Kool ET. Oximes and Hydrazones in Bioconjugation: Mechanism and Catalysis. Chem Rev. 2017. doi:10.1021/acs.chemrev.7b00090

16. Brisson ERL, Xiao Z, Levin L, Franks G V., Connal LA. Facile synthesis of histidine

functional poly(N-isopropylacrylamide): Zwitterionic and temperature responsive materials. Polym Chem. 2016. doi:10.1039/c5py01915j

17. Muzammil EM, Khan A, Stuparu MC. Post-polymerization modification reactions of poly(glycidyl methacrylate)s. RSC Adv. 2017. doi:10.1039/c7ra11093f

18. Godula K, Bertozzi CR. Synthesis of glycopolymers for microarray applications via ligation of reducing sugars to a poly(acryloyl hydrazide) scaffold. J Am Chem Soc. 2010. doi:10.1021/ja103009d

19. Kumar A, Ujjwal RR, Mittal A, Bansal A, Ojha U. Polyacryloyl hydrazide: An efficient, simple, and cost effective precursor to a range of functional materials through hydrazide based click reactions. ACS Appl Mater Interfaces. 2014. doi:10.1021/am404837f

20. Priegue JM, Crisan DN, Martínez-Costas J, Granja JR, Fernandez-Trillo F, Montenegro J. In Situ Functionalized Polymers for siRNA Delivery. Angew Chemie - Int Ed. 2016. doi:10.1002/anie.201601441

21. Kumar A, Ujjwal RR, Mittal A, Bansal A, Ojha U. Polyacryloyl hydrazide: An efficient, simple, and cost effective precursor to a range of functional materials through hydrazide based click reactions. ACS Appl Mater Interfaces. 2014. doi:10.1021/am404837f

22. Priegue JM, Lostalé-Seijo I, Crisan D, Granja JR, Fernández-Trillo F, Montenegro J. Different-Length Hydrazone Activated Polymers for Plasmid DNA Condensation and Cellular Transfection. Biomacromolecules. 2018. doi:10.1021/acs.biomac.8b00252

23. Juanes M, Creese O, Fernández-Trillo P, Montenegro J. Messenger RNA delivery by hydrazone-activated polymers. Medchemcomm. 2019. doi:10.1039/c9md00231f

24. Moskowitz JD, Abel BA, McCormick CL, Wiggins JS. High molecular weight and low

dispersity polyacrylonitrile by low temperature RAFT polymerization. J Polym Sci Part A Polym Chem. 2016. doi:10.1002/pola.27806

25. Abel BA, McCormick CL. Mechanistic Insights into Temperature-Dependent Trithiocarbonate Chain-End Degradation during the RAFT Polymerization of N-Arylmethacrylamides. Macromolecules. 2016. doi:10.1021/acs.macromol.5b02463

26. Hoff EA, Abel BA, Tretbar CA, McCormick CL, Patton DL. Aqueous RAFT at pH zero: Enabling controlled polymerization of unprotected acyl hydrazide methacrylamides. Polym Chem. 2017. doi:10.1039/c6py01563h

27. Chalmers BA, Alzahrani A, Hawkins G, Aldabbagh F. Efficient synthesis and RAFT polymerization of the previously elusive N-[(cycloalkylamino)methyl]acrylamide monomer class. J Polym Sci Part A Polym Chem. 2017. doi:10.1002/pola.28607

28. Perrier S. 50th Anniversary Perspective: RAFT Polymerization - A User Guide. Macromolecules. 2017. doi:10.1021/acs.macromol.7b00767

29. Skey J, O'Reilly RK. Facile one pot synthesis of a range of reversible addition-fragmentation chain transfer (RAFT) agents. Chem Commun. 2008. doi:10.1039/b804260h

30. Moad G. A Critical Assessment of the Kinetics and Mechanism of Initiation of Radical Polymerization with Commercially Available Dialkyldiazene Initiators. Prog Polym Sci. 2019. doi:10.1016/j.progpolymsci.2018.08.003

31. Zhou Y, Zhang Z, Postma A, Moad G. Kinetics and mechanism for thermal and photochemical decomposition of 4,4'-azobis(4-cyanopentanoic acid) in aqueous media. Polym Chem. 2019. doi:10.1039/c9py00507b

32. Gody G, Maschmeyer T, Zetterlund PB, Perrier S. Rapid and quantitative one-pot synthesis of sequence-controlled polymers by radical polymerization. Nat Commun.

2013. doi:10.1038/ncomms3505

33. Gody G, Maschmeyer T, Zetterlund PB, Perrier S. Exploitation of the degenerative transfer mechanism in RAFT polymerization for synthesis of polymer of high livingness at full monomer conversion. Macromolecules. 2014. doi:10.1021/ma402286e

34. Gody G, Barbey R, Danial M, Perrier S. Ultrafast RAFT polymerization: Multiblock copolymers within minutes. Polym Chem. 2015. doi:10.1039/c4py01251h

35. Zhou Y, He J, Li C, Hong L, Yang Y. Dependence of thermal stability on molecular structure of RAFT/MADIX agents: A kinetic and mechanistic study. Macromolecules. 2011. doi:10.1021/ma201570f

36. Legge TM, Slark AT, Perrier S. Thermal stability of reversible addition-fragmentation chain transfer/macromolecular architecture design by interchange of xanthates chain-transfer agents. J Polym Sci Part A Polym Chem. 2006. doi:10.1002/pola.21803

37. Gardiner J, Martinez-Botella I, Tsanaktsidis J, Moad G. Dithiocarbamate RAFT agents with broad applicability-the 3,5-dimethyl-1H-pyrazole-1-carbodithioates. Polym Chem. 2016. doi:10.1039/c5py01382h

38. Keddie DJ, Guerrero-Sanchez C, Moad G, Rizzardo E, Thang SH. Switchable reversible addition-fragmentation chain transfer (raft) polymerization in aqueous solution, n, n -dimethylacrylamide. Macromolecules. 2011. doi:10.1021/ma200760q

39. Chen M, Zhong M, Johnson JA. Light-Controlled Radical Polymerization: Mechanisms, Methods, and Applications. Chem Rev. 2016. doi:10.1021/acs.chemrev.5b00671

Supporting Information

Poly(Boc-acryloyl hydrazide): The importance of temperature and RAFT agent degradation on its preparation

Oliver Creese, Pavan Adoni, Guanlong Su, Andrey Romanyuk and Paco Fernandez-Trillo*

School of Chemistry, and Institute of Microbiology and Infection, University of Birmingham, Edgbaston, B15 2TT Birmingham

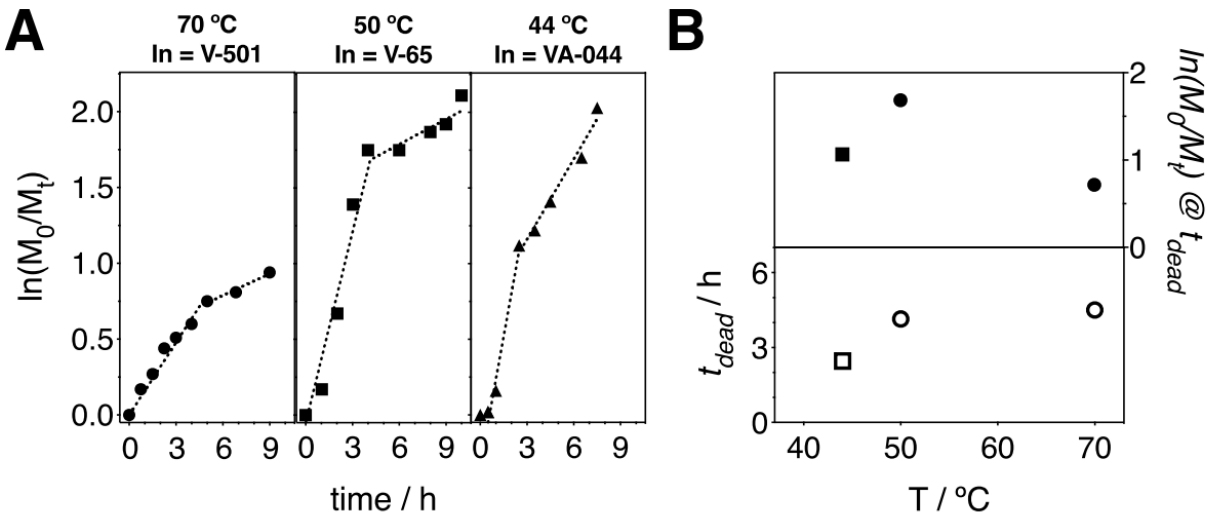

Figure S1. A) Plot of fractional concentration of monomer $ln(M_0/M_t)$ vs time for polymerisations of N'-(tert-butoxycarbonyl)acryloyl hydrazide (1) performed at different temperatures. Conditions: [M]=0.9M, [M]/[CTA]/[In]=100/1/0.2. 4,4'-Azobis(4-cyanovaleric acid) (V-501) - circles, 2,2'- azobis(2,4-dimethylvaleronitrile) (V-65) - squares, and 2,2'-azobis[2-(2-imidazolin-2- yl)propane]dihydrochloride (VA-044) - triangles. Adapted with permission from Crisan, D. N.; Creese, O.; Ball, R.; Brioso, J. L.; Martyn, B.; Montenegro, J.; Fernandez-Trillo, F. Polym. Chem. 2017, 8 (31), 4576– 4584 - Published by The Royal Society of Chemistry. B) For polymerisations carried out in S1A, effect of temperature on the time at which deviation from linearity for the plot of $ln[M]_0/[M]_t$ vs time is observed (t_{dead}), and the fractional concentration of monomer $ln(M_0/M_t)$ at this point.

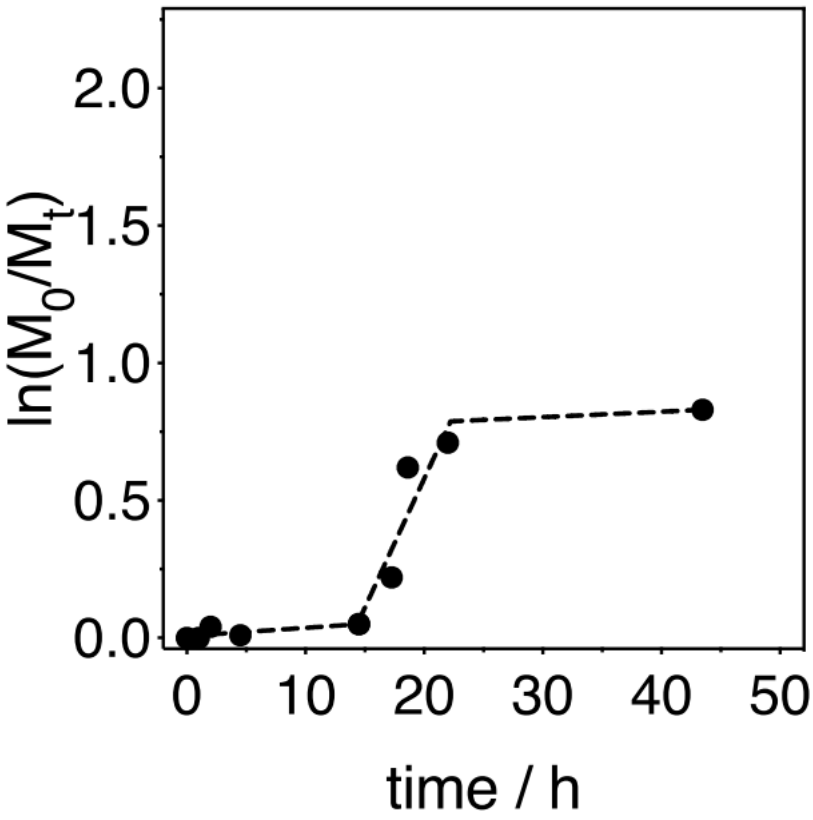

Figure S2. Plot of ln(M_0/M_t) vs time for the polymerisation of N'-(tert butoxycarbonyl)acryloyl hydrazide (1) at 30 ºC. Conditions: [M]=0.9M, [M]/[CTA]/[VA-044]=50/1/0.2.

Small molecule analogue of a DP= 1 of N'-(tert-butoxycarbonyl)acryloyl hydrazide (1).

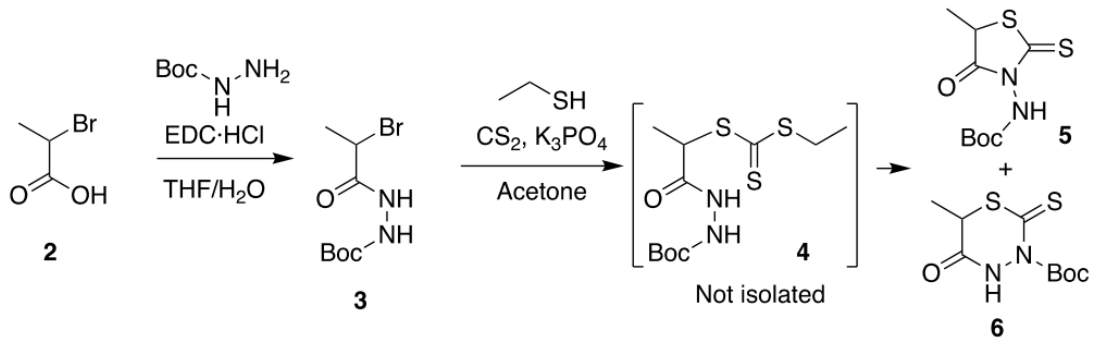

Scheme S1. Attempted route for the synthesis of a DP= 1 analogue of N'-(tert-butoxycarbonyl)acryloyl hydrazide (1).

tert-butyl 2-(2-bromopropanoyl)hydrazine-1-carboxylate (3)

2-Bromopropionic acid (2) (10 g, 59.9 mmol) and tert-butyl carbazate (6.56 g, 49.6 mmol) were dissolved in a 2:1 mixture of water/THF (180 ml). N-(3-Dimethylaminopropyl)-N'-ethylcarbodiimide hydrochloride (13.3 g, 69.5 mmol) was added in portions to the solution over 15 minutes and the mixture was left stirring for 3h at room temperature. The solution was extracted into EtOAc (3 x 60 ml) and a basic work-up performed with NaCO3 (3 X 60 ml). The organic layer was further washed with water (2 x 60 ml), dried with Na2SO4, filtered and the solvent removed under reduced pressure to leave a white solid. This solid was then recrystallised using ethyl acetate to afford white crystalline material which was washed with ice cold diethyl ether and dried under reduced pressure (8.9 g, 64 %): 1H NMR (300MHz, DMSO-d6) δ (ppm) 9.9 (s, 1H), 9.0-8.3 (s, 1H), 4.45 (q, 1H), 1.65 (d, 3H), 1.38 (s, 9H).

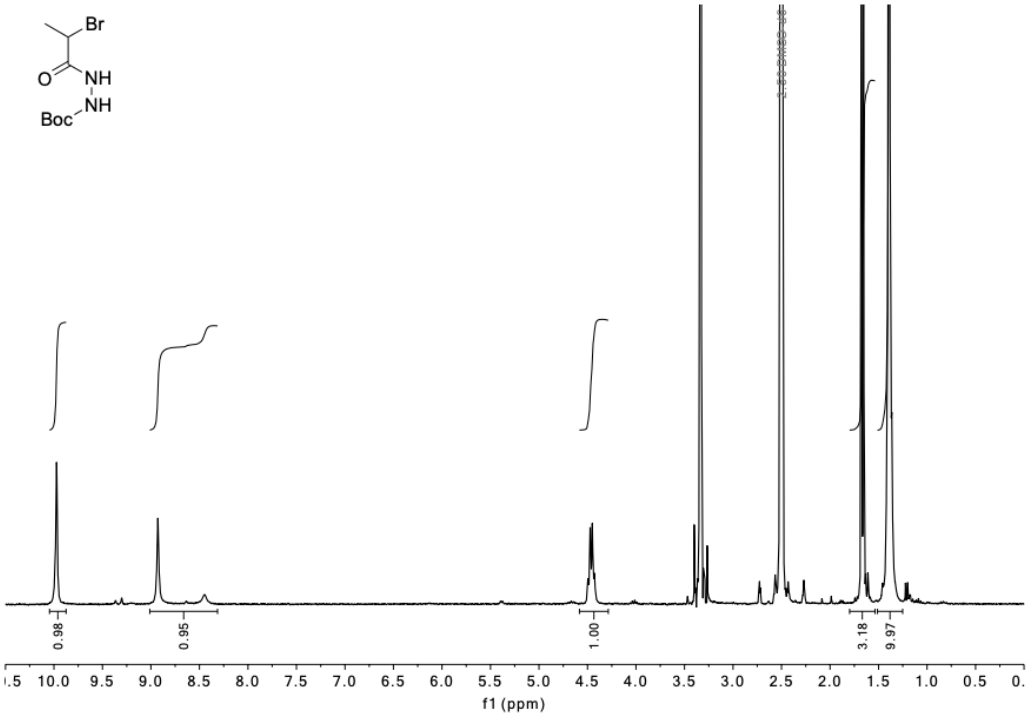

Figure S3. 1H NMR (300 MHz, CDCl3) spectrum of tert-butyl 2-(2-bromopropanoyl)hydrazine-1-carboxylate (3).

tert-butyl 2-(2-(((ethylthio)carbonothioyl)thio)propanoyl)hydrazine-1-carboxylate (4) (not isolated):

Ethanethiol (0.49 ml, 6.59 mmol) was added to a suspension of K3PO4 (1.4 g, 6.59 mmol) in acetone (20 ml) and was left stirring at room temperature for 10 minutes. CS2 (1.09 ml, 6.59 mmol) was then added and the reaction mixture was left for a further 10 minutes. tert-butyl 2-(2- bromopropanoyl)hydrazine-1-carboxylate (1) (1.6 g, 5.99 mmol) was added in one portion and the mixture left to react for 13 hours. The solvent was then removed under reduced pressure and HCl (100 ml, 1 M) was added to the crude of the reaction. The resulting mixture extracted into DCM (2 x 100 ml). The organic layer was then washed with water (2 x 100 ml) and brine (2 x 100 ml), dried with Na2SO4, filtered and the solvent removed under reduced pressure. The resulting orange oil was purified by column chromatography using a 7:3 ratio of diethyl ether and hexane, then dried under reduced pressure to leave a viscous orange liquid (0.12 g, 7 %) which consisted of two compounds, none of which is the title compound. a; 1H NMR (300MHz, CDCl3) δ (ppm) 10.3-9.7 (1H, s, NH), 4.66 (q, 1H), 1.58 (d, 3H), 1.44 (s, 9H) and b; 1H NMR (300MHz, CDCl3) δ (ppm) 10.3-9.7 (1H, s, NH), 4.73 (q, 1H), 1.59 (d, 3H), 1.44 (s, 9H).

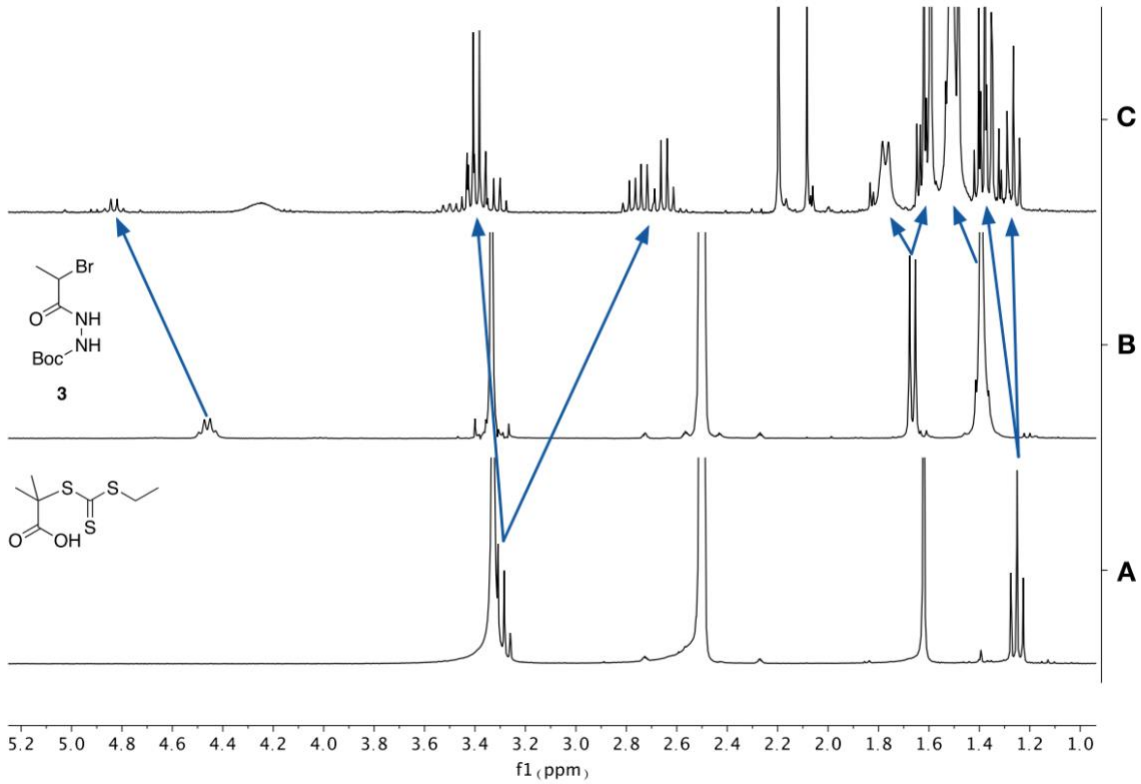

Figure S4. A) 1H NMR (300 MHz, DMSO) spectrum of 2-((ethylthio)carbonothioyl)thio-2-methylpropanoic acid (CTA). B) 1H NMR (300 MHz, CDCl3) spectrum of tert-butyl 2-(2-bromopropanoyl)hydrazine-1-carboxylate (3). C) 1H NMR (300 MHz, CDCl3) spectrum of the reaction of ethanethiol with carbon disulfide and tert-butyl 2-(2-bromopropanoyl)hydrazine-1-carboxylate (3).

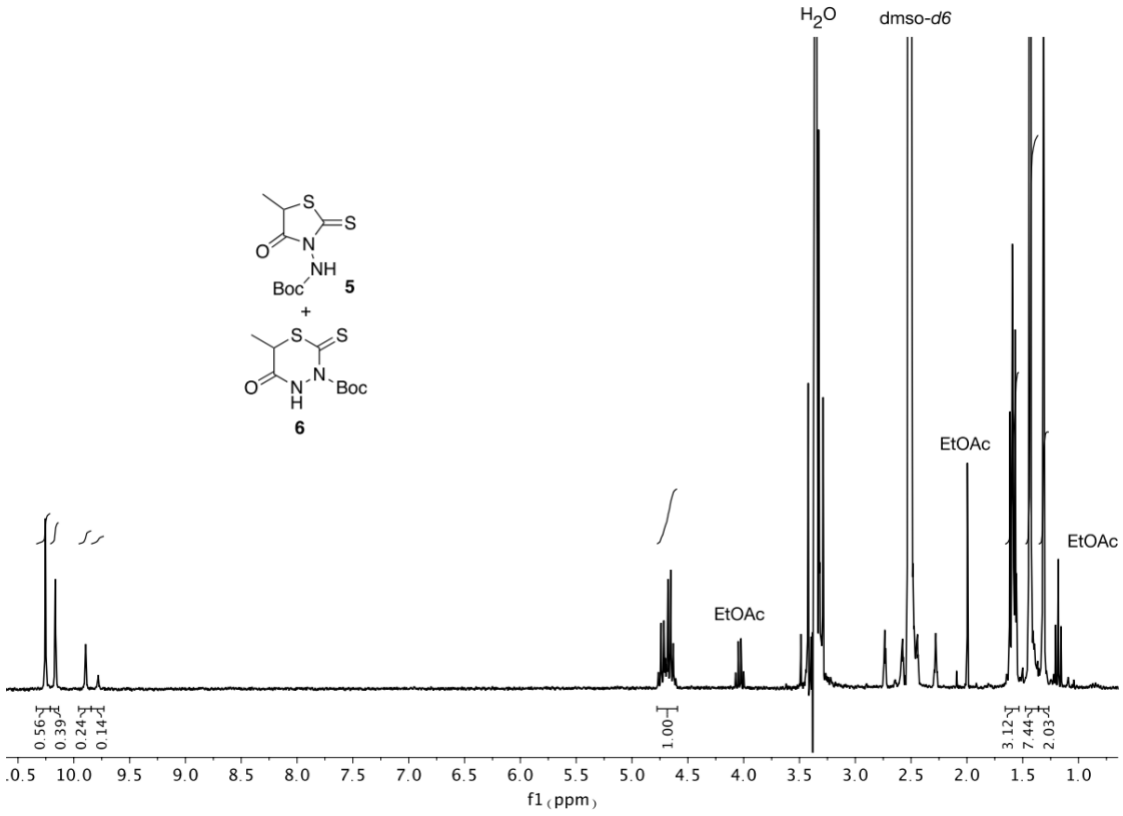

Figure S5. 1H NMR (300 MHz, CDCl3) spectrum of the main fraction isolated following the reaction of ethanethiol with carbon disulfide and tert-butyl 2-(2-bromopropanoyl)hydrazine-1-carboxylate (3).

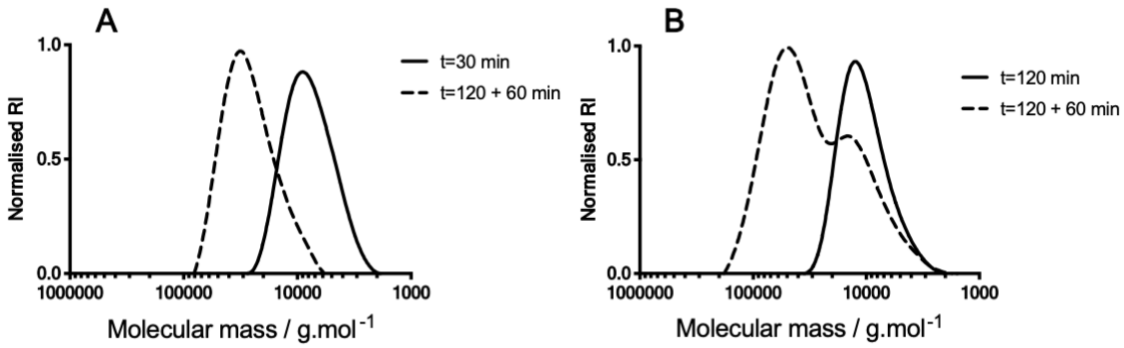

Figure S6. A) GPC traces (DMF LiBr 0.05M) of "living" Boc-Px after (t=30 min) and subsequent chain extension with (1)(t=30+60 min). B) "dead" Boc-Px (t=120 min) and subsequent inability to chain extend with (1) (t=120+60 min).

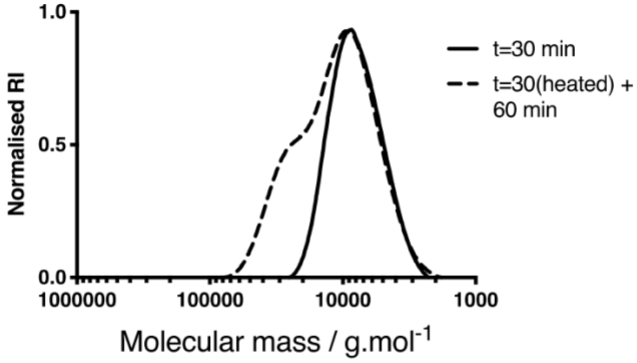

Figure S7. GPC traces (DMF LiBr 0.05M) of isolated "living" Boc-Px after (t=30 min) after further heating (60 ºC t=90 min), and subsequent inability to chain extend with (1) (t=30+60 min)

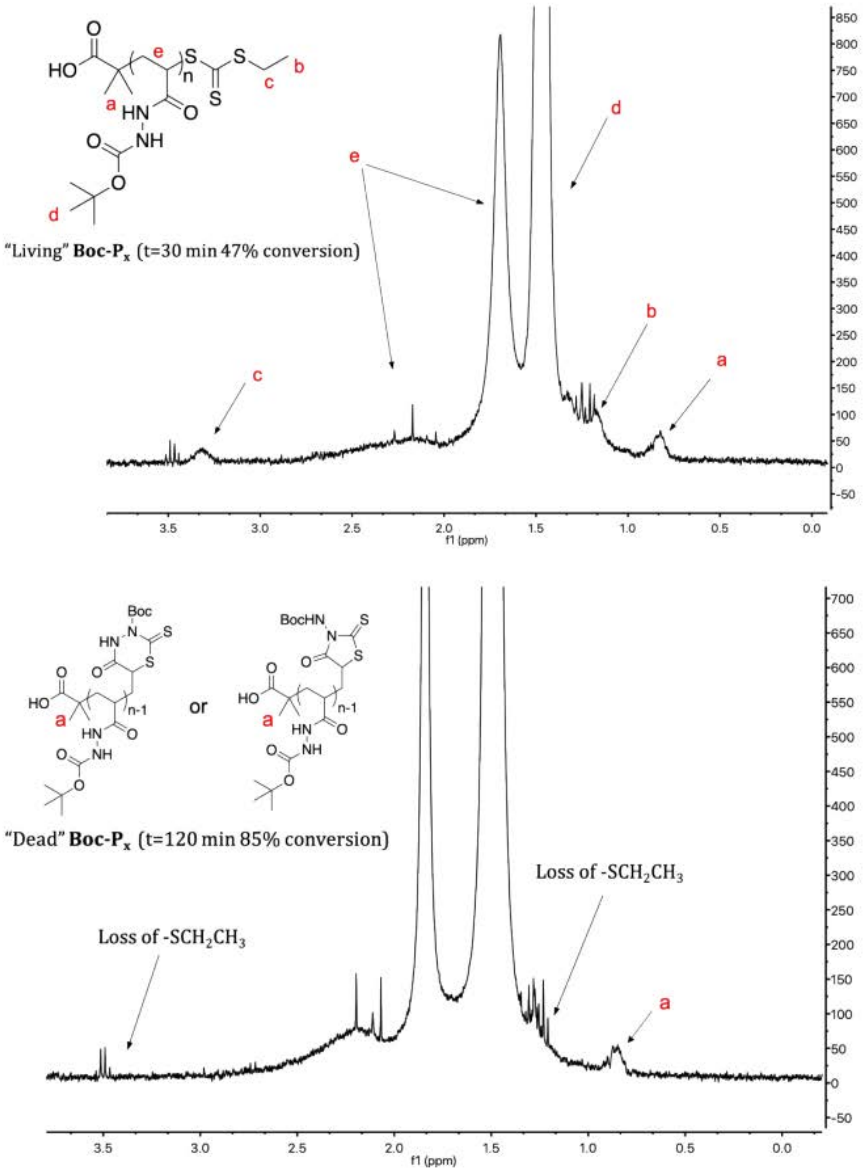

Figure S8. Top: 1H NMR (300 MHz, CDCl3) of "living" Boc-Px after polymerisation reaction was stopped after 30 minutes, before full conversion (47%). Bottom: 1H NMR (300 MHz, CDCl3) of "dead" Boc-Px after polymerisation for 120 minutes to maximum conversion (85%).

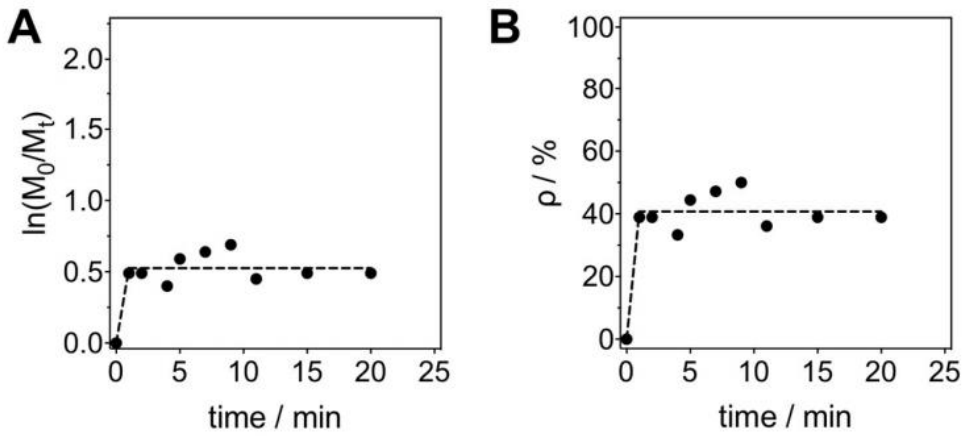

Figure S9. Plot of ln(M0/Mt) vs time (A) and conversion (ρ) vs time (B) for the polymerisation of N'-(tertbutoxycarbonyl)acryloyl hydrazide (1) at 150 ºC. Conditions: [M]=0.9M, [M]/[CTA]/[VA-044]=50/1/0.2.

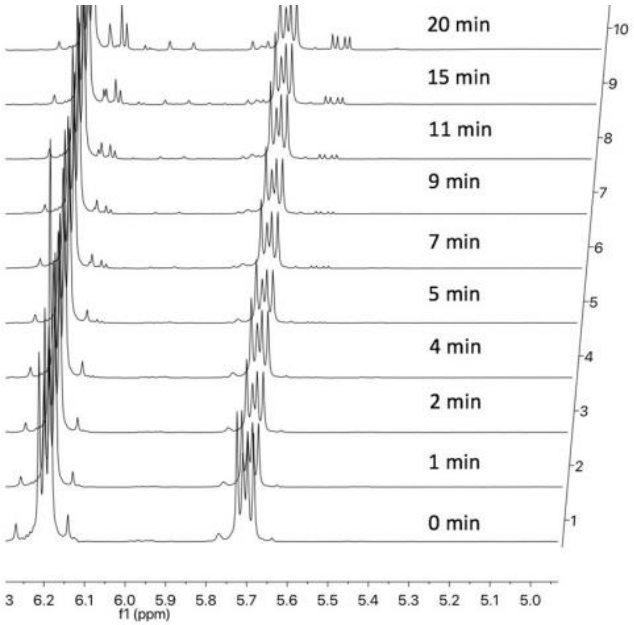

Figure S10. 1H NMR (300 MHz, CDCl3) spectrum showing vinyl region at varying time points in the polymerisation of N'-(tert-butoxycarbonyl)acryloyl hydrazide (1) at 150 ºC. Conditions: [M]=0.9M, [M]/[CTA]/[VA-044]=50/1/0.2. New vinyl protons can be observed from 7 minutes, suggestive of βelimination products

Chapter 4 – Screening of poly(acryloyl hydrazide) based polymers for bacterial aggregation and the stimulation of functional *E.coli* K-12 biofilms

(i) Abstract

Functional polymers based on a poly(acryloyl hydrazide) scaffold were screed with the biofilm forming *Escherichia coli* K-12 strain PHL644 for potential polymer-induced aggregation of cells. Poly(acryloyl hydrazide) was functionalised with a range of aldehydes resulting in a library of polymers with differing physiochemical properties, including hydrophobicity and pKa. It was found that polymer induced aggregation of PHL644 cells was driven primarily by hydrophobic interactions, with charged polymers inducing minimal aggregation via charge interaction.

(ii) Introduction

Bacterial biofilms are made up of surface associated bacterial cells that form a co-operative community that protects them from predators, supports the division of labour and conservation of genotype. Cells within a biofilm are embedded in a self-produced extracellular matrix that provides structural integrity and provides a physical barrier against mechanical and physical stimuli[1]. The transition of cells from planktonic to a sessile biofilm lifestyle is driven by complex changes in gene expression which serve to add to their persistent characteristics[2]. Historically therefore biofilms are seen as problematic as they are difficult to remove from surfaces, display resistance to chemical treatment[3], cause infection[4] and are associated with antibiotic resistance[5]. These resilient characteristics however can be exploited in different fields in biotechnology including biocatalysis[6] and bioremediation[7] where normal planktonic bacterial cells may be susceptible to harsh conditions. To this end, we wanted to form a platform for the control of biofilm formation,

in the hope of subsequent control over biofilm functionality e.g. in the field of biocatalysis. The first stage of the biofilm lifecycle is the attachment of bacteria to a surface and in this sense synthetic polymers have been shown to interact and aggregate bacteria through non-specific and specific interactions, with potentially interesting changes in cell phenotype including biofilm expression[8,9,10,11]. To this end a series of functional polymers based on a poly(acryloyl hydrazide) scaffold[12] (pAH) were made by post-polymerisation functionalisation of pAH. The resulting polymers varied in terms of their physiochemical properties including pKa values and hydrophobicity. These polymers were then tested with the biofilm forming *E. coli* K-12 strain PHL644 to monitor potential polymer-bacterial interactions such as the polymer-induced aggregation of cells, and the overall amount of aggregating biomass associated with each polymer when incubated with PHL644 for a set amount of time. It was found that on the whole, poly(acryloyl hydrazide) functionalised with hydrophobic moieties were able to interact and aggregate PHL644 cells primarily through hydrophobic interactions. The next chapter builds on the data gathered in this section to optimise polymer-induced biofilm formation, including analysis of the functionality of polymer-induced biofilms in the biocatalysis arena.

.

(iii) Results and Discussion

(a) Synthesis of functional polymers used to aggregate PHL644 cells

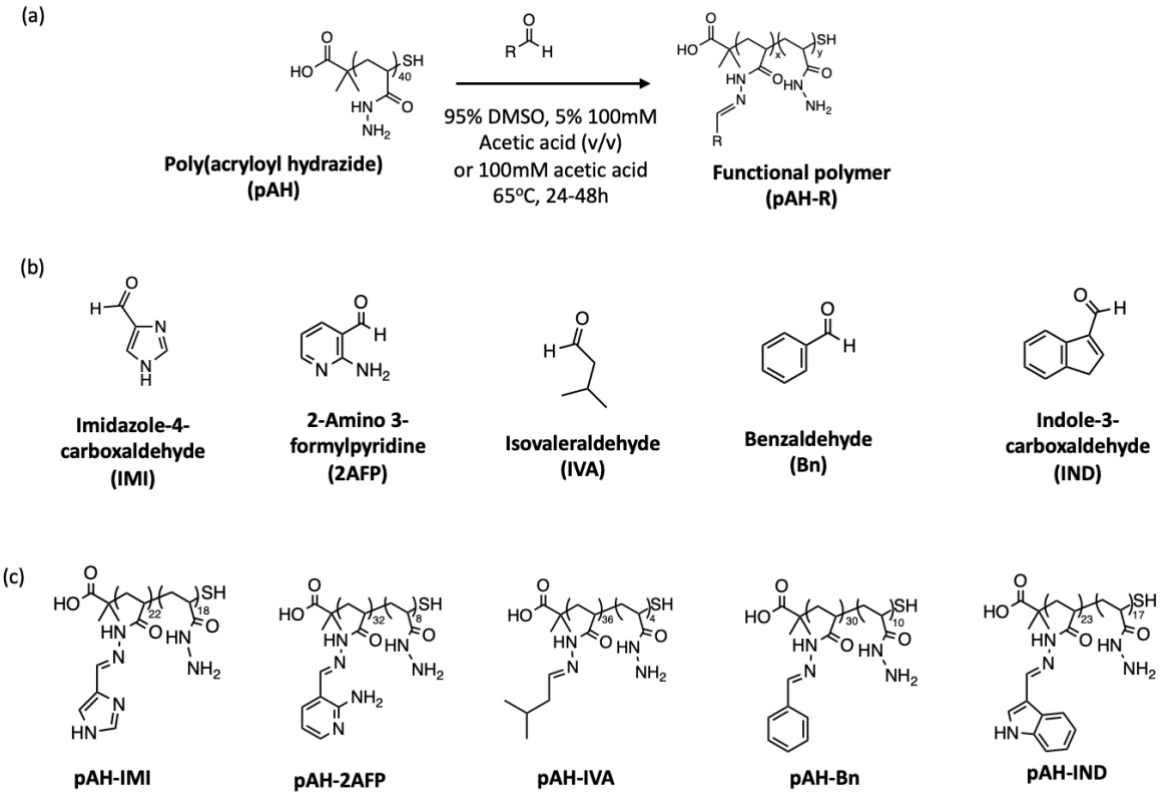

Figure 1: (a) Reaction scheme for the post-polymerisation functionalisation of pAH. (b) Aldehydes used for the functionalisation of pAH. (c) Resulting functional polymers (number of functional hydrazone groups and unfunctionalised hydrazide groups on each polymer is given within the chemical structure).

Functional pAH based polymers were made by post polymerisation functionalisation of the hydrazide repeating units of a 40-mer pAH with respective aldehydes as presented in figure 1. pAH was synthesised according to the protocols used in Crisan et. al[12], resulting in pAH of chain length 40 (a full detailed description of pAH synthesis and characterisation can be found in chapter 2(ii)(a). The coupling reaction (figure 1a) between pAH and aldehyde is acid catalysed hence the presence of acetic acid in the reaction buffer. Isovaleraldehyde, benzaldehyde and indole-3-carboxaldehyde are insoluble in water, so the coupling reaction

with pAH was performed in 95% DMSO, 5% 100 mM acetic acid (v/v). Imidazole-4-caboxaldehyde and 2-Amino 3-formyl pyridine are water soluble (as is pAH), hence the coupling reaction for these two aldehydes was performed in 100 mM acetic acid. Consequently the water soluble coupling reactions (containing more acetic acid) were completed within 24h whilst the coupling reactions performed in 95% DMSO, 5% 100 mM acetic acid (v/v) took around 48h. Equimolar amounts of pAH and the respective aldehyde were reacted. The coupling does not go to completion and can be monitored by ^{1}H-NMR to deduce the final amount of aldehyde coupled onto pAH (a full description of this can be found in chapter 2(i), full ^{1}H-NMR characterisations of each functional polymer can be found in chapter 5 supplementary figures. The final polymers therefore contain a known proportion of unreacted hydrazide groups and a known proportion of reacted hydrazone groups containing the aldehyde moiety (figure 1c). Furthermore, respective pAH polymers of increasing benzaldehyde and imidazole-4-carboxyladehyde functionality were also made, creating a small library of pAH-Bn and pAH-IMI polymers with increasing functionality and hydrophobicity. These sub functional polymers were made by adding sub molar equivalents of the required aldehyde to the pAH and incubating as before in the same solvents. Dual functional polymers i.e. pAH-Bn/IMI were made by incubation of pAH with the desired molar equivalents of both benzaldehyde and imidazole-4-carboxyaldehyde in 95% DMSO, 5% 100 mM acetic acid (v/v). ^{1}H NMR characterisations of the dual functional polymers can be found in the supplementary figures section of this chapter. The physiochemical properties of each respective polymer (cLogD and pKa) could be obtained by using the partition and protonation plugins on MarvinSketch after drawing out each characterised functional polymer respectively.

(b) Physiochemical properties of functional polymers

The polymers shown in figure 1c can be split into two groups; polymers in which the functional group is protonatable (pAH, pAH-2AFP and pAH-IMI) and polymers where the functional group cannot take part in proton exchange (pAH-Bn, pAH-IVA and pAH-IND). All functionalised polymers also contain proportion of unfunctionalised hydrazide groups that can take part in proton exchange, and hence the unfunctionalised pAH polymer is also able exchange protons. Figure 2 shows the locations on each polymer where protonation is possible. The level of protonation for each polymer at a given pH can be calculated based on the pKa values of the polymer. Background theory on pKa's, including how to calculate the degree of protonation at a certain pH given a known pKa can be found in chapter 2(i).

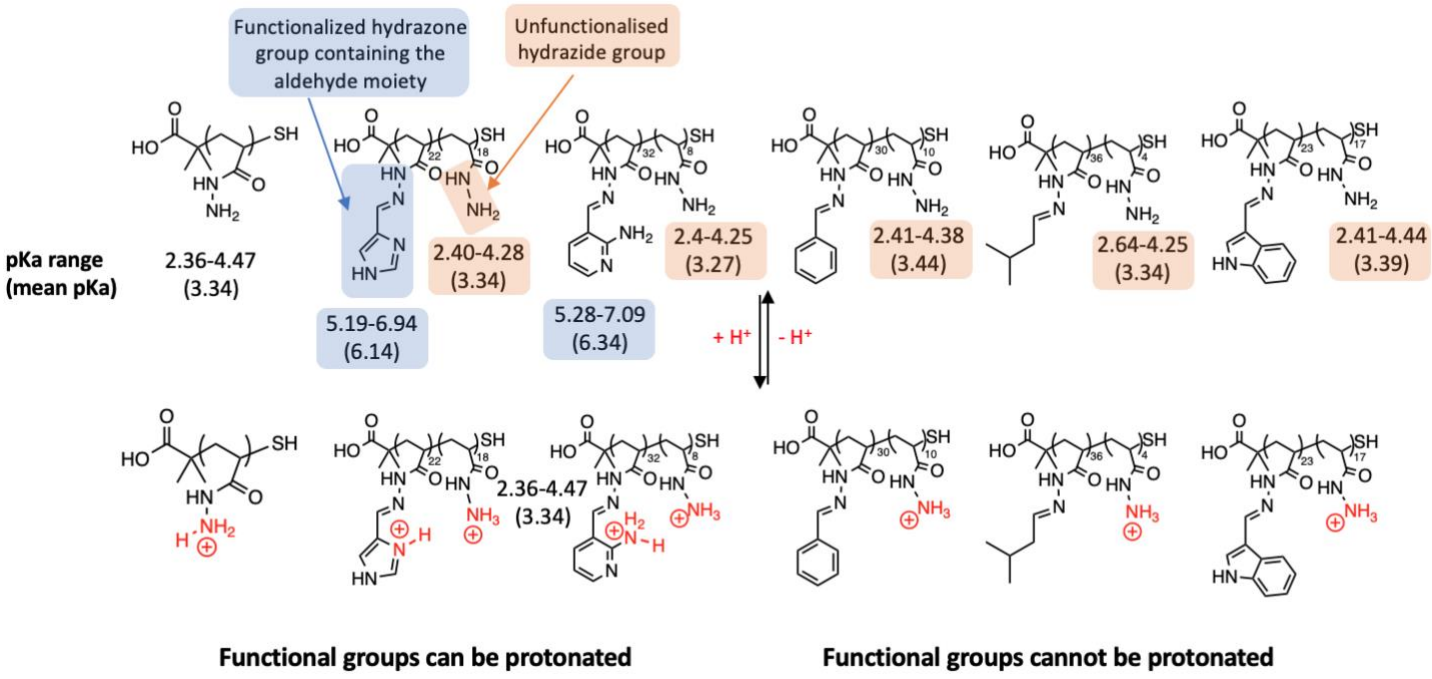

Figure 2: Potential regions of protonation for each polymer. Along with the pKa range (and average) of each segment of each polymer (i.e. the functionalised hydrazone segment and the unfunctionalised hydrazide segment)

Each polymer (except pAH) can be split into two segments; the functional hydrazone groups (containing the aldehyde moiety) and a proportion of uncoupled hydrazide groups as illustrated in figure 2 for pAH-IMI. Each repeating functional group of the polymer will contain its own pKa value, leading to a range of similar pKa's for each repeating functional group; in the case of pAH-IMI, the pKa's of the functional imidazole moieties range from 5.19-6.94 with a mean value of 6.14. This is also the case for the remaining unfunctionalized hydrazides each of which will have a its own pKa value. The pKa's of the unfunctionalised hydrazide units of pAH-IMI range from 2.40-4.28 at an average of 3.34. pAH-IMI and also pAH-2AFP are therefore given two mean pKa values each, one that corresponds to the mean pKa of the functional hydrazone groups and one that corresponds to the mean pKa of unfunctionalised hydrazide groups. As pAH-Bn, pAH-IVA and pAH-IND do not have any sites on the functional group to allow for proton exchange, they do not possess pKa values. So these polymers only contain one mean pKa value corresponding to the pKa range of the unfunctionalised hydrazide units. The unfunctionalised pAH polymer also only contains one pKa range corresponding to the pKa's of each hydrazide unit. By knowing the mean pKa value of a particular segment of a polymer, an estimation of the proportion of fully neutral to fully protonated groups in that segment at a given pH can be calculated using the equation below, defined R.

$$R = \frac{[Unprotonated\ species]}{[Protonated\ species]} = 10^{(pH-pKa)}$$

Figure 3: Equation to calculate the proportion of uncharged to charged species at a given pH

Using this value, an estimation can be made of the proportion (and number) of protonated groups in each protonatable segment of each polymer on average at pH 2.8 and pH 7.

Take pAH-IMI for example; the average pKa value of the imidazole moieties is 6.14. Therefore the average ratio of fully unprotonated pAH-IMI imidazole groups to fully protonated groups is: $10^{7-6.14} = 7.24 : 1$ (figure 3). From this we can therefore roughly say that at any one time, the ratio of uncharged to charged imidazole groups within a pAH-IMI polymer is 7.24 : 1. Therefore at pH 7, an average of 7.24 imidazole moieties will be uncharged per 8 imidazole's within pAH-IMI, or 12% charged. From this the number of charged functional imidazole moieties within the fully characterised pAH-IMI can be estimated (table 1):

Table 1: Table of values showing the number of functionalised aldehyde repeating units and the number of unfunctionalised hydrazide units for each polymer. Furthermore the degree of protonation of each polymer segment at pH 2.8 and pH 7 was calculated based on pKa values by using the equations described.

Polymer (40-mer)	**Number of functionalized aldehyde groups**	**Number of unfunctionalised hydrazide groups**	**Average proportion of charged functional groups (and the number of charged functional groups) at:**		**Average proportion of charged hydrazide groups (and the number of charged hydrazide groups) at:**	
			pH 2.8	**pH 7**	**pH 2.8**	**pH 7**
pAH	0	40	-	-	78% (31)	0.02% (0)
pAH-IMI	22	18	99.9% (22)	12% (3)	78% (14)	0.02% (0)
pAH-2AFP	32	8	99.9% (32)	18% (6)	74% (24)	0.02% (0)
pAH-BN	30	10	-	-	78% (8)	0.03% (0)
pAH-IVA	36	4	-	-	78% (3)	0.02% (0)
pAH-IND	23	17	-	-	80% (18)	0.02% (0)

pAH, pAH-2AFP and pAH-IMI are all made in 100 mM acetic acid which corresponds to a pH of 2.8. Starting with the unfunctionalised pAH polymer, the pKa values of the hydrazides of pAH range between 2.36-4.47 (figure 2, table 1). Therefore taking the mean value (pKa 3.34), it is estimated that at a pH 2.8, around 78% of the hydrazides of pAH will be protonated. Conversely, at pH 7 only 0.02% will be protonated. For pAH-IMI, the polymer contains 22 functionalised imidazole groups and 18 unfunctionalised hydrazide groups. The pKa range of the functional imidazole groups lie between 5.19-6.94 at an average of 6.14. This means that at a pH of 2.8, all 22 imidazole moieties will be protonated. The pKa range of the unfunctionalised hydrazides on pAH-IMI are between 2.4-4.28 at an average of 3.34 meaning that at pH 2.8, 78% of these groups will be protonated corresponding to 14 protonated hydrazide groups on pAH-IMI. At a pH of 7, only 12% of the imidazole moieties will be protonated (i.e. 3 groups) whilst only 0.02% of the hydrazide groups will be protonated. The third and final polymer with protonatable functional groups is pAH-2AFP. The pKa range of the 32 functional groups lie between 5.28-7.09 at an average of 6.34, whilst the 8 hydrazide groups have pKa values between 2.4-4.25 at an average of 3.27. At a pH of 2.8, all 32 2-amino 3-formylpyridene functional groups will be protonated, whilst 74% of the unfunctionalised hydrazides will be protonated. At a pH of 7, only 18% of the 2-amino 3-formylpyridene functional groups will be protonated (i.e. 6 groups) whilst only 0.02% protonation of the unreacted hydrazides. Consequently, these three polymers will have very different physiochemical properties at differing pHs. The remaining polymers (pAH-Bn, pAH-IVA and pAH-IND) do not have any sites on the functional groups that can be protonated (figure 2) however the unfunctionalised portions of these polymers can. In general for all these three polymers, at pH 2.8 around 78-80% of the unfunctionalised hydrazides will be protonated whilst at pH 7, all will be unprotonated.

In addition to pKa values, the respective hydrophobicities of each polymer at pH 7 were also calculated by drawing out the full polymer on MarvinSketch and using the partitioning plugin to calculate hydrophobicity, given as the calculated partition coefficient clogD at pH 7 (table 2).

Table 2: Hydrophobicity of each polymer as given by the calculated partition coefficient (clogD)

Polymer	Hydrophobicity at pH 7 (clogD)
pAH	-39.1
pAH-IMI	-34.45
pAH-2AFP	-9.08
pAH-Bn	29.03
pAH-IVA	25.77
pAH-IND	19.17

(c) Analysis of polymer induced aggregation of *E. coli* K-12 PHL644

The biofilm forming *E. coli* K-12 strain PHL644 was inoculated and grown overnight in LB. Polymer-cell suspensions were prepared as detailed in chapter 2 (ii) (b). Bacterial aggregation was monitored spectrophotometrically according to the protocol described by Foster et. al[12] by recording absorbance (600 nm) every 30 minutes for 4h and then finally once at 24h with the assumption that if bacterial aggregation were to occur, the absorbance of the suspension (turbidimetry) would increase due to the formation of aggregates which then settle to the bottom of the cuvette over time due to their weight, accompanied by a reduction in absorbance.

The absorbance traces for when the respective polymers were added to PHL644 suspended in a buffered (pH 7) solution can be seen as thick blue traces whilst the response of polymers added to PHL644 in NaCl solution can be seen as thick red traces (figure 4).

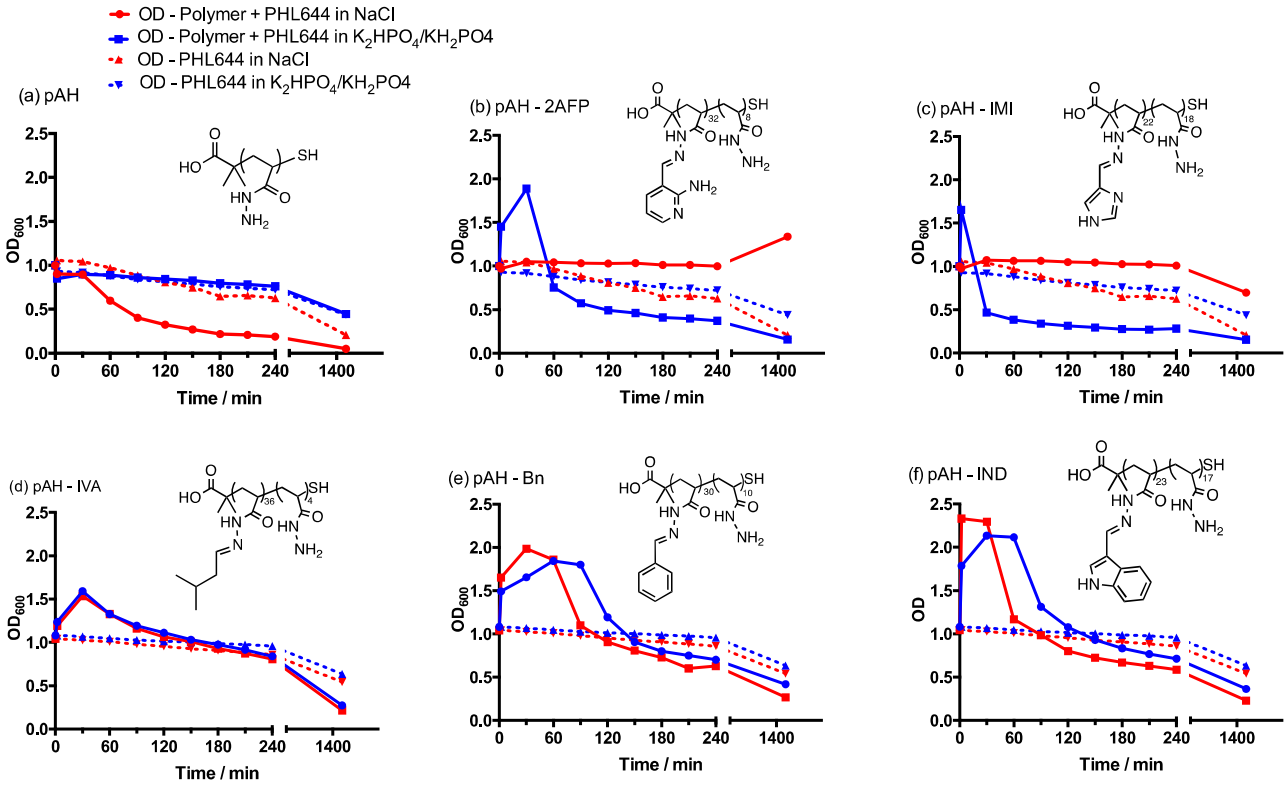

Figure 4: Spectrophotometric assay to monitor polymer induced aggregation of PHL644. PHL644 aggregation when mixed with (a) pAH (b) pAH-2AFP (c) pAH-IMI (d) pAH-IVA (e) pAH-Bn (f) pAH-IND

Control experiments were also performed without the addition of polymer to monitor potential autoaggregation (dashed lines) and this is shown in each separate graph to compare autoaggregation with polymer induced aggregation. In buffered conditions it can be seen that on addition of all polymers except pAH to PHL644, immediate aggregation proceeds as shown by a sharp increase in absorbance (corresponding to the formation of aggregates) followed by a period where the aggregates slowly settle to the bottom of the cuvette due to their weight. The unfunctionalised pAH induces minimal change from the bacterial control suggesting that in these conditions (i.e. pH 7), pAH induces no additional aggregation of bacteria. This is unsurprising as pAH does not contain any hydrophobic moieties, nor is it charged at pH 7. However when pAH is added to an unbuffered PHL644 suspension, aggregation can be seen as given by the drop in absorbance. As mentioned, the initial stock solution of pAH is in 100 mM acetic acid at a pH 2.8, hence all its hydrazide groups will be charged. When this initially highly charged pAH is added to a pH 7 buffered solution, the number of protonated hydrazides reduces to 10% as the KH_2PO_4/K_2HPO_4 buffer sequesters the protons away from the pAH. In salt solution however, the pAH charges are not sequestered and may remain on the polymer. Therefore it can be assumed that in the absence of buffer, pAH induces PHL644 aggregation via charge interaction. pAH-IMI and pAH-2AFP are also highly charged in their initial stock solutions at pH 2.8 but neither of these polymers induced aggregation when added to PHL644 in salt where charges may not be removed. Therefore aggregation by charge interaction does not occur for these functional polymers in these conditions at pH 2.8. When the same two polymers are added to PHL644 in a pH 7 buffed solution, the charges get removed and this leads to aggregation, most likely through hydrophobic interactions between the polymer functional groups and the bacterial envelope. The remaining polymers (pAH-Bn, pAH-IVA and pAH-IND) are not

able to accept protons onto their functional groups but can accept protons onto the remaining unfunctionalized hydrazides. However, these three polymers are synthesised in 95% DMSO, 5% 100 mM acetic acid which corresponds to a pH of around 7 and in these conditions none of the polymer hydrazide repeating groups will be charged. Hence it makes no difference to the electrostatic nature of the polymers whether they are added to a PHL644 in pH 7 buffered or salt solution – the polymers will remain uncharged. Hence the aggregating response is very similar when the respective polymers are added to PHL644 in buffer and in salt respectively. Therefore due to the absence of charge, it is assumed that these functional polymers interact and aggregate bacteria primarily through hydrophobic interactions.

(d) Analysis of polymer-induced aggregate biomass intensity

Given that the functional polymers were able to aggregate PHL644 cells in set conditions, it was decided to monitor the overall amount of aggregate biomass attached to each polymer after incubation for 24h. PHL644 was prepared as previously and suspended into either 0.1M KH_2PO_4/K_2HPO_4 (buffered to pH 7) or 0.1 M NaCl at OD_{600} 1. The culture was split into 1 ml aliquots in eppendorfs and the polymers were added to a final concentration of 0.5 mg/ml respectively. The polymer-bacteria suspensions were then incubated for 24h, 48h and 72h respectively at 30^{o}C with shaking at 150 rpm. After this, the overall amount of biomass attached to the respective polymers was measured as described in the literature via the crystal violet assay. The full detailed experimental protocol can be found in the materials and methods section in chapter 2 (ii) (b).

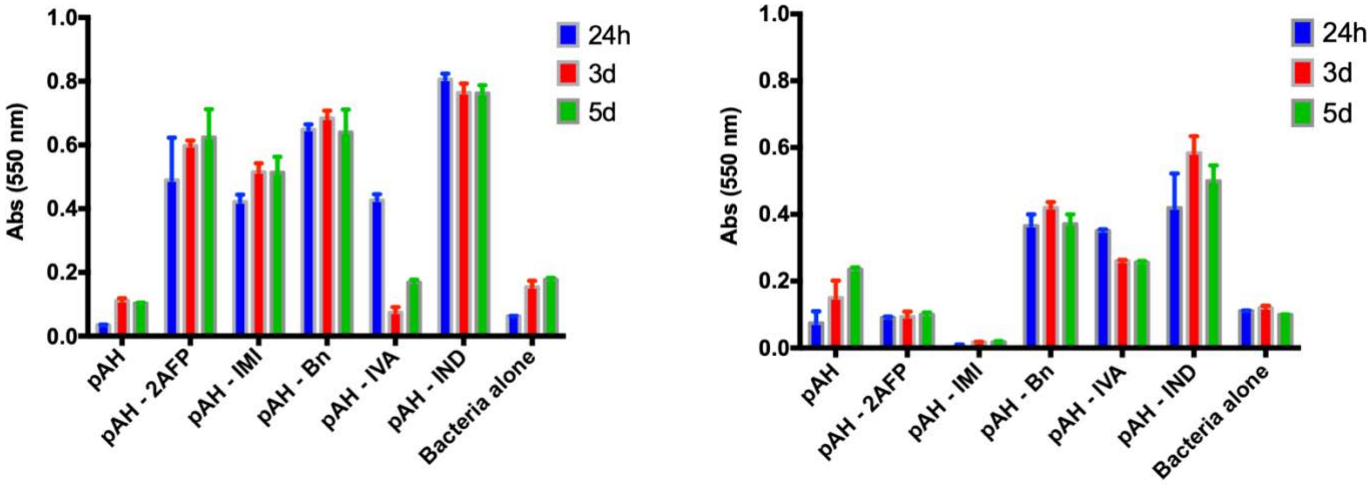

Figure 5: Analysis of overall polymer induced PHL644 aggregate biomass after 24, 48 and 72h of incubation with respective polymers. Polymers are added to PHL644 suspended in either 0.1M KH_2PO_4/K_2HPO_4 buffered to pH 7 (left) or in 0.1 M NaCl (right)

As explained in chapter 1, PHL644 is a biofilm forming strain. It contains an *ompR234* point mutation which allows for the overexpression of curli, the main biofilm adhesin produced by K-12 strains. Hence over a period of 24h it is likely the polymer-induced PHL644 bacterial aggregates are in biofilm form, unless the polymers specifically reduce curli (or other EPS) expression; work performed on this has not yet been presented hence the polymer-induced aggregates will not yet be referred to as biofilms. The crystal violet assay was therefore used to measure overall polymer-induced aggregate biomass, rather that referring to it as polymer-induced biofilms at this stage (figure 5). When functional polymers were added to PHL644 in buffered solution, immediate PHL644 aggregation proceeded and this was monitored spectrophotometrically (figure 4). The unfunctionalised pAH was the only polymer that did not induce aggregation of cells in buffer. As a result, the overall amount of biomass attached to pAH after 24, 48 and 72h is very low suggesting that even after 24h of incubation with pAH, pAH does not induce aggregation when in its uncharged state in the presence of pH 7 buffer. The remaining functional polymers which did induce aggregation in

buffered conditions via hydrophobic interactions, resulted in high amounts of biomass attached to the polymers at each timepoint relative to the bacterial control without the addition of polymer where PHL644 may bind naturally to the sample container. Intriguingly the amount of aggregate biomass associated with pAH-IVA dramatically reduced after 24h in buffered conditions. At this stage it is not known why, but it would indicate that bacterial binding to pAH-IVA is much weaker than all other functional polymers and that bacteria are able to detach from the pAH-IVA aggregates over time. This polymer is also different from the other functional polymers as it contains an aliphatic functional group rather than an aromatic group, suggesting the importance of aromaticity in the polymer induced aggregation of PHL644. Unsurprisingly, when pAH was added to PHL644 cells in salt solution, the amount of biomass attached was increased due to interaction via electrostatics. However this was still significantly lower than all other polymers suggesting that aggregation via charge interaction is not as intense as aggregation via hydrophobic interactions with the functional polymers. Unsurprising when pAH-IMI and pAH-2AFP were added to PHL644 in salt solution respectively, very little biomass was attached after all timepoints and this is because these polymers do not interact with PHL644 cells via charge interaction as confirmed by the spectrophotometric assay. As expected, the remaining polymers that do not accept charges onto their functional groups (pAH-Bn, pAH-IVA and pAH-IND) and that showed similar levels of polymer induced aggregation in both buffered and salt solution also showed similar levels of polymer-induced aggregate biomass after each timepoint in both conditions. An important point to make is that the amount of biomass attached to a particular polymer does not seem to increase between 24 and 72 h, but stays rather similar. This is likely due to the fact that at this stage, no source of food was

added to the bacterial suspensions, likely hampering bacterial growth and preventing an increase in biomass over time.

Moving forward, it is clear that for the set of polymers tested so far, polymer induced bacterial aggregation is driven primarily through hydrophobic interactions which are maximal when polymers are added to buffered solution at pH 7. This is confirmed when plotting polymer hydrophobicity at pH 7 (given by clogD) with overall polymer induced aggregate biomass levels in buffered solution, with there being a direct correlation.

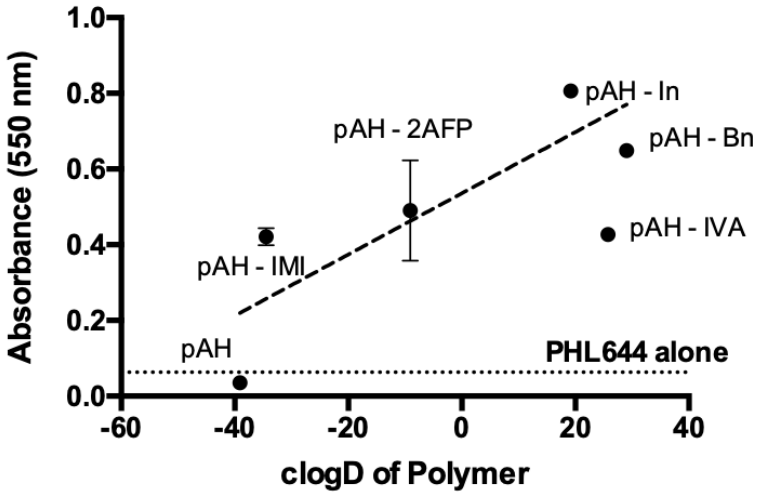

Figure 6: Polymer induced aggregate biomass after 24h in buffered conditions plotted against the respective calculated polymer hydrophobicities (clogD)

As can be seen from figure 6, a direct correlation is found between polymer hydrophobicity and the amount of biomass attached to each polymer. pAH-IVA is one notable outlier which induces less biomass that expected despite its high clogD value of 25.77 (table 2). As mentioned, pAH-IVA differs from all the other functional polymers in that its functional Isovaleraldehyde group is aliphatic whilst all other are aromatic, suggesting that aromaticity also plays a significant role in aggregating PHL644 cells.

Given the high level of control over aggregated biomass quantities, we wanted to assess if differing levels of aggregate biomass could also be by stimulated using the same functional polymer, but varying its degree of functionality (and subsequent hydrophobicity). For this pAH-IMI and pAH-Bn were chosen, with each polymer being functionalised with sub molar equivalents of the respective aldehyde to target pAH-IMI and pAH-Bn polymers of increasing functionality and subsequent hydrophobicity. Sub functional polymers were made by addition of sub molar equivalents of the respective aldehyde to pAH, and incubating as before. The polymers were then added to PHL644 cells as before for 24h, after which sub functional polymer induced aggregate/biomass was measured using crystal violet.

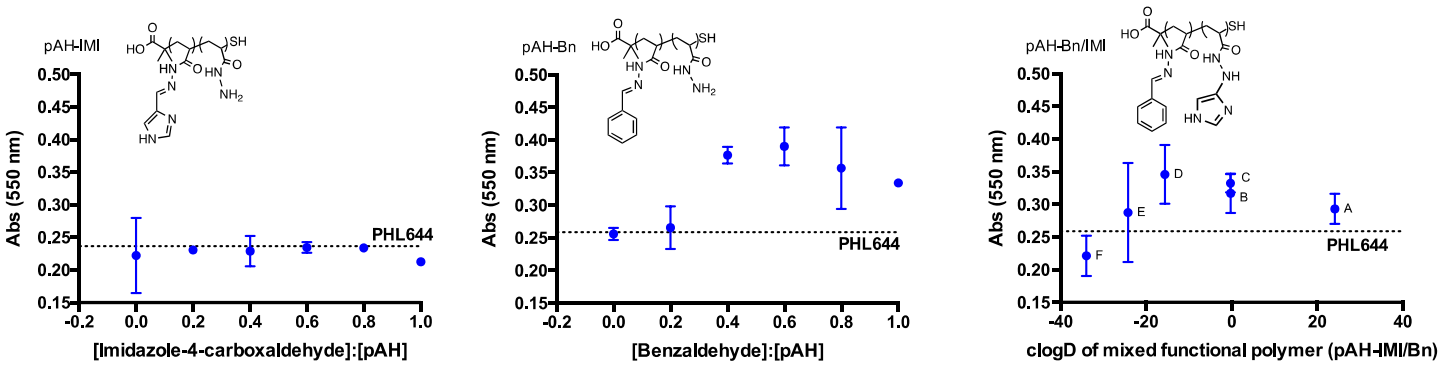

Figure 7: Polymer induced aggregate biomass after incubation for 24h. (Left) Sub functional pAH-IMI polymer induced biomass, (centre) Sub functional pAH-Bn polymer induced biomass, (right) Dual functional pAH-Bn/IMI polymer induced biomass. Details of polymers A,B,C,D,E, and F can be found in table 3.

Predictably, pAH-IMI polymer showed very little additional aggregation of biomass compared with the control sample (figure 7, left). This is not surprising due to the fact that both the unfunctionalised pAH and imidazole groups are hydrophilic and are of similar cLogD value (table 2). An increase in biomass was however found upon adding the more hydrophobic pAH-Bn sub functionalised polymers, with only 0.4 equivalents of benzaldehyde required to create highly functional aggregating pAH-Bn polymers

(figure 7, centre). Interestingly, above the addition of 0.6 equivalents of benzaldehyde a slight decrease in polymer aggregation was found despite these polymers likely being more hydrophobic. A potential theory for this could be that as more and more hydrophobic benzaldehyde functionality gets incorporated into the polymer, it may prefer to take a tighter orientation involving more intramolecular hydrophobic interactions rather than hydrophobic interactions with bacterial cell walls, resulting in slightly less aggregation.

Table 3: Table showing the equivalents of Bn and IMI aldehydes added to respective pAH polymers, their % functionality and resulting polymer hydrophobicity

Polymer Sample	**Equivalents of Benzaldehyde (Bn) used**	**Equivalents of Imidazole-4-carboxaldehyde (IMI) used**	**% Benzaldehyde functionality**	**% Imidazole-4-carboxyaldehyde functionality**	**Polymer hydrophobicity (cLogD)**
A – pAH-$Bn_{0.64}$	1	0	64	0	24.1
B – pAH-$Bn_{0.38}$/$IMI_{0.17}$	0.8	0.2	38	17	-0.26
C – pAH-$Bn_{0.36}$/$IMI_{0.31}$	0.6	0.4	37	31	-0.28
D – pAH-$Bn_{0.22}$/$IMI_{0.23}$	0.4	0.6	22	23	-15.6
E – pAH-$Bn_{0.14}$/$IMI_{0.11}$	0.2	0.8	14	11	-24.2
F – pAH-$IMI_{0.60}$	0	1	0	60	-33.9

Finally, a series of dual functionalised pAH polymers were made to target both imidazole and benzaldehyde incorporation in varying ratios as presented in table 3. Additionally, the polymers were characterised by ^{1}H NMR and so cLogD values of all polymers were also obtained (table 3). In general, pAH-Bn functionality tended to increase with increasing molar ratios of benzaldehyde despite the presence of imidazole in the reaction; conversely pAH-IMI incorporation does not increase linearly with increasing imidazole-4-carboxaldehyde molar ratios added to pAH, in the presence of benzaldehyde. Further kinetic studies involving the dual incorporation of these two aldehydes

simultaneously into pAH needs to be performed to understand this, however the resulting polymers varied in hydrophobicity enough for investigation with PHL644 (figure 7, right). The results look strikingly similar to that of the pAH-Bn sub functional polymers, with the most PHL644 aggregation resulting from polymers made from the addition of intermediate molar equivalents of benzaldehyde. Imidazole functionality seemed to have very little effect given its hydrophilicity, hence it is likely the dual functionalised polymer binds to bacteria exclusively via the benzaldehyde functionalities. Hence pAH-Bn/IMI induced bacterial aggregation was highest at intermediate hydrophobicities where it is more likely that polymer benzaldehyde functionalities interact with bacteria rather than with themselves intramolecularly as a result of over-functionalising with hydrophobic moieties.

(iv) Conclusions and next steps

A series of six functional pAH polymers were made by post polymerisation functionalisation of pAH with six aldehydes respectively. Three of the aldehydes were found to be moderately hydrophobic whilst two possessed heteroaromatic functionality and were hydrophilic in nature, along with the unfunctionalised pAH. In general, hydrophobic interaction were responsible for polymer induced aggregation of the *E. coli* K-12 strain PHL644, with the hydrophilic pAH inducing minimal aggregation. When the two heteroaromatic polymers (pAH-2AFP and pAH-IMI) were added to bacteria whilst positively charged (and subsequently highly hydrophilic), minimal aggregation was found confirming that aggregation does not proceed via charge interaction with polymers. The eventual amounts of biomass adhered to the polymers after 24-72h was found to be directly correlated to polymer hydrophobicity, indicating that polymers can be used to control biofilm quantities.

When single polymers were modified to contain a range of degree of functionality, bacterial aggregation was highest at when pAH was functionalised with sub molar equivalents of hydrophobic functionality. These results therefore suggest an ability to control bacterial aggregation/biofilm formation using hydrophobic polymers. In the next section, the library of polymers is extended to include highly hydrophobic functionality into pAH. Furthermore, detailed analysis is performed on the resulting polymer induced aggregates to define their characteristics. And finally, we demonstrate the functionality of these aggregate biofilms in two separate biocatalysis arenas.

(v) Supplementary figures

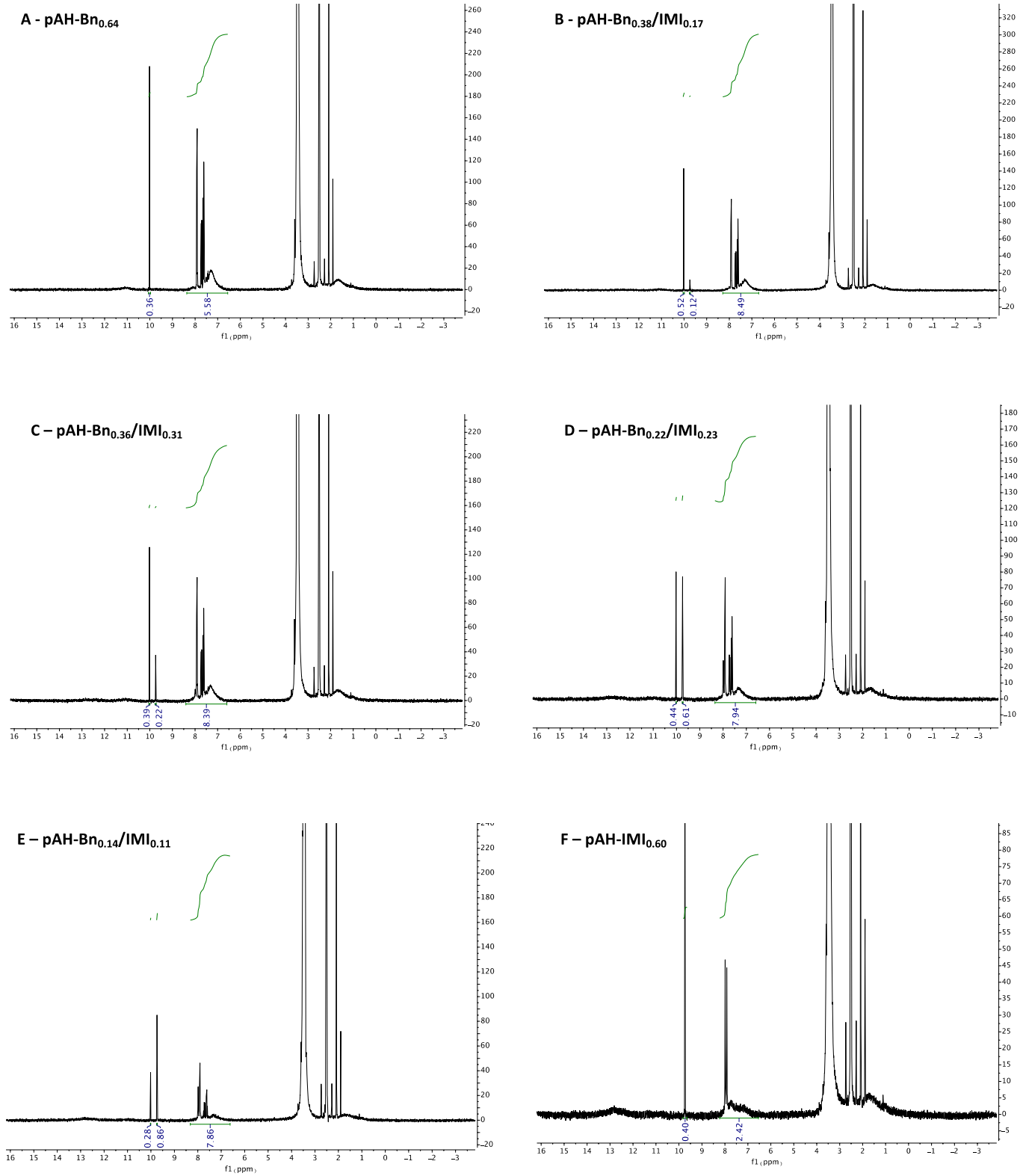

Figure S1: ^{1}H NMR spectroscopy of dual functionalised pAH-Bn/IMI polymers, note the fractional amounts of each aldehyde attached to each polymer

(vi) References

1. Renner LD, Weibel DB. Physicochemical regulation of biofilm formation. *MRS Bull*. 2011. doi:10.1557/mrs.2011.65
2. Stoodley P, Sauer K, Davies DG, Costerton JW. Biofilms as complex differentiated communities. *Annu Rev Microbiol*. 2002. doi:10.1146/annurev.micro.56.012302.160705
3. Bridier A, Briandet R, Thomas V, Dubois-Brissonnet F. Resistance of bacterial biofilms to disinfectants: A review. *Biofouling*. 2011. doi:10.1080/08927014.2011.626899
4. Lebeaux D, Ghigo J-M, Beloin C. Biofilm-Related Infections: Bridging the Gap between Clinical Management and Fundamental Aspects of Recalcitrance toward Antibiotics. *Microbiol Mol Biol Rev*. 2014. doi:10.1128/mmbr.00013-14
5. Stewart PS. Mechanisms of antibiotic resistance in bacterial biofilms. *Int J Med Microbiol*. 2002. doi:10.1078/1438-4221-00196
6. Tsoligkas AN, Winn M, Bowen J, Overton TW, Simmons MJH, Goss RJM. Engineering Biofilms for Biocatalysis. *ChemBioChem*. 2011. doi:10.1002/cbic.201100200
7. Maurya A, Raj A. Recent advances in the application of biofilm in bioremediation of industrial wastewater and organic pollutants. In: *Microorganisms for Sustainable Environment and Health*. ; 2020. doi:10.1016/b978-0-12-819001-2.00005-x
8. Perez-Soto N, Moule L, Crisan DN, et al. Engineering microbial physiology with synthetic polymers: Cationic polymers induce biofilm formation in: Vibrio cholerae and downregulate the expression of virulence genes. *Chem Sci*. 2017. doi:10.1039/c7sc00615b
9. Foster LL, Yusa SI, Kuroda K. Solution-mediated modulation of pseudomonas

aeruginosa biofilm formation by a cationic synthetic polymer. *Antibiotics*. 2019. doi:10.3390/antibiotics8020061

10. Zhang P, Lu H, Chen H, et al. Cationic Conjugated Polymers-Induced Quorum Sensing of Bacteria Cells. *Anal Chem*. 2016. doi:10.1021/acs.analchem.5b03920
11. Disney MD, Zheng J, Swager TM, Seeberger PH. Detection of bacteria with carbohydrate-functionalized fluorescent polymers. *J Am Chem Soc*. 2004. doi:10.1021/ja047936i
12. Crisan DN, Creese O, Ball R, et al. Poly(acryloyl hydrazide), a versatile scaffold for the preparation of functional polymers: Synthesis and post-polymerisation modification. *Polym Chem*. 2017. doi:10.1039/c7py00535k

Chapter 5 – Hydrophobic aldehyde functionalised poly(acryloyl hydrazide) based polymers for the controlled stimulation of biocatalytic *E. coli* K-12 biofilms

(Written in the format of a journal paper, with a Supplementary Figures section)

(i) Abstract

Bacterial biofilms are able to withstand chemical and physical extremes, making them problematic and difficult to eradicate in a wide variety of settings. These same characteristics however can be used to our advantage in the field of biotransformations. Previous work in our group has demonstrated the potential of recombinant *E. coli* K-12 biofilms in the biocatalysis of haloindoles to halotryptophans, with biofilms showing greater catalytic longevity when compared with their planktonic counterparts. More generally, using biofilms in biotransformations may be particularly useful when performing reactions that require harsh/toxic conditions that may not be suitable for bacteria or immobilised enzymes. Many of the resilient properties of biofilms are linked to their physical size/thickness and their composition with regard to the extracellular matrix, which provides structural integrity and acts as a physical barrier toward the diffusion of toxic compounds e.g. antibiotics, whilst also providing phase separation from any potentially toxic bulk medium. Many industrially relevant strains however are not capable of forming biofilms, and as such may limit their use in bioreactors toward a narrow set of conditions that are favourable for planktonic bacteria. Therefore, stimulating biofilm expression in industrially relevant strains not normally known to form them may provide a range of benefits, allowing for them to tolerate toxic chemicals and the physical extremes that many industrial reactions require.

To this end we attempted to control and optimise biofilm formation using synthetic polymers in the hope to provide an alternative and potentially more efficient platform for biofilm mediated processes. Synthetic polymers have been shown to interact and aggregate

bacteria, stimulating unique responses, many of which affect biofilm formation. In this study, we synthesised a range of functional polymers of increasing hydrophobicity based on a poly(acryloyl hydrazide) scaffold and monitored their effect on biofilm formation in two *E. coli* K-12 strains – PHL644 (containing an *ompR234* point mutation that causes the overexpression of curli) and MC4100 (the isogenic wild-type parental strain). We found that our synthetic polymers were able to aggregate cells and stimulate the expression of biofilm factors in a simple, predictable manner with polymer hydrophobicity and expression of biofilm determinants being directly linked. Furthermore, we have found that our polymers were are able to increase the expression of curli/biofilm in MC4100 to similar levels to that of the overproducing PHL644; demonstrating the potential of hydrophobic polymers to significantly boost biofilm levels in non-biofilm associated strains. The ability of these 'polymer-induced recombinant biofilms' in the biotransformation of 5-fluoroindole to 5-fluorotryptophan was assessed, with moderate-highly hydrophobic polymer induced biofilms showing greatly improved reaction yields when compared with naturally formed biofilms. Additionally, the natural esterase production of *E. coli* was harnessed for the degradation of a lipid ester 4-Nitrododecanoate, with hydrophobic polymer induced biofilms performing more favourably than hydrophilic polymer induced biofilms and natural biofilms, potentially due to the greater resistance of the hydrophobic polymer induced biofilms toward the toxic reaction conditions required.

(ii) Introduction

The vast majority of bacteria live on surfaces, which help nucleate cell growth due to the high local concentration of nutrients that tend to get deposited onto surfaces from the bulk media[1]. In many cases surface attachment triggers changes in phenotype as cells transition from a motile to sessile state, with this usually involving the expression of biofilm factors, changes in antibiotic susceptibility amongst many other strain specific changes[2]. The type of surface plays an important role in the eventual characteristics of a biofilm and to this end surface coatings have been developed that resist cell attachment and subsequent biofilm formation[3]. There are two stages of cell-surface attachment; the first is reversible and usually driven by non-specific physiochemical interactions, the second irreversible step sees the bacteria begin to produce surface adhesins and matrix-like extracellular polymeric substances (EPS) which effectively glue together and protect the bacteria from external stresses[2]. The resulting biofilm is therefore far more resistant to environmental, physical and chemical stresses compared with its planktonic counterpart[4]. Because of this, biofilms are normally seen as problematic in a wide variety of settings due to the fact they are difficult to eradicate; they are responsible for the biofouling of surfaces, contamination of food[5] and medical implants, hospital infections[6], and are responsible for antimicrobial resistance[7]. These same persistent characteristics however can be used to our advantage in industrial biotechnology, with biofilms showing promise in the field of biocatalysis[4]. *Pseudomonas* biofilms have been shown to catalyse the epoxidation of styrene to (S)-styrene oxide[8,9], *Zymomonas mobilis* biofilms can efficiently catalyse benzaldehyde to benzyl alcohol[10] and *Pseudomonas*, *Sphingomonas* and *Rhodococcus* biofilms have been shown to degrade organofluoride pollutants, converting them into useful intermediates[11].

Previous work in our lab has demonstrated that *E.coli* K-12 biofilms engineered to overproduce tryptophan synthase (an enzyme that catalyses the conversion of haloindoles to halotryptophans) are generally better catalysts than their planktonic counterparts and the purified tryptophan synthase enzyme[4] in the biotransformations of fluoroindoles to fluorotryptophan. Furthermore this biotransformation was also performed using a BL21 strain additionally engineered to increase levels of biofilm on the application of near infrared light, which lead to optimised reaction kinetics[12]. For this particular biotransformation, the main reason for biofilm efficiency was because biofilms showed catalytic longevity when compared with planktonic cells[13] and a further study found that this was at least in part due to constant regeneration of the recombinant tryptophan synthase enzyme within cells of a biofilm[14]. A more general reason to employ biofilms for biotransformations is that cells within biofilms may be able to resist some of the harsh environmental factors that reduce biotransformation efficiency e.g. extremes of temperature and pH (which denatures enzymes), and substrate/product/solvent toxicity[4,10] which may lead to cell death. Additionally, biofilms could be used as an immobilised whole cell catalyst, allowing for their use in flow reactors[15].

To this end we wanted to try to induce biofilm formation and subsequent biocatalytic performance by using synthetic polymers as the artificial scaffold onto which bacteria aggregate in a controlled manner via non-specific physiochemical interactions, resulting in the controlled stimulation of biofilm factors. The resulting polymer-induced biofilms were then assessed for the ability to convert 5-fluoroindole into the pharmaceutically relevant 5-fluorotryptophan. The vast majority of studies focussing on polymer-bacteria interactions involve the design of antimicrobial polymers designed to directly kill cells. A recent

approach involves the use of bacterial sequestering polymers, which are designed to prevent cell surface binding by sequestering and aggregating bacteria away from the potential site of infection without killing them, thereby eliminating evolutionary pressure on the bacteria. Previous work by Krachler et al. has demonstrated the ability of cationic synthetic polymers to sequester *V. cholerae* via charge interaction and dictate bacterial phenotype (intriguingly upregulating quorum sensing and biofilm production together, and downregulating virulence)[16,17]. Very little however can be found in the literature regarding the use of synthetic polymers designed to specifically stimulate biofilm expression for the development of applicable biofilms. Hence, we wanted to design synthetic polymers that were able to drive bacterial aggregation with subsequent control over biofilm properties, which could be used to our advantage in the biotransformation arena. The synthetic polymers used in this study were based on a poly(acryloyl hydrazide) scaffold[18] functionalised with a range of hydrophobic moieties to give a library of hydrophobic polymers that could be tested with *E. coli* – a biofilm forming strain widely used within industry[19]. As *E. coli* is Gram-negative with a hydrophobic cell wall, we postulated that its aggregation and subsequent biofilm formation could be driven by the addition of hydrophobic polymers. In this study, we demonstrate that polymer hydrophobicity dictates bacterial aggregation and subsequent biofilm properties including overall biofilm quantity and the expression of curli – a surface adhesin and one of the main EPS components in *E. coli* biofilms along with poly-β-1,6-N-acetyl-D-glucosamine (PGA) and colanic acid. The ability of the resulting polymer-induced biofilms in the biotransformation of 5-fluoroindole to 5-fluorotryptophan was then monitored with hydrophobic polymers stimulating large quantities of biofilm and showing higher catalytic activity than naturally formed biofilms. The two *E.coli* strains tested in this study were; PHL644 – a K-12 variant with an *ompR234*

mutation which causes this strain to constitutively express curli, the main proteinaceous component of *E.coli* biofilms[20], and MC4100 – the parental strain without the mutation resulting in less curli expression and a vastly lower ability to form biofilms[21]. In essence, we therefore conduced all experiments with high (PHL644) and low (MC4100) biofilm forming isogenic strains to see how our polymers could modulate biofilm properties, with results indicating that our polymers have the potential to significantly boost biofilm expression even in the poor MC4100 biofilm forming strain, hence opening up the possibility for these cells to experience the industrially relevant benefits of being in biofilm form.

(iii) Results

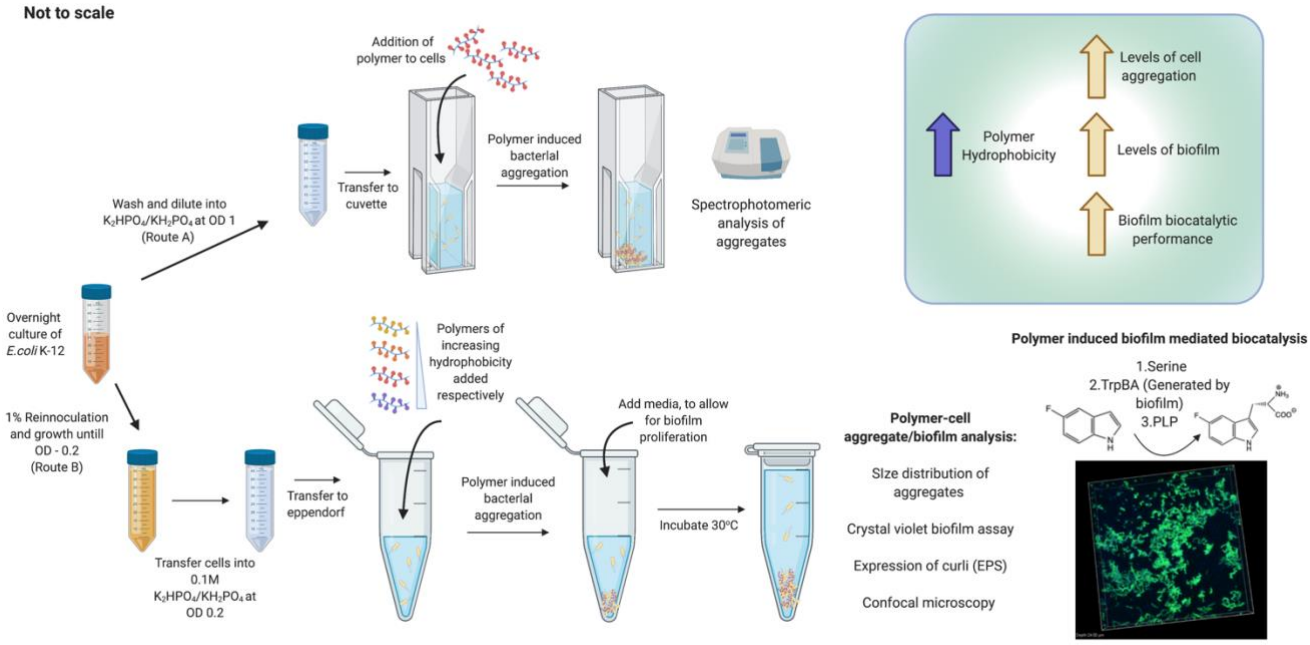

Figure 1: Schematic of experimental workflow. Route A was used to monitor polymer-induced bacterial aggregation. Route B includes the addition of media to induce biofilm expression; polymer induced biofilms were then analysed and used in the biotransformation of 5-fluoroindole to 5-fluorotryptophan.

(a) Hydrophobic polymers used in this study and their synthesis route

The interaction of bacteria with surfaces represents the first stage of biofilm formation, so it is unsurprising that much research has gone into bacteria-surface interactions, with vast examples in the literature describing the design of antifouling surfaces that resist bacterial attachment. In general, the surface free energies of the bacteria and the surface are most influential in governing preliminary non-specific interactions which are generally made up of weak Van der Waals forces, electrostatic and hydrophobic interactions[22]. Gram negative bacterial cell walls contain an outer hydrophobic layer composed primarily of lipopolysaccharides, outer membrane proteins and capsular polysaccharides[23]; hence we decided to synthesise a range of hydrophobic polymers based on the previously studied

poly(acryloyl hydrazide) scaffold (pAH)[18,24] in the hope of polymer-bacterial attachment and subsequent aggregation driven by hydrophobic interactions. Firstly (figure 2a), a boc-protected acryloyl hydrazide was synthesised (26 % yield, ^{1}H NMR figure S1) and RAFT polymerised to afford size controlled boc-protected pAH (68 %, DP-40, ^{1}H NMR figures S3 and S4) which in turn could be deprotected to pAH (43 %, ^{1}H NMR figure S6, GPC figure S7). pAH was then functionalised by reacting it with a range of increasingly hydrophobic aldehydes respectively to give a library of copolymers each with a proportion, x of functionalised hydrazone groups (containing the hydrophobic aldehyde moiety) and y, a proportion of unfunctionalised hydrazide groups as the coupling reaction doesn't reach full conversion (figure 2b). The percentage of incorporated functional groups was found using ^{1}H NMR, by monitoring the signal decrease in the aldehyde peak (with respect to its starting concentration) as it becomes incorporated within the polymer (figures S8-16). Given this, calculated polymer hydrophobicities (figure 2b) were determined using the partitioning plugin on MarvinSketch after drawing out the full polymers respectively. All functionalised polymers (figure 2b) were used in biological assays without further purification and so for completeness, all assays were performed with additional aldehyde controls whereby the respective free aldehyde (corresponding to each functional polymer) was added to bacteria instead of the polymer, so as to be sure any changes in bacterial phenotype was driven by polymer induced aggregation rather than simply an effect of the unreacted aldehyde. ^{1}H NMR characterisation of each polymer (figures S8-S16) can be found in the supplementary info.

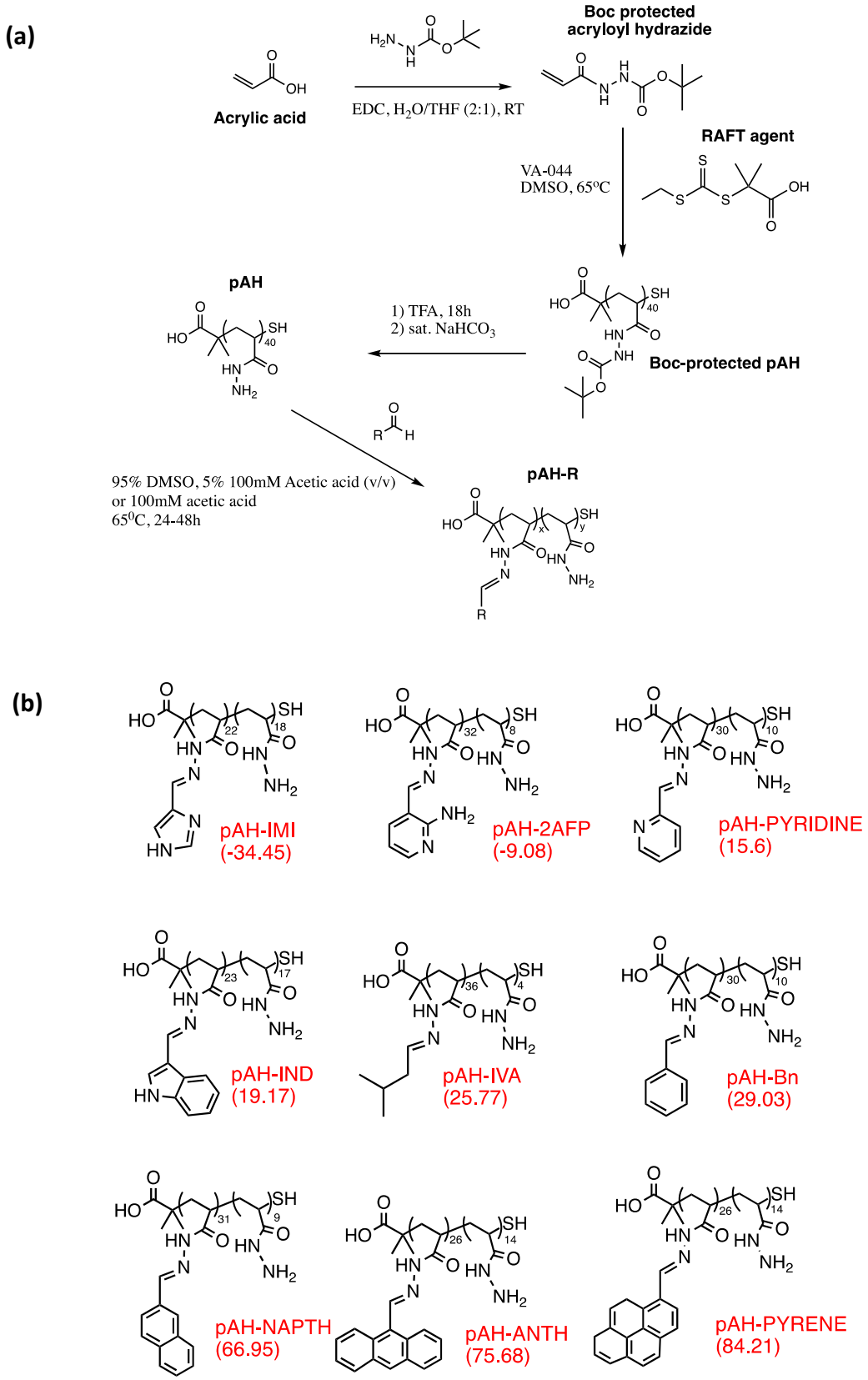

Figure 2: (A) Synthetic route to hydrophobic polymers based on a poly(acryloyl hydrazide) scaffold (A). (B) The final polymers are statistical copolymer of chain length 40, with hydrazone and hydrazide blocks in proportions x and y respectively, along with their calculated partition coefficients (clogD).

(b) Polymer induced bacterial aggregation

Initially we wanted to investigate if the polymers were able to aggregate *E. coli* K-12 over the course of 24h, and if polymer hydrophobicity dictated the levels of aggregation. The K-12 strain MC4100 was grown overnight, washed and transferred into a low osmolarity solution of 0.1M KH_2PO_4/K_2HPO_4 buffered at pH 7 to give a suspension at OD_{600} 1. Each of the polymers were then added separately to the bacteria in a cuvette to a final concentration of 0.5 mg/ml and incubated for 24h at 30 ^{0}C with shaking at 150 rpm. Aggregation was monitored spectrophotometrically, as performed by Xue et al.[25] by recording the absorbance of the polymer-bacteria suspensions at 600 nm every 30 minutes for 4h and then once again at 24h, with the assumption that if bacterial aggregation were to occur, the absorbance of the suspension would eventually be reduced due to clusters forming and sedimenting to the bottom of the cuvette due to their weight (figure 3).

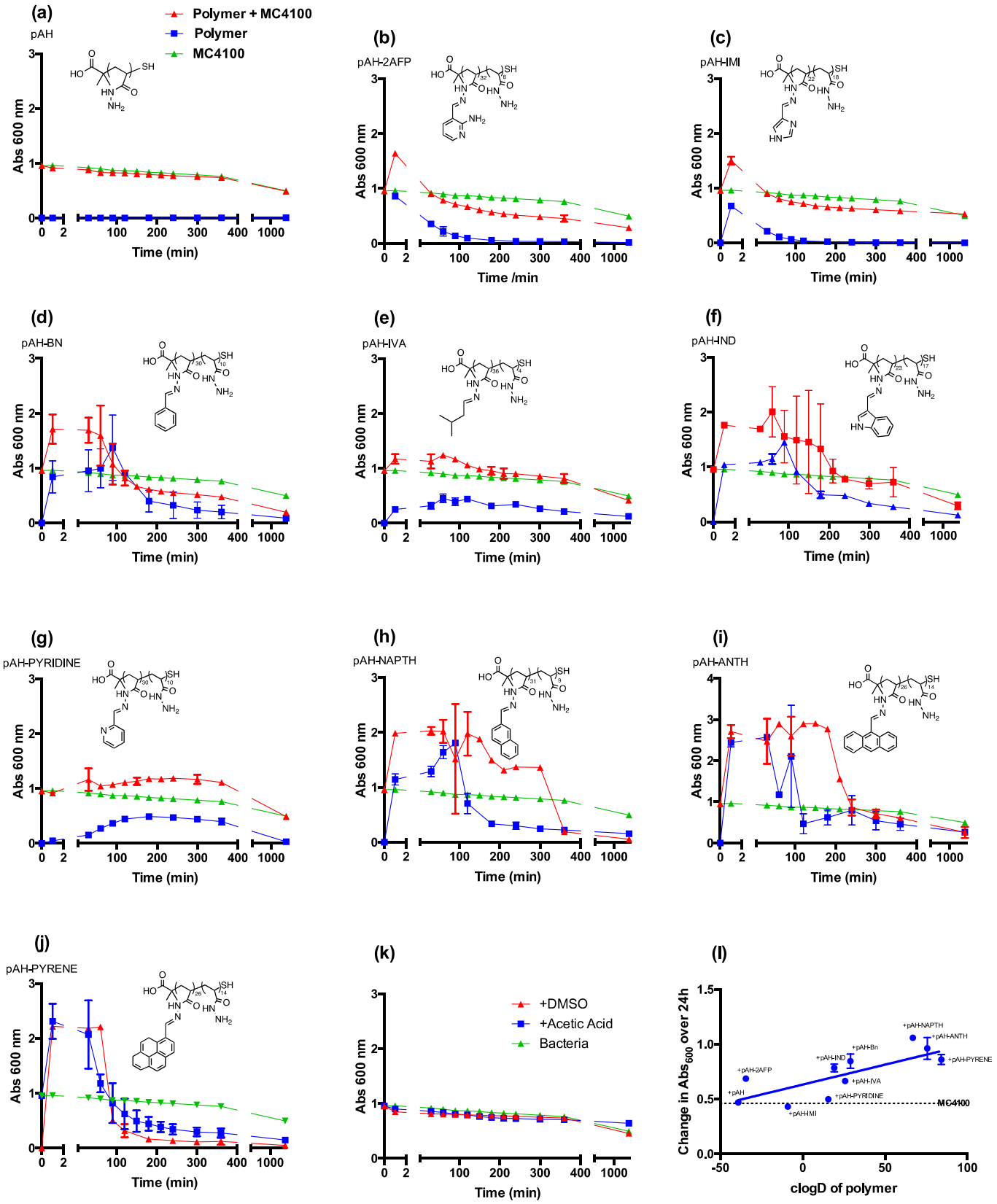

Figure 3: (a-j) Spectrophotometric assay to monitor polymer induced aggregation of MC4100. (k) Control experiment with the addition of DMSO and 100 mM acetic acid polymer solvent (without polymer) (l) Total levels of cell aggregation after 24h of incubation with respective polymers as a function of polymer hydrophobicity.

The graphs of figure 3 show 24h spectrophotometric traces of MC4100 cells when each polymer is added respectively to the cell culture (red trace), a cell culture control without the addition of polymer (green trace) and an additional blue trace which shows the response when polymer is added to the buffer solution without bacteria, so as to monitor turbidity as the respective polymers precipitate out of solution. Most of the polymers (except pAH and pAH-PYRIDINE) induce a distinct trend - on their addition to the aqueous solution with and without MC4100, absorbance immediately increases and then decreases over 24h (red and blue traces). In the absence of MC4100, the initial increase is due to the polymers precipitating out of solution upon addition, presumably forming hydrophobic polymer networks/aggregates that either settle immediately or after some time due to their weight, with each polymer having its own distinct trace (blue traces). In the case of bacteria alone (green trace) very limited aggregation of cells is found over 4h and the absorbance gradually decreases from 1 to around 0.5 over 24h presumably due to autoaggregation[26]. On the addition of polymers to MC4100, bacterial absorbance rapidly increases from 1 due to the formation of hydrophobic polymer networks with subsequent bacterial attachment via hydrophobic interactions. These polymer-bacteria networks then settle to the bottom of the cuvette in a very similar way to the polymer networks/aggregates alone, suggesting that the clustering patterns for polymer induced MC4100 cells are in general dictated by the hydrophobic polymer networks. Unfunctionalised pAH induced no additional bacterial clustering when compared with natural bacterial autoaggregation (green trace), presumably due to its hydrophilicity and subsequent high solubility in aqueous solution. Additionally, the pKa values of the hydrazides of pAH are around 3-4 and so pAH would be uncharged and unable to form electrostatic interactions with bacteria. pAH-PYRIDINE, pAH-IMI and to a lesser extent pAH-IVA induced limited MC4100 aggregation over 24h despite these

polymers inducing their own aggregating polymer networks. Aldehyde controls were also performed to monitor any potential aldehyde induced aggregation, however no significant effects were found except in the case of 1-Pyrene carboxaldehyde which did induce bacterial aggregation (figure S18). 1-Pyrene carboxaldehyde is the most hydrophobic of the aldehydes used and it would make sense that this aldehyde could potentially bind to bacteria and induce aggregation via charge neutralisation. In order to quantify the total degree of bacterial aggregation over 24h by the different polymers, the total change in absorbance from start to end of the experiment (24h) was plotted against calculated polymer distribution coefficient, clogD (figure 3l) with the graph showing a strong correlation between the total degree of bacterial aggregation and polymer hydrophobicity.

(c) Polymer induced biofilms

Now that it was confirmed that polymer induced *E. coli* aggregation was driven by polymer hydrophobicity, we wanted to see if this translated into overall biofilm levels using a simple and commonly used crystal violet biofilm quantification assay[27]. In the spectrophotometric assay, the cells were grown overnight (for around 16h), washed and transferred into phosphate buffer to an OD_{600} 1 (figure 1, route A). Hence the data corresponds to cells that were already 16h old at the start of the experiment (likely in the stationary phase), and 40h old by the end of the 24h point. It would be safe to assume therefore that at 16h, cells will have started expressing biofilm components with previous work suggesting PGA expression after only 4h[28]. Additionally, data shown in the later section confirms that expression of curli starts after just 20h of incubation in MC4100 and after 10h for PHL644. This was not of concern for the spectrophotometric assay as we simply wanted to monitor the degree of polymer induced cell clustering. Moving forward however, we thought it a good idea to add polymers to cells that were fresh and in the early log phase (i.e. not from an overnight stationary phase culture) so as to get a more thorough understanding of how the polymers affect biofilm expression levels from the start of proliferation (figure 1, route B). In all the proceeding experiments, it was therefore decided that overnight cultures (grown in LB) would be re-inoculated to 1% in the morning and grown for around 3h, washed and resuspended in phosphate buffer to an OD_{600} of 0.2. Polymers would then be added to these fresh 3h old cell suspensions at concentration of 0.1mg/ml so as to induce bacterial aggregation. An equal volume of 1X M63 minimal media (with respect to buffer volume) was added and the suspension incubated for 24h and 48h respectively (final polymer concentration of 0.05mg/ml), after which biofilms were stained with UV active crystal violet,

washed to remove unbound stain, and absorbance (550 nm) of the resulting suspension was measured. Increasing levels of absorbance correspond to a higher level of crystal violet staining as a result of more biofilm[27].

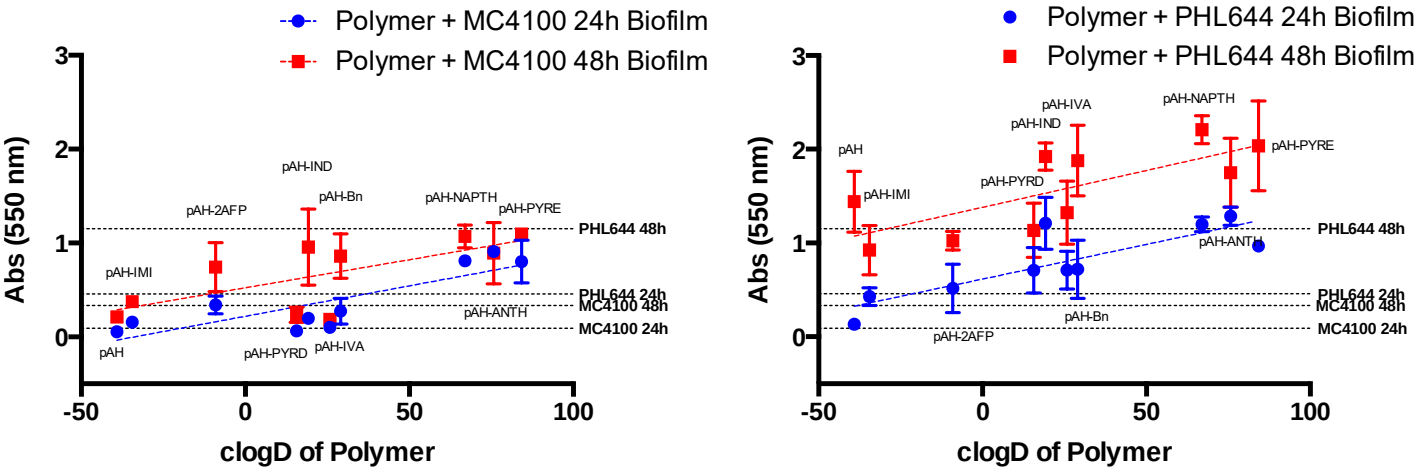

Figure 4: Polymer induced MC4100 (left) and PHL644 (right) biofilms after 24 and 48h incubation with polymers performed using crystal violet. MC4100 and PHL644 natural biofilm levels (without addition of polymer) also shown as dashed lines

As mentioned previously, the two strains are isogenic mutants differing only in one gene, *ompR* with PHL644 containing a point mutation (*ompR234*) which allows for the constitutive overexpression of curli resulting in thicker biofilms when compared with the parental MC4100 strain and this is conformed here for naturally formed MC4100 and PHL644 biofilms (dashed lines, figure 4) which are initiated by bacterial aggregates formed at the bottom of the container due to autoaggregation. One of the objectives therefore was to see if MC4100 biofilm levels could be boosted to that comparable of naturally formed PHL644 biofilms by inducing increasing levels of aggregation using our polymers. Looking at figure 4 it can be seen that overall polymer induced biofilm levels at both 24h and 48h were directly proportional to polymer hydrophobicity in both strains, indicating that the more the polymer is able to aggregate bacteria, the higher the final biofilm levels will be. After 24h,

almost all polymer induced MC4100 biofilm levels (figure 4, left) were boosted to exceed natural 24h MC4100 biofilm levels, with the more hydrophobic polymers (pAH-NAPTH, pAH-ANTH and pAH-PYRENE) stimulating more biofilm in 24h when compared with 48h MC4100 natural biofilm levels, 24h natural PHL644 biofilm levels and producing similar levels to that of 48h natural PHL644 biofilms. In the case of PHL644 a similar response to the addition of polymers is shown, with the most hydrophobic polymers stimulating almost twice the amount of biofilm than the naturally formed PHL644 biofilms at both timepoints (figure 4, right). Unsurprisingly, in general the addition of the respective aldehyde to the cells did not boost biofilm levels due to their inability to aggregate bacteria, except in the case of 1-Pyrene carboxaldehyde, which did induce a slight increase in biofilm levels (figure S19). Overall, the data demonstrates that hydrophobic polymer induced bacterial aggregation can increase biofilm levels in a predictable manner, and also shows that we can potentially use highly hydrophobic polymers to stimulate large amounts of biofilm in strains not normally known to do so, in this case MC4100. Given the high level of control over biofilm quantities, we wanted to asses if differing levels of biofilm could also be by stimulated using the same functional polymer, but varying its degree of functionality (and subsequent hydrophobicity). For this pAH-IMI and pAH-Bn were chosen, with each polymer being functionalised with the respective aldehyde to target polymer functionalities

(d) Size and strength of polymer induced bacterial aggregates/biofilm

Given the ability of the polymers to interact with and form controlled levels of biofilm, it was decided to monitor the size distributions of these polymer induced bacterial aggregates/biofilm after the 24 and 48h mark using laser diffraction based particle size analysis. Given that the data so far suggests that the most hydrophobic polymers cause the most overall bacterial aggregation and resulting biofilm, we hypothesised that these polymers would be stimulating the largest, most cell dense aggregates.

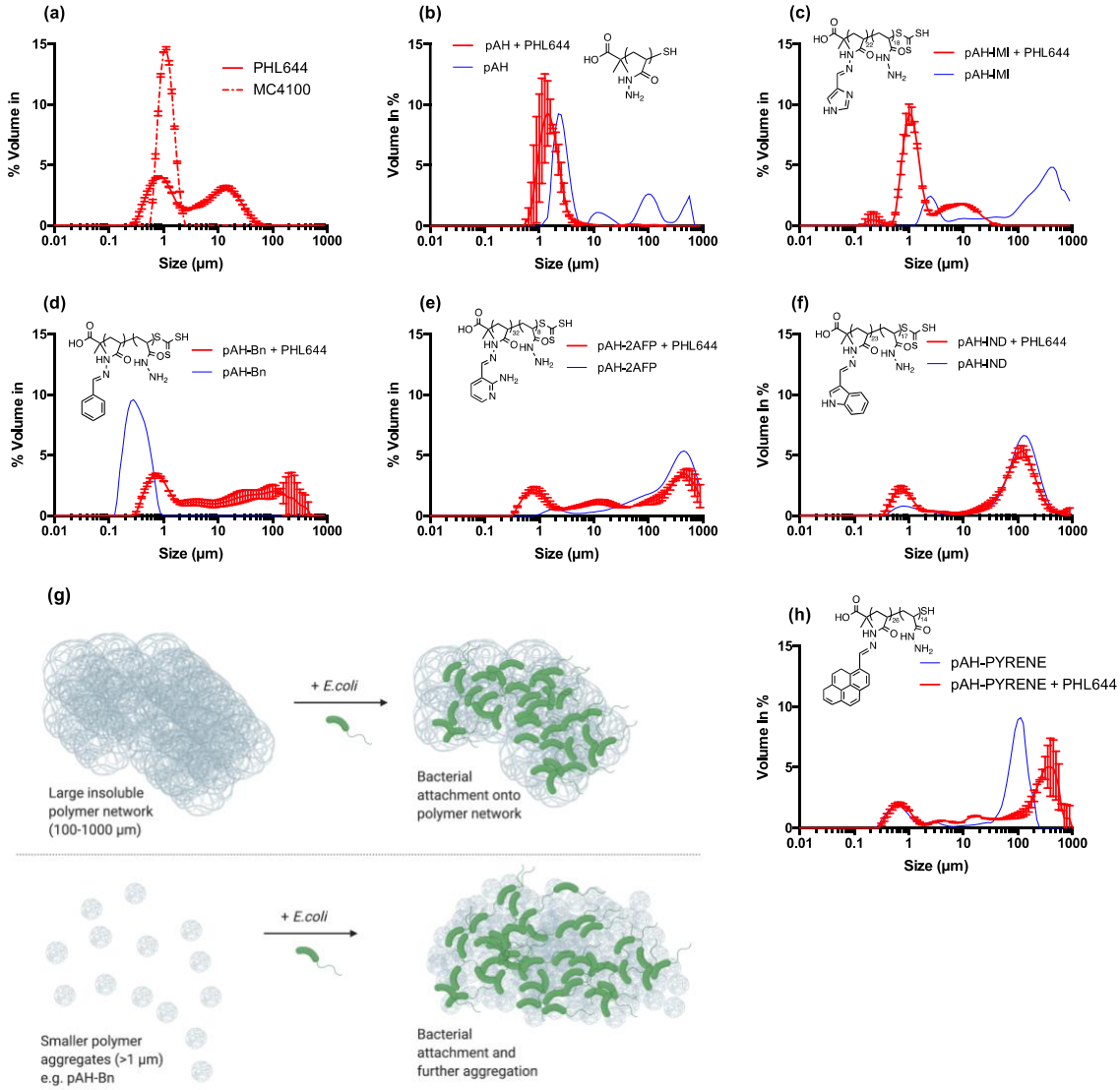

Figure 5: (a-f) Size distributions of selected polymers and their respective 24h polymer-induced PHL644 aggregates. (g) The proposed mechanisms of polymer-bacterial aggregation (h) Size distribution of pAH-PYRENE PHL644 aggregates

Polymers were mixed with either fresh MC4100 or PHL644 cells as previously (figure 1, route B) and left to incubate for 24 and 48h. The samples were then transferred into, and were continually stirred in a mastersizer dispersion unit set at 500 rpm. The size distributions of aggregates were measured by laser diffraction as the aggregates passed through the laser. As most of the polymers were shown to be insoluble in water creating aggregates of their own (figure 3), the respective polymer size distributions were also measured in the absence of bacteria. Some selected examples of polymer induced PHL644 aggregate size distributions after 24h are shown in figure 5. Firstly, it needs to be mentioned that upon addition of polymer to *E. coli*, large clusters were immediately visible by the naked eye, so it is likely that the size of these aggregates are on the millimetre scale. When the samples are placed into the dispersion chamber set at 500 rpm, it is more than likely that these large aggregates/biofilm are broken down into smaller sizes, which will depend on the strength of the aggregating interactions. In general, most polymer induced MC4100 aggregates were simply not strong enough both after 24 and 48h of incubation, and only showed a single population distribution corresponding to single cells (figures S22 and S23). Only 4 of the polymers (pAH-2AFP, pAH-IND, pAH-NAPTH and pAH-ANTH) were able to induce strong enough MC4100 aggregates that resisted breaking apart by stirring after 24 and 48h with the respective polymer (figures S22 and S23).

The size distribution of PHL644 alone, without the addition of polymer showed two distinct populations; single cells (around 1 μm) and naturally formed aggregates which were between 10-100 μm in size (figure 5a). This was expected as this strain is an over-expresser of curli, which presumably encourages and strengthens bacterial aggregation. The size distribution of MC4100 alone did not show this natural aggregation even after 48h (figure 5a and S23) however it is completely possible that MC4100 does produce weaker

aggregates (due to less curli expression) which simply get broken up due to the shear of stirring. In both strains, very similar polymer induced bacterial aggregate size distributions were found after incubation for 24 and 48h respectively (compare equivalent strains of figures 5, S20 and S22 (24h) with figures S21 and S23 (48h)). One would expect that after 48h bacterial aggregates would be larger due to increased biofilm expression. This may well be the case but again, they may be broken down in these conditions to the match the 24h aggregate sizes. As expected, the hydrophilic unfunctionalised pAH induced no PHL644 aggregation and also prevented the formation of the naturally formed aggregates at 24h (figure 5b), but not after 48h (figure S21). Later on it is shown that pAH severely disrupts the expression of curli in PHL644 and somewhat in MC4100 too. Surprisingly, pAH alone showed 4 separate polymer size distributions up to 1000 μm in size (figure 5b), however in the presence of either strain of bacteria these do not lead to strong bacterial aggregates within the dispersion chamber. pAH-IMI also generated large polymer aggregates (100-1000 μm) but again in the presence of either strain, these are absent (figure 5c and S23) suggesting that for these two hydrophilic polymers, polymer induced bacterial aggregation is weak and bacterial aggregates get broken up in the dispersion chamber. Additionally, the fact that only one distribution can be seen at 1 um in the presence of these polymers suggests that the bacteria actually disrupt the insoluble polymer network, resulting in the polymers binding to the bacteria despite not inducing aggregating effects. Many of the polymers do however seem to bind strongly to both strains, forming aggregates that stay intact; pAH-2AFP and pAH-IND polymeric size distributions are almost identical to that of the large polymer induced bacterial aggregates (100-1000 μm) (figure 5e, f, S21-S23), and this is also expectedly seen in two of the most hydrophobic polymers (pAH-NAPTH and pAH-ANTH, figures S20-S23) where one would expect the polymeric/bacterial aggregates to be larger

and more intact due to increasing levels of hydrophobic interactions between polymer chains and with bacteria. pAH-2AFP and pAH-IND may not be as hydrophobic but both contain heterocyclic repeating units which could potentially form strong hydrogen bonds with neighbouring chains and/or the bacterial cell surface. Intriguingly, unlike pAH-NAPTH and pAH-ANTH, the similarly hydrophobic pAH-PYRENE only induced large aggregates in PHL644 but not in MC4100. The reason for this is unclear at this stage, however pAH-PYRENE was the only polymer to induce larger bacterial aggregates than that of its own polymer aggregate network for PHL644 (figure 5h). Later on, we show that pAH-PYRENE significantly boosts PHL644 curli expression levels, and this is likely the reason. Therefore only pAH-2AFP, pAH-IND, pAH-NAPTH and pAH-ANTH were able to form any bacterial aggregates in the weakly aggregating MC4100 (figures S22 and S23). These respective polymers in general induce very similarly sized bacterial aggregates in both strains, however the volume densities of these are always lower in the respective polymer induced MC4100 aggregates. This is expected due to the higher levels of curli expression in PHL644. From this it can be said that the size of the polymer induced bacterial aggregates depends on the mediating polymer, whereas the volume intensity of the aggregates is mediated by curli expression.

Interestingly, pAH-Bn does not seem to produce large polymeric aggregate networks in the absence of bacteria, instead showing a smaller size distribution on the nano scale. In the presence of PHL644 however, large aggregates (100-1000 μm) can be found (figure 5d) indicating that bacterial aggregation may occur via a slightly different mechanism. Most of the data so far suggests that upon addition of polymers to a culture of bacteria, they immediately form large polymeric networks onto which bacteria attach. In the case of pAH-Bn, it seems that the bacteria attach to the smaller pAH-Bn aggregates which then seem to

increase in size dramatically. Unsurprisingly, the addition of corresponding aldehydes induced no strong aggregates in either strain, including when 1-Pyrene carboxaldehyde was added (Data not shown).

(e) Influence of polymers on curli expression

So far, all analysis has looked into the ability of the polymers to cluster bacteria; the crystal violet assay is widely used to measure overall biofilm quantity but it does not give much information with regards to the expression specific of extracellular polymeric substances. Curli is the most widely studied EPS component in *E. coli*[20], and its expression levels can be easily monitored with the use of reporter genes, and as such we wanted to see the effect of polymer induced bacterial aggregation on curli expression levels. Curli formation is directed by the *csgBA* and *csgDEF* operons[20] and as such a GFP reporter plasmid (pJLC-A) was used to effectively monitor the rate of expression of curli in both strains by reporting promoter activity of the *csgBA* operon. Bacteria-polymer suspensions were prepared as usual and GFP fluorescence was monitored over 48h using a plate reader, see chapter 2 materials and methods section (ii) (b).

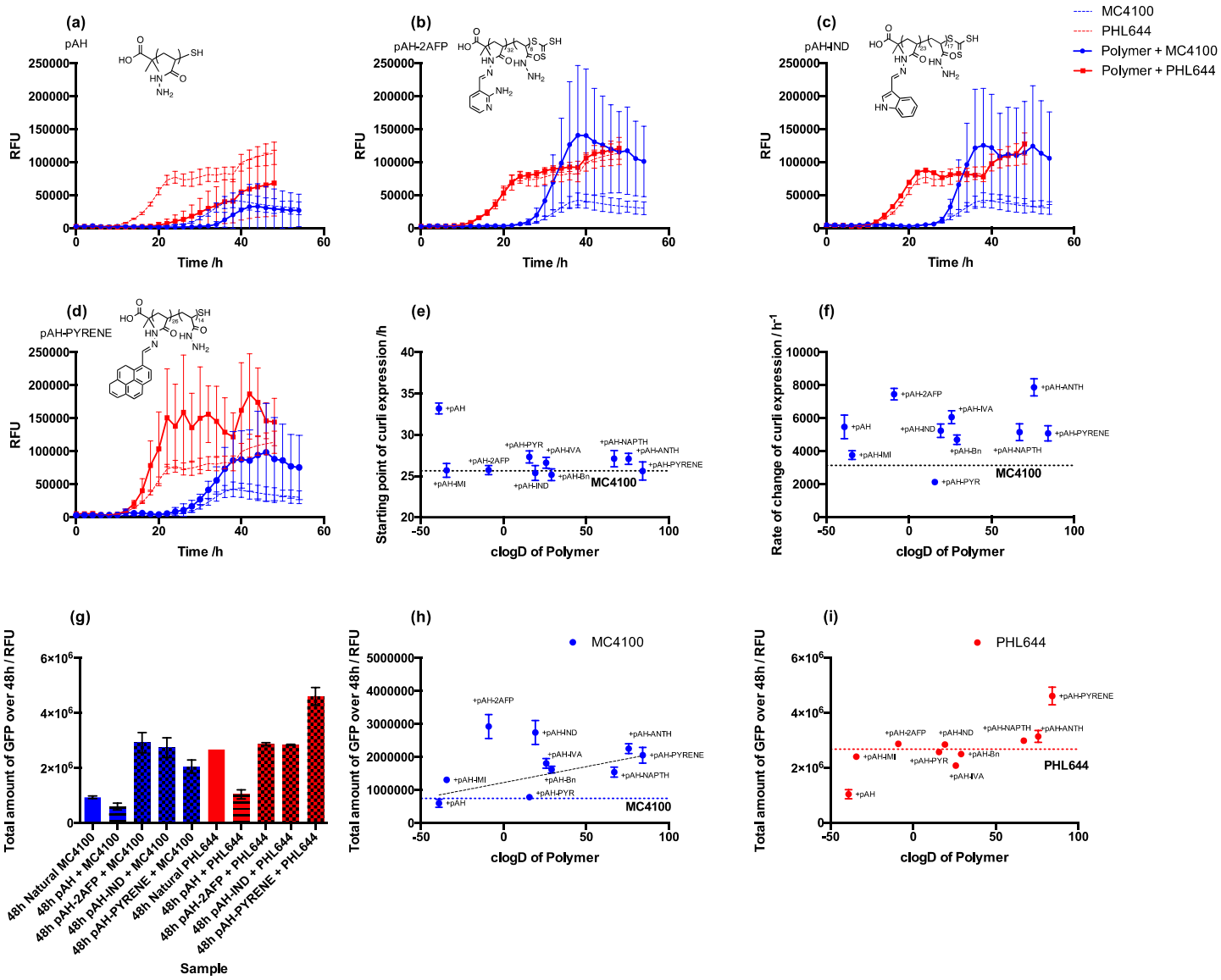

Figure 6: (a-d) Rate of expression of curli over 48h in polymer induced clusters (thick traces) and in cultures without the addition of polymer (thin traces). (e) Time of onset of curli expression in MC4100 samples (f) Initial rate of curli expression on its onset (g) Comparison of total curli expression after 48h in different conditions (h) Total amount of curli expression in polymer induced MC4100 biofilms (i) Total amount of curli expression in polymer induced PHL644 biofilms. Horizontal dotted lines represent data for cultures without the addition of polymer.

As expected without the addition of polymers, PHL644 generates more curli than MC4100 (figure 10a-d, thin traces) due to the *ompR234* point mutation. PHL644 seems to start expressing curli much earlier than MC4100 (at around 10h compared with around 20h for MC4100), additionally PHL644 shows another period at around 40h whereby the rate of curli expression increases again. In contrast MC4100 only has one initial gradient followed

by a plateau/decrease in the rate of expression at around the 40h mark and these trends are followed on the addition of polymers too. For PHL644, the addition of only two polymers (pAH and pAH-PYRENE) significantly affects overall curli expression levels (figure 6 a, d and i). All other polymers seem to have little effect (figure 6b, c, i and figure S24), suggesting that in general the polymer induced aggregation of PHL644 does not affect curli expression in this already overproducing strain. Of the two polymers; pAH, the most hydrophilic of polymers dramatically reduces curli expression by delaying its onset (figure 6a) and pAH-PYRENE, the most hydrophobic dramatically increases initial expression rates, without affecting the time of onset (figure 6d). Later it is shown that pAH dramatically reduces cell metabolism and so its detrimental effect on curli expression is understandable, however the reason for the spike in pAH-PYRENE samples in PHL644 is unclear at this stage given that the similarly hydrophobic polymers pAH-NAPTH and pAH-ANTH did not have any effect (figure S24 and 6i).

In contrast, the addition of increasingly hydrophobic polymers to MC4100 cells significantly increased total levels of curli expression with respect to the natural MC4100 levels in all but the hydrophilic pAH and pAH-PYRIDINE induced samples (figures 6b-d, S24 and 6h), which do not aggregate cells. pAH which like for PHL644, reduces overall expression by delaying its onset (figure 6a). pAH-PYRIDINE on the other hand reduced the initial rate of expression (figure S24), despite having no effect on PHL644. The most hydrophobic polymers (pAH-ANTH and pAH-PYRENE) significantly increased initial expression rates in MC4100 (figure 6d and figure S24) resulting in significantly higher total amounts of curli over 48h, and comparable to that of the overexpressing natural PHL644 sample (figure 6h, i). Interestingly, the moderately hydrophobic heteroaromatic polymers pAH-2AFP and pAH-IND were the

best of all candidates with the highest levels of MC4100 curli being generated (figure 6b, c, h). Previous analysis on the size distributions of aggregates showed that these two polymers induced strong hydrophobic networks that were not broken up in the presence of bacteria suggesting strongly aggregating interactions between the respective polymer chains and bacteria, which could be from the result of additional cooperative hydrogen bonding made possible by the heterocyclic nature of these two polymers. This increased level of bacterial surface binding could influence the production of curli, which is after all a surface adhesin produced on bacterial surface contact[21,20]. In all cases except for pAH and pAH-PYRIDINE, polymers were able to increase the total expression of MC4100 curli over 48h entirely due to an increased rate of expression on the onset when compared with the control without polymer (figure 6b-d and figure S24), with expression increasing, levelling off and decreasing at similar times compared with the natural MC4100 biofilm. The effect of each aldehyde on the expression of curli was also monitored in both strains, with the corresponding aldehyde generally inducing less curli than its respective polymer. One exception was for 1-Pyrene carboxaldehyde which has been shown to aggregate bacteria, and did stimulate large levels of curli (figure S25) by increasing the initial rate of expression. A point of note to make is that the error bars for polymer induced curli expression are rather large and increase with higher levels of induced expression. Each data point represents 6 replicates, the results of which do tend to vary and a possible reason for this could be due to the slightly differing polymer induced bacterial aggregating patterns for each replicate of a given sample, reflected greatly in curli expression. These variations were not seen in the respective aldehyde induced biofilms due to the fact that they do not significantly aggregate cells (figure S25, S18).

For the purposes of completeness, we decided to visualise these bacterial aggregates using a confocal microscope. pAH-2AFP was attached to a blue-fluorescent label (7-methoxycoumarin-3-carboxylic acid, MCCA) and was added to the curli dependant GFP expressing bacteria as usual in a chamber slide and left to incubate for 24h. After this, the resulting polymer-cell aggregates were additionally stained and incubated for 1h with red fluorescent wheat germ agglutin (WGA) - a lectin which binds to N-acetyl-D-glucosamine moieties. Excess unbound stain was then removed and the aggregates imaged to confirm the presence of poly-β-1,6-N-acetyl-D-glucosamine (PGA) in the biofilms (figure 7). A control without the addition of polymer was also imaged (figure S27).

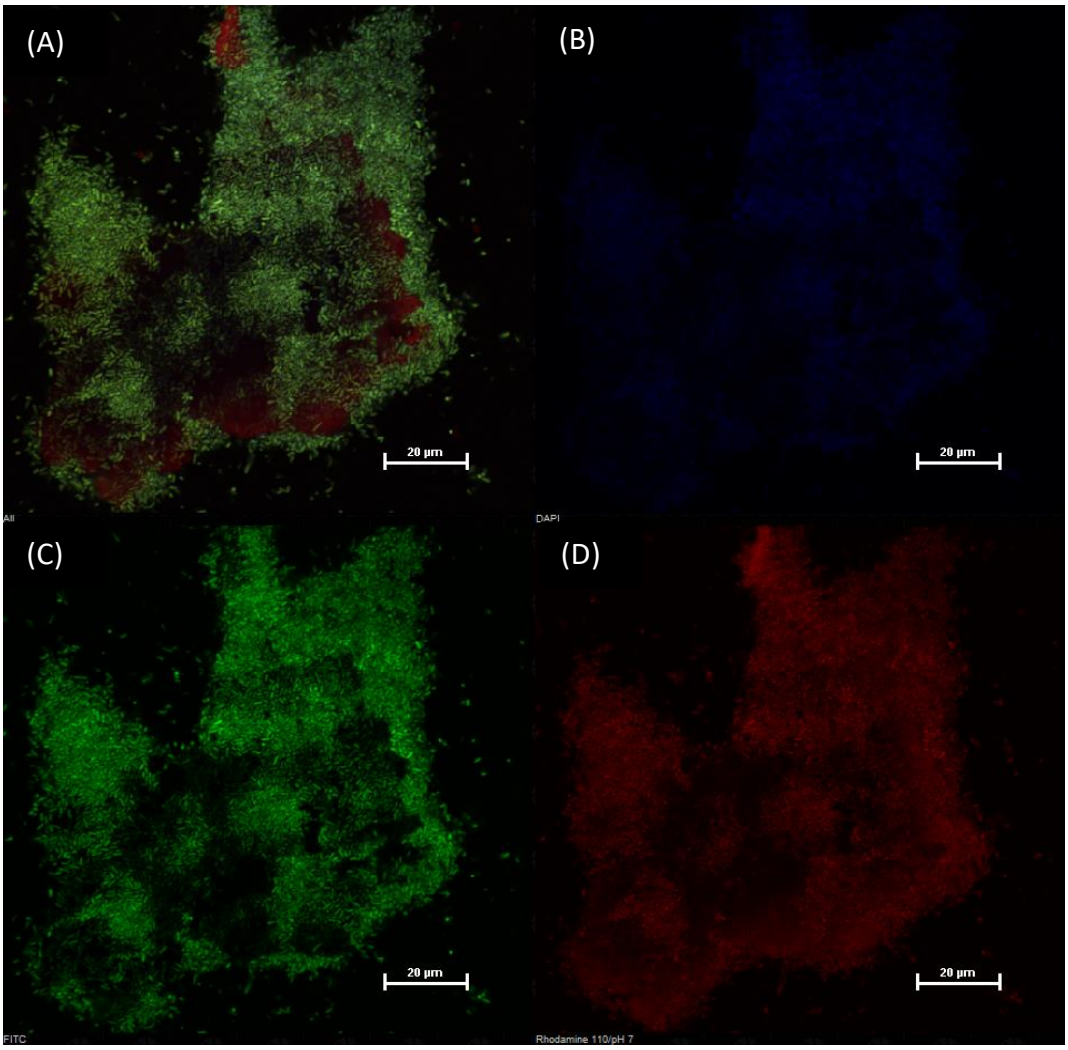

Figure 7: Confocal image (40X objective) of pAH-2AFP induced PHL644 aggregate/biofilm. Cells expressed GFP as a reporter for the expression of curli. Red fluorescence confirmed the presence of PGA, blue fluorescence was associated with the MCCA labelled pAH-2AFP. (A) merged image of pAH-2AFP induce aggregate/biofilm (B-D) individual images for blue, green and red channels

The structure of the pAH-2AFP aggregates in general was found to be very heterogenous with little control over aggregate shape in the presence of polymer. The different components of the aggregate could be visualised through the different stains; all aggregates showed blue fluorescence confirming that polymer aggregates were associated with polymer. All aggregates contained cells that were expressing GFP indicating high curli expression, furthermore planktonic cells were also expressing GFP. The red fluorescence additionally confirms the presence of PGA on the aggregates. Interestingly, neither the GFP or the WGA fluoresce intensities were found to be consistent throughout the aggregate structure indicating heterogeneity in the composition of overall EPS. This level of heterogeneity was not however found in the naturally formed biofilms without the addition of polymer (figure S27). In general most biofilms used for industrial purposes are targeted to be highly heterogeneous; forming sub-communities, voids and channels which increase the mass transfer of nutrients, oxygen, and other substrates throughout the biofilm, increasing its metabolism and productivity[29,30].

(f) Biocatalytic ability of polymer induced biofilms

Finally, we wanted to assess the functionality of our polymer induced biofilms in the biocatalytic arena. Previous work within our group has shown the ability of 7-day old spin coated *E.coli* K-12 MG1655 and MC4100 biofilms and their respective isogenic *ompR234* mutants PHL628 and PHL644 to convert haloindoles into their respective halotryptophans[13] when transformed with pSTB7, a plasmid expressing the tryptophan synthase gene. In this this study, only the conversion of 5-fluoroindole to 5-fluorotryptophan was monitored and it was previously shown that the mutant overexpressing biofilms outperformed their respective wild type counterparts in terms of 5-fluoroindole consumption, 5-fluorotryptophan generation, and overall selectivity of conversion after 24h of incubation of biofilms with starting material[13]. A later study suggested the reason for this was a least in part due to the constant and complete regeneration of the tryptophan synthase enzyme within thick spin coated biofilms[14]. We therefore wanted to assess the performance of our alternative polymer induced biofilm platform in this biotransformation, where we can control biofilm production. Both strains of polymer-bacteria samples were prepared as usual in eppendorf tubes and incubated at 30 ^{0}C for 24 and 48h respectively with shaking at 150 rpm. Before addition of reagents to the settled biofilms, the supernatants of each sample were removed so as to remove any planktonic cells, with supernatant cell density being checked so as to be sure we were not removing significantly different amounts of bacteria that could skew results accordingly (figure S28). Biofilm mediated biocatalysis of 5-fluoroindole was then performed respectively as described in the materials section with all biotransformation reactions proceeding for 24h, after which the reaction was stopped and HPLC was used to measure final concentrations of 5-fluoroindole and 5-fluorotryptophan.

Additionally, as the reaction is reversible (figure 8a, catalysed by the native *E. coli* enzyme tryptophanase, TnaA) an additional parameter, selectivity of conversion was also calculated and can be defined as the percentage of 5-fluorotryptophan generated directly from the cell uptake of 5-fluoroindole.

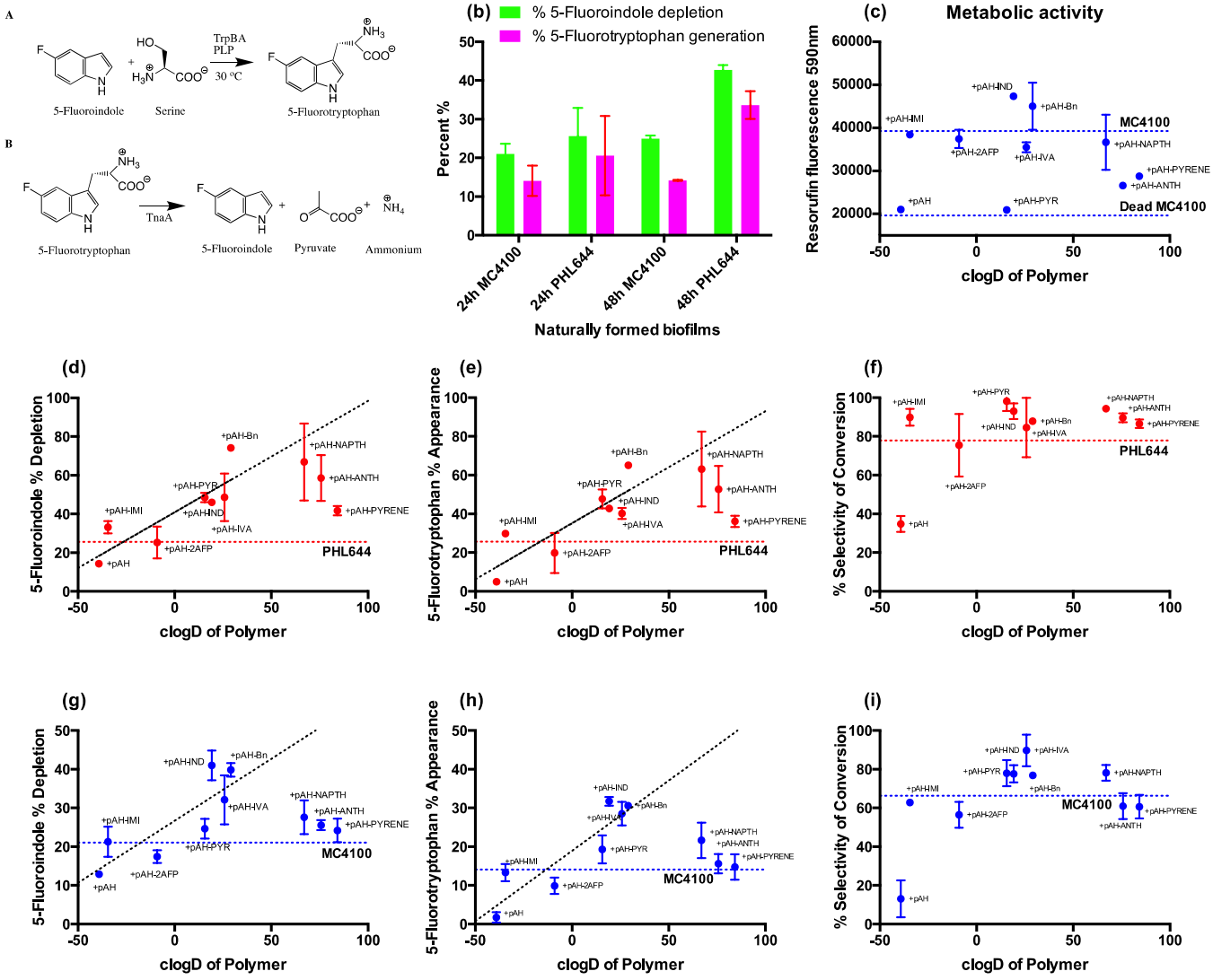

Figure 8: (a) Reaction scheme for the biocatalysis of 5-fluoroindole to 5-fluorotryptophan, and the reverse reaction catalysed by tryptophanase, TnaA. (b) Performance of naturally formed 24 and 48h PHL644 and MC4100 biofilm after 24h incubation with starting reagents. (c) Metabolic activity of 24h old polymer induced biofilms. (d-f) Biotransformation data for 24h polymer-induced PHL644 and MC4100 (g-i) biofilms.

In the case of naturally formed PHL644 biofilms (figure 8b), performance was greater for 48h biofilms with respect to its 24h counterpart in terms of 5-fluorindole depletion and 5-fluorotryptohan generation. It has been shown that natural biofilm levels increase after 24h (figure 4) and hence it is no surprise that the thicker 48h biofilms perform better given the reasoning above. This effect was much less so in the less dense naturally formed MC4100 biofilms, with 24h and 48h performances being comparable likely due to the limited increase in overall biofilm levels (figure 4). As expected, PHL644 performed significantly better that its parent MC4100 at the 48h mark, and slightly better at the 24h timepoint.

Somewhat unexpectedly only minimal differences were found between respective 24h and 48h polymer induced biofilm performances in both strains (figure S29), despite the increase in biofilm levels. In general it was found that the moderately hydrophobic polymers (pAH-Bn, pAH-IVA, pAH-IND and pAH-PYRIDINE) induced cells to perform slightly better at the 24h mark, whilst the hydrophilic (pAH-IMI, pAH-2AFP) and most hydrophobic polymers (pAH-NAPTH, pAH-ANTH and pAH-PYRENE) induced cells to perform better at the 48h mark. Most of these differences are however not statistically significant, hence in general it can be said that there is no need to wait for 48h before starting this polymer mediated biotransformation and that 24h polymer induced biofilms perform similarly to their 48h counterparts.

Therefore, focussing on 24h polymer induced biofilms (figure 8d-i), the addition of increasingly hydrophobic polymers clearly boosts the biotransformation in both strains up to a point, with respect to the natural biofilm controls. As expected, pAH which reduces biofilm production had a detrimental effect on the biotransformation with moderately

hydrophobic polymers boosting performance almost twofold in each strain when compared with their naturally formed counterparts. For MC4100 biofilms especially, this only reaches a certain point whereby the addition of excessively hydrophobic polymers (pAH-ANTH and pAH-PYRENE, and to a lesser extent pAH-NAPTH) begin having a detrimental effect on the biocatalysis (figure 8g and h). In some ways this is not surprising as the addition of highly hydrophobic polymers may induce a level of cell membrane damage, reducing viability. To test this the metabolic activity of MC4100 biofilms were assessed after incubation with the respective polymer for 24h, via the widely used resazurin assay. Upon addition of resazurin, it diffuses into the cells where it can be reduced to the highly fluorescent resorufin probably as the result of the action of several different redox enzymes and intracellular coenzymes such as NADH[31,32,33], hence it is commonly used to probe overall metabolic activity of cells. Unsurprisingly, the addition of both highly hydrophobic pAH-ANTH and pAH-PYRENE reduced the metabolic activity of cells (figure 8c), potentially due to cell envelope damage[34,35] and this is reflected in biotransformation performance in both 24 and 48h biofilms, albeit less so at the 48h mark where cells may recover during the additional 24h period of incubation (figure S28, S30). In PHL644 this detrimental effect of the hydrophobic polymers is somewhat less, with pAH-NAPTH induced 24h PHL644 biofilms performing as expected and can be tentatively explained by the increased resistance of cells within thick PHL644 biofilms. pAH and pAH-PYRIDINE completely reduced metabolic activity after 24h, similar to the levels of dead cells and so it was surprising that pAH-PYRIDINE unlike pAH induced biofilms are able to catalyse the reaction at all, confirmed by its relatively high selectivity of conversion suggesting these cells recover their metabolism during the additional 24h biocatalysis process. Another potential reason for the drop in activity for the hydrophobic polymer induced biofilms could be due to limitations in mass transfer within

the aggregate structure, which is tightly bound together predominantly by strong hydrophobic interactions, where the transfer of flow could be limited. Therefore, mass transfer within these polymer induced aggregates/biofilm needs to be investigated further, and it is likely that it may depend on the physiochemical and rheological properties of the aggregating polymers.

Finally, we wanted to further assess the biocatalytic ability of the induced aggregate/biofilms by harnessing some of the useful native metabolic pathways of bacteria that are common within industry for the biocatalysis or bioremediation of organic substrates[36]. *E. coli* is known to produce and excrete esterases which can used for the hydrolysis of esters. Specifically K-12 strains are known to have a range of esterase activity with effective hydrolysis of acetyl esters[37], butyrate esters[38] and nitrophenyl esters[39] reported in the literature. As such we decided to analyse nitrophenyl hydrolysis activity of our polymer induced biofilms using literature protocols[39]. 4-Nitrophenyldodecanoate was chosen as the substrate; it is insoluble in aqueous conditions hence the reaction mixture for the biocatalysis was made to contain 33% ethanol to improve solubility. This added an additional dimension to the experiment as the this was now a reaction performed in harsh conditions for bacteria – ethanol is toxic. We saw this as an effective way to challenge our polymer induced biofilms and monitor how they would perform when compared with naturally formed biofilms. Polymer-bacteria suspensions were prepared is usual (chapter 2 materials and methods (ii) (b)) and left to incubate for 24h, after which an ethanol containing solution with the substrate 4-Nitrophenyldodecanoate was added to the aggregates. The reaction was monitored at set timepoints for a total of 240h, by measuring reaction buffer absorbance (410 nm) as the product 4-Nitrophenol us UV active.

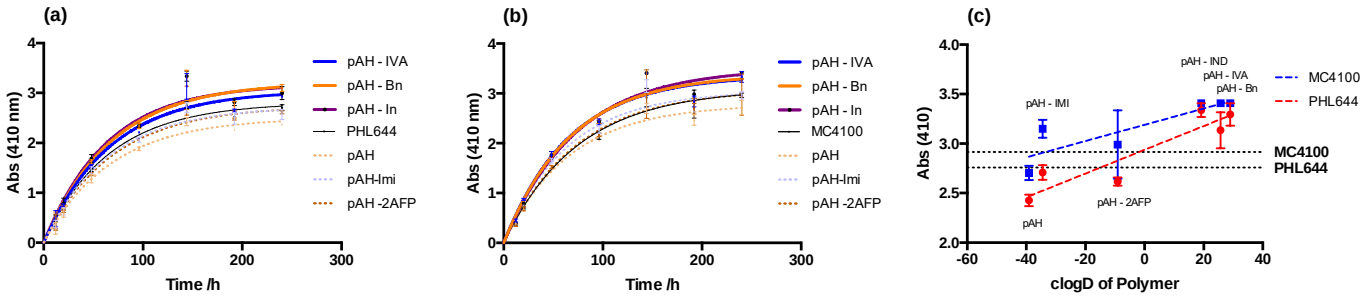

Figure 9: Reaction curve for the biocatalysis of 4-Nitrophenyldodeconoate to the UV_{410} active 4-Nitrophenol by polymer induced PHL644 biofilms (a) and for polymer induced MC4100 biofilms (b). Graph showing the relative amounts of 4-Nitrophenol generation after144h as a function of calculated polymer hydrophobicity cLogD for both strains (c)

In these conditions, the reaction is extremely slow due to the low amounts of 4-nitrophenyldodecanoate used (0.08 mM) and perhaps a detrimental effect on the cells by the levels of ethanol. However, it can be clearly seen that the moderately hydrophobic polymer induced biofilms (pAH-IVA, pAH-Bn and pAH-IND) generate higher amounts of product throughout the 240h (figure 9a and b), and it is evident this is due to polymer hydrophobicity (figure 9c). Surprisingly, MC4100 cells performed slightly better than PHL644 in both the naturally formed biofilms and the polymer induced biofilms (figure 9c). We also performed this reaction in slightly less challenged conditions using only 10% ethanol, and even less substrate (as this is dependent on the amount of ethanol used in the reaction mixture). In these conditions, however the reaction even slower indicating the need for a higher amount of substrate and ethanol (figure S34). Hence this is an example of a case whereby challenged conditions are needed to optimise reaction performance. Our moderately hydrophobic polymer induced biofilms were able to produce slightly more product over the course of the reaction when compared with naturally formed biofilms and biofilms stimulated by the hydrophilic pAH-2AFP and pAH-IMI polymer. The reasoning for this was due to increased resistance imparted by the hydrophobic polymer induced biofilms toward toxic conditions.

(iv) Discussion

In this study we have demonstrated the ability of hydrophobic poly(acryloyl hydrazide) functionalised polymers to interact and aggregate two *E. coli* K-12 strains; PHL644 and MC4100 via hydrophobic interactions, with levels of overall polymer induced aggregation over 24h being increased with increasingly hydrophobic polymers. Predictably, many of the polymers precipitated out of solution upon addition to aqueous solution forming aggregates of their own, onto which cells bind to in their presence. Hence in general, polymer mediated cell aggregation was dictated by the insoluble polymer aggregates/networks. The overall levels of polymer induced aggregation corresponded well with the resulting overall biofilm levels after 24h and 48h of incubation, as measured by crystal violet staining. Additionally it was shown that we could induce biofilm levels of the usually low biofilm forming MC4100 to match that of the naturally formed curli overproducing PHL644 biofilms. In general the most hydrophobic polymers (pAH-NAPTH, pAH-ANTH and pAH-PYRENE) induced large, strong bacterial aggregates/biofilm with almost identical size distributions to their respective insoluble polymer aggregates formed upon addition to aqueous solution suggesting that bacteria attach to the polymer only upon the formation of these insoluble polymer networks, without disrupting them. Hydrophilic polymers such as pAH and pAH-IMI also produce large soluble aggregates in aqueous solution, however in the presence of bacteria and continual stirring, the aggregates break up with the polymers seemingly adhering to the single cells. The moderately hydrophobic heteroaromatic polymers pAH-2AFP and pAH-IND surprisingly also induced a similar response to the hydrophobic pAH-NAPTH, pAH-ANTH and pAH-PYRENE, creating polymer aggregates strong enough to stay intact during continual stirring and in the presence of bacteria which adhere to the polymer network. We think that

this may be due potential additional hydrogen bonding within the heteroaromatically functionalised polymer aggregates of pAH-2AFP and pAH-IND. Intriguingly upon addition of the moderately hydrophobic pAH-Bn to aqueous solution, significantly smaller aggregates of 1 um were formed. However in the presence of bacteria, large aggregates were found suggesting a different mechanism of bacterial attachment to pAH-Bn (figure 5g).

On the whole our polymers did not affect curli expression in the already overexpressing PHL644, but did in a predictable manner for MC4100; in general with increasingly hydrophobic polymers inducing increasing levels of curli over 48h of incubation. This was a somewhat intriguing result due to the fact that an earlier study conducted in our labs showed that curli expression was decreased upon cell attachment to a solid surface and within sedimented cell aggregates, whilst expression was maximal in planktonic cells[40]. Therefore curli acts as an adhesin which is maximally expressed in planktonic cells in preparation for (and to mediate) solid surface attachment[41]. Surface attachment is then sensed by the outer membrane protein NIpE[42] which activates the CpxRA two component regulatory system, which represses *csgD* and *csgB* expression and hence curli expression[20]. It is therefore not surprising that curli expression in cultures without the addition of polymer is low owing to the level of autoaggregation (figure 3) leading to the formation of solid surface associated sediment biofilms. Additionally high cell-cell contact within these aggregates increases osmolarity – also known to be detrimental to curli expression[40,20]. Interestingly, it was shown that cells within a pellicle biofilm (a floating biofilm formed at the liquid-air interface, figure 9a) expressed curli at higher levels[40]. The authors reasoned that this was due to the lack of solid surface contact, and also the additional structural role required of curli within non-solid supported biofilms leading to its continual expression[40]. Despite the fact that the polymer induced aggregates do form sediments at the bottom of

the container, there could still be some level of hijacking of the curli-downregulating NIpE/CpxRA surface sensing/regulatory pathway due to the high level of association of cells with a soft unsupported surface (i.e. the polymer network) rather than a solid like surface – similarly to pellicles where the surface is a 'soft' air-liquid interface (figure 10).

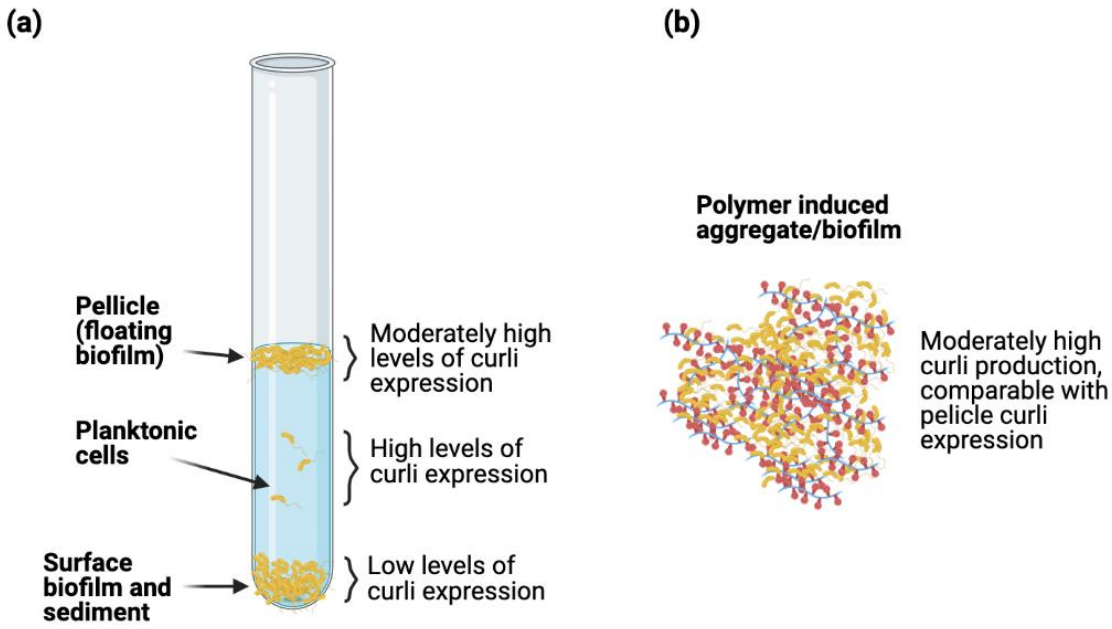

Figure 10: (a) Schematic illustrating the differences in curli expression based on location of growth within a solid tube, from ref 36. (b) Unsupported polymer induced biofilm may require extra curli for structural integrity – very much like a pellicle

The reason why MC4100 curli expression gets progressively higher in increasingly hydrophobic polymer networks remains unknown and requires further investigation. Intriguingly the heteroaromatically functionalised pAH-2AFP and pAH-IND both induced the largest amounts of overall curli. We postulated that these polymers formed tightly aggregating networks through hydrogen bonding interactions and that bacteria could also form hydrogen bonds with these polymers. It is possible that the less hydrophobic nature of these aggregates results in lower levels of local osmolarities where water soluble nutrients can flow more freely within the structure, resulting in a boost in curli expression. Given that

we could control and increase overall biofilm quantity in both strains using our polymers, we decided to monitor their ability in the biocatalytic area. Cells were transformed with pSTB7, a plasmid that allows for the expression of the enzyme tryptophan synthase and incubated with polymers to stimulate biofilm expression. The biofilm mediated biotransformation of 5-fluoroindole to 5-fluorotryptophan was monitored and as expected, biocatalytic performance over 24h was linked to polymer induced biofilm levels with our moderately hydrophobic polymers generating around double the amount of product when compared to its respective naturally formed biofilm. These polymers also stimulated MC4100 cells to outperform their PHL644 naturally formed biofilm counterparts, hence opening up the possibility of using low biofilm forming strains in biofilm mediated biocatalysis. Unexpectedly however two most hydrophobic polymers (pAH-ANTH and pAH-PYRENE) had a detrimental effect on performance and it was show that this was at least in part due to a reduced metabolic activity of these biofilms, potentially due to polymer induced cell membrane disruption and a reduction in viability. Additionally, there could be limitations in the mass transfer of material through these tightly bound hydrophobic structures, limiting their performance. Hence for optimal performance in this biotransformation a balance needs to be formed between overall quantities of polymer induced biofilm (resulting in cell protection, continual regeneration of the tryptophan synthase and catalytic longevity) and metabolic activity/mass transfer of the system which is affected upon the use of highly hydrophobic polymers. Finally we also tested the ability of the esterase producing *E. coli* biofilms on the biocatalysis of 4-Nitrophenyldodecanoate to 4-Nitrophenol with data suggesting that the moderately hydrophobically functionalised polymers pAH-IVA, pAH-IND and pAH-Bn formed biofilm structures that were more resilient to the toxic reaction conditions, thereby optimising the reaction kinetics when compared

with naturally formed biofilms (the highly hydrophobic pAH-NAPTH, pAH-ANTH and pAH-PYRENE were not tested).

(v) Supplementary figures

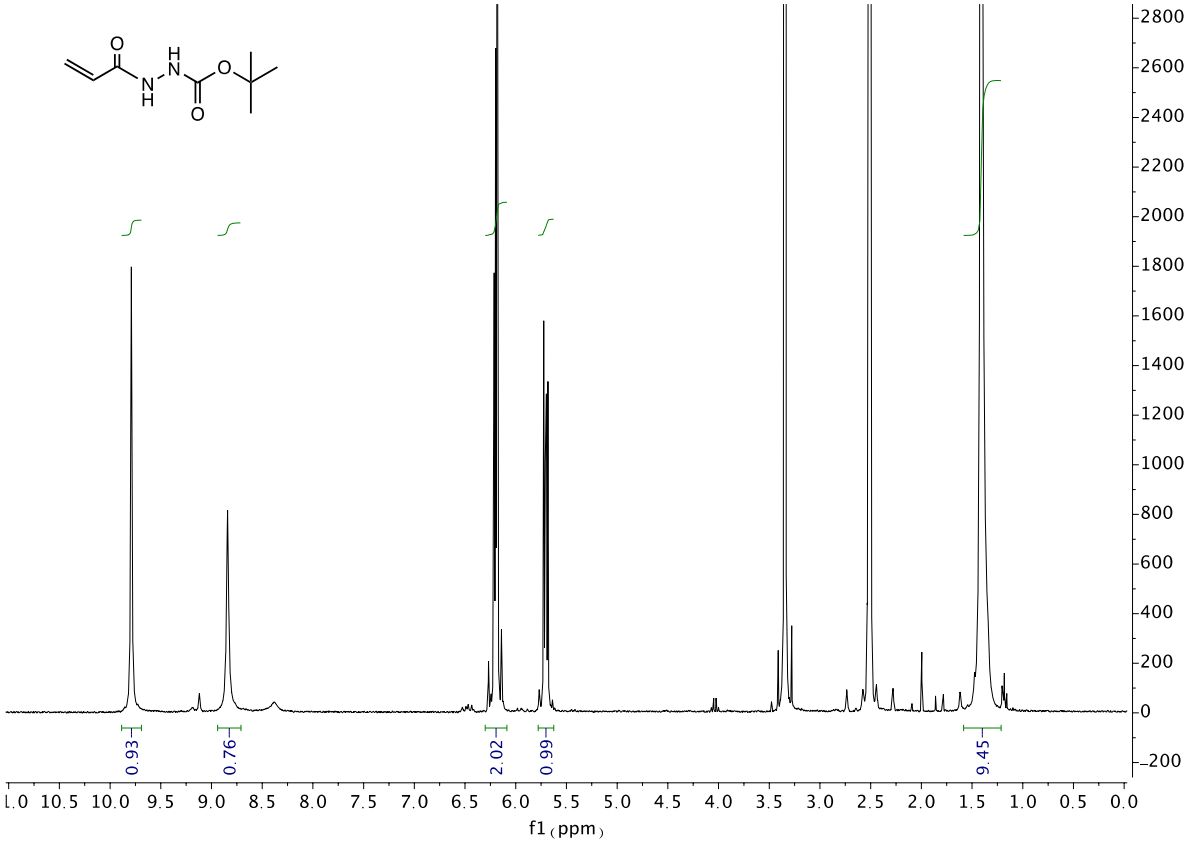

Figure S1: 1H-NMR of tert-butyl 2-acryloylhydrazinecarboxylate (Referred to in the text as 'Boc-acryloyl hydrazide')

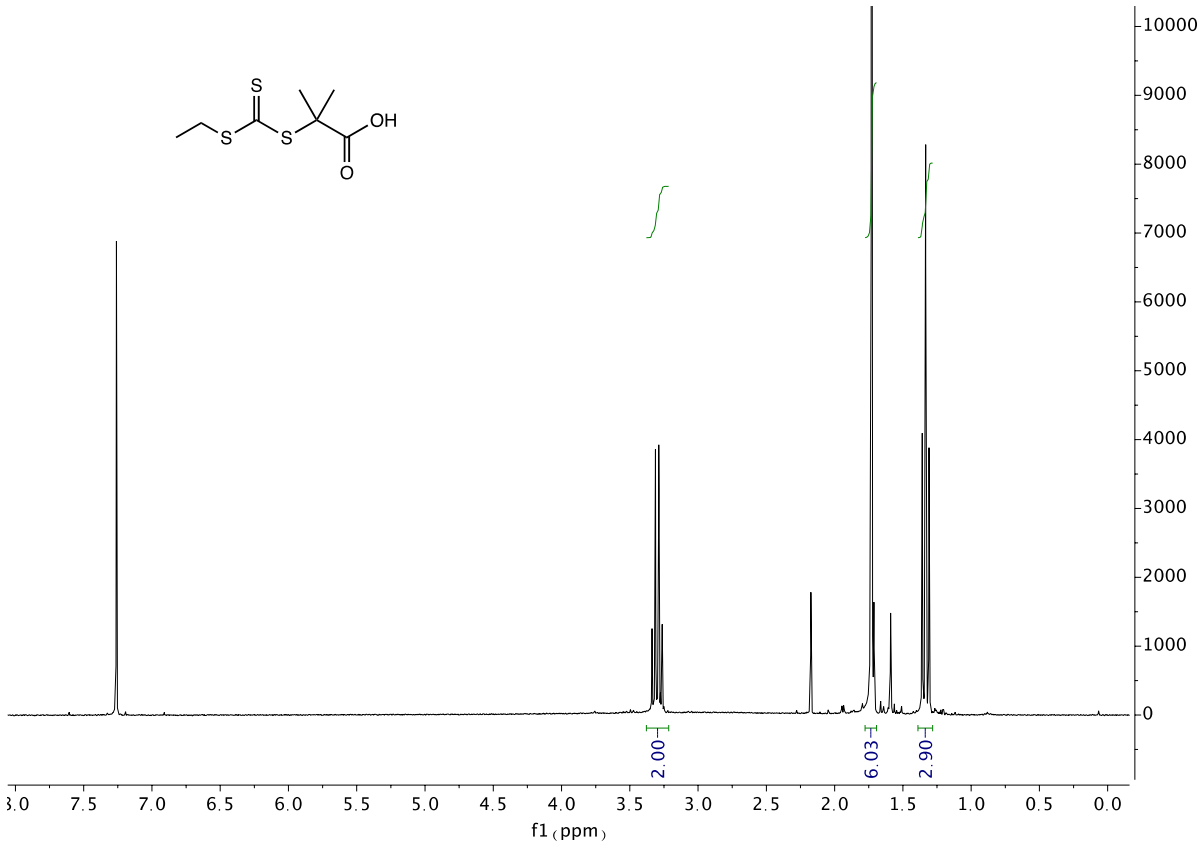

*Figure S2: [1]H NMR of 2-((Ethylthio)carbonothioyl)thio-2-methylpropanoic acid (**CTA**)*

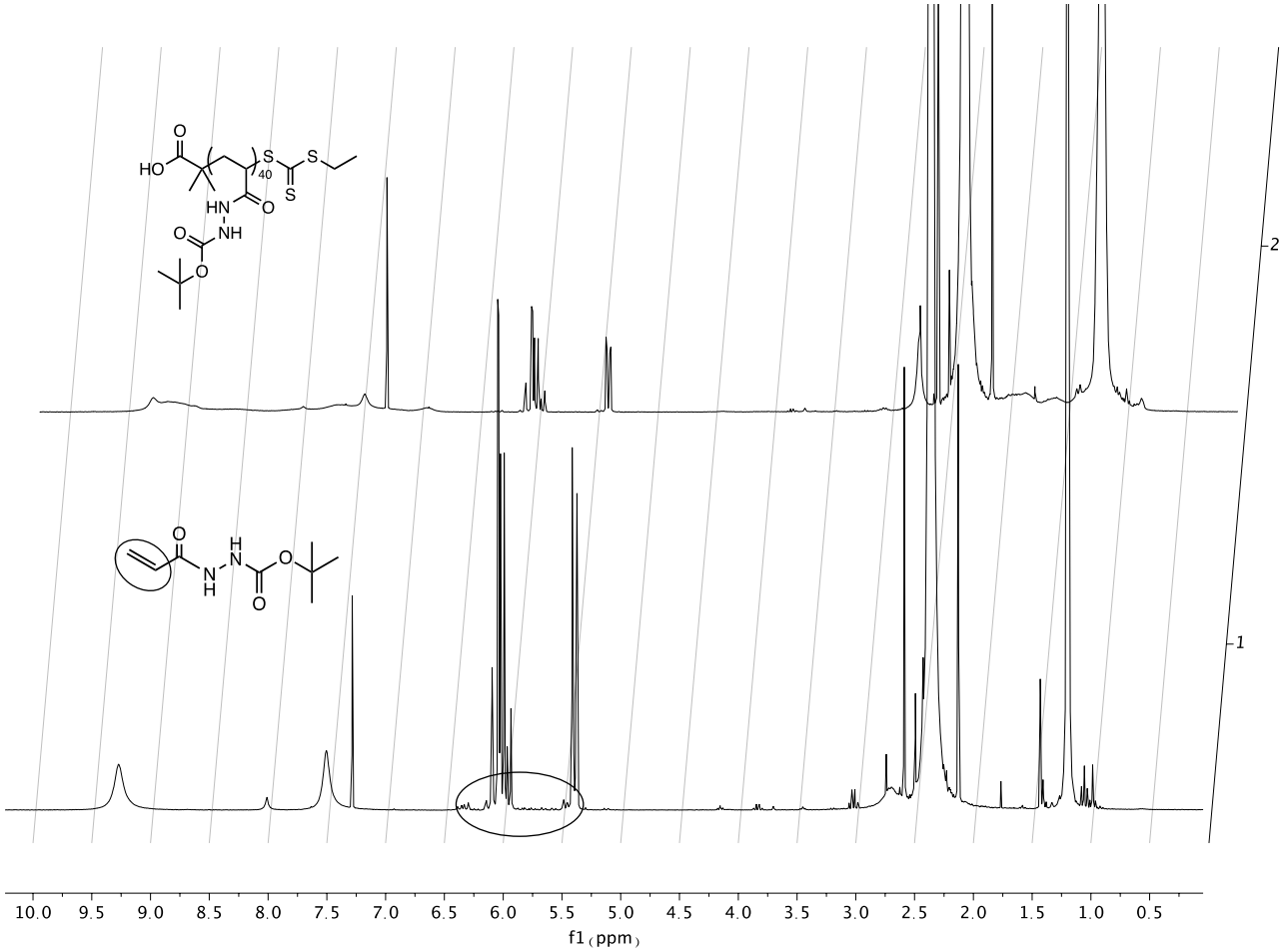

Figure S3: ^{1}H-NMR (top) of crude Boc-protected poly(acryloyl hydrazide) and (bottom) aliquot of boc-acryloyl hydrazide starting material before polymerisation. Monomer conversion into polymer was monitored by the decrease in intensity of the vinyl peaks of Boc-acryloyl hydrazide.

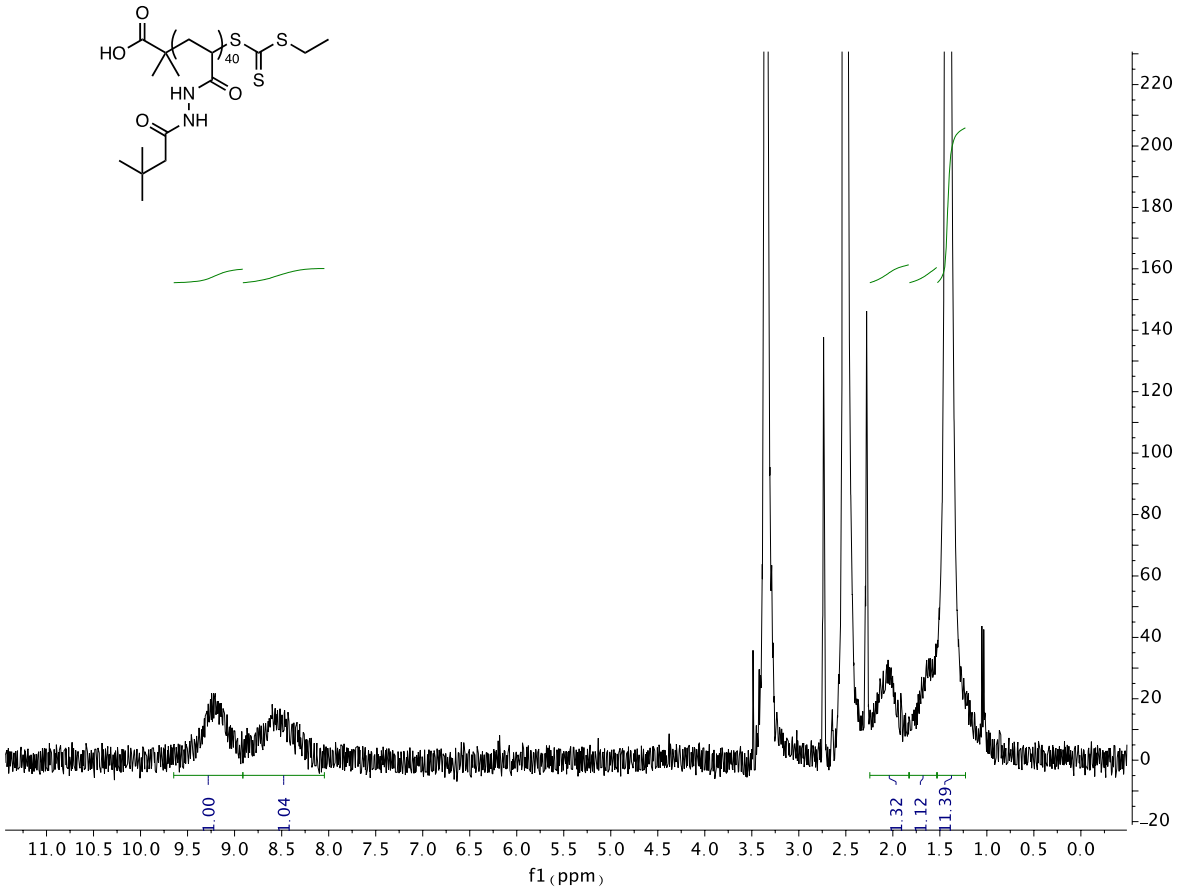

Figure S4: ^{1}H-NMR of purified Boc-protected poly(acryloyl hydrazide)

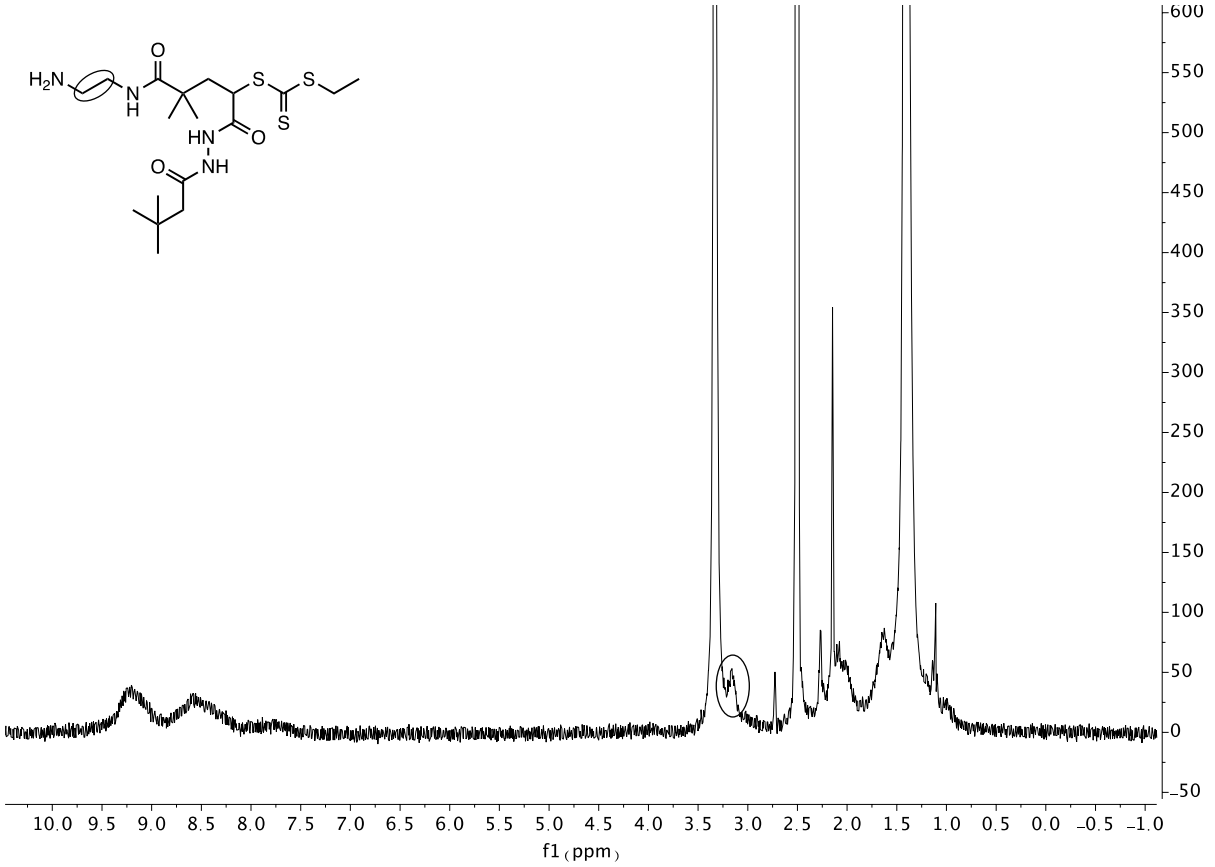

Figure S5: ^{1}H NMR of pure Boc-pAH-NH_2

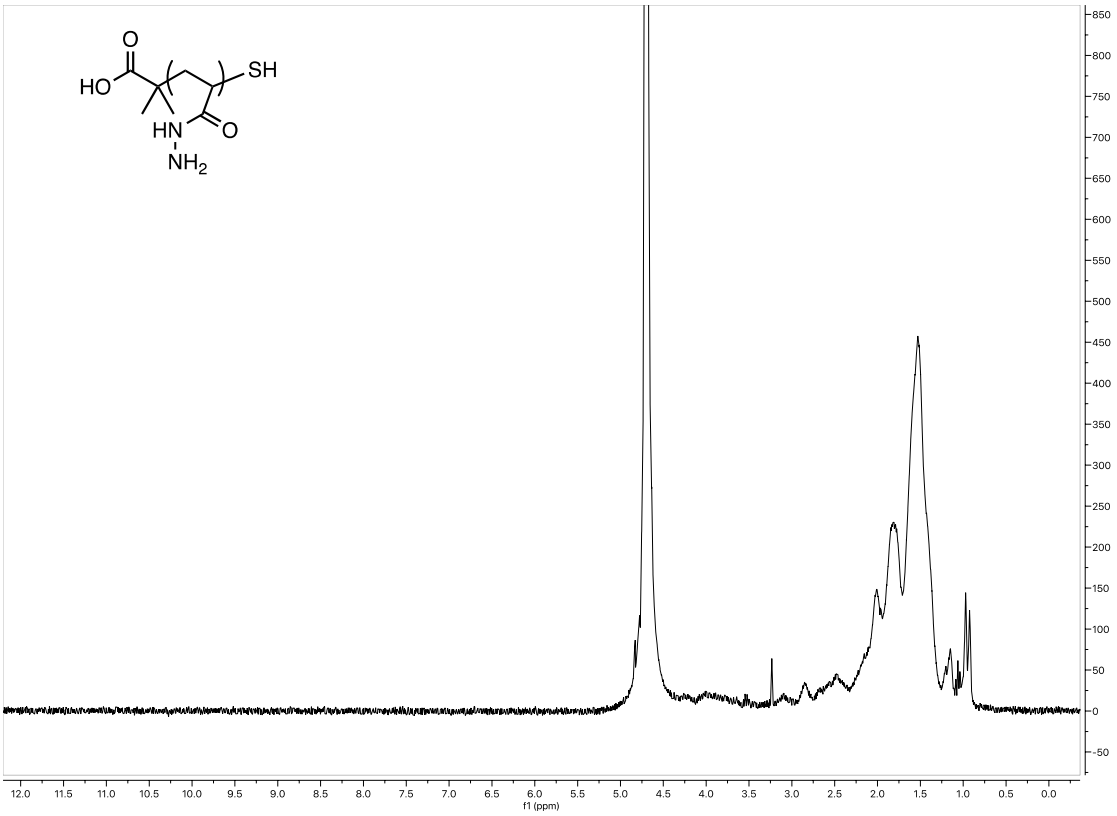

Figure S6: ^{1}H-NMR of purified poly(acryloyl hydrazide)

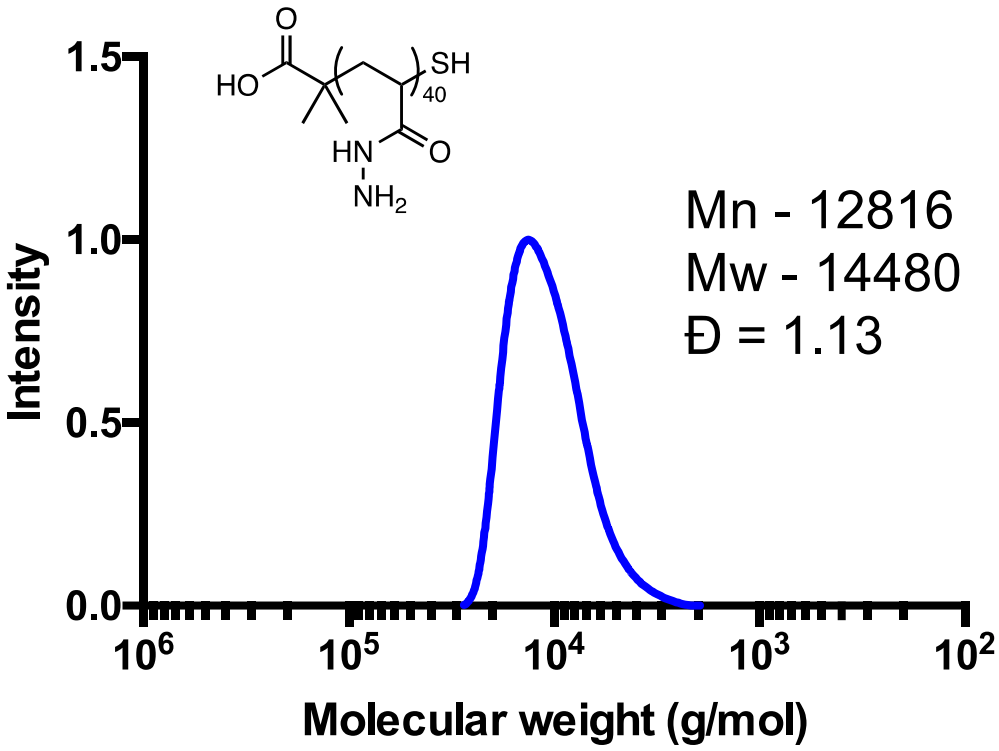

Figure S7: GPC trace of purified poly(acryloyl hydrazide)

Poly(acryloyl hydrazide) – aldehyde coupling H-NMR analysis to ascertain % functionalisations.

It must be noted that all polymer coupling reactions except pAH-2AFP and pAH-IMI were performed in 95% DMSO, 5% 100mM acetic acid. 2-Amino 3-formypyridine and Imidazole-4-carboxaldehyde couplings were performed in 100mM acetic acid due these two polymers not being soluble in DMSO.

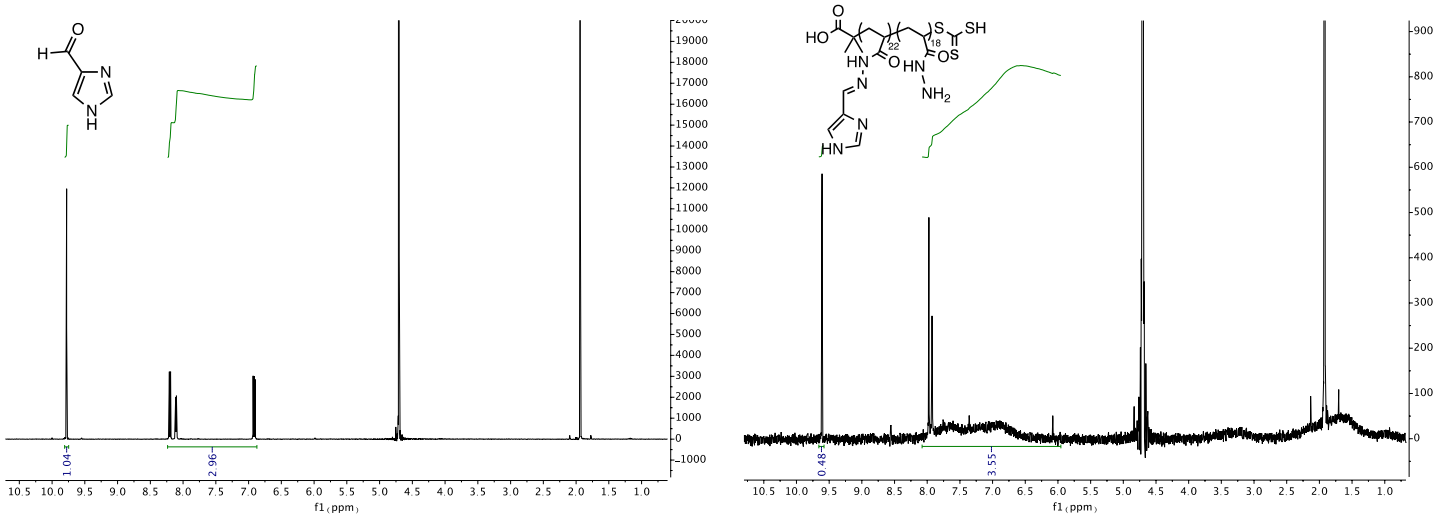

Figure S8: [1]H-NMRs of (left) Imidazole-4-carboxaldehyde before the coupling reaction, (right) pAH-IMI without further purification

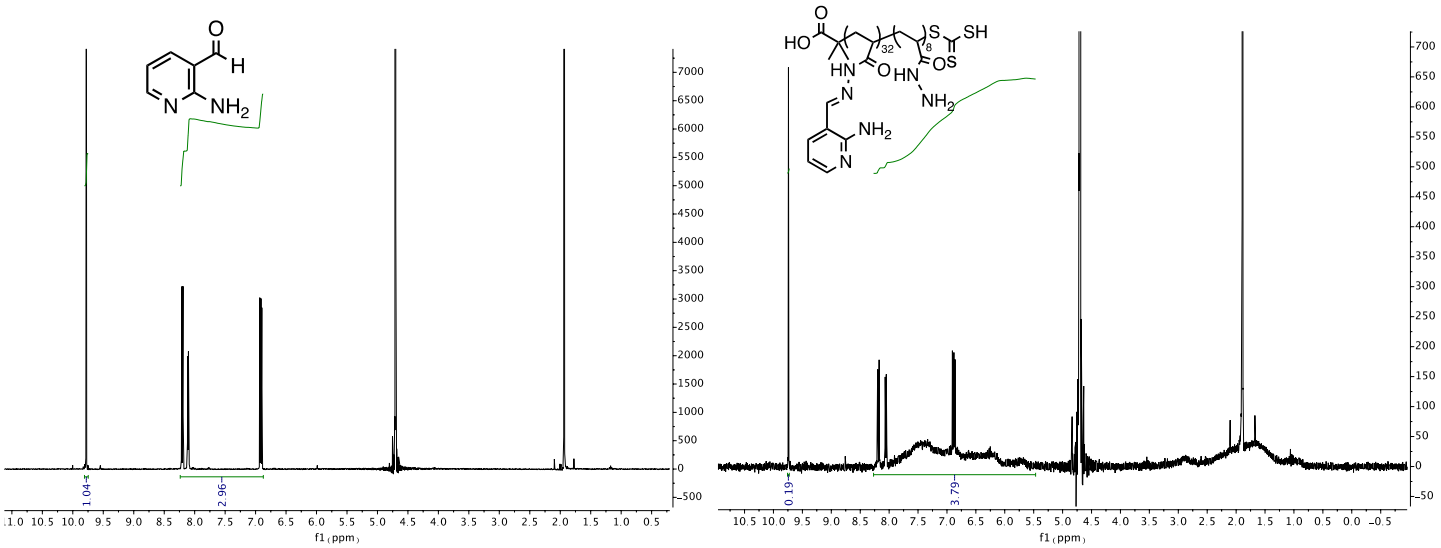

Figure S9: [1]H-NMRs of (left) 2-Amino 3-formylpyridine before the coupling reaction, (right) pAH-2AFP without further purification

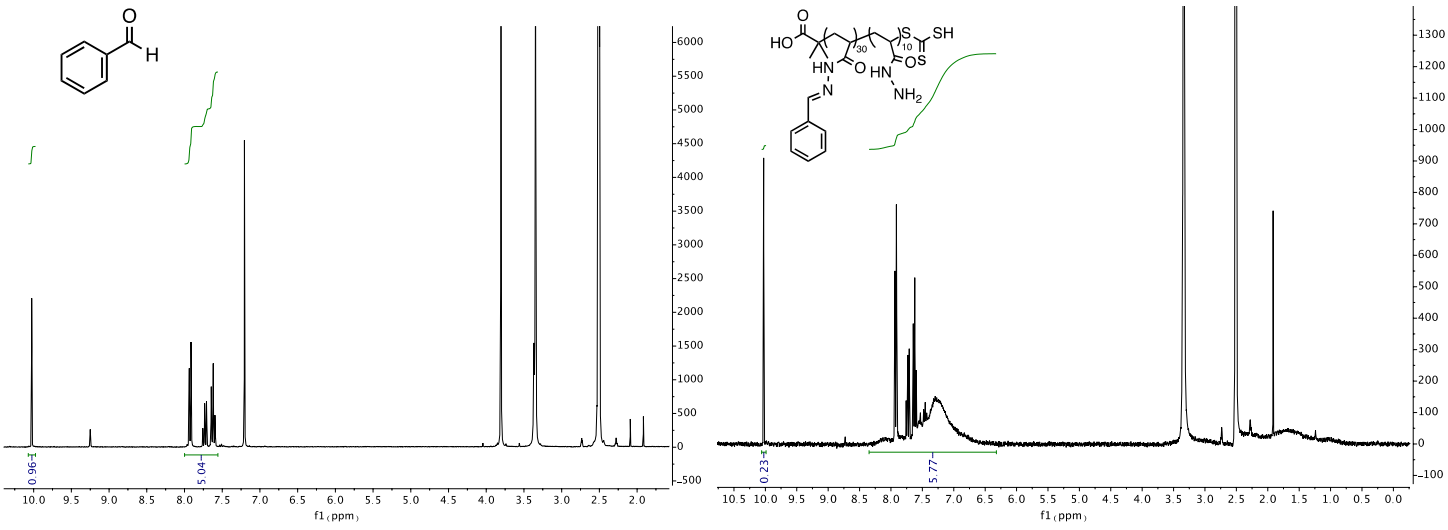

Figure S10: [1]H-NMRs of (left) Benzaldehyde before the coupling reaction, (right) pAH-Bn without further purification

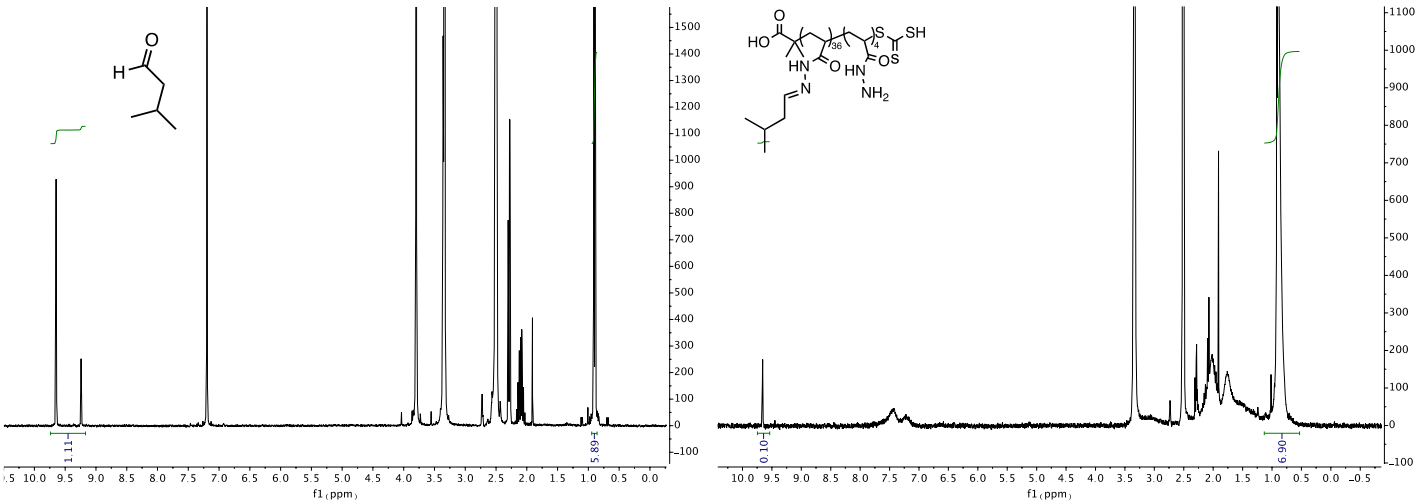

Figure S11: [1]H-NMRs of (left) Isovaleraldehyde before the coupling reaction, (right) pAH-IVA without further purification

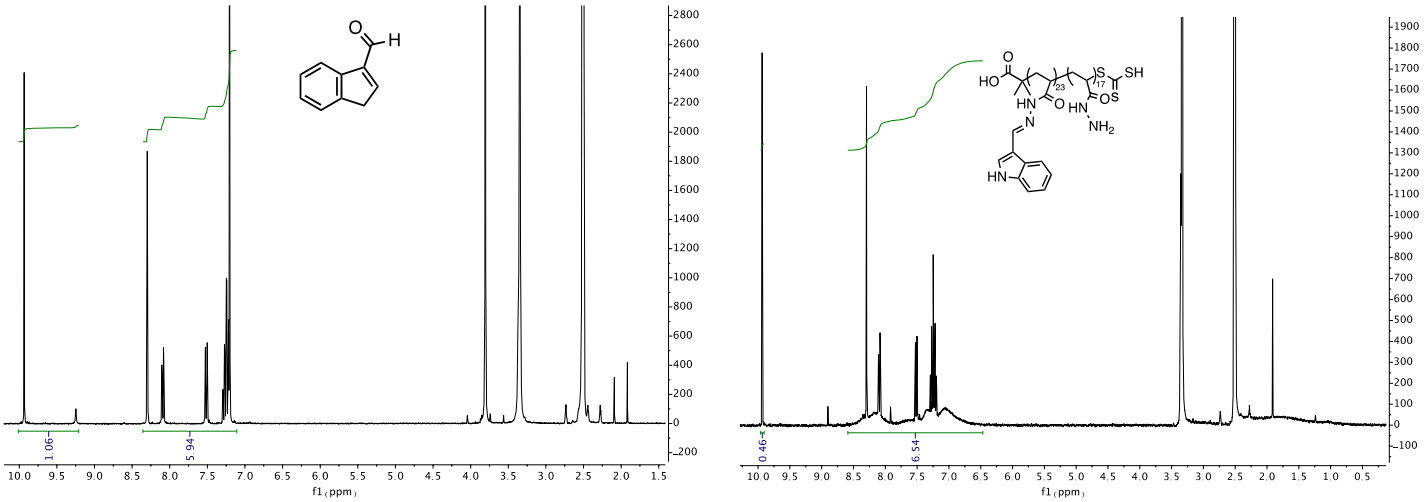

Figure S12: [1]H-NMRs of (left) Indole-3-carboxaldehyde before the coupling reaction, (right) pAH-IND without further purification

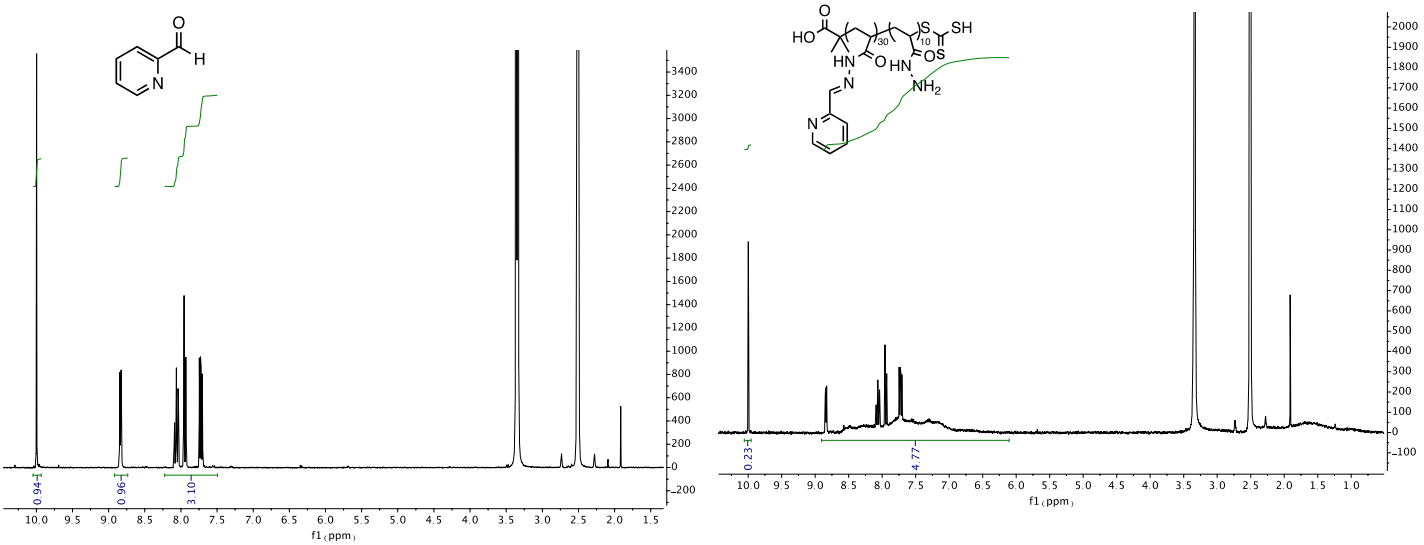

Figure S13: [1]H-NMRs of (left) Pyridine-2-carboxaldehyde before the coupling reaction, (right) pAH-PYRD without further purification

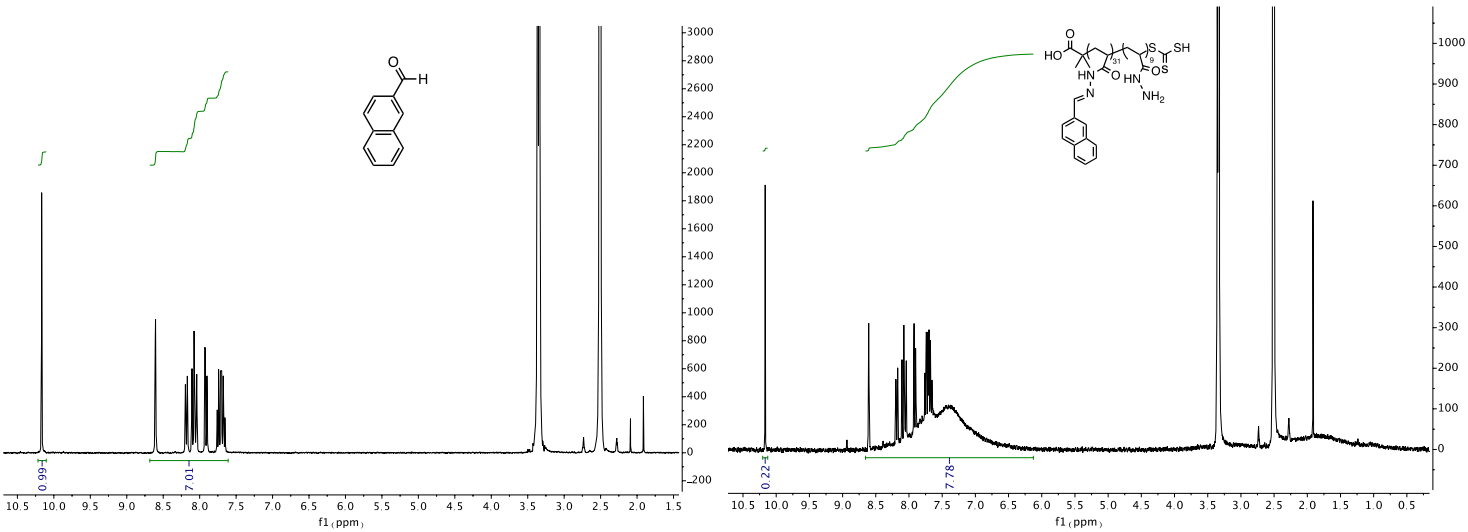

Figure S14: [1]H-NMRs of (left) 2-Napthaledehyde before the coupling reaction, (right) pAH-NAPTH without further purification

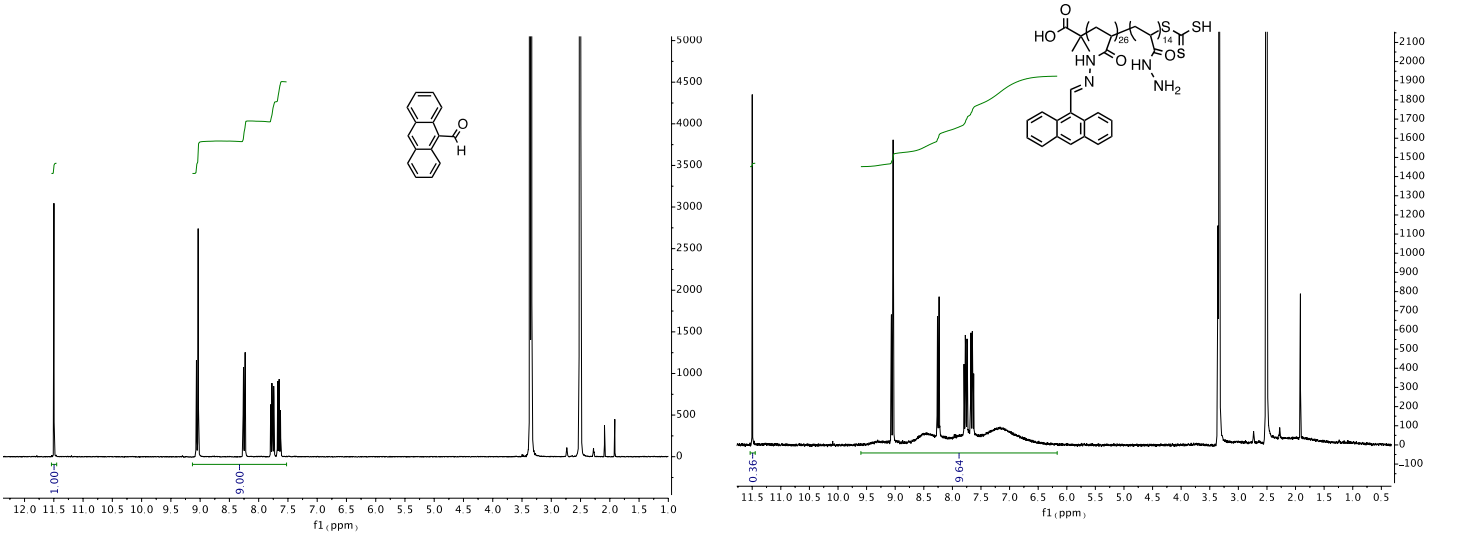

Figure S15: [1]H-NMRs of (left) 9-Anthraledehyde before the coupling reaction, (right) pAH-ANH without further purification

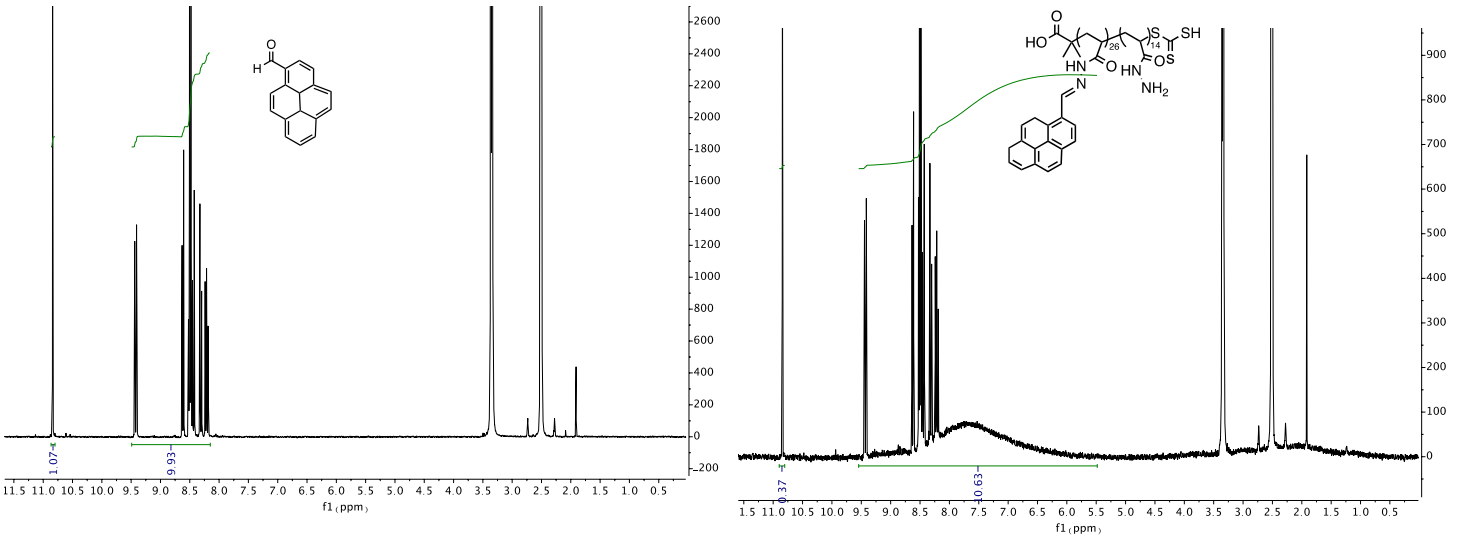

Figure S16: [1]H-NMRs of (left) 9-Anthraledehyde before the coupling reaction, (right) pAH-ANH without further purification

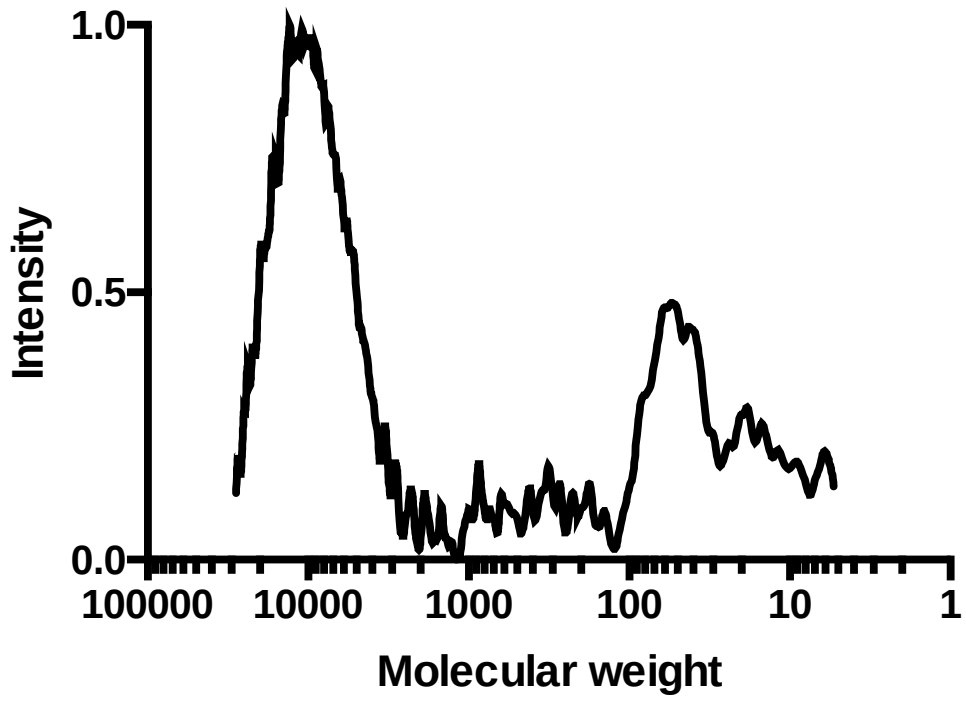

Figure S17: GPC trace (UV-402 nm) of MCCA-pAH-2AFP.

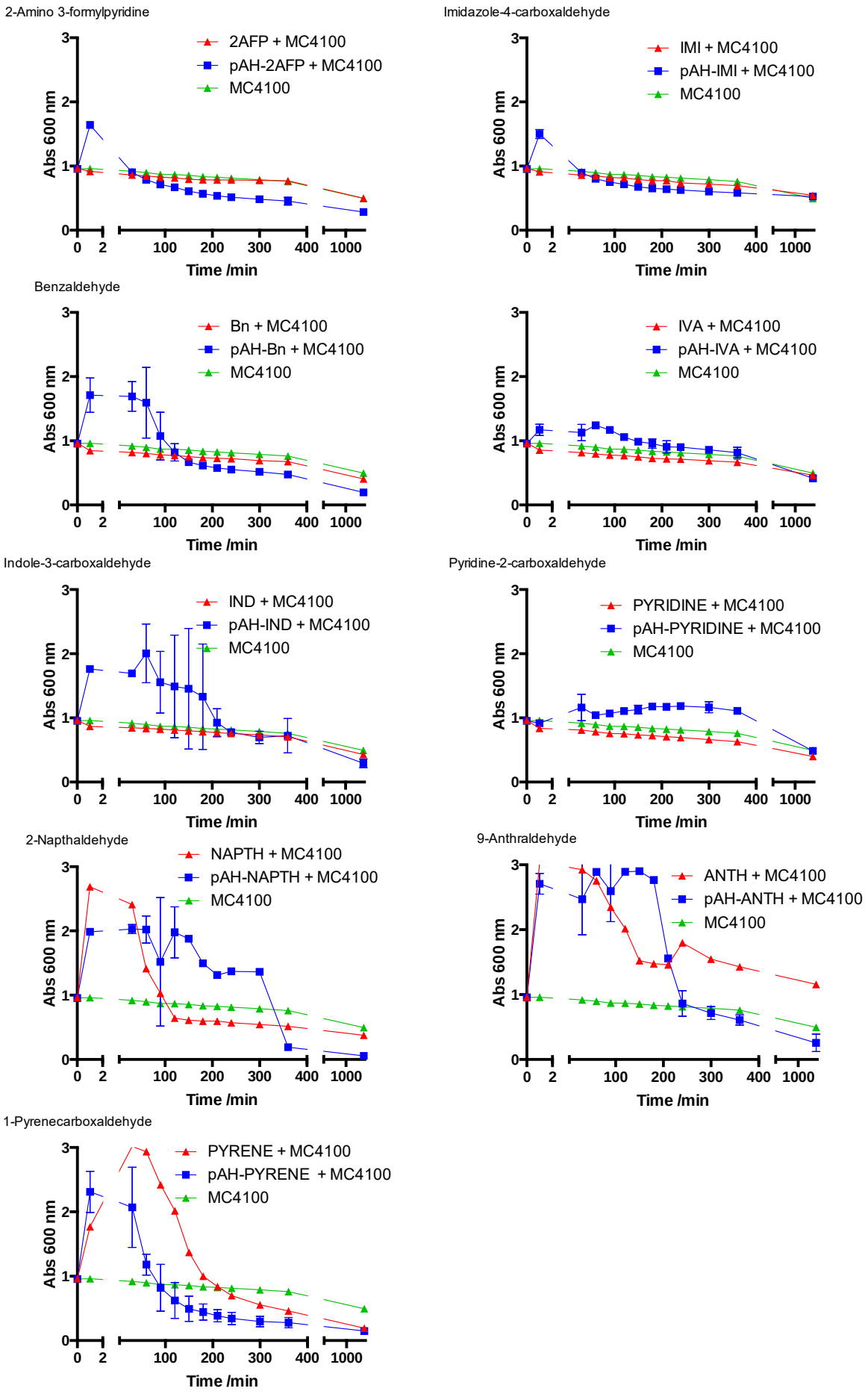

Figure S18: Spectrophotometric assay to monitor aldehyde induced MC4100 aggregation (red traces) in comparison with the respective polymer induced MC4100 aggregates (blue traces), and MC4100 without the addition of polymer (green traces)

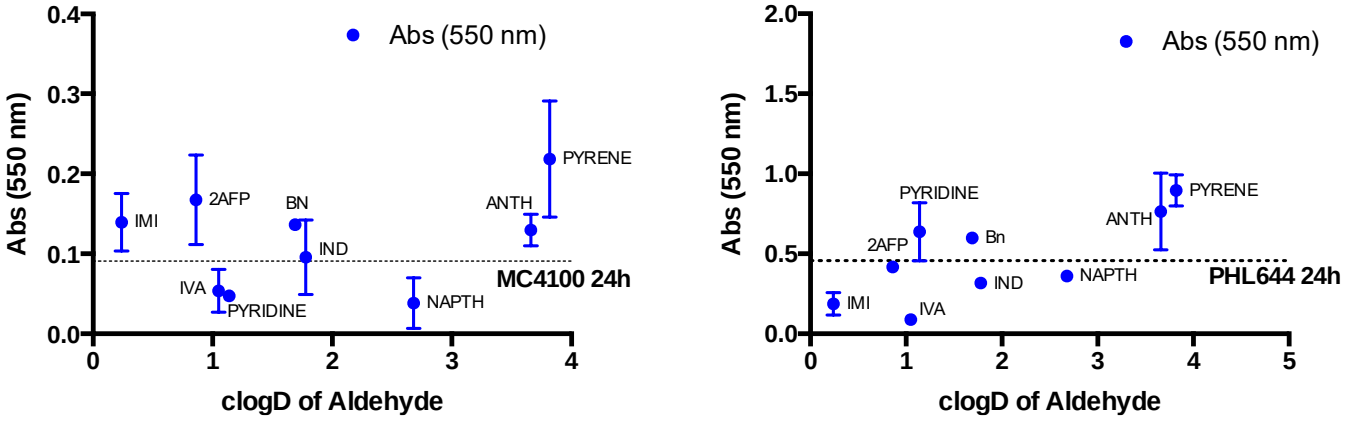

Figure S19: Abs_{550} of MC4100 (left) and PHL644 (right): samples incubated with aldehydes for 24h correlated to aldehyde clogD. Dotted line shows A_{550} of no aldehyde control for each strain. Note the different y axis scale for each strain.

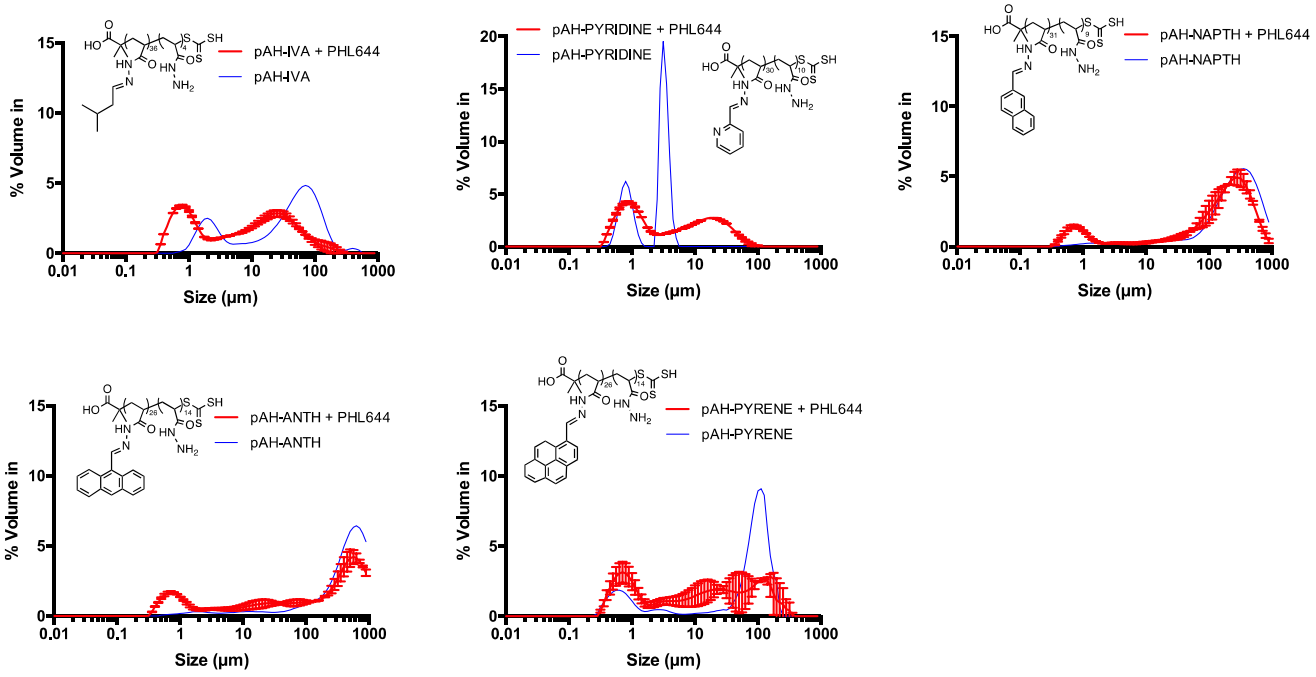

Figure S20: 24h Polymer induced PHL644 aggregate/biofilm size distributions, along with polymer size distributions (blue lines)

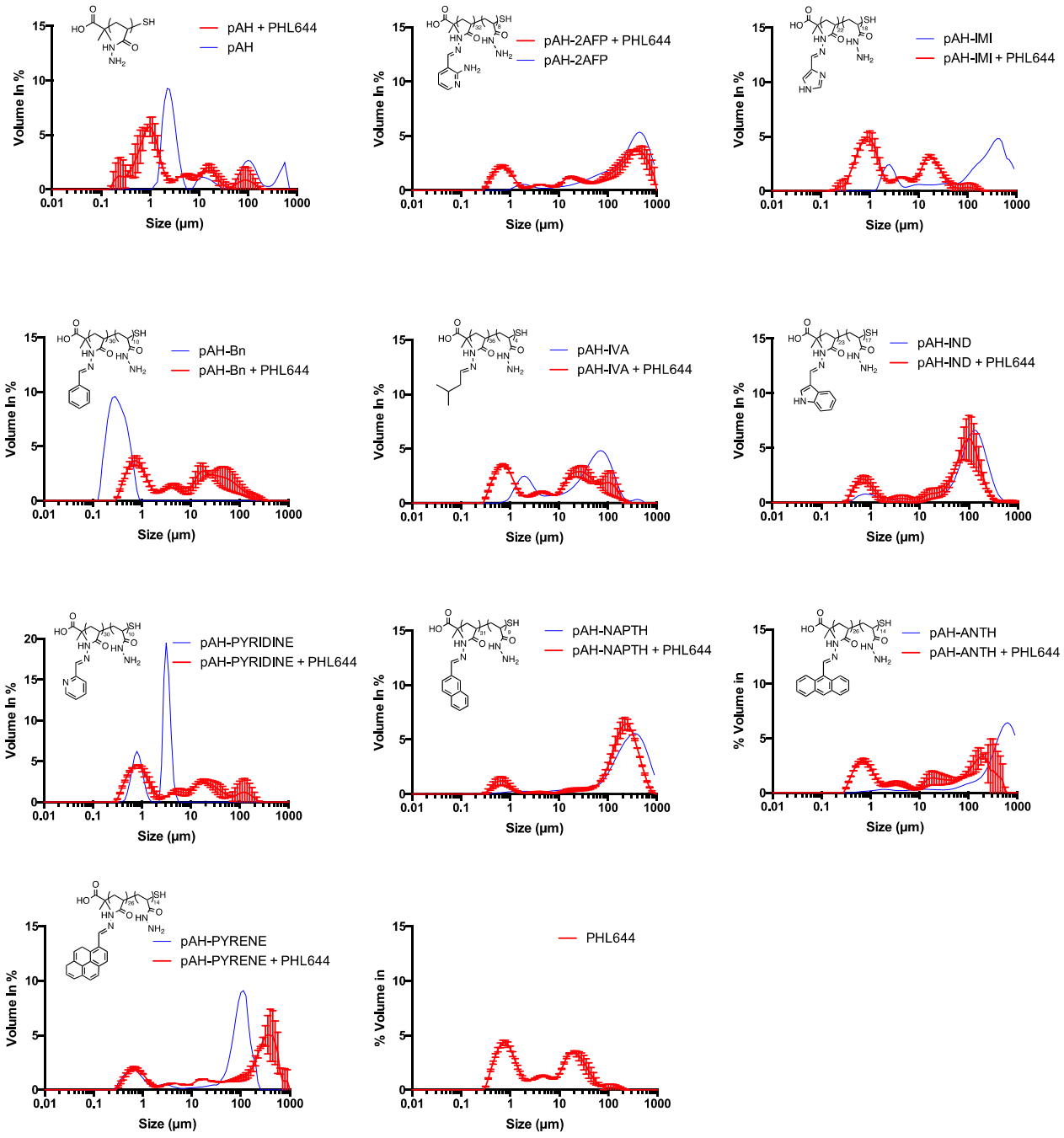

Figure S21: 48h polymer induced PHL644 aggregate/biofilm size distributions along with polymer size distributions

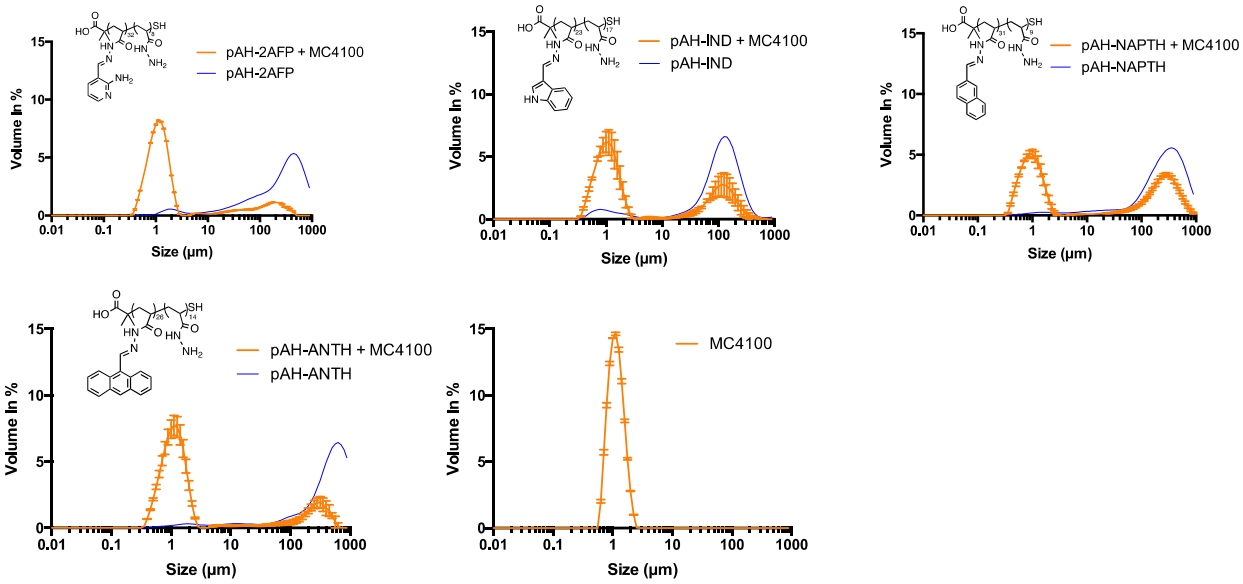

Figure S22: 24h polymer induced MC4100 aggregate/biofilm size distributions, along with polymer size distributions. All other polymer induced MC4100 aggregates were not broken up inside the dispersion chamber, resulting in a distribution identical to the MC4100 control without the addition of polymer

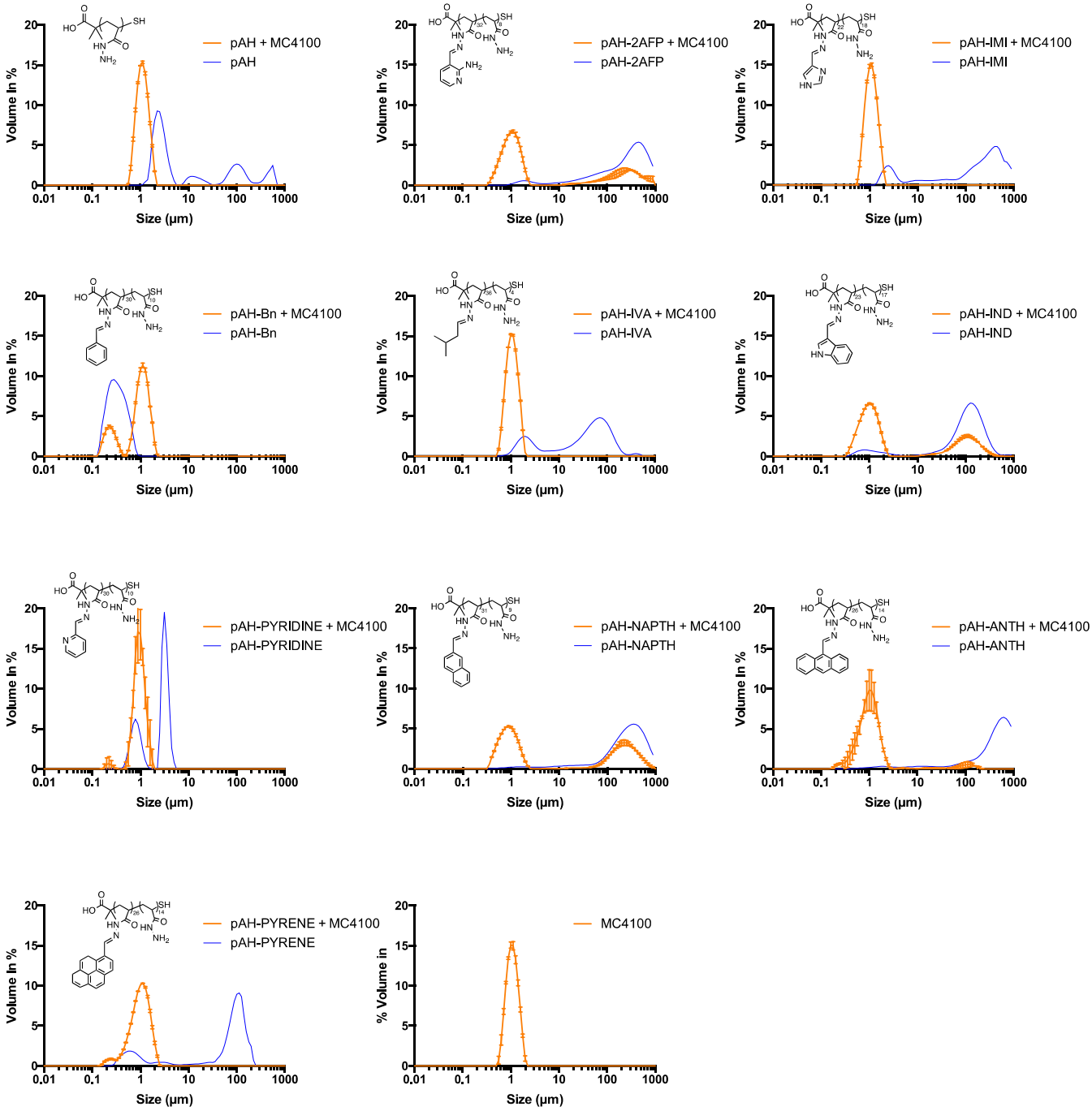

Figure S23: 48h polymer induced MC4100 aggregate/biofilm size distributions, along with polymer size distributions.

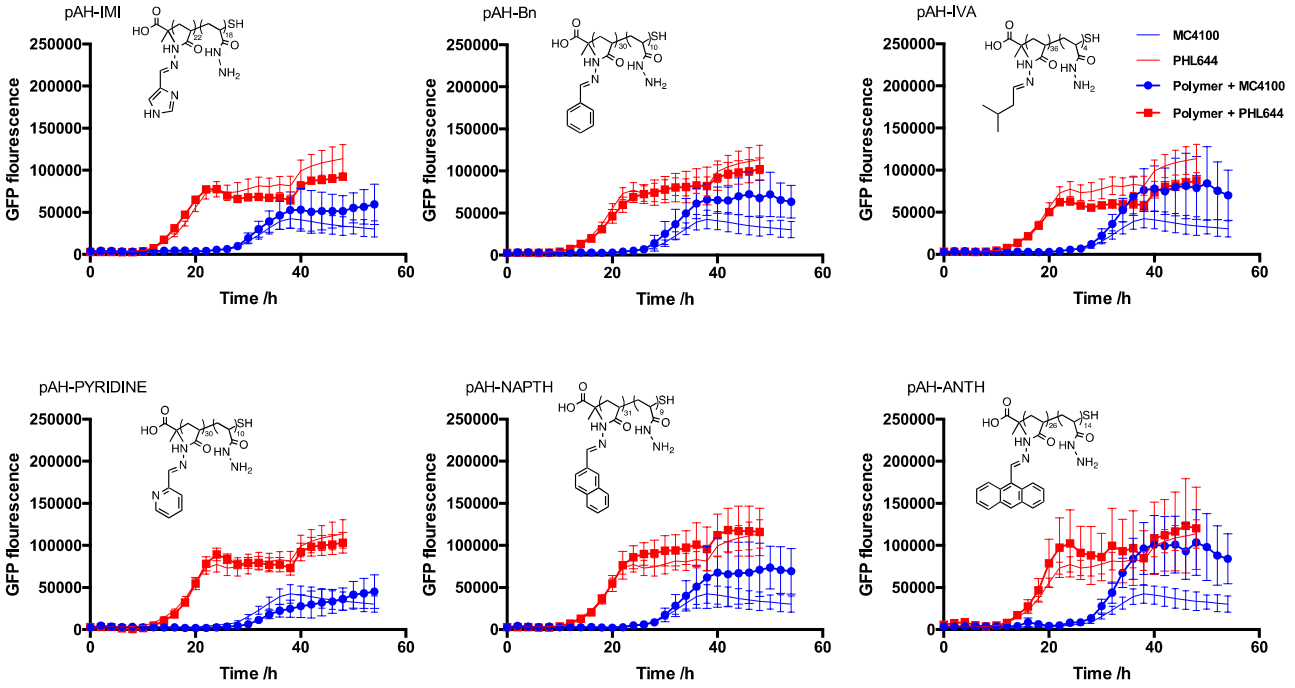

Figure S24: Expression of curli over 48h for polymer induced MC4100 (blue) and PHL644 (red) biofilms, compared with natural expression of curli in MC4100 and PHL644

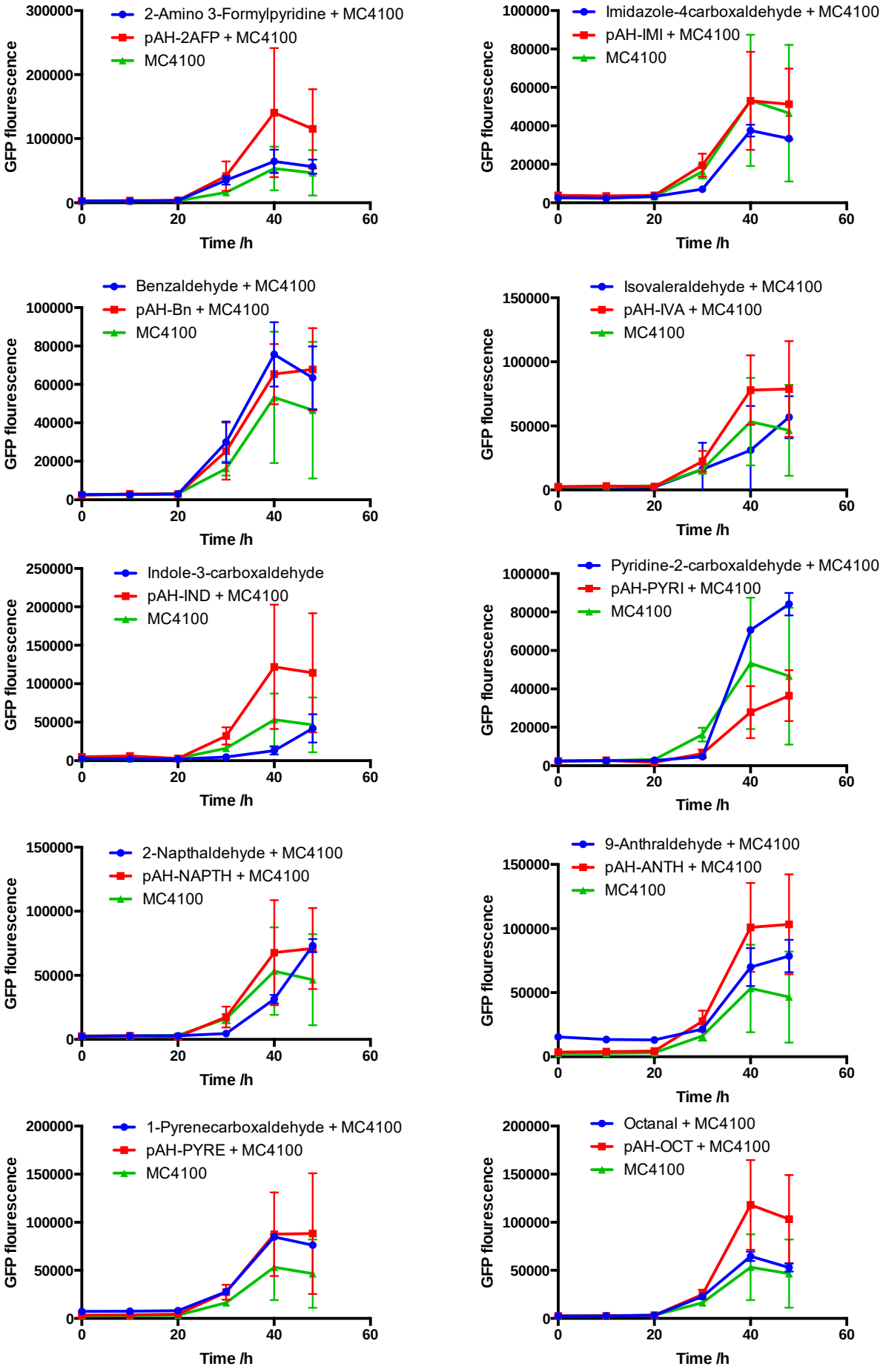

Figure S25: Rate of expression of curli over 48h for MC4100 + Aldehyde suspensions, compared with polymer induced MC4100 and MC4100 alone

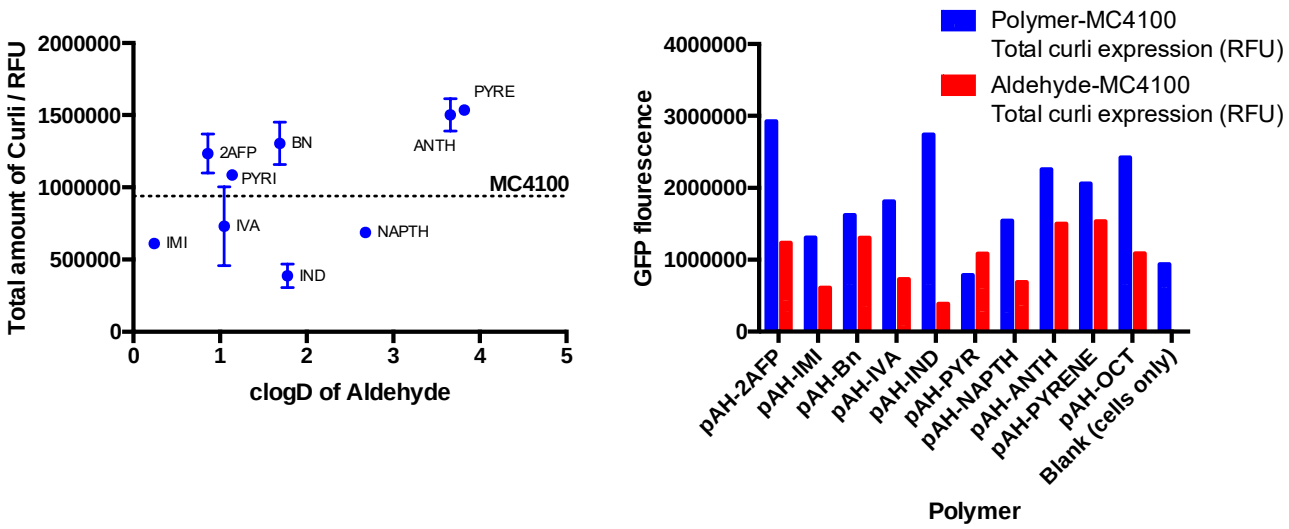

Figure S26: Total curli expression in MC4100 + Aldehyde suspensions over 48h (left) and comparison of total aldehyde induced curli expression over 48h with polymer induced MC4100

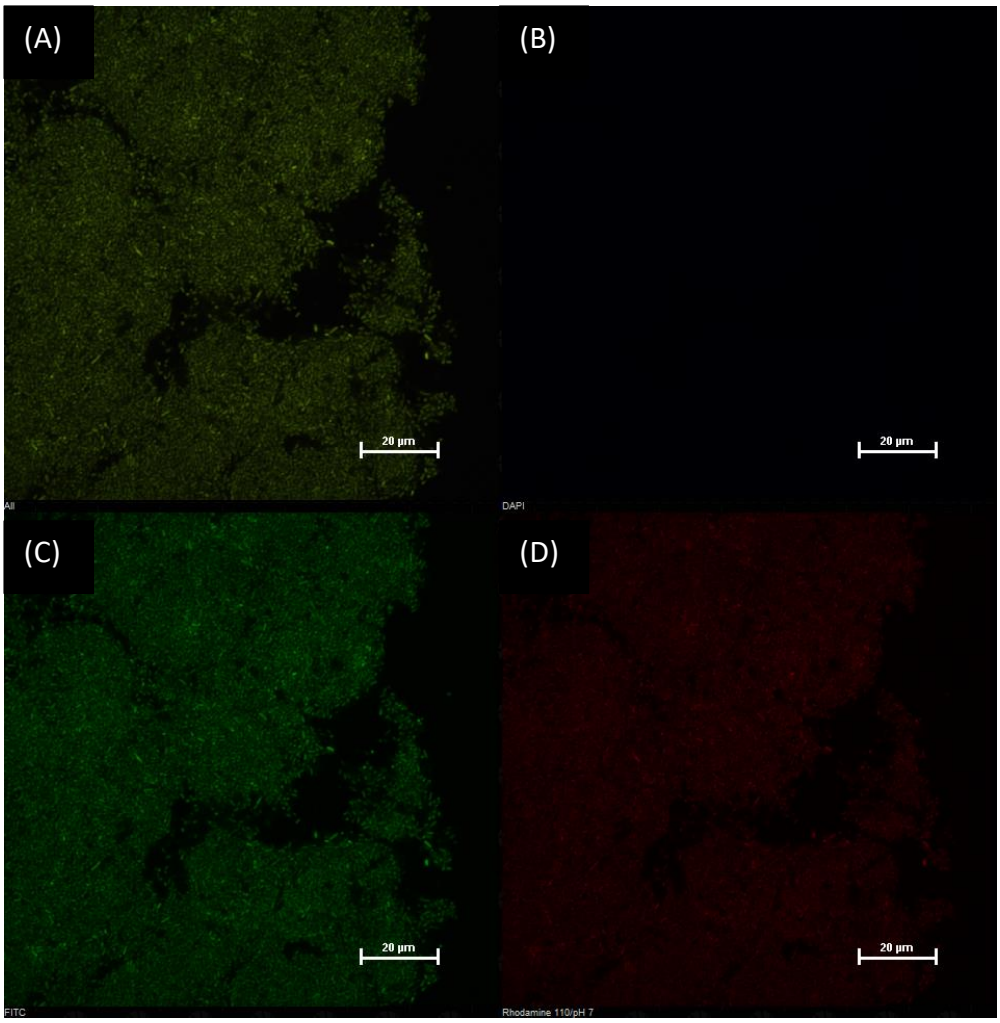

Figure S27: Confocal image (40X) of naturally formed biofilms without the addition of polymer. (A) Merged image of E. coli aggregate/biofilm expressing GFP and stained with red fluorescent wheat germ agglutinin. (B-D) Individual images for blue, green and red channels

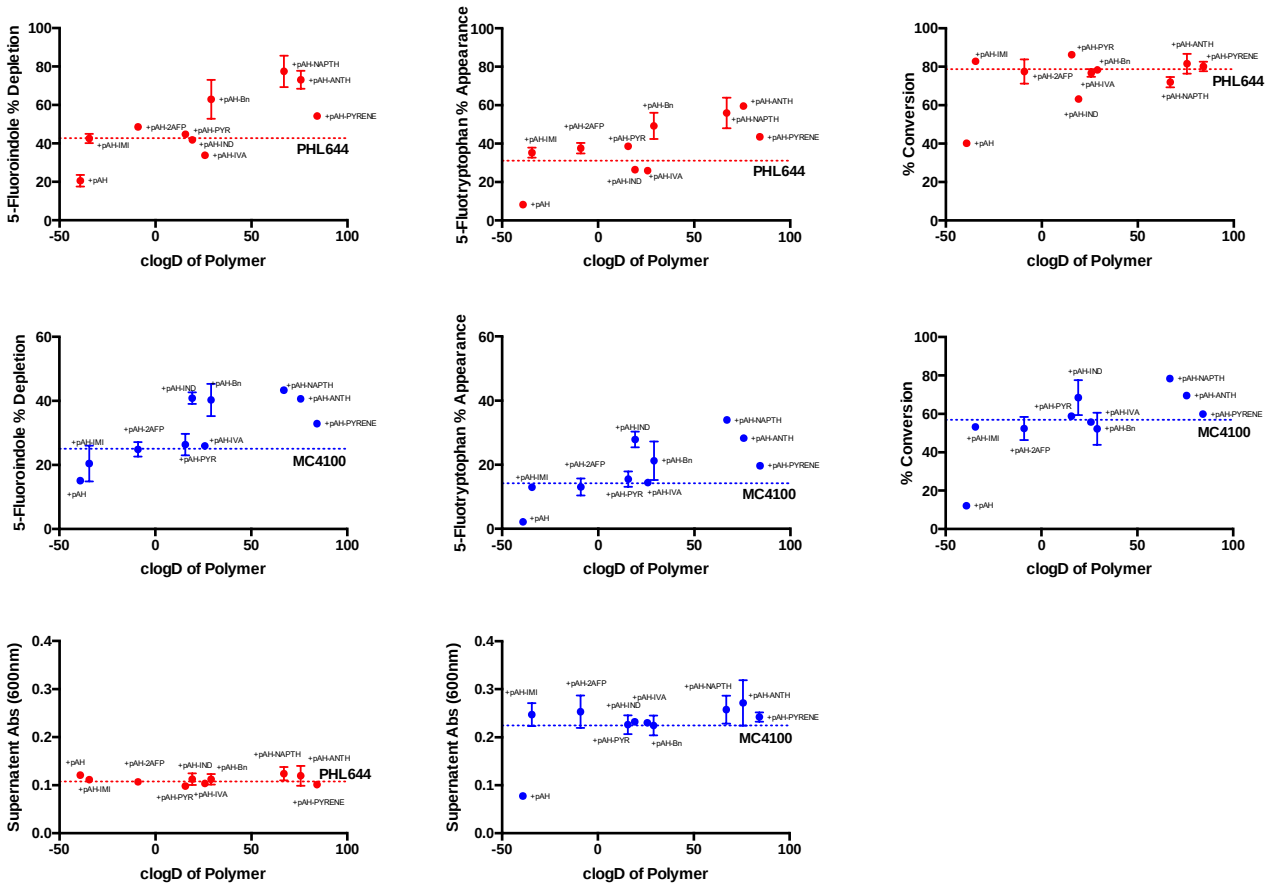

Figure S28: Biotransformation data for 48h polymer-induced PHL644 and MC4100 biofilms.

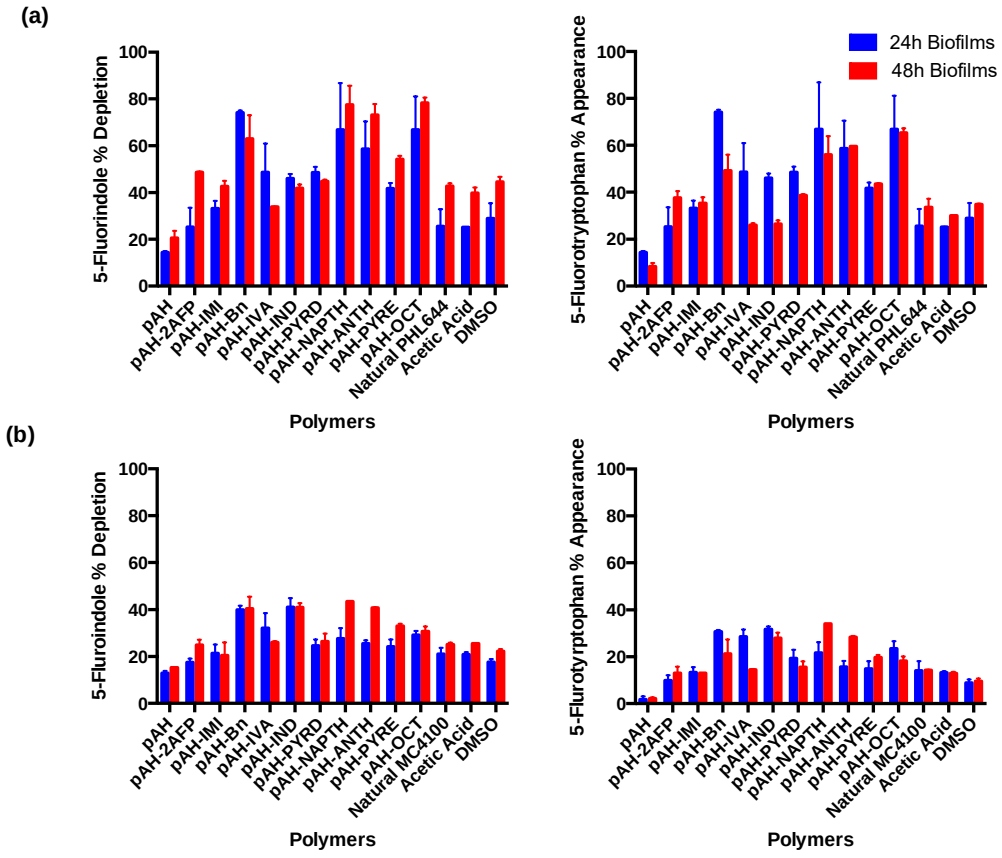

Figure S29: Comparison of biocatalytic activity of respective 24h and 48h polymer induced (a) PHL644 biofilms, (b) MC4100 biofilms

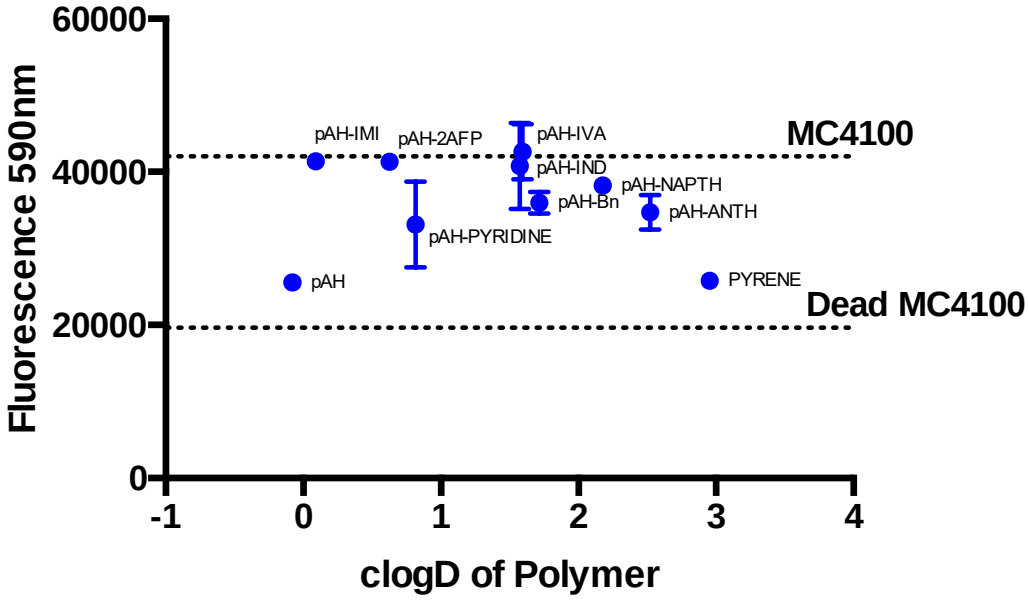

Figure S30: Metabolic activity of 48h polymer induced biofilms, measured using the resazurin probe

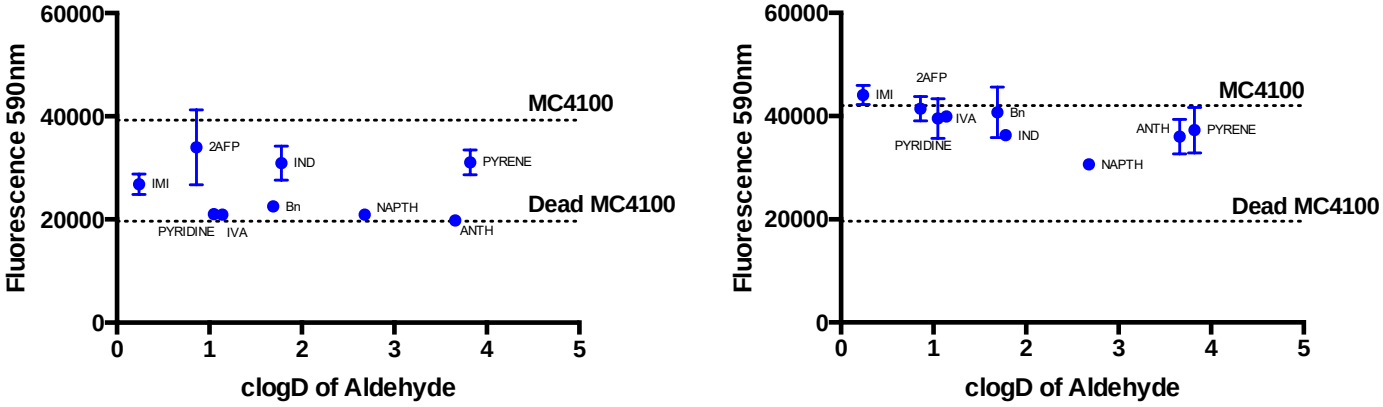

Figure S31: Metabolic activity of (left) 24h and (right) 48h aldehyde + MC4100 suspensions

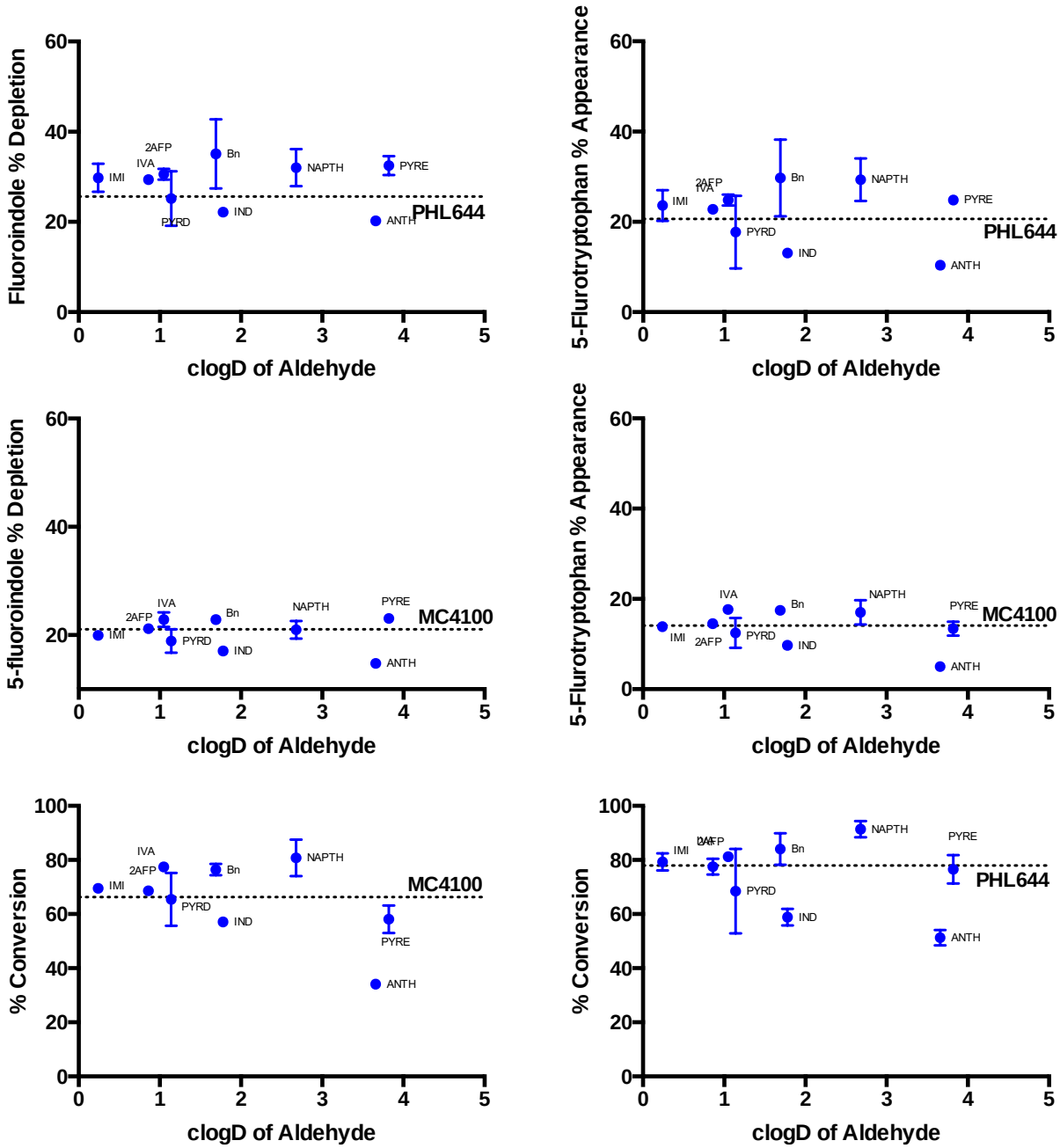

Figure 32: Biotransformation data for 24h aldehyde + PHL644 and MC4100 suspensions respectively

Figure S33: Time course showing increase of mobile phase (methanol) over time for HPLC analysis

Time (min)	% Methanol
0-0.5	10
0.5-12.5	10-90
12.5-15	90
15-16	90-10
16-21	10

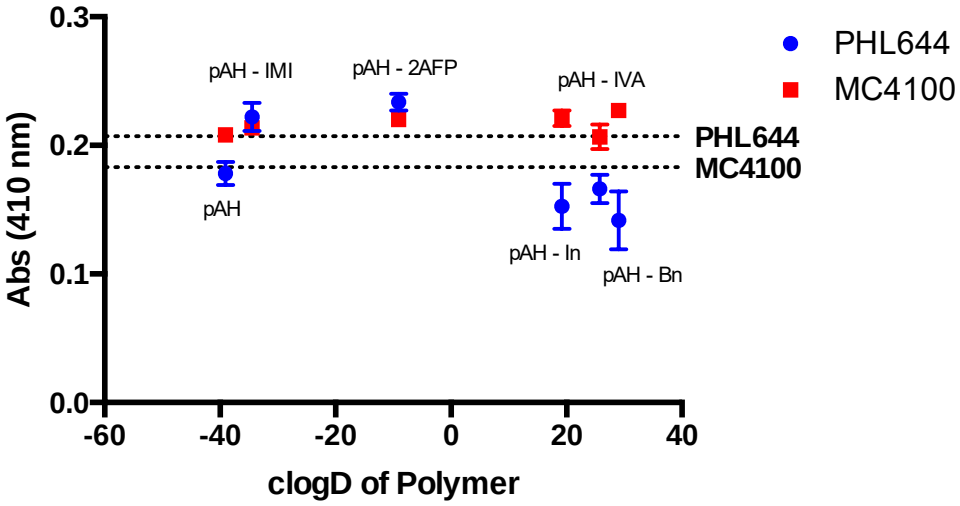

Figure S34: Relative amounts of UV_{400} active 4-Nitrophenol produced after 144h by polymer induced biofilms in less challenged conditions

(vi) References

1. Zobell CE. The Effect of Solid Surfaces upon Bacterial Activity. *J Bacteriol*. 1943.
2. Tuson HH, Weibel DB. Bacteria-surface interactions. *Soft Matter*. 2013. doi:10.1039/c3sm27705d
3. Banerjee I, Pangule RC, Kane RS. Antifouling coatings: Recent developments in the design of surfaces that prevent fouling by proteins, bacteria, and marine organisms. *Adv Mater*. 2011. doi:10.1002/adma.201001215
4. Tsoligkas AN, Winn M, Bowen J, Overton TW, Simmons MJH, Goss RJM. Engineering Biofilms for Biocatalysis. *ChemBioChem*. 2011. doi:10.1002/cbic.201100200
5. Galié S, García-Gutiérrez C, Miguélez EM, Villar CJ, Lombó F. Biofilms in the food industry: Health aspects and control methods. *Front Microbiol*. 2018. doi:10.3389/fmicb.2018.00898
6. Bryers JD. Medical biofilms. *Biotechnol Bioeng*. 2008. doi:10.1002/bit.21838
7. Flemming HC, Wingender J, Szewzyk U, Steinberg P, Rice SA, Kjelleberg S. Biofilms: An emergent form of bacterial life. *Nat Rev Microbiol*. 2016. doi:10.1038/nrmicro.2016.94
8. Karande R, Halan B, Schmid A, Buehler K. Segmented flow is controlling growth of catalytic biofilms in continuous multiphase microreactors. *Biotechnol Bioeng*. 2014. doi:10.1002/bit.25256
9. Schmutzler K, Kupitz K, Schmid A, Buehler K. Hyperadherence of Pseudomonas taiwanensis VLB120ΔC increases productivity of (S)-styrene oxide formation. *Microb Biotechnol*. 2017. doi:10.1111/1751-7915.12378
10. Li XZ, Webb JS, Kjelleberg S, Rosche B. Enhanced benzaldehyde tolerance in

Zymomonas mobilis biofilms and the potential of biofilm applications in fine-chemical production. *Appl Environ Microbiol*. 2006. doi:10.1128/AEM.72.2.1639-1644.2006

11. Murphy CD, Casey E. Biofilm-catalysed transformation of organofluorine compounds. *Chim Oggi/Chemistry Today*. 2013.

12. Hu Y, Liu X, Ren ATM, Gu JD, Cao B. Optogenetic Modulation of a Catalytic Biofilm for the Biotransformation of Indole into Tryptophan. *ChemSusChem*. 2019. doi:10.1002/cssc.201902413

13. Perni S, Hackett L, Goss RJM, Simmons MJ, Overton TW. Optimisation of engineered Escherichia coli biofilms for enzymatic biosynthesis of L-halotryptophans. *AMB Express*. 2013. doi:10.1186/2191-0855-3-66

14. Tong X, Barberi TT, Botting CH, et al. Rapid enzyme regeneration results in the striking catalytic longevity of an engineered, single species, biocatalytic biofilm. *Microb Cell Fact*. 2016. doi:10.1186/s12934-016-0579-3

15. Wood TL, Guha R, Tang L, Geitner M, Kumar M, Wood TK. Living biofouling-resistant membranes as a model for the beneficial use of engineered biofilms. *Proc Natl Acad Sci U S A*. 2016. doi:10.1073/pnas.1521731113

16. Perez-Soto N, Moule L, Crisan DN, et al. Engineering microbial physiology with synthetic polymers: Cationic polymers induce biofilm formation in: Vibrio cholerae and downregulate the expression of virulence genes. *Chem Sci*. 2017. doi:10.1039/c7sc00615b

17. Perez-Soto N, Creese O, Fernandez-Trillo F, Krachler AM. Aggregation of Vibrio cholerae by Cationic Polymers Enhances Quorum Sensing but Overrides Biofilm Dissipation in Response to Autoinduction. *ACS Chem Biol*. 2018. doi:10.1021/acschembio.8b00815

18. Crisan DN, Creese O, Ball R, et al. Poly(acryloyl hydrazide), a versatile scaffold for the preparation of functional polymers: Synthesis and post-polymerisation modification. *Polym Chem*. 2017. doi:10.1039/c7py00535k

19. Baeshen MN, Al-Hejin AM, Bora RS, et al. Production of biopharmaceuticals in E. Coli: Current scenario and future perspectives. *J Microbiol Biotechnol*. 2015. doi:10.4014/jmb.1412.12079

20. Barnhart MM, Chapman MR. Curli Biogenesis and Function. *Annu Rev Microbiol*. 2006. doi:10.1146/annurev.micro.60.080805.142106

21. Vidal O, Longin R, Prigent-Combaret C, Dorel C, Hooreman M, Lejeune P. Isolation of an Escherichia coli K-12 mutant strain able to form biofilms on inert surfaces: Involvement of a new ompR allele that increases curli expression. *J Bacteriol*. 1998.

22. Meinders JM, van der Mei HC, Busscher HJ. Deposition Efficiency and Reversibility of Bacterial Adhesion under Flow. *J Colloid Interface Sci*. 1995. doi:10.1006/jcis.1995.9960

23. May KL, Grabowicz M. The bacterial outer membrane is an evolving antibiotic barrier. *Proc Natl Acad Sci U S A*. 2018. doi:10.1073/pnas.1812779115

24. Creese O, Adoni P, Su G, Romanyuk A, Fernandez-Trillo P. Poly(Boc-acryloyl hydrazide): the importance of temperature and RAFT agent degradation on its preparation. *Polym Chem*. 2019;10(41):5645-5651. doi:10.1039/C9PY01222B

25. Xue X, Pasparakis G, Halliday N, et al. Synthetic polymers for simultaneous bacterial sequestration and quorum sense interference. *Angew Chemie - Int Ed*. 2011. doi:10.1002/anie.201103130

26. Danese PN, Pratt LA, Kolter R. Exopolysaccharide production is required for development of Escherichia coli K-12 biofilm architecture. *J Bacteriol*. 2000.

doi:10.1128/JB.182.12.3593-3596.2000

27. O'Toole GA. Microtiter dish Biofilm formation assay. *J Vis Exp*. 2010. doi:10.3791/2437

28. Wang X, Preston JF, Romeo T. The pgaABCD Locus of Escherichia coli Promotes the Synthesis of a Polysaccharide Adhesin Required for Biofilm Formation. *J Bacteriol*. 2004. doi:10.1128/JB.186.9.2724-2734.2004

29. Costerton JW. Overview of microbial biofilms. *J Ind Microbiol*. 1995. doi:10.1007/BF01569816

30. de Beer D, Stoodley P, Roe F, Lewandowski Z. Effects of biofilm structures on oxygen distribution and mass transport. *Biotechnol Bioeng*. 1994. doi:10.1002/bit.260431118

31. Chen JL, Steele TWJ, Stuckey DC. Metabolic reduction of resazurin; location within the cell for cytotoxicity assays. *Biotechnol Bioeng*. 2018. doi:10.1002/bit.26475

32. Riss TL, Moravec RA. Cell proliferation assays: Improved homogeneous methods used to measure the number of cells in culture. In: *Cell Biology, Four-Volume Set*. ; 2006. doi:10.1016/B978-012164730-8/50005-8

33. Wu G. Assays Based on Integrated Cell System Properties. In: *Assay Development*. ; 2010. doi:10.1002/9780470583128.ch11

34. Ganewatta MS, Tang C. Controlling macromolecular structures towards effective antimicrobial polymers. *Polymer (Guildf)*. 2015. doi:10.1016/j.polymer.2015.03.007

35. Yang Y, Cai Z, Huang Z, Tang X, Zhang X. Antimicrobial cationic polymers: From structural design to functional control. *Polym J*. 2018. doi:10.1038/pj.2017.72

36. Edwards SJ, Kjellerup B V. Applications of biofilms in bioremediation and biotransformation of persistent organic pollutants, pharmaceuticals/personal care products, and heavy metals. *Appl Microbiol Biotechnol*. 2013. doi:10.1007/s00253-

013-5216-z

37. Kanaya S, Koyanagi T, Kanaya E. An esterase from Escherichia coli with a sequence similarity to hormone-sensitive lipase. *Biochem J*. 1998. doi:10.1042/bj3320075

38. Kuznetsova E, Proudfoot M, Sanders SA, et al. Enzyme genomics: Application of general enzymatic screens to discover new enzymes. *FEMS Microbiol Rev*. 2005. doi:10.1016/j.femsre.2004.12.006

39. Zhu Y, Li J, Cai H, Ni H, Xiao A, Hou L. Characterization of a new and thermostable esterase from a metagenomic library. *Microbiol Res*. 2013. doi:10.1016/j.micres.2013.04.004

40. Golub SR, Overton TW. Pellicle formation by Escherichia coli K-12: Role of adhesins and motility. *J Biosci Bioeng*. 2021. doi:10.1016/j.jbiosc.2020.12.002

41. Leech J, Golub S, Allan W, Simmons MJH, Overton TW. Non-pathogenic Escherichia coli biofilms: effects of growth conditions and surface properties on structure and curli gene expression. *Arch Microbiol*. 2020. doi:10.1007/s00203-020-01864-5

42. Otto K, Silhavy TJ. Surface sensing and adhesion of Escherichia coli controlled by the Cpx-signaling pathway. *Proc Natl Acad Sci U S A*. 2002. doi:10.1073/pnas.042521699

Chapter 6 - Conclusions and future work

In this project, poly(acryloyl) hydrazide (pAH) was used as scaffold onto which functionality could be introduced via a simple post polymerisation step, resulting in a small library of aldehyde functionalised pAH polymers with varying physiochemical properties that could be used to our advantage to modulate bacterial aggregation mechanisms with subsequent control over phenotype. Firstly however, a study collaborative study was conducted to optimise boc-pAH RAFT mediated synthesis in order to try to target long chain polymers with improved control over polymer dispersity from previous protocols. It was found that a temperature dependant intramolecular nucleophilic attack toward the trithiocarbonate of the mediating RAFT agent during propagation lead to loss of control over polymer dispersities. This was of particular concern for longer targeted polymers due to the fact that these polymerisations took longer to complete, but only reached low conversions owing to temperature dependant early RAFT degradation. Kinetic experiments were performed using a low temperature initiator (so as to control the rate of propagation by temperature) and a 'goldilocks temperature of polymerisation' – 65 ^{o}C, was found where a balance between increasing the rate of propagation and delaying onset of raft agent degradation was found resulting in greater monomer conversions and higher polymer dispersities. This was particularly prevalent when targeting the synthesis of longer polymers.

Moving forward, the now optimised polymerisation route was used to synthesize the functional pAH polymers to be tested with *E. coli* K-12. It was found that polymer induced bacterial aggregation was driven primarily by hydrophobic interactions between insoluble polymer aggregates and bacteria, generating bacterial aggregates which increased in biofilm intensity as a function of polymer hydrophobicity. Furthermore, it was shown that MC4100

biofilm levels could be stimulated to surpasses that of the thick biofilm forming PHL644 using our most hydrophobic polymers. This was an encouraging result and suggests that other non/low biofilm forming strains that could be industrially important, can experience the benefits of being in biofilm.

Furthermore, curli expression was investigated in these polymer induced aggregates with only the most hydrophobic polymer pAH-PYRENE inducing significantly affecting curli expression in the already overexpressing PHL644 strain. MC4100 curli expression on the other hand, which does not express curli to a high extent in its native form, was greatly influenced by the addition polymers with in general, increasingly hydrophobic pAH polymers stimulating increasing levels of curli expression. Intriguingly, the low-moderately hydrophobic pAH-2AFP and pAH-IND stimulated the largest amounts of curli, and these two polymers also generated large and strong bacterial aggregates as determined by laser particle size analysis, along with the most hydrophobic polymers pAH-NAPTH, pAH-ANTH and pAH-PYRENE. Therefore the higher level of strong polymer induced bacterial aggregation from the pAH-2AFP and pAH-IND polymers is likely because of additional hydrogen bonding interactions between the polymer aggregates/bacteria. Intriguingly, in a previous study conducted in our labs curli expression has actually been found to decrease upon solid surface attachment/sedimentation when compared with planktonic cells, suggesting its use primarily as an adhesin for cells in preparation for surface attachment. However, in pellicles which are formed on a soft air-liquid interface, curli expression is significantly higher with curli thought to be required for additional structural integrity of the biofilm potentially due to the lack of a solid support. It could be possible that this is the reason for the high levels of curli expression within our soft material based bacterial

aggregates, where curli downregulation has been suppressed in a similar manner to pellicles. Further work is required to elucidate the specific reasons for this and could involve assessing and comparing rheological properties of pellicles with that of our polymer induced aggregate biofilms, in order to ascertain viscoelastic properties of both. If the properties are comparable, it could be likely that curli regulation is dependent on the viscoelastic properties of the biofilm/pellicle. Imaging the biofilms via high resolution transmission electron microscopy (TEM) could also give information about the biofilm structure. Investigating how bacteria are patterned onto the polymers, and if they are densely packed or more sparsely populated compared with naturally formed biofilms. Ideally, the polymer induced biofilms would present porous biofilm structures that would allow for greater levels of flow, and a reduction in osmolarity which is also known to increase curli expression. Overall the most encouraging result however was the fact that control over *E. coli* biofilm levels could be imparted using our functional polymers in a predictable manner. Furthermore the fact we are able to induce and surpass overall biofilm levels and curli expression to that over its mutant curli overproducing PHL644 strain opens up the possibility that other potentially industrially useful non/low biofilm forming strains could experience the benefits of being in biofilm form through the use of our polymers.

The functionality of the polymer induced biofilms in the biocatalytic arena was also assessed, with encouraging results. In general for the biocatalysis of 5-fluoroindole, an increase in reaction kinetics after 24h was seen for increasingly hydrophobic polymer induced biofilms, however this reached a certain point where increasingly hydrophobic pAH-ANTH and pAH-PYRENE were detrimental to performance. Metabolic activity assessment of the biofilms revealed that indeed pAH-ANTH and pAH-PYRENE had a detrimental effect on

bacterial metabolic activity, and this was thought the reason for the drop in biocatalysis performance. Furthermore, a bioconversion involving harnessing the native metabolism of *E. coli* was performed; specifically for esterase activity. In environmentally challenging conditions for the bacteria (33% ethanol), the lipid ester 4-Nitrophenldodecanoate was converted into the UV_{410} active 4-Nitrophenol by selected polymer induced biofilms. Kinetic analysis showed that the hydrophobic polymer induced aggregate biofilms performed better than their naturally formed counterparts, with hydrophilic polymers inducing no increase in activity. The optimised performance related to hydrophobic polymers induced biofilms was thought to be down to the increased resistance towards toxic ethanol, imparted by the increased levels of biofilm. The immediate future work on polymer induced biocatalysis could involve potentially assessing the performance of these polymers with different strains of industrially relevant bacteria with a range of strain specific bioconversions performed under different conditions. Bioremediating properties could also be easily assessed.

An additional advantage of aldehyde functionalised poly(acryloyl hydrazide) polymers is that the aldehyde functionality is pH dynamic. The pAH-aldehyde coupling reaction is performed in acidic conditions and the equilibrium of the coupling reaction is shifted towards the functional hydrazone. The relative percentage incorporation of aldehydes into pAH depends on this. In less acidic conditions however, this hydrazone bond may be hydrolysed, thereby reversing the equilibrium back to the unfunctionalised pAH and aldehyde. Initial experiments have been performed in attempting to manipulate this dynamism in our polymer induced biofilms (see figure 1) with promising results, indicating that polymer induced biofilm levels can be manipulated by modulating pH *in situ*. Whether this is directly

down to pH modulated changes in pAH-aldehyde functionality within these bacterial aggregates remains to be seen and pursuing this research could lead to additional functionality of the polymer-bacterial aggregate system, whereby biofilm levels can be reduced and increased *in situ* by the pAH polymers as a result of simple changes in pH.

(a)

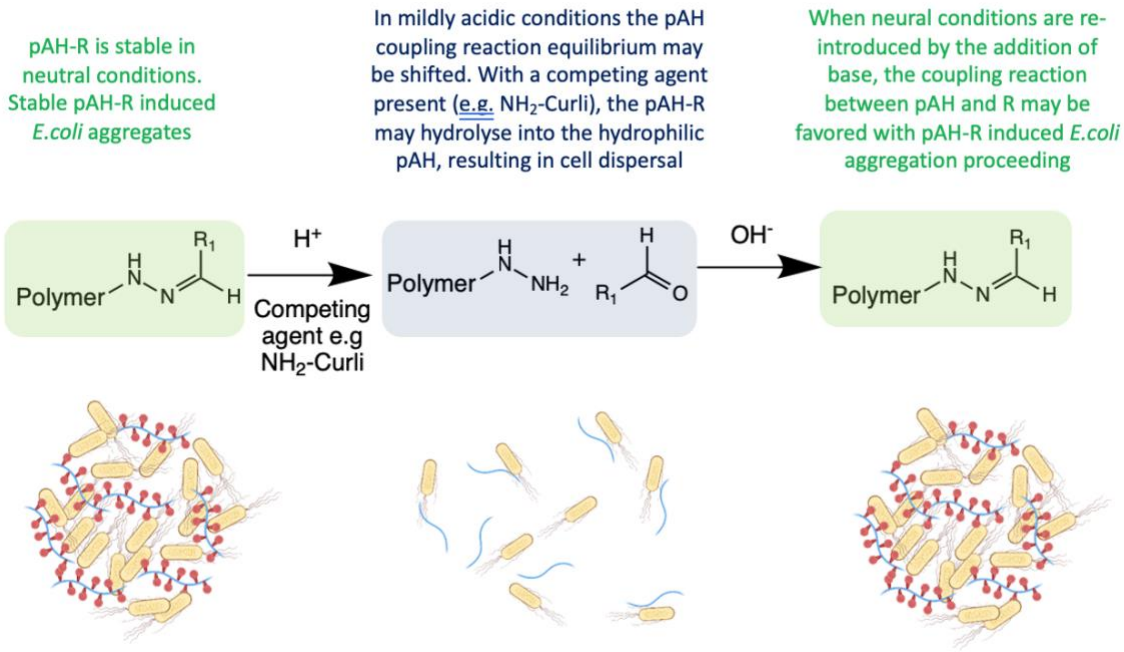

(b)

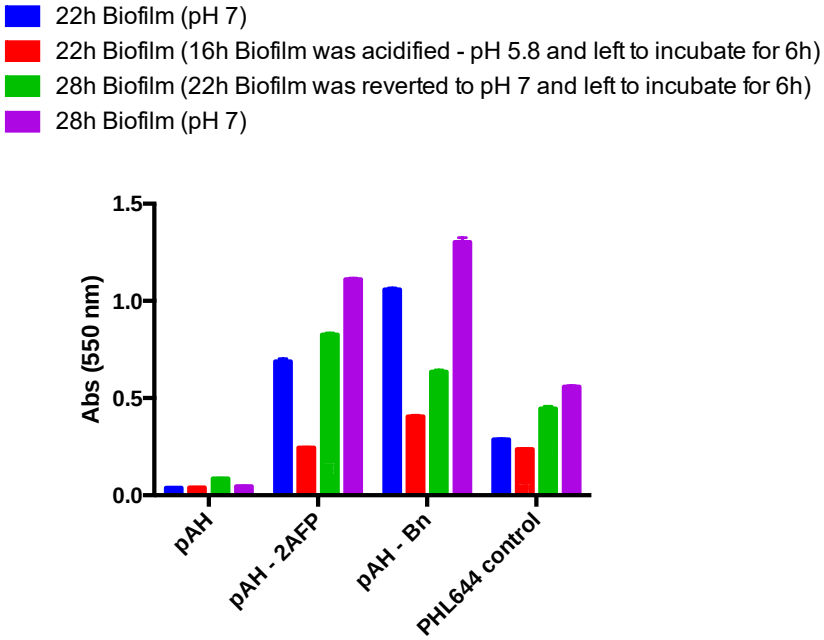

Figure 1: (a) Schematic representing the potential pH responsive dynamism of the pAH-aldehyde bond. (b) Polymer induced biofilm levels (as determined by crystal violet) before and after pH changes. Polymer-cell suspensions were prepared as detail in chapter 2 section (ii)